

博士論文

Correlation Functions
of $\mathcal{N} = 4$ Supersymmetric Yang-Mills Theory
in $\text{AdS}_5/\text{CFT}_4$ Correspondence
– Perturbation and Integrability

($\text{AdS}_5/\text{CFT}_4$ 対応における
 $\mathcal{N}=4$ 超対称 Yang-Mills 理論の相関関数
– 摂動論と可積分性)

東京大学大学院 総合文化研究科

桐生 直輝

Doctor Dissertation

**Correlation Functions
of $\mathcal{N} = 4$ Supersymmetric Yang-Mills Theory
in $\text{AdS}_5/\text{CFT}_4$ Correspondence
– Perturbation and Integrability**

Naoki Kiryu*

A thesis submitted to
the University of Tokyo, Komaba,
Graduate school of Arts and Sciences

Tokyo, Japan, March 27, 2019

*naokiri0311 AT gmail.com

Abstract

This dissertation is devoted to the study of $\text{AdS}_5/\text{CFT}_4$ correspondence, which is a duality between $\mathcal{N} = 4$ Supersymmetric Yang-Mills theory in four dimensions and type IIB superstring theory on $\text{AdS}_5 \times \text{S}^5$. In particular, we focus on a fundamental physical quantity in $\mathcal{N} = 4$ supersymmetric Yang-Mills theory which is correlation functions. In this thesis, there are two main results for computations of correlators of operators on the 1/2 BPS Wilson loop. The first result is a proposal for a finite coupling expression of large-volume correlators by an integrability-based approach. The second result is that we calculate finite-size corrections of the correlators at lower order from the perturbation.

After a general introduction, we begin with a brief review of the $\text{AdS}_5/\text{CFT}_4$ correspondence, and give generic preliminaries of correlators of $\mathcal{N} = 4$ supersymmetric Yang-Mills theory in Part I. The main text in this thesis is split into two parts explained in Part II and in Part III. Part II, the first half of the main contents of the thesis, deals with the correlation functions of single trace operators, which correspond to an interaction process of closed strings. Then, we review several developments of integrability-based approaches for computations of correlators in a short course to explain a proposal for large-volume correlators with finite coupling.

As a natural question, it is interesting to consider an open string version of the finite coupling method. In Part III, the second half of the main contents of the thesis, we deal with correlation functions of operators inserted into the 1/2 BPS Wilson loop. Such configuration corresponds to open strings attached D3-brane in the dual AdS theory. Then, we explain integrability-based computations of the correlators at lower order, and then we propose large-volume correlators with finite coupling. In addition, we explain computations of finite-size corrections of the correlators at lower order from the perturbation. It is a significant advantage to consider the open string configuration.

Acknowledgement

First of all, I would like to express my gratitude to Shota Komatsu. He was my main collaborator, and discussion with him for several topics was always exciting and stimulating. Secondly, I would like to thank all the collaborators, Takuya Nishimura and Minkyoo Kim. The collaboration with them was enjoyed.

I next would like to acknowledge my supervisor Mitsuhiro Kato and all the former and current members of the particle theory group at Komaba. In particular, I thank Keiyu Goto, Hiroaki Matsunaga and Toko Sasaki. Without their help, I couldn't make nice PhD days.

Lastly, I would like to acknowledg various discussions of AdS/CFT and integrability with Katsushi Ito, Yoichi Kazama, Hideki Kyono, Junichi Sakamoto, Yuji Sato, Hongfei Shu and Kentaroh Yoshida.

Contents

I	Introduction and AdS₅/CFT₄	8
1	Introduction	9
1.1	Opening act	9
1.2	Outline of this thesis	14
1.2.1	Organization of the thesis	14
1.2.2	Contents of the thesis organized in two figures	14
2	AdS₅/CFT₄ correspondence and $\mathcal{N} = 4$ SYM	17
2.1	AdS ₅ /CFT ₄ correspondence	17
2.1.1	Open string side	17
2.1.2	Closed string side	18
2.1.3	AdS ₅ /CFT ₄ correspondence	19
2.2	$\mathcal{N} = 4$ SYM	19
2.2.1	Correlation functions and BPS operator	20
2.2.2	Weak coupling expansion of correlators	21
II	Correlators of single trace operators	24
3	BPS operators – perturbation	25
3.1	Four-point functions at tree-level	25
3.2	Correlation functions at one-loop	28
3.2.1	One-loop insertion formula	29
3.2.2	Four-point functions	30
4	Non-BPS operators – perturbation and integrability	35
4.1	Two-point functions at one-loop	35

4.1.1	The anomalous dimension matrix and XXX spin chain Hamiltonian	36
4.1.2	Anomalous dimensions and coordinate Bethe ansatz	37
4.2	Three-point functions at tree-level	40
4.2.1	Structure constants at tree-level	40
4.2.2	Weight factors and Tree-level hexagon form factor	49
5	Complete method – integrability	50
5.1	Structure constants at finite coupling	50
5.1.1	Symmetry of the three-point functions	52
5.1.2	Symmetry and hexagon form factor	53
5.1.3	Integrability and hexagon form factor	57
5.1.4	Three-point functions at tree-level	59
5.1.5	Finite-size correction and mirror transformation	59
5.2	Four-point functions and hexagon method	62
5.2.1	Length two BPS operators	63
5.2.2	Conformal transformation of the hexagon	64
5.2.3	Gluing the hexagons	65
5.2.4	BPS four operators at one-loop	66
5.2.5	Some developments of the hexagonalization	67
III	Correlators of operators on the Wilson loop	69
6	Maldacena-Wilson loop	70
6.1	Maldacena-Wilson loop	70
6.1.1	Wilson loop at the strong coupling	71
6.1.2	Wilson loop in perturbation theory	71
6.2	Cusp and operator insertions in Wilson loop	72
6.3	Set-up and notations	73
7	BPS operators – perturbation	76
7.1	Four-point functions at tree-level	76
7.2	One-loop correlation functions of the BPS operators on the Wilson loop . .	81
7.2.1	One-loop insertion formulas without Wilson loop boundary	81
7.2.2	One-loop insertion formulas with Wilson loop boundary	82

7.3	One-loop correlation functions	85
7.3.1	Two- and three-point functions	85
7.3.2	Four-point functions	87
8	Zero-length operators – perturbation	91
8.1	Two-point functions at two loops	92
8.1.1	One loop	92
8.1.2	Two loops	93
8.2	Three-point functions at two loop	98
8.2.1	One loop	98
8.2.2	Two loop	99
8.3	Three-point functions in the ladders limit	100
8.3.1	Set-up	101
8.3.2	Bridge kernel and the SD-equation	102
8.3.3	Two-point functions and renormalization	104
8.3.4	Case I: one nontrivial and two trivial DCOs	106
8.3.5	Case II: two nontrivial and one trivial DCOs	107
8.3.6	Case III: three nontrivial DCOs	109
9	Non-BPS operators – perturbation and integrability	112
9.1	Open spin-chain and wave functions	113
9.1.1	One-magnon	113
9.1.2	Two-magnon	114
9.1.3	Multi-magnon	115
9.2	Structure constants and the hexagon form factor	116
9.2.1	A nontrivial operator with one-magnon : $C_{123}^{Y\infty}$	116
9.2.2	A nontrivial operator with two-magnon : $C_{123}^{Y^2\infty}$	117
9.2.3	A nontrivial operator with M -magnon : $C_{123}^{Y^M\infty}$	118
10	Complete method – integrability	125
10.1	Conjecture for finite coupling structure constants	125
10.2	Hexagonalization and the perturbation	127
10.2.1	Summary of the hexagonalization and perturbation	127
10.2.2	Hexagonalization data from the one-loop correlators	128

IV	Conclusions and future directions	136
11	Conclusions	137
12	Future directions	139
12.1	Higher rank sector	139
12.2	$1/N$ correction	139
12.3	Hexagonalization of multi-magnon	140
12.4	Application to higher spin holography	140
V	Appendix	142
A	Basic integrals	143
B	Three-point functions with double-magnon states at tree-level $C_{123}^{XX^\circ}$	145
C	Vertex and self-energy diagrams for the three-point functions	148
D	Excited states and conformal descendants	150
E	Contribution from the integral of Γ_{UV}	154
F	Explicit calculation of the $C_{123}^{\bullet\circ\circ}$ in (8.63)	156
G	An infinite sum representation for $C_{123}^{\bullet\bullet\bullet}$	158
H	Open spin chain wave functions	160
H.1	One-magnon	160
H.2	Two-magnon	161
I	Multi-magnon hexagon form factor	163
J	Bridge length independent terms	166
K	Two nontrivial operators with one-magnon : $C_{123}^{YY^\circ}$	168
L	On norms of structure constants for open string	171

Part I

Introduction and $\text{AdS}_5/\text{CFT}_4$

Chapter 1

Introduction

1.1 Opening act

In 1997, Maldacena proposed a duality between d -dimensional conformal field theory and $d + 1$ -dimensional gravity theory on the anti-de Sitter space, which is so-called AdS/CFT correspondence [1]. Since the AdS/CFT correspondence has many interesting aspects, it has several ways to call it: holographic duality, gauge/gravity duality and so on. In addition, many models with such duality have been discovered, and then many researchers have studied or used the AdS/CFT correspondence in the various topics.

Among them, we focus on the most prototypical case of the AdS₅/CFT₄ correspondence, which is the duality between Type IIB superstring theory on AdS₅ × S⁵ background and $\mathcal{N} = 4$ supersymmetric Yang-Mills theory in four-dimension ($\mathcal{N}=4$ SYM). Since the AdS₅/CFT₄ correspondence has a strong/weak property, we should be away from the perturbative computation naively in order to verify it. This is, actually, not only a nice property to be used, but also a cause of difficulty.

It is no doubt that one of the general goals in the context of the AdS₅/CFT₄ correspondence has been how to give a finite coupling result of correlation functions. In the long history, the symmetry and integrability-based approach has been developed greatly [2], for instance computations of correlators with finite coupling, since both sides of the AdS₅/CFT₄ correspondence have large symmetries and integrable structures [3–6].

At the initial stage in the long history, the study was focused on the computation of two-point functions of single trace operators, that is, spectrum problem. Since an anomalous dimension matrix in $\mathcal{N} = 4$ SYM is considered to be identified with a Hamiltonian of spin chain system, the spectrum problem has been deeply related to a diagonalization problem of the Hamiltonian.¹ With an assumption that the anomalous dimensions correspond to the spin chain system at finite coupling,² S-matrices of magnons on the spin chain are strongly constrained by the symmetry of the two-point functions in $\mathcal{N} = 4$

¹We believe that the identification is true even at finite coupling.

²And also, we assume that there is a finite coupling spin chain model.

SYM:

$$[\mathcal{J}, S] = 0,$$

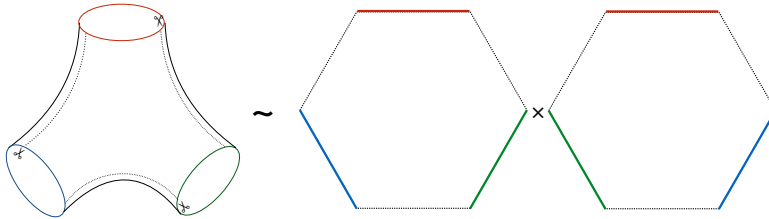
where \mathcal{J} are generators of such symmetry. Solving the equation, one can analytically determine the exact S -matrices [7–11]. Thus, momentums of the magnons are also determined by using the Bethe ansatz equation $1 = \exp(ip_k L) \prod_{k \neq l} S(p_k, p_l)$. Finally, the dispersion relation teaches us the spectrum from the momentum [12].³ Such a integrability-based results were surprisingly matched to all perturbative results till now.

At the next stage, the study of three-point functions in the AdS₅/CFT₄ correspondence also has a long history.⁴ The three-point functions in $\mathcal{N} = 4$ SYM are composed not only of the anomalous dimensions but also of structure constants C_{123} defined by the operator product expansion (OPE) of the conformal field theory. On the string theory side, the three-point functions can be interpreted as a three-string interaction, which is the joining or splitting process of the three strings. The interaction of three operators is characterized three-string string field theory vertex \mathcal{V}_{SFT} including three-string Hilbert spaces \mathcal{H}_i :

$$|\mathcal{V}_{\text{SFT}}\rangle \in \mathcal{H}_1 \otimes \mathcal{H}_2 \otimes \mathcal{H}_3, \quad \langle \mathcal{V}_{\text{SFT}} | (|1\rangle \otimes |2\rangle \otimes |3\rangle).$$

In fact, in the context of the AdS₅/CFT₄ correspondence, it is shown that structure constants in the pp-wave limit are related to the three-string field theory vertex in the pp-wave string field theory [24–30]. However, for the general AdS₅ background, it is still an open problem.⁵

Recently, a remarkable development for studying the three-point functions in the AdS₅/CFT₄ correspondence has been done. It is because the structure constants are proposed at finite coupling [34]. Roughly speaking, the idea comes from the world sheet picture interacting with three closed strings, that is, a pair of pants diagram, and such diagram is graphically decomposed into two hexagon form factors:



Thus, the finite coupling method says that the structure constants in $\mathcal{N} = 4$ SYM are given by a function of the hexagon form factor \mathfrak{h} :

$$C_{123}(\mathfrak{h}), \quad \mathfrak{h} \equiv \langle h | (|1\rangle \otimes |2\rangle \otimes |3\rangle).$$

³Moreover, a resummation formula of the finite size correction called quantum spectrum curve was also important development [13, 14].

⁴Some researches are successful in analysing the three-point functions in the AdS₅/CFT₄ correspondence [15–23].

⁵Some developments are in [31–33]

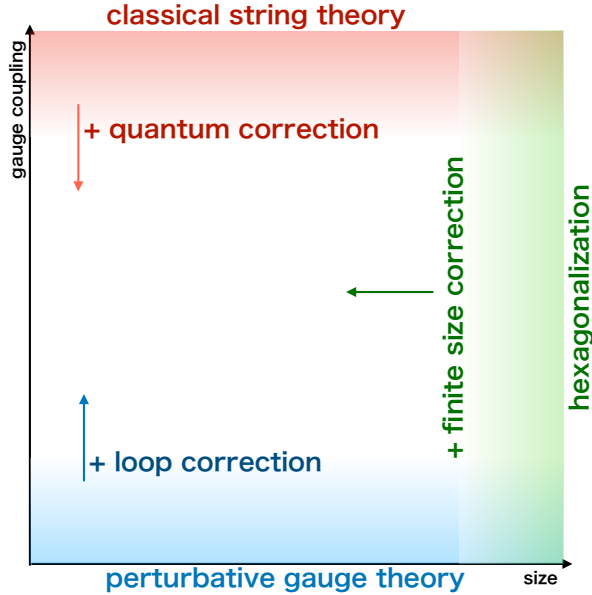


Figure 1.1: Chart for the three-point functions of the $\text{AdS}_5/\text{CFT}_4$ correspondence

Then, the hexagon form factor is strongly constrained by the symmetry:

$$\langle h | \tilde{\mathcal{J}} = 0,$$

where $\tilde{\mathcal{J}}$ is generators of symmetry of the three-point functions in $\mathcal{N} = 4$ SYM. Thereby, the hexagon form factor is completely fixed by the symmetry and further integrability constraints. Although we could get the finite coupling answer of the structure constants (if we believe the hexagon method), we do not understand physical explanation at all.

The hexagon method is a technique introduced very recently. It certainly gives a new aspect for studying the three-point functions in the $\text{AdS}_5/\text{CFT}_4$ correspondence. Until now, the weak coupling region in the $\text{AdS}_5/\text{CFT}_4$ correspondence is sufficiently calculated by perturbative gauge theory (perturbative gauge theory realm), and the strong coupling region is also studied by classical string theory (classical string theory realm). In addition, the hexagon method teaches us another region which is the finite coupling within large-volume limit (hexagonalization realm),⁶ see in figure 1.1. In other words, each three realm can be studied by using each of the established methods.⁷ Then, we find the two overlapping regions: between the classical string theory realm and hexagonalization realm and between perturbative gauge theory realm and hexagonalization realm. It is worth studying the relations since we will eventually have an ambitious question, *how does the string emerge from the gauge theory* through the integrability realm in the future.

In what follows, we explain more specific motivation, and then we shall connect the contents in this thesis. Then, notable topics are split into three directions.

⁶The large volume limit is a technical word which is used in the Hexagonalization realm. The volume (or size) is defined in terms of a length $\ell_{ij} = (L_i + L_j - L_k)/2$, where L_i s are the length of the external operators. The length ℓ_{ij} means the number of tree-level contractions between operators \mathcal{O}_i and \mathcal{O}_j .

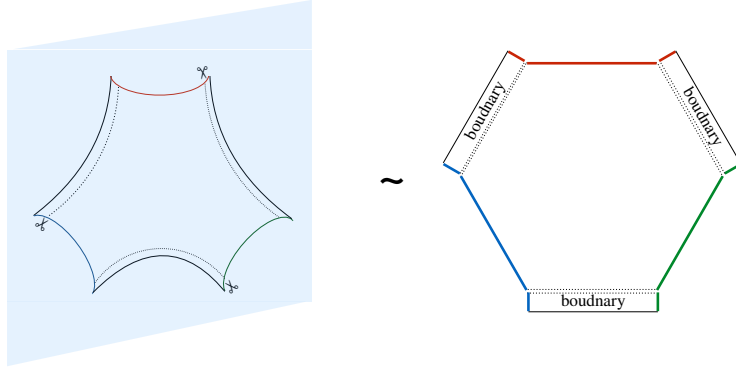
⁷Rigorously, the hexagonalization method is a proposal. However, we will assume the validity of the proposal in this thesis.

Perturbation and hexagonalization

In this thesis, we focus on studying the relation between the perturbative gauge theory realm and hexagonalization realm. One of the main differences in these method is diagrams. The perturbative method is based on the calculation of Feynman diagrams. Furthermore, loop diagrams produce divergences and regularization. However, the hexagon method doesn't know such familiar phenomena. On the other hand, the hexagon method has the hexagon form factor, which is a 2-dimensional world-sheet like object. It is interesting to reproduce such object from the perturbative method. The most hopeful task is to produce the hexagon form factor from the tailoring method, which can calculate tree-level structure constants by using both the perturbation and an integrability. In this thesis, we shall see it in chapter 4 and 9.

Closed string and open string

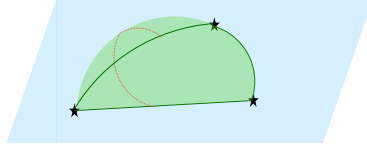
As a natural question, we would like to consider an open string version of the hexagon method. In the perturbative gauge theory realm, a gauge invariant operator corresponding to the open strings attached D3-brane, is given by three local operators inserted into the 1/2-BPS Wilson loop. The three-point functions of the open strings can also apply the hexagon method since it is decomposed into one hexagon and three boundaries in chapter 10:



Surprisingly, in our proposal, the hexagon form factor in the three-point functions of the open strings is the same object with one of the closed strings. One may seem that the closed string correlator will be written in terms of the open string correlator at finite coupling. Actually, we shall sometimes see that the open string correlator naturally appears in computations of the closed string correlator in this thesis, for instance in chapter 3 and 7.

Open string correlator and finite-size corrections

Finally, we would like to mention a further motivation to consider the open string correlator. One of the big differences from the closed correlator is the fact that the open string worldsheet is always attached to the boundary. Because of that, we can define diagrams propagated from a boundary to another boundary in $\mathcal{N} = 4$ SYM:



Since such loop diagrams will have the order of operator length $O(e^L)$, it is often called finite-size corrections (or mirror collections in terms of the integrability realm). In practice, the two-loop and the ladder resummed diagrams can be calculated by perturbative method in chapter 8 and 10. This is one of the advantages to consider the open string configuration.

1.2 Outline of this thesis

1.2.1 Organization of the thesis

This thesis is devoted to the study of correlation functions in the $\text{AdS}_5/\text{CFT}_4$ correspondence. Among them, we focus on computations of correlators of $\mathcal{N} = 4$ SYM from the perturbation and an integrability-based approach. In the rest of Part I, we start with an introduction of the $\text{AdS}_5/\text{CFT}_4$ correspondence, and then we summarize basic things of correlators of $\mathcal{N} = 4$ SYM.

The Part II deals with correlators of single trace operators. In chapter 3, we calculate correlators of single trace BPS operators up to one-loop by using the well known perturbative method. In chapter 4, we review correlators of non-BPS operators. In particular, we consider two-point functions at one-loop and three-point functions at tree-level. Then, we use integrability techniques, spin chain system and tailoring method, in order to efficiently solve an operator mixing problems. In chapter 5, we review a proposal for finite coupling prescription of three- and four-point functions, which is called hexagon method and hexagonalization. Such correlators are given by bootstrap techniques for symmetry and integrability.

The Part III is a main part of this thesis, since all contents are composed by the author's published papers. There, we consider correlation functions of operators inserted into the 1/2 BPS Wilson loop. After introducing the set-ups in chapter 6, we start with calculation of correlators of BPS operators up to one-loop by using the perturbative method in chapter 7. In chapter 8, we consider correlator of length zero operators, which is defect changing operators, by using the perturbative method. Then, we calculate two-loop and ladder-resummed diagrams [37]. In chapter 9, we calculate the three-point functions of non-BPS operators at tree-level by using tailoring method. In section 10, we propose a finite coupling conjecture of the correlator [35,37]. Thus, from the perturbative results showed in chapter 7, we predict hexagonalization data whose integrability-based calculations are difficult because it is technically challenging [36].

In Part IV, we discuss the results explained in this thesis and comment on further directions. In Part V, we add some appendices to help reading the main contexts.

Before ending the organization of this thesis, it is better to more clarify which parts of this thesis are on the basis of the author's works. In Part II, the one-loop results of sections 3.2 were proposed by previous papers [39]. However, the tree-level results in section 3.1 and more rigorous proof of the one-loop results in section 3.2 was done by the author in unpublished notes. In the section 4.2, the multi-magnon proof is also first worked out by the author. In the Part III, the chapter 8 are on the basis of the author's work [37]. On the other hand, the chapter 7, 9 and 10 are on the basis of the author's work heavily [35,36].

1.2.2 Contents of the thesis organized in two figures

The story of this thesis is arranged in figure 1.2. The main text in this thesis is split into

	closed	open
AdS ₅ /CFT ₄	② Preliminary	⑥ Preliminary
Perturbation	③ BPS	⑦ BPS ⑧ Zero – length
Perturbation & Integrability	④ Non – BPS	⑨ Non – BPS
Integrability	⑤ Hexagon	⑩ Hexagon

Figure 1.2: The arrangement of the contents based on the ordering of the chapters in this thesis.

two parts: Part II and Part III. The contents of Part II, which have from chapter 2 to chapter 5, correspond to closed string configuration, and correlators of each chapter are calculated by perturbation, not only perturbation but also integrability and integrability-based approach respectively. The contents of Part III, which have from chapter 6 to chapter 10, correspond to open string configuration, and most chapters have parallel contents with Part III. However, the configuration in chapter 8, which is the correlators of zero-length operators, is only on the open string side.

We can explain the arrangement of chapters in terms of studying the computations of correlators of AdS₅/CFT₄ correspondence in figure 1.3. The studies in chapter 3 and in chapter 7 are located in the perturbation realm. In chapter 4 and chapter 9, these studies are relied not only on perturbation but also on integrability techniques. In chapter 5 and chapter 10, the studies with finite coupling are in the hexagonalization realm available for the large-volume. Conversely, the configuration in chapter 8 is a zero-volume region in the perturbative realm.

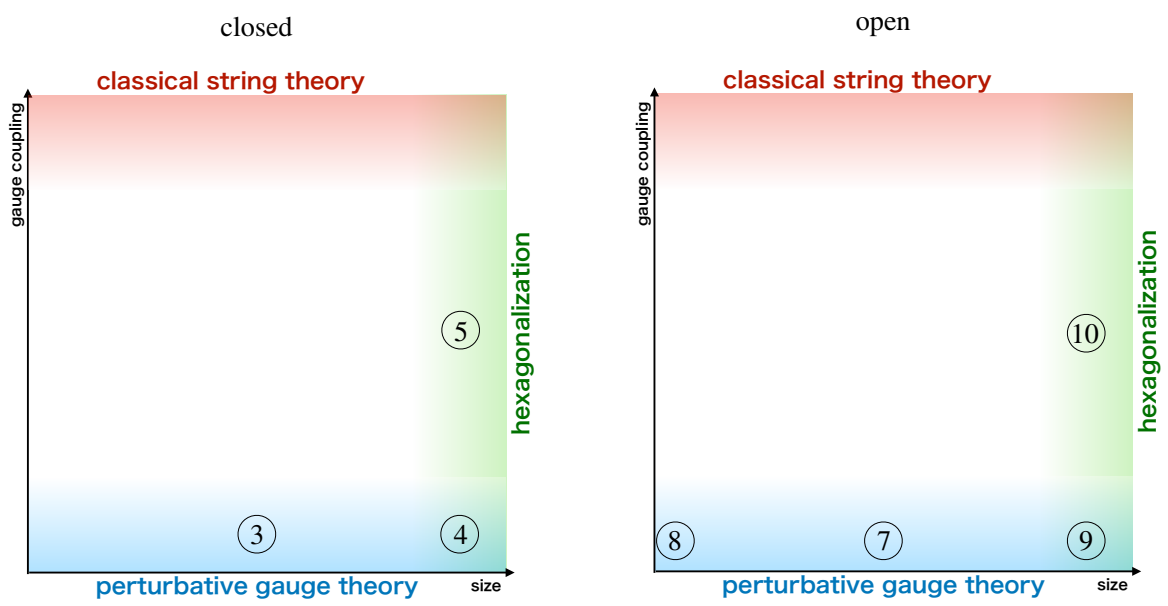


Figure 1.3: Chapters in this thesis and $\text{AdS}_5/\text{CFT}_4$ correspondence.

Chapter 2

AdS₅/CFT₄ correspondence and $\mathcal{N} = 4$ SYM

The aim of this chapter is to introduce the AdS₅/CFT₄ correspondence, which is the duality between $\mathcal{N} = 4$ Supersymmetric Yang-Mills theory in four-dimensions ($\mathcal{N} = 4$ SYM) and type IIB superstring on $AdS_5 \times S^5$.

2.1 AdS₅/CFT₄ correspondence

Let us start with the situation where there is a stack of N D3-branes in type IIB superstring theory on the ten-dimensional flat space. Since the type IIB superstring theory is a closed string theory, there is closed string interacting with the D3-branes. Furthermore, an open string attached to the D3-branes is also included.

We would like to discuss the low energy limit of the situation from two different perspectives: open string and closed string. The AdS₅/CFT₄ correspondence shall be stated as a duality between these two perspectives.

2.1.1 Open string side

We first focus on the open strings attached to the D3-branes. By quantizing them, the action includes the four-dimensional vector field A^μ ($\mu = 0 \sim 3$) which live in parallel to the four direction of D3-brane, six scalar fields ϕ^i ($i = 1 \sim 6$) which live in the six-direction perpendicular to D3-brane and supersymmetric partners, four fermions ψ_A ($A = 1 \sim 4$) as a massless sector. The massless sector of the low energy effective action of the N

D3-branes is known as the action of $\mathcal{N} = 4$ SYM

$$S = \frac{1}{g_{\text{YM}}^2} \int d^4x \mathcal{L}, \quad (2.1)$$

$$\mathcal{L} = \text{Tr} \left[-\frac{[D_\mu, D_\nu]^2}{2} + (D_\mu \phi_i)^2 + \frac{[\phi_i, \phi_j]^2}{2} + i\bar{\psi}\Gamma^\mu D_\mu \psi + \bar{\psi}\Gamma^i[\phi_i, \psi] + \partial^\mu \bar{c} D_\mu c + (\partial_\mu A^\mu)^2 \right]. \quad (2.2)$$

Unfortunately, the practical action, which comes from string theory includes not only the massless sector but also massive sectors and interactions with the closed strings, which are hard to deal with. In order to decouple and ignore these terms, we take a doubles scaling limit: $l_s \rightarrow 0$ and $g_s = \text{fixed}$. Then, the mass and coupling constant of the closed string become

$$\kappa \sim g_s \alpha'^2 \rightarrow 0, \quad m \propto \frac{1}{\alpha'} \rightarrow \infty. \quad (2.3)$$

Thereby, it is often called the decoupling limit.

From above, under the decoupling limit, $\mathcal{N} = 4$ SYM appears in the low energy effective theory of the D3-branes. In addition, there is ten-dimensional supergravity theory from the closed string decoupling with the open string. Therefore, from the open string side, we see the following theories:

$$4\text{-dim } \mathcal{N} = 4 \text{ SYM} \oplus 10\text{-dim supergravity}$$

2.1.2 Closed string side

We next discuss the situation from the closed string side. Immediately, we faced with a problem of the scattering of the closed string by the D-branes. If we attempt to straightforwardly attack the problem, we must calculate the all passible Feynman diagrams, that is, sum over Riemann surface with any number of holes. In order to avoid such terrible and hopeless calculation, we image the scene that the light closed string move into the potential made by the heavy D3-branes. In fact, it is known to the classical solution of D3-brane in the supergravity theory, which is called black 3-brane as follows:

$$ds^2 = f^{-1/2} dx^\mu dx_\mu + f^{1/2} (dr^2 + r^2 d\Omega_5^2), \quad (2.4)$$

$$f = 1 + \frac{r_0^4}{r^4}, \quad r_0 = 4\pi g_s N l_s^4.$$

After doing so, we should further consider the decoupling limit in the same way as the open string. Here, it is better to divide the two regions: $r > r_0$ and $r < r_0$, and discuss separately:

$$\underline{r > r_0}$$

In this region, the (2.4) become the ten-dimensional flat space metric

$$ds^2 = dx^\mu dx_\mu + dr^2 + r^2 d\Omega_5^2. \quad (2.5)$$

In the same argument as the open string side, the massive modes of the closed string are decoupled. Therefore, we get a ten-dimensional flat space supergravity theory in the region $r > r_0$.

$$\underline{r < r_0}$$

By performing coordinate transformation $Z = \frac{r_0^2}{r}$, we have

$$ds^2 = r_0^2 \left(\frac{dx_\mu dx^\mu + dZ^2}{Z^2} + d\Omega^2 \right), \quad (2.6)$$

where is nothing but the $\text{AdS}_5 \times S^5$ space-time with radius r_0 . Even though we take the decoupling limit $l_s \rightarrow 0, g_s = \text{fixed}$, it remains to show the curved metric. The fact is understood as the red-shift. Thus, the massive modes cannot be neglected. Furthermore, since the decoupling limit implies the limit $r_0 \rightarrow 0$, it is so-called the near horizon limit.

From above arguments, we find that there is a ten-dimensional flat-space supergravity in the $r > r_0$ region and type IIB superstring on the $\text{AdS}_5 \times S^5$ background in the $r < r_0$:

type IIB superstring on $\text{AdS}_5 \times S^5 \oplus 10\text{-dim supergravity}$

2.1.3 $\text{AdS}_5/\text{CFT}_4$ correspondence

According to the arguments of both sides, we finally have the $\text{AdS}_5/\text{CFT}_4$ correspondence:

type IIB superstring on $\text{AdS}_5 \times S^5 \leftrightarrow 4\text{-dim } \mathcal{N} = 4 \text{ SYM}$

We further state of parameters of the correspondence. In $\mathcal{N} = 4$ SYM and type IIB superstring theory on $\text{AdS}_5 \times S^5$, there are two parameters (g_{YM}, N) and (g_s, α') respectively. Here, it is better for discussions below to introduce the so-called 't Hooft coupling constant $\lambda = g_{\text{YM}}^2 N$. Thus, the relations between the parameters are

$$\lambda \equiv g_{\text{YM}}^2 N = g_s N = \frac{R^4}{\alpha'^2}. \quad (2.7)$$

Notice that the parameter α' is proportional to the inverse of the λ . Due to the fact, the $\text{AdS}_5/\text{CFT}_4$ correspondence is a duality of weak/strong. This is one of the nontrivial and interesting feature of $\text{AdS}_5/\text{CFT}_4$ correspondence.

In this thesis, we only discuss a special double scaling limit: $N \rightarrow \infty$ and $\lambda = \text{fixed}$, which is called planar limit or large N limit [38]. In this limit, planar Feynman diagrams are the only dominant contributions.

2.2 $\mathcal{N} = 4$ SYM

In this section, we summarize basic properties of correlation functions in $\mathcal{N} = 4$ SYM as a preliminary.

We first recall the action of $\mathcal{N} = 4$ SYM

$$S = \frac{1}{g_{\text{YM}}^2} \int d^4x \mathcal{L}, \quad (2.8)$$

$$\mathcal{L} = \text{Tr} \left[-\frac{[D_\mu, D_\nu]^2}{2} + (D_\mu \phi_i)^2 + \frac{[\phi_i, \phi_j]^2}{2} + i\bar{\psi}\Gamma^\mu D_\mu \psi + \bar{\psi}\Gamma^i[\phi_i, \psi] + \partial^\mu \bar{c} D_\mu c + (\partial_\mu A^\mu)^2 \right] \quad (2.9)$$

with $D_\mu \equiv \partial_\mu - i[A_\mu, \cdot]$. The c and \bar{c} are the ghosts and $\Gamma^A = (\Gamma^\mu, \Gamma^i)$ are the ten-dimensional Dirac matrices satisfying

$$\text{tr}(\Gamma^A \Gamma^B) = 16\delta^{AB}. \quad (2.10)$$

Using this action, one can compute the propagators in the Feynman gauge as follows:

$$\begin{aligned} \text{Gluon : } \quad \mu \begin{array}{c} a \\ \text{~~~~~} \\ b \end{array} \text{~~~~~} \begin{array}{c} c \\ \text{~~~~~} \\ d \end{array} \nu &= \frac{g_{\text{YM}}^2 \delta^{ac} \delta^{bd}}{8\pi^2} \frac{\delta_{\mu\nu}}{|x-y|^2}, \\ \text{Scalar : } \quad i \begin{array}{c} a \\ \text{-----} \\ b \end{array} \text{-----} \begin{array}{c} c \\ \text{-----} \\ d \end{array} j &= \frac{g_{\text{YM}}^2 \delta^{ac} \delta^{bd}}{8\pi^2} \frac{\delta_{ij}}{|x-y|^2}, \\ \text{Fermion : } \quad \begin{array}{c} a \\ \text{-----} \\ b \end{array} \text{-----} \begin{array}{c} c \\ \text{-----} \\ d \end{array} &= \frac{g_{\text{YM}}^2 \delta^{ac} \delta^{bd}}{8\pi^2} \frac{1}{|x-y|^2}, \\ \text{Ghost : } \quad \begin{array}{c} a \\ \text{-----} \\ b \end{array} \text{-----} \begin{array}{c} c \\ \text{-----} \\ d \end{array} &= \frac{g_{\text{YM}}^2 \delta^{ac} \delta^{bd}}{8\pi^2} \frac{1}{|x-y|^2}. \end{aligned} \quad (2.11)$$

Here $a-d$ are the color indices and all the propagators are proportional to $\delta^{ac} \delta^{bd}$.

2.2.1 Correlation functions and BPS operator

Since $\mathcal{N} = 4$ SYM is a conformal field theory, correlation functions are constrained by conformal symmetry. Thus, two- and three-point functions of single trace operators have following forms:

$$\begin{aligned} \langle \mathcal{O}_1(x_1) \mathcal{O}_2(x_2) \rangle &= n_1 \times \frac{1}{|x_{12}|^{2\Delta_1}}, \\ \frac{\langle \mathcal{O}_1(x_1) \mathcal{O}_2(x_2) \mathcal{O}_3(x_3) \rangle}{\sqrt{n_1 n_2 n_3}} &= \frac{C_{123}}{\sqrt{N}} \times \frac{1}{|x_{12}|^{\Delta_{12|3}}} \frac{1}{|x_{23}|^{\Delta_{23|1}}} \frac{1}{|x_{31}|^{\Delta_{31|2}}}. \end{aligned} \quad (2.12)$$

where $\Delta_{ij|k} \equiv \Delta_i + \Delta_j - \Delta_k$. Δ_i and C_{ijk} are conformal dimensions and the structure constants respectively.

On the other hand, four-point functions

$$\frac{\langle \mathcal{O}_1(x_1) \mathcal{O}_2(x_2) \mathcal{O}_3(x_3) \mathcal{O}_4(x_4) \rangle}{\sqrt{n_1 n_2 n_3 n_4}} \equiv \frac{G_{1,2,3,4}}{N} \quad (2.13)$$

is a nontrivial function of the cross ratios. To see this explicitly, we strip off the space-time dependence from $G_{1,2,3,4}$ as

$$G_{1,2,3,4} = \frac{1}{|x_{12}|^{\Delta_1+\Delta_2}} \frac{1}{|x_{34}|^{\Delta_3+\Delta_4}} \left(\frac{x_{14}}{x_{24}}\right)^{\Delta_2-\Delta_1} \left(\frac{x_{14}}{x_{13}}\right)^{\Delta_3-\Delta_4} g_{1,2,3,4}(\chi). \quad (2.14)$$

Then, the remaining quantity $g_{1,2,3,4}$ depends only on the cross ratios, defined by

$$\frac{x_{12}^2 x_{34}^2}{x_{13}^2 x_{24}^2} = z\bar{z}, \quad \frac{x_{14}^2 x_{23}^2}{x_{13}^2 x_{24}^2} = (1-z)(1-\bar{z}), \quad (2.15)$$

As a special case, we next discuss correlation functions of BPS operators, which do not receive the quantum correlations. In $\mathcal{N} = 4$ SYM, the BPS operator is given by

$$\mathcal{O}_i^{\text{BPS}(L_i)}(x_i) = \text{tr}[(Y_i \cdot \Phi)^{L_i}](x_i), \quad (2.16)$$

where Y is a complex six-dimensional null vector $Y^i \cdot Y^i = 0$. Then, contractions of the operators produce not only the differences of the space-time variables x_{ij} , but also inner product of the SO(6) R-symmetry vector $Y_i \cdot Y_j$. Namely, the two- and three-point function of the BPS operators become

$$\begin{aligned} \langle \mathcal{O}_1^{\text{BPS}(L_1)}(x_1) \mathcal{O}_2^{\text{BPS}(L_2)}(x_2) \rangle &= n_1 \delta_{1,2} \times (d_{12})^{L_1}, \\ \frac{\langle \mathcal{O}_1^{\text{BPS}(L_1)}(x_1) \mathcal{O}_2^{\text{BPS}(L_2)}(x_2) \mathcal{O}_3^{\text{BPS}(L_3)}(x_3) \rangle}{\sqrt{n_1 n_2 n_3}} &= \frac{c_{1,2,3}}{\sqrt{N}} \times (d_{12})^{\frac{L_{12|3}}{2}} (d_{23})^{\frac{L_{23|1}}{2}} (d_{31})^{\frac{L_{31|2}}{2}}, \end{aligned} \quad (2.17)$$

where $L_{ij|k} \equiv L_i + L_j - L_k$ is the combinations of the bare dimensions. Furthermore, d_{ij} is defined as

$$d_{ij} \equiv \frac{\lambda}{8\pi^2} \frac{Y_i \cdot Y_j}{x_{ij}^2}. \quad (2.18)$$

The four-point functions also depend on cross ratios not only of the space-time but also of R-symmetry denoted by α and $\bar{\alpha}$:

$$\frac{\langle \mathcal{O}_1^{\text{BPS}(L_1)}(x_1) \mathcal{O}_2^{\text{BPS}(L_2)}(x_2) \mathcal{O}_3^{\text{BPS}(L_3)}(x_3) \mathcal{O}_4^{\text{BPS}(L_4)}(x_4) \rangle}{\sqrt{n_1 n_2 n_3 n_4}} \equiv \frac{1}{N} d_{12}^{\frac{L_1+L_2}{2}} d_{34}^{\frac{L_3+L_4}{2}} \left(\frac{d_{24}}{d_{14}}\right)^{\frac{L_2-L_1}{2}} \left(\frac{d_{13}}{d_{14}}\right)^{\frac{L_3-L_4}{2}} g_{1,2,3,4}(\chi, \bar{\chi}, \alpha, \bar{\alpha}). \quad (2.19)$$

with

$$\frac{(Y_1 \cdot Y_2)(Y_3 \cdot Y_4)}{(Y_1 \cdot Y_3)(Y_2 \cdot Y_4)} = \alpha \bar{\alpha}, \quad \frac{(Y_1 \cdot Y_4)(Y_2 \cdot Y_3)}{(Y_1 \cdot Y_3)(Y_2 \cdot Y_4)} = (1-\alpha)(1-\bar{\alpha}). \quad (2.20)$$

2.2.2 Weak coupling expansion of correlators

In this subsection, we explain how to extract the anomalous dimensions and structure constants from the actual perturbative computations. Because, the two- and three-point

functions given in (2.12) are applied to the correlators of the renormalized operators. However, the actual perturbative computations have divergence due to the un-renormalized (or equivalently bare) operators.

By introducing the cut off parameter $\epsilon \sim \Lambda^{-1}$, the bare operator \mathcal{O}^B is related to the renormalized operator \mathcal{O}^R in general as follows:¹

$$\mathcal{O}^R \equiv \frac{\epsilon^{-\gamma}}{\sqrt{a}} \mathcal{O}^B, \quad (2.21)$$

where a is the finite renormalization constant which need to bring the renormalized correlator into a canonical form (2.12). Then, substituting (2.21) to (2.12), the two-point functions of the un-renormalized operators are given by

$$\langle \mathcal{O}^B(t_1) \mathcal{O}^B(t_2) \rangle = \frac{a}{|x_{12}|^{2\Delta^{(0)}}} \frac{1}{(|x_{12}|/\epsilon)^{2\gamma}}, \quad (2.22)$$

where $\Delta^{(0)}$ is the bare dimension. Both γ and a are functions of the 't Hooft coupling constant $\lambda \equiv g_{\text{YM}}^2 N$, and can be expanded as

$$a = 1 + \lambda a^{(1)} + \lambda^2 a^{(2)} + \dots, \quad \gamma = \lambda \gamma^{(1)} + \lambda^2 \gamma^{(2)} + \dots. \quad (2.23)$$

Here, we assumed the tree-level renormalized constant become one $a|_{\lambda=0} = 1$. By expanding the right hand side of (2.22), we obtain the expression at weak coupling,

$$\langle \mathcal{O}^B(x_1) \mathcal{O}^B(x_2) \rangle = \frac{(1 + \lambda A^{(1)} + \lambda^2 A^{(2)} + \dots)}{|x_{12}|^{2\Delta_1^{(0)}}}, \quad (2.24)$$

with

$$\begin{aligned} A^{(1)} &= a^{(1)} - 2\gamma^{(1)} \log \frac{|x_{12}|}{\epsilon}, \\ A^{(2)} &= a^{(2)} - 2a^{(1)}\gamma^{(1)} \log \frac{|x_{12}|}{\epsilon} + 2 \left(\gamma^{(1)} \log \frac{|x_{12}|}{\epsilon} \right)^2 - 2\gamma^{(2)} \log \frac{|x_{12}|}{\epsilon}. \end{aligned} \quad (2.25)$$

From the relation (2.21) and three-point functions of the renormalized operators (2.12), we can also determine the structure constants C_{123} of the un-renormalized operators at weak coupling. To simplify the expression, below we set $a^{(1)} = 0$ ². Then, using the expansion of the structure constant,

$$C_{123} = C_{123}^{(0)} \left(1 + \lambda c_{123}^{(1)} + \lambda^2 c_{123}^{(2)} + \dots \right), \quad (2.26)$$

one can write the result as

$$\langle \mathcal{O}_1^B(x_1) \mathcal{O}_2^B(x_2) \mathcal{O}_3^B(x_3) \rangle = \frac{C_{123}^{(0)} (1 + \lambda B^{(1)} + \lambda^2 B^{(2)} + \dots)}{|x_{12}|^{\Delta_1^{(0)} + \Delta_2^{(0)} - \Delta_3^{(0)}} |x_{23}|^{\Delta_2^{(0)} + \Delta_3^{(0)} - \Delta_1^{(0)}} |x_{31}|^{\Delta_3^{(0)} + \Delta_1^{(0)} - \Delta_2^{(0)}}}, \quad (2.27)$$

¹Here, we ignored the operator mixing. If there is an operator mixing, γ should be anomalous dimension matrix Γ defined by $\Gamma = -\frac{d \log Z}{d \log \epsilon}$ where $\mathcal{O}_i^R = Z_i^j \mathcal{O}_j^B$.

²In fact, when we calculate correlation functions up to two-loop order, such a case occurred in chapter 8, we will see the condition $a^{(1)} = 0$.

with

$$\begin{aligned}
B^{(1)} &= c_{123}^{(1)} - \sum_i \gamma_i^{(1)} \log u_i, \\
B^{(2)} &= c_{123}^{(2)} + \frac{1}{2} \sum_i a_i^{(2)} - \sum_i \left(\gamma_i^{(2)} + c_{123}^{(1)} \gamma_i^{(1)} \right) \log u_i + \frac{1}{2} \sum_{i,j} \gamma_i^{(1)} \gamma_j^{(1)} \log u_i \log u_j.
\end{aligned} \tag{2.28}$$

Here a_i and γ_i are the normalization and the anomalous dimension of the operator \mathcal{O}_i respectively and u_i is given by

$$u_i \equiv \left| \frac{x_{ij} x_{ki}}{x_{jk} \epsilon} \right| \tag{2.29}$$

where $\{i, j, k\}$ is a cyclic permutation of $\{1, 2, 3\}$.

Part II

Correlators of single trace operators

Chapter 3

BPS operators – perturbation

In this chapter, we discuss the correlation functions of the BPS operators up to one-loop by using the perturbative method.

The tree-level contribution is merely given by the Wick contraction. Actually, the two- and three-point functions of the BPS operators at tree-level surely have following contraction patterns:

$$\langle \mathcal{O}_1^{\text{BPS}(L)}(x_1) \mathcal{O}_2^{\text{BPS}(L)}(x_2) \rangle_{\text{tree}} : d_{12}^L, \quad (3.1)$$

$$\langle \mathcal{O}_1^{\text{BPS}(L_1)}(x_1) \mathcal{O}_2^{\text{BPS}(L_2)}(x_2) \mathcal{O}_3^{\text{BPS}(L_3)}(x_3) \rangle_{\text{tree}} : d_{12}^{\frac{L_{12}|3}} d_{23}^{\frac{L_{23}|1}} d_{31}^{\frac{L_{31}|2}}. \quad (3.2)$$

On the other hand, the four-point functions are non-trivial and have interesting structures. Because, even if the operator's lengths are minimum such as the length one, the four-point functions have following three contraction patterns:¹

$$\langle \mathcal{O}_1^{\text{BPS}(1)}(x_1) \mathcal{O}_2^{\text{BPS}(1)}(x_2) \mathcal{O}_3^{\text{BPS}(1)}(x_3) \mathcal{O}_4^{\text{BPS}(1)}(x_4) \rangle_{\text{tree}} : \begin{array}{l} d_{23}d_{41}, \quad d_{12}d_{34}, \\ d_{13}d_{24}. \end{array} \quad (3.3)$$

Furthermore, the contractions are corresponding to the diagrams in figure 3.1.

If the operator lengths become long, the four-point functions have a lot of contraction patterns. Thereby, a structure of the four-point functions seems complicated problem even though it is the tree-level computations. In section 3.1, we try to study the combinatorial problems of the four-point functions. After doing so, we calculate the one-loop corrections by dressing the tree-level diagrams in section 3.2.

3.1 Four-point functions at tree-level

Let us begin with the simplest operator set whose lengths are same and two: $L_1 = L_2 = L_3 = L_4 = 2$. Then, there are six contraction patterns as follows:

¹We now consider the length one operators. However, in practice, such an operator should vanish due to the trace of the gauge group indices, $\phi^a \text{Tr}[T^a] = 0$.

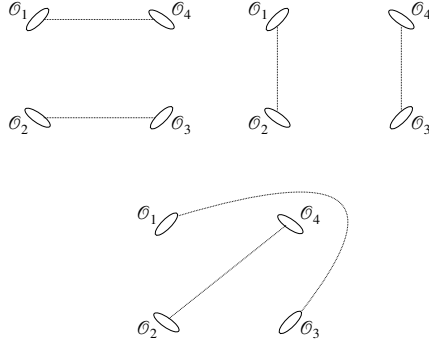
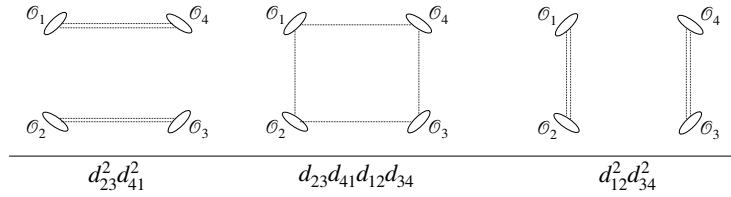


Figure 3.1: Four-point functions of the length one operators.

$$\begin{aligned}
 & d_{23}^2 d_{41}^2, & d_{34} d_{41} d_{12} d_{23}, & d_{12}^2 d_{34}^2, \\
 & d_{23} d_{41} d_{13} d_{24}, & d_{12} d_{34} d_{13} d_{24}, & \\
 & & d_{13}^2 d_{24}^2. &
 \end{aligned}$$

Notice that we now arranged the contractions in triangle. The arrangement shall be suggestive for the generalization and for one-loop computation. Then, we first focus on the contractions in the first line of the triangle:



Here, we would like to mention following two points:

1. There are no cross contractions, that is, d_{13} or d_{24} , in the first line. In other words, all contractions are parallel or vertical to the arrow being below the diagrams.
2. With following the directions of the arrow, the vertical contraction pairs, $d_{23} d_{41}$, vanish and the parallel contraction pairs, $d_{12} d_{34}$, are added.

The remains diagrams in the triangle, the second line and the third line, are depicted in figure 3.2

Then, we next mention the following properties:

3. The diagrams in n -th line have $n - 1$ pair cross contractions, $d_{13}^{n-1} d_{24}^{n-1}$. Namely, the diagrams in the second line have one-pair cross contraction, $d_{13} d_{24}$. On the other hand, the diagrams in the third line have two-pair cross contractions $d_{13}^2 d_{24}^2$

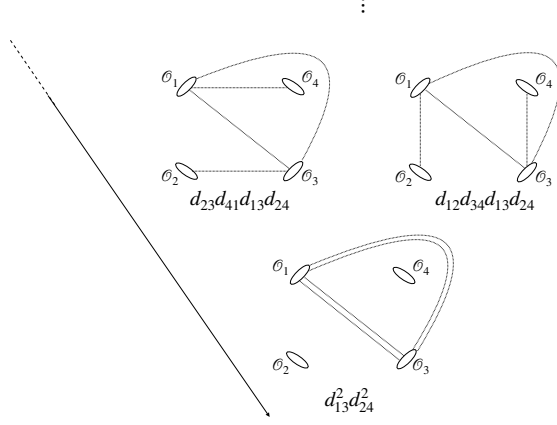


Figure 3.2: The most-below diagram has contraction $d_{13}^2d_{24}^2$, which comes the one pair cross contraction $d_{13}d_{24}$ times common factor between the $d_{23}d_{41}d_{13}d_{24}$ and $d_{12}d_{34}d_{13}d_{24}$.

4. a n -th diagram is given by the one-pair cross contraction times common contractions of two diagrams in $n + 1$ -th diagrams just above the n -th diagram.

With the lessons from 1.to 4., the contractions of the length-four operators are easily given by

$$\begin{aligned}
& d_{12}^3d_{34}^3, & d_{12}^2d_{34}^2d_{23}d_{41}, & d_{12}d_{34}d_{23}^2d_{41}^2, & d_{23}^3d_{41}^3, \\
& d_{12}^2d_{34}^2d_{13}d_{24}, & d_{12}d_{34}d_{23}d_{41}d_{13}d_{24}, & d_{23}^2d_{41}^2d_{13}d_{24}, \\
& d_{12}d_{34}d_{13}^2d_{24}^2, & d_{23}d_{41}d_{13}^2d_{24}^2, \\
& d_{13}^3d_{24}^3.
\end{aligned}$$

Here, we subtract the most combinations below $d_{13}^{\ell_{13}}d_{24}^{\ell_{24}}$ from the all diagrams and introduce the following notations²

$$\frac{d_{12}d_{34}}{d_{13}d_{24}} = \frac{\alpha\bar{\alpha}}{\chi\bar{\chi}} \equiv \bar{s} (= s^{-1}) \quad \text{and} \quad \frac{d_{23}d_{41}}{d_{13}d_{24}} = \frac{(1-\alpha)(1-\bar{\alpha})}{(1-\chi)(1-\bar{\chi})} \equiv \bar{t} (= t^{-1}). \quad (3.4)$$

Then, the contractions are simply written in terms of \bar{s}, \bar{t} down as:

$$\begin{aligned}
& \bar{s}^3, & \bar{s}^2\bar{t}, & s\bar{t}^2, & \bar{t}^3, \\
& \bar{s}^2, & \bar{s}\bar{t}, & \bar{t}^2, \\
& \bar{s}, & \bar{t}, \\
& 1.
\end{aligned}$$

In general, the four-point functions with any length operators will be following multiplet:

²The s and t are ordinary notations. On the other hand, we here used the inverse of them.

$$\begin{array}{ccccccc}
\bar{s}^n, & \bar{s}^{n-1}\bar{t}, & \dots & \bar{s}\bar{t}^{n-1}, & \bar{t}^n, & & \\
& \ddots & & & & \ddots & \\
& & \bar{s}, & & \bar{t}, & & \\
& & & & & & 1.
\end{array}$$

Here, we don't explain the details. Because the combination in the first line is the same as the tree-level four-point functions of operators inserted into Wilson line explained in section 7.1. Thereby, we devote to the section 7.1 for the more detail explanation of generalization.

3.2 Correlation functions at one-loop

We now discuss the one-loop correlation functions by using the perturbative method. A compact formula for n -point functions was suggested by Drukker and Plefka [39]. In particular, the one-loop four-point functions are suggested as

$$\langle \mathcal{O}_1^{\text{BPS}(L_1)} \mathcal{O}_2^{\text{BPS}(L_2)} \mathcal{O}_3^{\text{BPS}(L_3)} \mathcal{O}_4^{\text{BPS}(L_4)} \rangle_{\text{one-loop}} \quad (3.5)$$

$$\begin{aligned}
&= L_1 L_2 L_3 L_4 \left(D_{1234} \langle \mathcal{O}_1^{(L_1-1)} \mathcal{O}_2^{(L_2-1)} \mathcal{O}_3^{(L_3-1)} \mathcal{O}_4^{(L_4-1)} \rangle_{\text{tree, disc}} \right. \\
&\quad + D_{1324} \langle \mathcal{O}_1^{(L_1-1)} \mathcal{O}_3^{(L_3-1)} \mathcal{O}_2^{(L_2-1)} \mathcal{O}_4^{(L_4-1)} \rangle_{\text{tree, disc}} \\
&\quad \left. + D_{1243} \langle \mathcal{O}_1^{(L_1-1)} \mathcal{O}_2^{(L_2-1)} \mathcal{O}_4^{(L_4-1)} \mathcal{O}_3^{(L_3-1)} \rangle_{\text{tree, disc}} \right), \quad (3.6)
\end{aligned}$$

where

$$D_{1234} \equiv \frac{\lambda}{32\pi^2} \Phi(z, \bar{z}) (2d_{13}d_{24} - ((1-z) + (1-\bar{z}))d_{14}d_{23} - (z + \bar{z})d_{12}d_{34}). \quad (3.7)$$

The $\Phi(s, t)$ is a one-loop conformal integral and the explicit form is shown in appendix A. The correlator $\langle \dots \rangle_{\text{tree, disc}}$ is the tree-level four-point functions of the four operators at the boundary of the disc.

Referring the previous paper [39], we introduce the one-loop insertion formulas and calculate the one-loop dressed diagrams from the tree-level result. Eventually, we shall see that the compact formula (3.6) is reproduced.

3.2.1 One-loop insertion formula

Let us begin with introducing the fundamental materials at one-loop in $\mathcal{N} = 4$ SYM. Using the Lagrangian, self-energy, scalar quartic interaction and gluon exchange are given by

$$\begin{aligned}
 \text{self}_{12} : & \quad Y_1 \cdot \phi(x_1) \text{---} \text{---} \text{---} Y_2 \cdot \phi(x_2) \quad = \quad -\lambda(Y_1 \cdot Y_2) I_{12} \frac{Y_{112} + Y_{122}}{I_{12}}, \\
 G_{1234} : & \quad \begin{array}{ccc} Y_1 \cdot \phi(x_1) \text{---} & & Y_2 \cdot \phi(x_2) \\ & \text{---} & \\ Y_3 \cdot \phi(x_3) \text{---} & & Y_4 \cdot \phi(x_4) \end{array} \quad = \quad \lambda(Y_1 \cdot Y_2)(Y_3 \cdot Y_4) I_{12} I_{34} F_{12,34}, \\
 S_{1234} : & \quad \begin{array}{ccc} Y_1 \cdot \phi(x_1) & & Y_2 \cdot \phi(x_2) \\ & \diagdown & / \\ & & \\ & / & \diagdown \\ Y_3 \cdot \phi(x_3) & & Y_4 \cdot \phi(x_4) \end{array} \quad = \quad \lambda [2(Y_2 \cdot Y_3)(Y_1 \cdot Y_4) - (Y_2 \cdot Y_4)(Y_1 \cdot Y_3) - (Y_1 \cdot Y_2)(Y_3 \cdot Y_4)] X_{1234},
 \end{aligned} \tag{3.8}$$

where $I_{12}, Y_{123}, F_{12,34}$ and X_{1234} are usual functions to present the one-loop diagrams. We summarized the details in appendix A.

By combing above three fundamental materials, we calculate the two- and three-point functions as a preliminary. In addition, we make the D_{1234} functions (3.7), which constructs the four-point functions.

(i) Two-point functions

We first calculate the two-point functions with operator's length L at one-loop. They have L self-energy, quartic scalar interaction and gluon exchanges. Then, their contributions are canceled out and the two-point functions vanish:

$$\begin{aligned}
 \langle \mathcal{O}_1^{\text{BPS}(2)}(x_1) \mathcal{O}_2^{\text{BPS}(2)}(x_2) \rangle_{\text{one-loop}} &= (2\text{self}_{12} + S_{1212} + G_{1212}) d_{12}^L \\
 &= 0.
 \end{aligned} \tag{3.9}$$

The result implies the BPS property. Namely there are no quantum corrections of spectrum due to the supersymmetry.

(ii) Corner interactions and three-point functions

It is useful to combine the one-half of the self-energy and three-body interactions, and such diagram appears at a corner of the diagrams:

$$\begin{aligned}
 & \begin{array}{ccc} & & Y_3 \cdot \phi(x_3) \\ & \diagdown & / \\ Y_2 \cdot \phi(x_2) & \text{---} & \\ & / & \diagdown \\ & & Y_1 \cdot \phi(x_1) \end{array} \quad \equiv \quad \frac{1}{2} \left[\begin{array}{ccc} & & \\ & \diagdown & / \\ & \text{---} & \\ & / & \diagdown \\ & & \end{array} + \begin{array}{ccc} & & \\ & \text{---} & \\ & & \end{array} \right] + \begin{array}{ccc} & & \\ & \text{---} & \\ & & \end{array} + \begin{array}{ccc} & & \\ & \text{---} & \\ & & \end{array} \quad \equiv \quad \text{CI}_{123} d_{12} d_{23}, \tag{3.10}
 \end{aligned}$$

where the corner interaction CI_{123} is given by

$$\text{CI}_{123} = \lambda Y_{123} \left(\frac{1}{I_{12}} + \frac{1}{I_{23}} - \frac{2}{I_{31}} \right). \tag{3.11}$$

Using the function (3.10), one can show that the one-loop three-point functions also vanish:

$$\begin{aligned}
\langle \mathcal{O}_1^{\text{BPS}(2)}(x_1) \mathcal{O}_2^{\text{BPS}(2)}(x_2) \mathcal{O}_3^{\text{BPS}(2)}(x_3) \rangle_{\text{one-loop}} &= \text{triangle diagram} \Big|_{\text{one-loop dressed}} \\
&= 2^3 (\text{CI}_{123} + \text{CI}_{231} + \text{CI}_{312}) d_{12} d_{23} d_{31} = 0.
\end{aligned} \tag{3.12}$$

Therefore, the one-loop structure constants are also zero.

(iii) D -function

In order to construct the D_{1234} -functions, we start with the four-body interactions:

$$\begin{aligned}
&\text{cross diagram} + \text{wavy line diagram} + \text{zigzag line diagram} = \text{S}_{1234} + \text{G}_{1234} + \text{G}_{1324}.
\end{aligned} \tag{3.13}$$

Here, the $F_{12,43}$ function in the G_{1234} diagram can be written as

$$\lambda F_{12,43} d_{12} d_{34} = \left[\lambda \frac{X_{1234}}{I_{13} I_{24}} (t-1) + \text{CI}_{12,43} \right] d_{12} d_{34}, \tag{3.14}$$

where $\text{CI}_{12,43}$ function is related as the corner interaction CI_{ijk} by

$$\text{CI}_{12,43} = -\frac{1}{3} (\text{CI}_{123} + \text{CI}_{412} + \text{CI}_{341} + \text{CI}_{234} - \text{CI}_{124} - \text{CI}_{243} - \text{CI}_{431} - \text{CI}_{312}). \tag{3.15}$$

Thus, subtracting the corner interactions, we obtain the D_{1234} -function as follows:

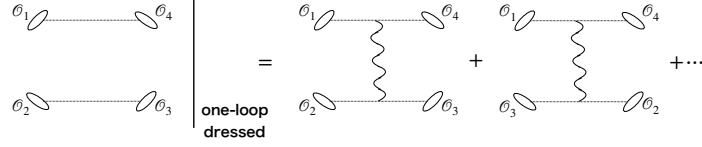
$$\begin{aligned}
D_{1234} &= \text{S}_{1234} + \text{G}_{1234} + \text{G}_{1324} - \text{CI}_{12,43} d_{12} d_{34} - \text{CI}_{14,23} d_{14} d_{23} \\
&= \lambda \frac{X_{1234}}{I_{13} I_{24}} (2d_{13} d_{24} + (s-1-t) d_{14} d_{23} + (t-1-s) d_{12} d_{34}) \\
&= \frac{\lambda}{16\pi^2} \Phi(s, t) (2d_{13} d_{24} + (s-1-t) d_{14} d_{23} + (t-1-s) d_{12} d_{34}).
\end{aligned} \tag{3.16}$$

The function is manifestly cyclic-symmetric as well as the reflection symmetry $2 \leftrightarrow 4$ and $s \leftrightarrow t$.

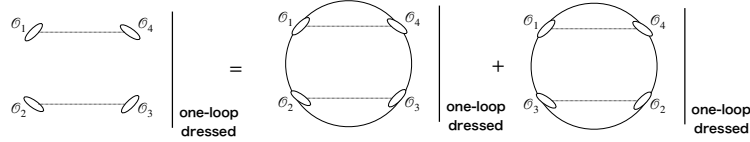
3.2.2 Four-point functions

Let us calculate the four-point functions at one-loop and reproduce the suggestion (3.6). Key point in the calculation is how to remove the corner interactions $\text{CI}_{ij,kl}$ and get only the D_{1234} functions.

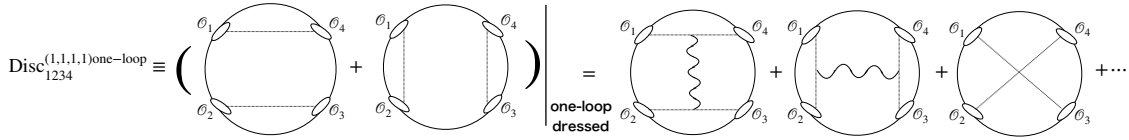
Let us begin with the simplest correlator with length one operators. The tree-level contributions were given by (3.3). Using the one-loop insertion formulas, we dress the tree-level diagrams, and then we shall get the one-loop four-point functions. However, when we use the one-loop dressed diagrams from tree-level contractions, we must be careful of the ordering of the operators. For example, the one-loop dressed diagrams of the tree-level contraction $d_{23}d_{41}$ are



Then, the ordering of between the operators \mathcal{O}_2 and \mathcal{O}_3 in diagrams is irrelevant at tree-level. However, we must distinguish them at one-loop level. In order to avoid such difficulty, we fix the operators at the boundary on the disc:



Thus, we define a tree-level disc four-point function $\text{Disc}_{1234}^{(1,1,1,1)\text{one-loop}}$ whose length one operators are arranged in the order of $\mathcal{O}_1\mathcal{O}_2\mathcal{O}_3\mathcal{O}_4$ on the disc:



Then, other one-loop dressed diagrams are given only by the replacement of the operators. Therefore, the one-loop four-point function is given by

$$\text{Disc}_{1234}^{(1,1,1,1)\text{one-loop}} + \text{Disc}_{1324}^{(1,1,1,1)\text{one-loop}} + \text{Disc}_{4231}^{(1,1,1,1)\text{one-loop}} \quad (3.17)$$

Each term comes from the one-loop diagrams of the tree-level contraction $(d_{23}d_{41} + d_{12}d_{34})$, $(d_{23}d_{41} + d_{13}d_{24})$ and $(d_{23}d_{41} + d_{12}d_{34})$ respectively, see also in figure 3.3. We find that each edge of the triangle in the tree-level contractions corresponds to each disc one-loop four-point function.

We next consider the length two operators. In the same way as the length one case, we first divide the diagrams into three parts corresponding to the three edges of the triangle at tree-level. Then, the one-loop four-point functions are given by

$$\text{Disc}_{1234}^{(2,2,2,2)\text{one-loop}} + \text{Disc}_{1324}^{(2,2,2,2)\text{one-loop}} + \text{Disc}_{4231}^{(2,2,2,2)\text{one-loop}}, \quad (3.18)$$

where the function $\text{Disc}_{1234}^{(2,2,2,2)\text{one-loop}}$ is defined as

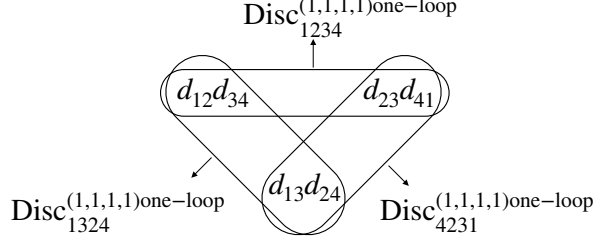
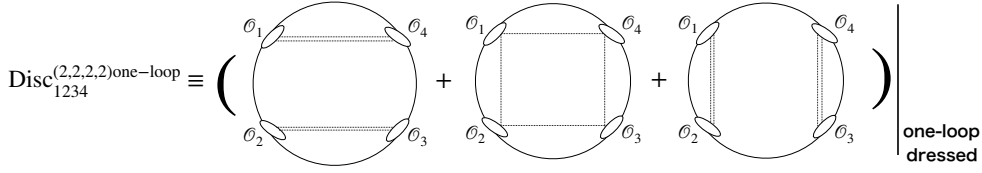


Figure 3.3: The tree-level contractions and one-loop diagrams in the disc. The $\text{Disc}_{ijkl}^{(1,1,1,1)\text{one-loop}}$ comes from the tree-level contraction of the operators arranged in the order of $\mathcal{O}_i\mathcal{O}_j\mathcal{O}_k\mathcal{O}_l$ on the disc.



From here, we discuss how to kill the corner interactions and how to produce the D_{1234} functions.

Let us see the details of the function $\text{Disc}_{1234}^{(2,2,2,2)\text{one-loop}}$. The function includes the following one-loop diagrams, see also in figure 3.4

$$\begin{aligned} \text{Disc}_{1234}^{(2,2,2,2)\text{one-loop}} &= (\text{S}_{1234} + \text{G}_{1234} + \text{G}_{1324}) (d_{12}d_{34} + d_{23}d_{41}) \\ &\quad + (\text{CI}_{123} + \text{CI}_{234} + \text{CI}_{341} + \text{CI}_{412})(d_{12}d_{23}d_{34}d_{41}). \end{aligned} \quad (3.19)$$

Here, we used the property (3.9). Using the definition of the D_{1234} -function (3.16), the disc four-point function become

$$\begin{aligned} \text{Disc}_{1234}^{(2,2,2,2)\text{one-loop}} &= D_{1234}(d_{12}d_{34} + d_{23}d_{41}) \\ &\quad + \text{CI}_{12,43}d_{12}^2d_{34}^2 + \text{CI}_{14,23}d_{14}^2d_{23}^2. \end{aligned} \quad (3.20)$$

It is because the corner interactions are canceled with a part of the $\text{CI}_{ij,kl}$ function in the D_{1234} function as³

$$\text{CI}_{12,43} + \text{CI}_{13,24} + \text{CI}_{123} + \text{CI}_{234} + \text{CI}_{341} + \text{CI}_{412} = 0. \quad (3.21)$$

Although the corner interactions were not completely canceled out, the remained corner interactions, $\text{CI}_{12,43}d_{12}^2d_{34}^2 + \text{CI}_{14,23}d_{14}^2d_{23}^2$, can be canceled with the corner interactions in the other disc four-point functions $\text{Disc}_{1324}^{(2,2,2,2)\text{one-loop}}$ and $\text{Disc}_{4231}^{(2,2,2,2)\text{one-loop}}$ functions. Therefore, the one-loop four-point functions are given by

$$\begin{aligned} &\text{Disc}_{1234}^{(2,2,2,2)\text{one-loop}} + \text{Disc}_{1324}^{(2,2,2,2)\text{one-loop}} + \text{Disc}_{4231}^{(2,2,2,2)\text{one-loop}} \\ &= D_{1234}(d_{12}d_{34} + d_{23}d_{41}) + D_{1324}(d_{13}d_{24} + d_{23}d_{41}) + D_{4231}(d_{42}d_{31} + d_{23}d_{41}). \end{aligned} \quad (3.22)$$

³When we prove the cancelation (3.21), we use the property $\text{CI}_{123} + \text{CI}_{231} + \text{CI}_{312} = 0$

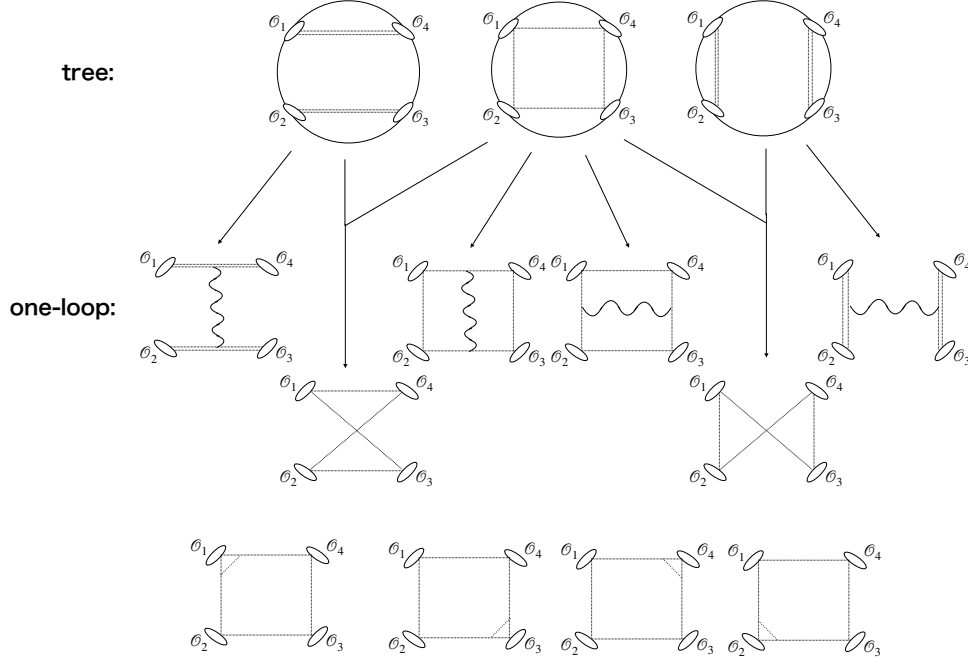


Figure 3.4: One-loop diagrams of the $\text{Disc}_{1234}^{(2,2,2,2)\text{one-loop}}$. It has six four-body diagrams and four corner interactions diagrams.

As expected, the result is represented by only the D_{1234} functions. Furthermore, the pre-factors of the D_{1234} functions are just tree-level disc four-point functions of the length one operators. Therefore, we finally have

$$\begin{aligned}
\langle \mathcal{O}_1^{\text{BPS}(2)} \mathcal{O}_2^{\text{BPS}(2)} \mathcal{O}_3^{\text{BPS}(2)} \mathcal{O}_4^{\text{BPS}(2)} \rangle_{\text{one-loop}} &= 2^4 \left(D_{1234} \langle \mathcal{O}_1^{(1)} \mathcal{O}_2^{(1)} \mathcal{O}_3^{(1)} \mathcal{O}_4^{(1)} \rangle_{\text{tree, disc}} \right. \\
&\quad + D_{1324} \langle \mathcal{O}_1^{(1)} \mathcal{O}_3^{(1)} \mathcal{O}_2^{(1)} \mathcal{O}_4^{(1)} \rangle_{\text{tree, disc}} \\
&\quad \left. + D_{4231} \langle \mathcal{O}_4^{(1)} \mathcal{O}_2^{(1)} \mathcal{O}_3^{(1)} \mathcal{O}_1^{(1)} \rangle_{\text{tree, disc}} \right). \quad (3.23)
\end{aligned}$$

In particular, the four-point functions of the length two BPS operators are written as

$$\langle \mathcal{O}_1^{\text{BPS}(2)} \mathcal{O}_2^{\text{BPS}(2)} \mathcal{O}_3^{\text{BPS}(2)} \mathcal{O}_4^{\text{BPS}(2)} \rangle_{\text{one-loop}} = -\frac{\lambda}{\pi^2} \Phi(s, t) \mathcal{R}_{\mathcal{N}=4}, \quad (3.24)$$

where the pre-factor $\mathcal{R}_{\mathcal{N}=4}$ is known as a universal refactor [40, 41] given by

$$\mathcal{R}_{\mathcal{N}=4} = (z(d_{12}d_{34} - d_{23}d_{41} + d_{41}d_{23} - d_{13}d_{24})) (\bar{z}(d_{12}d_{34} - d_{23}d_{41} + d_{41}d_{23} - d_{13}d_{24})) \quad (3.25)$$

The above discussions can be easily generalized for the general four-point functions. Namely, even though the operator lengths are general, the all corner interactions are canceled out and the remaining functions are only the D_{ijkl} function. In addition, the

pre-factors become the tree-level disc four-point functions of the operator length $L_1 - 1, L_2 - 1, L_3 - 1, L_4 - 1$.

Here, it is instructive to consider the length-three operators. The tree-level contribution is surely written by the triangle in section 3.1. In the same way as the length-two operators, we make the one-loop dressed diagrams from the three edges of the triangle in tree-level combinatorics. Then, the D_{1234} functions are produced and the all corner interactions are canceled out. As a result, the four-point function is given by

$$\begin{aligned} & \text{Disc}_{1234}^{(3,3,3,3)\text{one-loop}} + \text{Disc}_{1324}^{(3,3,3,3)\text{one-loop}} + \text{Disc}_{4231}^{(3,3,3,3)\text{one-loop}} \\ &= D_{1234} \langle \mathcal{O}_1^{(2)} \mathcal{O}_2^{(2)} \mathcal{O}_3^{(2)} \mathcal{O}_4^{(2)} \rangle_{\text{tree, disc}} + D_{1324} \langle \mathcal{O}_1^{(2)} \mathcal{O}_3^{(2)} \mathcal{O}_2^{(2)} \mathcal{O}_4^{(2)} \rangle_{\text{tree, disc}} \\ &+ D_{4231} \langle \mathcal{O}_4^{(2)} \mathcal{O}_2^{(2)} \mathcal{O}_3^{(2)} \mathcal{O}_1^{(2)} \rangle_{\text{tree, disc}}. \end{aligned}$$

Although the diagrams corresponding to the edges of triangle are relevant, the interior of the triangle should vanish in order to produce the correct answer. So as to check this, we now focus on the one-loop dressed diagram in the interior of the triangle, $d_{12}d_{34}d_{23}d_{41}d_{13}d_{24}$. The diagram is given by

$$\left[\text{Diagram of a triangle with vertices } \phi_1, \phi_2, \phi_3, \phi_4 \text{ and internal lines } d_{12}, d_{34}, d_{23}, d_{41}, d_{13}, d_{24} \right] \Big|_{\text{one-loop dressed}} = \sum_{\{i,j,k\}} (\text{CI}_{ijk} + \text{CI}_{jki} + \text{CI}_{kij}) \times \left[\text{Diagram of a triangle with vertices } \phi_1, \phi_2, \phi_3, \phi_4 \text{ and internal lines } d_{12}, d_{34}, d_{23}, d_{41}, d_{13}, d_{24} \right] = 0$$

where $(\{1, 2, 4\}, \{2, 3, 4\}, \{1, 3, 4\}, \{1, 2, 3\}) \in \{i, j, k\}$. This imply that the all diagrams in the interior of the triangle are given by the summation of the three-point functions. Thereby, these contribution become zero.

Overall, we get the general four-point functions as follows:

$$\begin{aligned} \langle \mathcal{O}_1^{\text{BPS}(L_1)} \mathcal{O}_2^{\text{BPS}(L_2)} \mathcal{O}_3^{\text{BPS}(L_3)} \mathcal{O}_4^{\text{BPS}(L_4)} \rangle_{\text{one-loop}} &= L_1 L_2 L_3 L_4 \left(D_{1234} \langle \mathcal{O}_1^{(L_1-1)} \mathcal{O}_2^{(L_2-1)} \mathcal{O}_3^{(L_3-1)} \mathcal{O}_4^{(L_4-1)} \rangle_{\text{tree, disc}} \right. \\ &+ D_{1324} \langle \mathcal{O}_1^{(L_1-1)} \mathcal{O}_3^{(L_2-1)} \mathcal{O}_2^{(L_3-1)} \mathcal{O}_4^{(L_4-1)} \rangle_{\text{tree, disc}} \\ &\left. + D_{4231} \langle \mathcal{O}_4^{(L_1-1)} \mathcal{O}_2^{(L_2-1)} \mathcal{O}_3^{(L_3-1)} \mathcal{O}_1^{(L_4-1)} \rangle_{\text{tree, disc}} \right). \end{aligned} \quad (3.26)$$

The result is just the same as the suggestion by the Drukker and Plefka (3.6).

Chapter 4

Non-BPS operators – perturbation and integrability

In this chapter, we discuss the correlation functions with a non-BPS operator. In section 4.1, we first consider the two-point functions at one-loop. For the case of non-BPS operator, the operator has nontrivial anomalous dimensions due to operator mixings. Namely, if there are no operator mixing, the all one-loop diagrams of two-point function vanish such as (3.9). On the other hand, if the operators include impurity, the scalar quartic interaction S_{1234} exchange the position of the impurity. Such mixing has tensor structure and the diagrams of two-point functions of operators with impurity are not canceled out. As a result, the two-point functions produce anomalous dimensions. Then, to diagonalize such tensor structure and calculate one-loop anomalous dimensions, we use an integrability technique which is so-called *spin chain system*. The study is just the first discovery of the relation between the integrability and $\mathcal{N} = 4$ SYM. In section 4.1, we briefly explain the relation, following the paper [6].

We next consider the three-point functions at tree-level in section 4.2. Then, we use the one-loop spin chain system. Even if it is the tree-level computation, we should rely on the integrability technique in order to efficiently count the contractions. It is because a large number of operators have the identical conformal dimensions, and the degeneracy will be lifted by the one-loop corrections. Therefore, we need to use the one-loop eigenstate, which correspond to the one-loop spin chain state, in the same way as the standard degenerated perturbation theory in quantum mechanics. Such technique to efficiently compute the tree-level structure constants is called *tailoring method* and suggested by previous papers [42–45]. The section 4.2 is devoted to give the incentive lessons for finite coupling method explained in next chapter 5.

4.1 Two-point functions at one-loop

In this section, we discuss the two-point functions of non-BPS operators which is in $SU(2)$ sub-sector at one-loop.

4.1.1 The anomalous dimension matrix and XXX spin chain Hamiltonian

Let us start with a special class of the single-trace operators which consist only of a scalar fields as follows:

$$\mathcal{O}_{i_1 i_2, \dots} = \text{tr}[\phi_{i_1} \phi_{i_2} \cdots], \quad (4.1)$$

which is the so-called $SO(6)$ sector. Notice that we do not impose the symmetric and null property. The tree-level two-point functions of the operator is easily given by

$$\langle \mathcal{O}_{i_1 i_2, \dots}(x_1) \mathcal{O}^{j_1 j_2, \dots}(x_2) \rangle_{\text{tree}} = \frac{\lambda^L}{(8\pi^2)^L} \frac{1}{|x_{12}|^{2L}} \delta_{i_1}^{j_1} \delta_{i_2}^{j_2} \cdots. \quad (4.2)$$

At one-loop level, the operators receive the quantum correction as the anomalous dimension γ , $\Delta = L + \gamma$. To determine the one-loop anomalous dimension, we calculate the one-loop Feynman diagrams in the similar way as correlators of the BPS operator 3.8. However, we must be careful of the $SO(6)$ indices. The only scalar quartic interaction has non-trivial tensor structure of the $SO(6)$ indices. The interaction comes from the commutator square term

$$[\phi_i, \phi_j]^2 = 2\phi_i \phi_j \phi_i \phi_j - 2\phi_i \phi_i \phi_j \phi_j \quad (4.3)$$

in the action of $\mathcal{N} = 4$ SYM. Therefore we have the following contribution:

$$\frac{\lambda}{16\pi^2} \left(2\delta_{I_\ell}^{J_{\ell+1}} \delta_{I_{\ell+1}}^{J_\ell} - \delta_{I_\ell}^{J_\ell} \delta_{I_{\ell+1}}^{J_{\ell+1}} - \delta_{I_\ell I_{\ell+1}} \delta^{J_\ell J_{\ell+1}} \right). \quad (4.4)$$

Since the others have trivial tensor structures, we use the previous results in 3.8.

$$\begin{aligned} \begin{array}{c} I_\ell \text{ --- } \bullet \text{ --- } J_\ell \\ I_{\ell+1} \text{ --- } J_{\ell+1} \end{array} &= -\frac{\lambda}{16\pi^2} 2\delta_{I_\ell}^{J_\ell} \delta_{I_{\ell+1}}^{J_{\ell+1}}, \\ \begin{array}{c} I_\ell \text{ --- } J_\ell \\ I_{\ell+1} \text{ --- } J_{\ell+1} \\ \text{---} \text{ } \text{---} \\ \text{---} \text{ } \text{---} \end{array} &= \frac{\lambda}{16\pi^2} \delta_{I_\ell}^{J_\ell} \delta_{I_{\ell+1}}^{J_{\ell+1}}. \end{aligned}$$

Adding all one-loop corrections, we therefore have

$$\begin{aligned} \langle \mathcal{O}_{i_1 i_2, \dots}(x_1) \mathcal{O}^{j_1 j_2, \dots}(x_2) \rangle &= \frac{1}{|x_{12}|^{2L}} (1 - 2\Gamma \log(\Lambda|x_{12}|)) \delta_{i_1}^{j_1} \delta_{i_2}^{j_2} \cdots, \\ \Gamma &= \frac{\lambda}{16\pi^2} \sum_n (-2\mathbf{P}_{n,n+1} + 2\mathbf{I}_{n,n+1} + \mathbf{K}_{n,n+1}), \end{aligned} \quad (4.5)$$

where $\mathbf{P}_{n,n+1}$, $\mathbf{I}_{n,n+1}$ and $\mathbf{K}_{n,n+1}$ act on the $SO(6)$ indices defined as

$$\begin{aligned} \mathbf{I}_{n,n+1} | \cdots, i, j, \cdots \rangle &= | \cdots, i, j, \cdots \rangle, \\ \mathbf{P}_{n,n+1} | \cdots, i, j, \cdots \rangle &= | \cdots, j, i, \cdots \rangle, \\ \mathbf{K}_{n,n+1} | \cdots, i, j, \cdots \rangle &= \delta_{ij} \sum_{k=1}^6 | \cdots, k, k, \cdots \rangle. \end{aligned}$$

Notice that if the state is the BPS, which satisfy the symmetric and null condition, we can check that such anomalous dimension becomes zero due to

$$(-\mathbf{P}_{n,n+1} + \mathbf{I}_{n,n+1})|\text{BPS}\rangle = (-\mathbf{I}_{n,n+1} + \mathbf{I}_{n,n+1})|\text{BPS}\rangle = 0, \quad \mathbf{K}_{n,n+1}|\text{BPS}\rangle = 0. \quad (4.6)$$

Here, we make a two complex scalars of four real scalars. For example, we define as

$$Z = \phi_1 + i\phi_2, \quad Y = \phi_3 + i\phi_4. \quad (4.7)$$

Furthermore, we consider the operators of $SU(2)$ sub-sector,

$$\mathcal{O} = \text{tr}[\dots Z \dots Y \dots]. \quad (4.8)$$

Then, we can identify the anomalous dimension matrix with the Hamiltonian of the XXX Heisenberg spin chain:

$$\Gamma \rightarrow H_{XXX} = \frac{\lambda}{16\pi^2} \sum_n (-2\mathbf{P}_{n,n+1} + 2\mathbf{I}_{n,n+1}). \quad (4.9)$$

Namely, we define that the all Z operator, which is the BPS operator is a spin chain vacuum state denoted uparrow \uparrow . On the other hand, the Y scalars inserted in BPS operator are corresponding to the excitation on the vacuum called *magnon*, which is denoted downarrow \downarrow . Namely, the single trace operators are mapped to the spin chain states are as follows:

$$\text{tr}[Z \dots Z] \longleftrightarrow |\uparrow \dots \uparrow\rangle, \quad (4.10)$$

$$\text{tr}[\dots Z Y Z \dots] \longleftrightarrow |\dots \uparrow \downarrow \uparrow \dots\rangle. \quad (4.11)$$

4.1.2 Anomalous dimensions and coordinate Bethe ansatz

In what follows, we explain the details of the spin chain states in coordinate Bethe ansatz. By using the coordinate Bethe ansatz, we can capture the physical intuition from the movement of the magnons, rather than the algebraic Bethe ansatz.

One-magnon state

We first start with the one-magnon state corresponding to the operator inserted one X scalar, which is the one spin flipping state as follows:

$$\text{tr}[\dots Z Y Z \dots] \longleftrightarrow |\dots \uparrow \downarrow \uparrow \dots\rangle.$$

Acting the Hamiltonian on the spin chain state, we have

$$H_{XXX}|\dots \uparrow \downarrow \uparrow \dots\rangle = \frac{\lambda}{8\pi^2} \left((L - (L - 2))|\dots \uparrow \downarrow \uparrow \dots\rangle - |\dots \downarrow \uparrow \uparrow \dots\rangle - |\dots \uparrow \uparrow \downarrow \dots\rangle \right), \quad (4.12)$$

where L denoted the length of the spin chain. Here, we assume a eigenstate which is so-called Bethe ansatz state as follows:

$$|p\rangle \equiv \sum_{x=1}^L e^{ipx} |\dots \uparrow \downarrow \uparrow \dots\rangle_x, \quad (4.13)$$

where p was the momentum of the magnon. Then, the magnon will satisfy the periodic boundary condition: $e^{ipL} = 1$, which is often called Bethe ansatz equation¹. Using the Bethe ansatz state, the Hamiltonian is diagonalized and the eigenvalue is given by

$$H_{XXX}|p\rangle = \epsilon(p)|p\rangle, \quad \epsilon(p) = \frac{\lambda}{2\pi^2} \sin^2 \frac{p}{2}. \quad (4.14)$$

Two-magnon state

We next consider the two-magnon state, which has the two down spins. The Bethe ansatz state have two terms for the ordering of the magnons as follows:

$$|p_1, p_2\rangle \equiv \sum_{x_1 < x_2}^L e^{ip_1 x_1 + ip_2 x_2} |\dots \uparrow \downarrow \uparrow \dots \uparrow \downarrow \uparrow \dots\rangle_{x_1, x_2} + S(p_2, p_1) \sum_{x_1 < x_2}^L e^{ip_2 x_1 + ip_1 x_2} |\dots \uparrow \downarrow \uparrow \dots \uparrow \downarrow \uparrow \dots\rangle_{x_1, x_2}. \quad (4.15)$$

where $S(p_2, p_1)$ is a factor of magnon scattering. In addition, the magnons will satisfy the following Bethe ansatz equation:

$$e^{ip_1 L} S(p_2, p_1) = 1. \quad (4.16)$$

There is the S-matrix factor since the magnons are scattered when the magnon of the momentum p_1 go around on the spin chain.

Then, we act the Hamiltonian on the Bethe ansatz state. If each magnon is not lived in the site next to the other magnon: $x_2 > x_1 + 1$, we have

$$H_{XXX}|p_1, p_2\rangle = 4|p_1, p_2\rangle - |p_1 - 1, p_2\rangle - |p_1 + 1, p_2\rangle - |p_1, p_2 - 1\rangle - |p_1, p_2 + 1\rangle. \quad (4.17)$$

On the other case: $x_2 = x_1 + 1$, we have

$$H_{XXX}|p_1, p_2\rangle = 2|p_1, p_2\rangle - |p_1 - 1, p_2\rangle - |p_1, p_2 + 1\rangle. \quad (4.18)$$

Solving these equations (4.17) and (4.18), the energy eigenvalue and S-matrix factor are given by

$$\begin{aligned} \epsilon(p_1, p_2) &= \frac{\lambda}{2\pi^2} \left(\sin^2 \frac{p_1}{2} + \sin^2 \frac{p_2}{2} \right) \\ &= \epsilon(p_1) + \epsilon(p_2) \end{aligned} \quad (4.19)$$

and

$$S(p_2, p_1) = - \frac{e^{i(p_1+p_2)} - 2e^{ip_2} + 1}{e^{i(p_1+p_2)} - 2e^{ip_1} + 1}. \quad (4.20)$$

¹The one magnon state have the momentum p . However, due to the trace of the single trace operator, the spin chain state is imposed the zero-momentum condition. Thereby, the only solution is $p = 0$ in the case. It means that the one-magnon state cannot practically exist.

Multi-magnon state

Finally, we consider the general spin chain system with M -magnon. The Bethe ansatz state is given by

$$|p_1, \dots, p_M\rangle = \sum_{1 \leq x_1 < \dots < x_M \leq L} \Psi^A(x_1, \dots, x_M) |\dots \downarrow \dots \downarrow \dots \downarrow\rangle, \quad (4.21)$$

where the wave function $\Psi^A(x_1, \dots, x_M)$ is

$$\Psi^A(x_1, \dots, x_M) = \sum_{\sigma \in P_M} A(\sigma) \prod_{j=1}^M e^{iP_{\sigma_j} x_j}. \quad (4.22)$$

The σ is a set of the momentums $\{\dots, p_i, \dots, p_j, \dots\}$ and $\sum_{\sigma \in P_M}$ means the sum over permutations. In addition, the pre-factor $A(\sigma)$ satisfied the following relation:

$$\frac{A(\dots, p_j, p_i, \dots)}{A(\dots, p_i, p_j, \dots)} = S(p_j, p_i). \quad (4.23)$$

For instance, if the number of magnon is three, $\sum_{\sigma \in P_3} A(\sigma)$ means the sum over the following terms

$$A(p_1, p_2, p_3), A(p_1, p_3, p_2), A(p_2, p_1, p_3), A(p_2, p_3, p_1), A(p_3, p_1, p_2), A(p_3, p_2, p_1). \quad (4.24)$$

Furthermore, by dividing the factor $A(p_1, p_2, p_3)$, each terms become

$$\begin{aligned} \frac{A(p_1, p_3, p_2)}{A(p_1, p_2, p_3)} &= S(p_3, p_2), \quad \frac{A(p_2, p_1, p_3)}{A(p_1, p_2, p_3)} = S(p_2, p_1), \quad \frac{A(p_3, p_2, p_1)}{A(p_1, p_2, p_3)} = S(p_3, p_1), \\ \frac{A(p_2, p_3, p_1)}{A(p_1, p_2, p_3)} &= \frac{A(p_2, p_3, p_1)}{A(p_2, p_1, p_3)} \frac{A(p_2, p_1, p_3)}{A(p_1, p_2, p_3)} = S(p_3, p_1) S(p_2, p_1), \\ \frac{A(p_3, p_1, p_2)}{A(p_1, p_2, p_3)} &= \frac{A(p_3, p_1, p_2)}{A(p_1, p_3, p_2)} \frac{A(p_1, p_3, p_2)}{A(p_1, p_2, p_3)} = S(p_3, p_1) S(p_3, p_2). \end{aligned}$$

Therefore, the wave function $\Psi(x_1, \dots, x_M)$ can also be written as

$$\Psi(x_1, \dots, x_M) = \sum_{\sigma \in P_M} \prod_{\substack{j < k \\ \sigma_k > \sigma_j}} S(p_{\sigma_k}, p_{\sigma_j}) \prod_{j=1}^M e^{iP_{\sigma_j} x_j}. \quad (4.25)$$

In addition, the Bethe ansatz equation is given by

$$e^{ip_k L} \prod_{\ell \neq k} S(p_\ell, p_k) = 1. \quad (4.26)$$

Here, in order to write more simply, we introduce the rapidity u which is defined by

$$u := \frac{1}{2} \cot \frac{p}{2}, \quad e^{ip} = \frac{u + \frac{i}{2}}{u - \frac{i}{2}}. \quad (4.27)$$

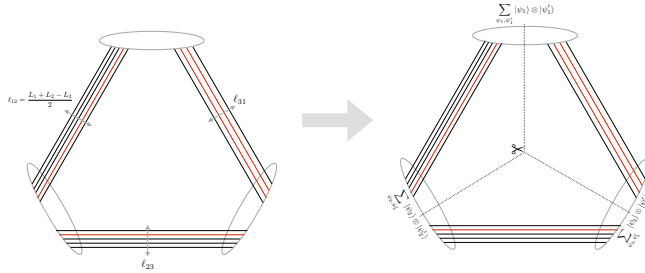


Figure 4.1: Tailoring method: the three-point functions have three bridge edges. We cut the three spin chains, and then we get three “two-point functions” with each bridge length.

Using the rapidity expression, the notations of the spin chain system become more simple. For example, the S-matrix factor and Bethe ansatz equation are written as

$$S(u_k, u_\ell) = \frac{u_k - u_\ell + i}{u_k - u_\ell - i}, \quad \left(\frac{u + \frac{i}{2}}{u - \frac{i}{2}} \right)^L \prod_{\ell \neq k}^M \frac{u_k - u_\ell + i}{u_k - u_\ell - i}. \quad (4.28)$$

Furthermore, the energy eigenvalue is also simplified as

$$\begin{aligned} E &= \sum_{k=1}^M \epsilon(u_k) \\ &= \frac{\lambda}{8\pi^2} \sum_{k=1}^M \frac{1}{u_k^2 + \frac{1}{4}}. \end{aligned} \quad (4.29)$$

4.2 Three-point functions at tree-level

In this section, we discuss the three-point functions of the non-BPS operators which is in $SU(2)$ sub-sector at tree-level.

4.2.1 Structure constants at tree-level

In general, the tree-level computation is given by the Wick contractions. For the three-point functions case, the contractions are divided by the three parts with the bridge length $l_{ij} \equiv \frac{L_i + L_j - L_k}{2}$ in figure 4.1. Referring to the previous papers, to calculate the three-point functions at tree-level, we first map the operators to spin chain states. Secondly, the spin chain states are cut in respect to the bridge lengths and flipping the cut spin chain states. Thirdly, the spin chain states are contracted with each other. Finally, we get the structure constants at tree-level.

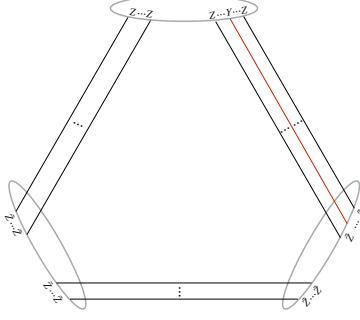


Figure 4.2: Three-point functions with one-magnon: The Y excitation can be contracted with only the operator \tilde{Z} .

One-magnon

Let us first consider the simplest configuration, which has one excitation as follows:

$$\mathcal{O}_1 = \text{Tr}[Z^{L_1}Y], \quad \mathcal{O}_2 = \text{Tr}[\bar{Z}^{L_2}], \quad \mathcal{O}_3 = \text{Tr}[\tilde{Z}^{L_3}], \quad (4.30)$$

where we set the scalars

$$Z = \phi_1 + i\phi_2, \quad Y = \phi_3 + i\phi_4, \quad (4.31)$$

$$\tilde{Z} = \frac{Z + \bar{Z} + Y - \bar{Y}}{2}. \quad (4.32)$$

Also, the notation \bar{Z} and \bar{Y} are complex conjugate of Z and Y respectively.

In order to systematically calculate the structure constants, we go on spin chain system. The operators are mapped to the each states with magnon as follows:

$$\mathcal{O}_1 \rightarrow |p\rangle_1 = \sum_x e^{ipx} |\cdots ZYZ \cdots\rangle_1,$$

$$\mathcal{O}_2 \rightarrow |0\rangle_2 = |\cdots \bar{Z} \cdots\rangle_2,$$

$$\mathcal{O}_3 \rightarrow |0\rangle_3 = |\cdots \tilde{Z} \cdots\rangle_3.$$

Next, these states are decomposed into two states. Then we must be careful of range of the excitations Y , because the excitation Y can only be contracted with the scalar \tilde{Z} in fig 4.2. Namely, we have

$$\mathcal{O}_1 \rightarrow \sum_{x=1}^{\ell_{12}} e^{ipx} |\cdots ZYZ \cdots\rangle_1 \otimes |\cdots Z \cdots\rangle_1,$$

$$\mathcal{O}_2 \rightarrow |\cdots \bar{Z} \cdots\rangle_2 \otimes |\cdots \bar{Z} \cdots\rangle_2,$$

$$\mathcal{O}_3 \rightarrow |\cdots \tilde{Z} \cdots\rangle_3 \otimes |\cdots \tilde{Z} \cdots\rangle_3.$$

Also, we perform a flipping operation which is merely change from the bra-state to ket-state for the right side states as follows:

$$\begin{aligned}\mathcal{O}_1 &\rightarrow \sum_{x=1}^{\ell_{12}} e^{ipx} |\cdots ZYZ \cdots\rangle_1 \otimes {}_1\langle \cdots Z \cdots|, \\ \mathcal{O}_2 &\rightarrow |\cdots \bar{Z} \cdots\rangle_2 \otimes {}_2\langle \cdots \bar{Z} \cdots|, \\ \mathcal{O}_3 &\rightarrow |\cdots \tilde{Z} \cdots\rangle_3 \otimes {}_3\langle \cdots \tilde{Z} \cdots|.\end{aligned}$$

Finally, by contracting them, the structure constants are given by

$$C_{123}^{Y\circ\circ} \propto \sum_{x=1}^{\ell_{12}} e^{ipx}. \quad (4.33)$$

Here, we normalized as $\langle Z|Z\rangle = \langle Y|Y\rangle = 1$. The geometric sum is calculated easy as

$$\sum_{x=1}^{\ell_{12}} e^{ipx} = N(p)(1 - e^{ip\ell_{12}}), \quad N(p) \equiv \frac{1}{e^{-ip} - 1}. \quad (4.34)$$

It is important to interpret the above equation as a movement of the magnon on the spin chain coordinate.

$$\sum_{x=1}^{\ell_{12}} \text{---} \overset{\bullet}{x} \text{---} \propto \overset{\bullet}{1} \text{---} \text{---} \text{---} \text{---} \text{---} \overset{\bullet}{\ell_{12}}$$

The magnon is denoted by the black dot. The first term of the right hand side shows that the magnon lives at the start point of site 1. The second term shows that the magnon lives at the end point of site ℓ_{12} on the spin chain coordinate. The propagation factor $e^{ip\ell_{12}}$ in (4.34) are raised when the magnon propagate from the start point to the end point.

Two-magnon

Next, we consider the operator with two excitations

$$\mathcal{O}_1 = \text{Tr}[\cdots ZYZ \cdots ZYZ \cdots]. \quad (4.35)$$

According to the section 4.1.2, the operator is mapped to the two-magnon state as follows:

$$|p_1, p_2\rangle = \sum_{x_1 < x_2} e^{ip_1 x_1 + ip_2 x_2} |\cdots \underset{x_1}{ZYZ} \cdots \underset{x_2}{ZYZ} \cdots\rangle + S(p_2, p_1) \sum_{x_1 < x_2} e^{ip_2 x_1 + ip_1 x_2} |\cdots \underset{x_1}{ZYZ} \cdots \underset{x_2}{ZYZ} \cdots\rangle. \quad (4.36)$$

In addition, by cutting, flipping and contracting the states, the structure constants are given by the geometric sum as follows:

$$C_{123}^{Y^2 \circ \circ} \propto \sum_{1 \leq x_1 < x_2 \leq \ell_{12}} e^{ip_1 x_1 + ip_2 x_2} + S(p_2, p_1) \sum_{1 \leq x_1 < x_2 \leq \ell_{12}} e^{ip_2 x_1 + ip_1 x_2}. \quad (4.37)$$

The first term become

$$\begin{aligned} \sum_{1 \leq x_1 < x_2 \leq \ell_{12}} e^{ip_1 x_1 + ip_2 x_2} &= N(p_2) \sum_{x_1=1}^{\ell_{12}} (e^{i(p_1+p_2)x_1} - e^{ip_1 x_1} e^{ip_2 \ell_{12}}) \\ &= N(p_2)N(p_1 + p_2)(1 - e^{i(p_1+p_2)\ell_{12}}) - N(p_1)N(p_2)(e^{ip_2 \ell_{12}} - e^{i(p_1+p_2)\ell_{12}}). \end{aligned} \quad (4.38)$$

This geometric sum can also be interpreted as a movement of the magnons on the spin chain coordinate as follows:

$$\begin{aligned} \sum_{x_1=1}^{\ell_{12}} \sum_{x_2=x_1+1}^{\ell_{12}} \text{---} \overset{\bullet}{x_1} \overset{\bullet}{x_2} \text{---} &= N(p_2) \sum_{x_1=1}^{\ell_{12}} (\text{---} \overset{\bullet}{x_1} \text{---} - \text{---} \overset{\bullet}{x_1} \text{---} \overset{\bullet}{} \text{---}) \\ &= N(p_2)N(p_1 + p_2) (\overset{\bullet}{} \text{---} \overset{\bullet}{} \text{---} - \text{---} \overset{\bullet}{} \text{---} \overset{\bullet}{} \text{---}) - N(p_1)N(p_2) (\overset{\bullet}{} \text{---} \overset{\bullet}{} \text{---} - \text{---} \overset{\bullet}{} \text{---} \overset{\bullet}{} \text{---}) \end{aligned}$$

When the two magnons are propagated together as a mass, the pre-factor become $N(p_1 + p_2)$ rather than $N(p_1)$ or $N(p_2)$.

Then, we notice that the interpretation of the summation depends on the ordering of the summation. Namely, if we first sum over x_2 and then sum over x_1 , the summation is given by

$$\begin{aligned} \sum_{x_2=1}^{\ell_{12}} \sum_{x_1=1}^{x_2-1} \text{---} \overset{\bullet}{x_1} \overset{\bullet}{x_2} \text{---} &= N(p_1) \sum_{x_2=1}^{\ell_{12}} (\overset{\bullet}{} \text{---} \overset{\bullet}{x_2} \text{---} - e^{-ip_1} \text{---} \overset{\bullet}{x_2} \text{---}) \\ &= N(p_1)N(p_2) (\overset{\bullet}{} \text{---} \overset{\bullet}{} \text{---} - \overset{\bullet}{} \text{---} \overset{\bullet}{} \text{---}) - N(p_1)N(p_1 + p_2)e^{-ip_1} (\overset{\bullet}{} \text{---} \overset{\bullet}{} \text{---} - \text{---} \overset{\bullet}{} \text{---} \overset{\bullet}{} \text{---}) \end{aligned}$$

Surely, it seems that the geometric sum apparently give the different answer as follows:

$$\sum_{1 \leq x_1 < x_2 \leq \ell_{12}} e^{ip_1 x_1 + ip_2 x_2} = N(p_1)N(p_2)(1 - e^{ip_2 \ell_{12}}) - N(p_1)N(p_1 + p_2)e^{-ip_1}(1 - e^{i(p_1+p_2)\ell_{12}}). \quad (4.39)$$

It teaches us that the terms should be summarized in respect to the each propagation factors, and then the representation has two types. According to the both (4.38) and (4.39), the summation can be rewritten as

$$\sum_{1 \leq x_1 < x_2 \leq \ell_{12}} e^{ip_1 x_1 + ip_2 x_2} = N(p_2)N(p_1 + p_2) - N(p_2)N(p_1)e^{ip_2 \ell_{12}} + N(p_1)N(p_1 + p_2)e^{-ip_1}e^{i(p_1+p_2)\ell_{12}}. \quad (4.40)$$

Notice that the non-trivial factors $N(\dots)$ are related to the the number of magnons at the left-(right-)most site. Thus, by substituting the result (4.40) for (4.37), we finally get the structure constants as follows:

$$C_{123}^{Y^2\circ\circ} \propto N(p_1)N(p_2)[h(u_1, u_2) - e^{ip_2\ell_{12}} - S(p_1, p_2)e^{ip_1\ell_{12}} + h(u_1, u_2)e^{i(p_1+p_2)\ell_{12}}], \quad (4.41)$$

where $h(u, v)$ is defined by

$$\begin{aligned} N(p_1)N(p_2)h(u, v) &\equiv N(p_1)N(p_2)\frac{u-v}{u-v+i} \\ &= N(p_2)N(p_1+p_2) + S(p_1, p_2)N(p_1)N(p_1+p_2) \\ &= N(p_1)N(p_1+p_2)e^{-ip_1} + S(p_1, p_2)N(p_2)N(p_1+p_2)e^{-ip_2}. \end{aligned} \quad (4.42)$$

In the next section, we will see that the factor $h(u, v)$ is just the tree-level hexagon form factor. In addition, we find the significant property of the relation between the factor $h(u, v)$ and S-matrix

$$\frac{h(u, v)}{h(v, u)} = S(u, v). \quad (4.43)$$

As an another case, we explain the structure constants of the two-magnon in different spin chain $C_{123}^{\bullet\bullet\circ}$ in appendix B

Multi-magnon

Finally, we discuss the operator with multi-magnon. According to the section 4.1.2, the Bethe ansatz state of the multi-magnon is given by

$$|p_1, \dots, p_M\rangle = \sum_{x_1 < \dots < x_M} \Psi(x_1, \dots, x_M) |ZY \dots YZ\rangle, \quad (4.44)$$

$$\Psi(x_1, \dots, x_M) = \sum_{\sigma \in P_M} \prod_{\substack{j < k \\ \sigma_k < \sigma_j}} S(P_{\sigma_k}, p_{\sigma_j}) \prod_{j=1}^M e^{ip_{\sigma_j} x_j} \quad (4.45)$$

Using the relation between S-matrix and $h(u, v)$ function (4.43), the product of S-matrices can be divided by

$$\prod_{\substack{\sigma_k < \sigma_j \\ j < k}} S(p_{\sigma_j}, p_{\sigma_k}) = \left(\prod_{\substack{\sigma_k < \sigma_j \\ j < k}} h(u_{\sigma_k}, u_{\sigma_j}) \right) \left(\prod_{\substack{\sigma_k < \sigma_j \\ j < k}} \frac{1}{h(u_{\sigma_j}, u_{\sigma_k})} \right). \quad (4.46)$$

Furthermore, the first bracket can be decomposed as

$$\left(\prod_{\substack{\sigma_k < \sigma_j \\ j < k}} h(u_{\sigma_k}, u_{\sigma_j}) \right) = \left(\prod_{\sigma_k < \sigma_j} h(u_{\sigma_k}, u_{\sigma_j}) \right) \left(\prod_{\substack{\sigma_k < \sigma_j \\ j > k}} \frac{1}{h(u_{\sigma_k}, u_{\sigma_j})} \right). \quad (4.47)$$

Next, by relabelling indices of the product, the S-matrices become

$$\prod_{\substack{\sigma_k < \sigma_j \\ j < k}} S(u_{\sigma_j}, u_{\sigma_k}) = \left(\prod_{j < k} h(u_j, u_k) \right) \left(\prod_{\substack{\sigma_k > \sigma_j \\ j < k}} \frac{1}{h(u_{\sigma_k}, u_{\sigma_j})} \right) \left(\prod_{\substack{\sigma_k < \sigma_j \\ j < k}} \frac{1}{h(u_{\sigma_k}, u_{\sigma_j})} \right). \quad (4.48)$$

Overall, we get the following form of the product of the S-matrices:

$$\prod_{\substack{\sigma_k < \sigma_j \\ j < k}} S(u_{\sigma_j}, u_{\sigma_k}) = \left(\prod_{j < k} h(u_j, u_k) \right) \left(\prod_{j < k} \frac{1}{h(u_{\sigma_j}, u_{\sigma_k})} \right). \quad (4.49)$$

Therefore, the structure constants are written as

$$C_{123}^{YM\infty} \propto \sum_{1 \leq x_1 \cdots < x_M \leq \ell_{12}} \Psi(x_1, \cdots, x_M) \quad (4.50)$$

$$= \prod_{j < k} h(u_j, u_k) \sum_{\sigma \in P_M} \left(\prod_{j < k} \frac{1}{h(u_{\sigma_j}, u_{\sigma_k})} \right) M(P_{\sigma_1}, \cdots, P_{\sigma_M}) \quad (4.51)$$

with

$$M(P_{\sigma_1}, \cdots, P_{\sigma_M}) \equiv \sum_{1 < x_1 \cdots < x_M \leq \ell_{12}} e^{i \sum_j p_j x_j}. \quad (4.52)$$

Let us next treat the factor $M(P_{\sigma_1}, \cdots, P_{\sigma_M})$, which is evaluated by geometric series. In advance, we state the result of the geometric sum of the multi-magnon:

$$M(P_{\sigma_1}, \cdots, P_{\sigma_M}) = \sum_{\substack{\alpha = \{1, \dots, m\} \\ \bar{\alpha} = \{m+1, \dots, M\}}} (-1)^{|\bar{\alpha}|} \left(\prod_{j \in \bar{\alpha}} e^{i p_j \ell_{12}} \right) \left(\prod_{j \in \alpha} \frac{1}{e^{-i \sum_{k=j}^m p_k} - 1} \right) \left(\prod_{j \in \bar{\alpha}} \frac{e^{i p_j}}{1 - e^{i \sum_{k=j+1}^M p_k}} \right). \quad (4.53)$$

By checking above result, we recall the two-magnon case. The lessons of geometric sum of the two-magnons are as follows:

- The non-trivial factors arise when the magnons are moved together as a mass.
- There are two different perspectives of the non-trivial factors, whether the magnons are at left-most site or right-most site.

First, we consider that the magnons are at the right-most site. For the cases of one-, two-

and three-magnon, the geometric sums are given by

$$\begin{aligned}
\sum_{x_1=1}^{\ell_{12}} e^{ip_1 x} &= \frac{e^{ip_1}}{1 - e^{ip_1}} (1 - e^{ip_1 \ell_{12}}), \\
\sum_{x_2=1}^{\ell_{12}} \sum_{x_1=1}^{x_2-1} e^{ip_1 x_1 + ip_2 x_2} &= \sum_{x_2=1}^{\ell_{12}} e^{ip_2 x_2} \times (-1) \frac{e^{ip_1}}{1 - e^{ip_1}} e^{ip_1(x_2-1)} + \dots \\
&= N(p_1)N(p_1 + p_2) e^{-ip_1} e^{i(p_1+p_2)\ell_{12}} + \dots \\
&= \frac{e^{i(p_1+p_2)}}{(1 - e^{ip_1})(1 - e^{i(p_1+p_2)})} e^{i(p_1+p_2)\ell_{12}} + \dots \\
\sum_{x_3=1}^{\ell_{12}} \sum_{x_2=1}^{x_3-1} \sum_{x_1=1}^{x_2-1} e^{ip_1 x_1 + ip_2 x_2 + ip_3 x_3} &= \sum_{x_3=1}^{\ell_{12}} e^{ip_3 x_3} \times (-1)^2 \frac{e^{i(p_1+p_2)}}{(1 - e^{ip_1})(1 - e^{i(p_1+p_2)})} e^{i(p_1+p_2)(x_3-1)} + \dots \\
&= (-1)^3 \frac{e^{i(p_1+p_2+p_3)}}{(1 - e^{ip_1})(1 - e^{i(p_1+p_2)})(1 - e^{i(p_1+p_2+p_3)})} e^{i(p_1+p_2+p_3)\ell_{12}} + \dots
\end{aligned}$$

It is easy to find the rules. Using the mathematical induction, the summation is given by

$$\sum_{1 < x_1 \dots < x_M \leq \ell_{12}} \prod_{i=1}^M e^{ip_i} = \sum_{x_M=1}^{\ell_{12}} e^{ip_M x_M} \times (-1)^{M-1} \prod_{i=1}^{M-1} \frac{e^{ip_i}}{1 - e^{i \sum_{j=1}^i p_j}} e^{ip_i(x_M-1)} + \dots \quad (4.54)$$

$$= (-1)^M \prod_{i=1}^M \frac{e^{ip_i}}{1 - e^{i \sum_{j=1}^i p_j}} e^{ip_M \ell_{12}} + \dots \quad (4.55)$$

The left-most side is also given by the same way as the right-most side:

$$\sum_{1 < x_1 \dots < x_M \leq \ell_{12}} \prod_{i=1}^M e^{ip_i} = \prod_{i=1}^M \frac{1}{e^{-i \sum_{j=1}^i p_j} - 1} + \dots \quad (4.56)$$

Therefore, in respect to the number of magnons at the left-(right-)most site, by using the (4.55) and (4.56), the summation (4.52) in figure 4.3 is rewritten as

$$\sum_{1 < x_1 \dots < x_M \leq \ell_{12}} = \sum_{\substack{\alpha=\{1, \dots, m\} \\ \bar{\alpha}=\{m+1, \dots, M\}}} (-1)^{|\bar{\alpha}|} \prod_{i \in \alpha} \frac{1}{e^{-i \sum_{j=1}^i p_j} - 1} \prod_{k \in \bar{\alpha}} \frac{e^{ip_k}}{1 - e^{i \sum_{j=1}^k p_j}} e^{ip_k \ell_{12}} \quad (4.57)$$

where α and $\bar{\alpha}$ denote the magnons lived at the left-(right-)most site. Thus, the structure constants become

$$C_{123}^{M \circ \circ} \propto \prod_{j < k} h(u_j, u_k) \sum_{\alpha \cup \bar{\alpha} = \{1, \dots, M\}} (-1)^{|\bar{\alpha}|} \left(\prod_{j \in \bar{\alpha}} e^{ip_j \ell_{12}} \right) \left(\prod_{\substack{i, j \\ i \in \alpha, j \in \bar{\alpha}}} \right) F(\alpha) \bar{F}(\bar{\alpha}) \quad (4.58)$$

$$\begin{aligned}
\sum_{1 < x_1 \dots < x_M \leq \ell_{12}} \text{---} \overset{\color{red}\bullet}{x_1} \dots \overset{\color{blue}\bullet}{x_M} \text{---} &= \sum_{\substack{\alpha = \{1, \dots, m\} \\ \bar{\alpha} = \{m+1, \dots, M\}}} (-1)^{|\bar{\alpha}|} \text{---} \underbrace{\overset{\color{red}\bullet}{\dots}}_{\alpha} \text{---} \underbrace{\overset{\color{blue}\bullet}{\dots}}_{\bar{\alpha}} \text{---} \\
&= \sum_{\substack{\alpha = \{1, \dots, m\} \\ \bar{\alpha} = \{m+1, \dots, M\}}} (-1)^{|\bar{\alpha}|} \text{---} \underbrace{\overset{\color{red}\bullet}{\dots}}_{\alpha} \text{---} \times \text{---} \underbrace{\overset{\color{blue}\bullet}{\dots}}_{\bar{\alpha}} \text{---} \\
&= \sum_{\substack{\alpha = \{1, \dots, m\} \\ \bar{\alpha} = \{m+1, \dots, M\}}} (-1)^{|\bar{\alpha}|} \prod_{i \in \alpha} \frac{1}{e^{-i \sum_{j=1}^i p_j} - 1} \times \prod_{k \in \bar{\alpha}} \frac{e^{ip_k}}{1 - e^{i \sum_{j=1}^k p_j}} e^{ip_k \ell_{12}}
\end{aligned}$$

Figure 4.3: The summation of propagation factors is divided into sum over partitions of magnons in α and $\bar{\alpha}$.

with

$$F(1, 2, \dots, m) \equiv \sum_{\sigma \in P_m} \left(\prod_{i < j} \frac{1}{h(u_{\sigma_i}, u_{\sigma_j})} \right) \left(\prod_{j=1}^m \frac{1}{e^{-i \sum_{k=j}^m P_{\sigma_k}} - 1} \right), \quad (4.59)$$

$$\bar{F}(1, 2, \dots, m) \equiv \sum_{\sigma \in P_m} \left(\prod_{i < j} \frac{1}{h(u_{\sigma_i}, u_{\sigma_j})} \right) \left(\prod_{j=1}^m \frac{e^{ip_{\sigma_j}}}{1 - e^{i \sum_{k=j}^m P_{\sigma_k}}} \right). \quad (4.60)$$

They seem tedious functions. However, we turn out that these functions can become following smart product

$$F(1, 2, \dots, m) = \bar{F}(1, 2, \dots, m) = \prod_{k=1}^m i(u_k + i/2). \quad (4.61)$$

Here, we deal with the relation of $F(1, 2, \dots, m)$. The function can be shown by the mathematical induction. For the preparation, the each factors in $F(1, 2, \dots, m)$ are written as

$$\begin{aligned}
M(p_1, \dots, p_m) &\equiv \prod_{j=1}^m \frac{1}{e^{-i \sum_{k=j}^m P_k} - 1} \\
&= \frac{1}{e^{-i \sum_{k=1}^m P_k} - 1} \times M(p_1, \dots, p_{m-1}), \\
H(p_1, \dots, p_m) &\equiv \prod_{i < j} \frac{1}{h(u_i, u_j)} \\
&= \prod_{k \neq m} \frac{1}{h(u_k, u_m)} \times H(p_1, \dots, p_{m-1}).
\end{aligned}$$

Using this relations, the function $F(1, 2, \dots, m)$ become

$$\begin{aligned} F(1, 2, \dots, m) &= \sum_{\sigma \in P_m} \left(\frac{1}{e^{-i \sum_{k=1}^m p_{\sigma_k}} - 1} \prod_{k \neq m} \frac{1}{h(u_{\sigma_k}, u_{\sigma_m})} \times M(p_{\sigma_1}, \dots, p_{\sigma_{m-1}}) H(p_{\sigma_1}, \dots, p_{\sigma_{m-1}}) \right) \\ &= \frac{1}{e^{-i \sum_{k=1}^M p_k} - 1} \sum_{j=1}^m \prod_{k \neq j} \frac{1}{h(u_k, u_j)} \times F(i, \dots, \check{j}, \dots, m), \end{aligned}$$

where $F(i, \dots, \check{j}, \dots, m)$ means that j -th excitation does not contribute. Thereby, we assume

$$F(1, 2, \dots, m) = \frac{1}{e^{-i \sum_{k=1}^M p_k} - 1} \sum_{j=1}^m \prod_{k \neq j} \frac{1}{h(u_k, u_j)} \frac{\prod_{k=1}^M i(u_k + 1/2)}{i(u_j + 1/2)}.$$

Here, by using the following counter integral, we can see

$$(e^{-i \sum_{k=1}^M p_k} - 1) = \prod_{k=1}^m \frac{u_k - i/2}{u_k + i/2} = \oint_{z=0} \frac{dz}{2\pi i} \frac{1}{z} \left(\frac{u_k - z - i/2}{u_k - z + i/2} - 1 \right) = \sum_{j=1}^m \prod_{k \neq j} \frac{1}{h(u_k, u_j)} \frac{1}{i(u_j + 1/2)}. \quad (4.62)$$

Therefore, we arrive at the relation

$$F(1, 2, \dots, m) = \prod_{k=1}^m i(u_k + i/2). \quad (4.63)$$

Overall, by considering the normalization, which is called the Gaudin norm [46, 47], we finally have the following correct form of the tree-level structure constants

$$C_{123}^{M\infty} = \frac{\mathcal{A}}{\sqrt{\prod_{i < j} S(u_i, u_j) \det \partial_{u_j} \phi_k}} \quad (4.64)$$

$$\mathcal{A} = \prod_{j < k} h(u_j, u_k) \sum_{\alpha \cup \bar{\alpha} = \{1, \dots, M\}} (-1)^{|\bar{\alpha}|} \left(\prod_{j \in \bar{\alpha}} e^{ip_j \ell_{12}} \right) \left(\prod_{\substack{i, j \\ i \in \alpha, j \in \bar{\alpha}}} \frac{1}{h(u_i, u_j)} \right), \quad (4.65)$$

where ϕ_j is defined by the Bethe equation as

$$e^{i\phi_j} \equiv e^{ip_j L} \prod_{k \neq j} S(u_j, u_k). \quad (4.66)$$

This form (4.65) is written as the sum over partitions of the magnons in α and $\bar{\alpha}$. It will be really helpful to the generalization for the finite coupling method.

4.2.2 Weight factors and Tree-level hexagon form factor

In this subsection, we would like to mention short interpretation about the tree-level hexagon form factor. In the (4.42), we define the function $h(p_1, p_2)$. As you can see later in subsection (5.1.4), the function is just the tree-level hexagon form factor. Then, we found how to produce the tree-level hexagon form factor from the tailoring method. Therefore, we would like to summarise the results here.

Let us recall the sum over the position of the magnons as

$$\sum_{x=1}^{\ell_{12}} e^{ipx} = N(p)(1 - e^{ip\ell_{12}}). \quad (4.67)$$

Of course, the result is written as the difference of the propagation factors and the weight factor $N(p)$. In other word, the factor $N(p)$ is given by the weight factor when one magnon move, and we depict as follows:

$$\text{weight} [\text{---} \bullet \text{---}] \equiv N(p)$$

Furthermore, by replacing the momentum p to $p_1 + p_2$, the two-magnon weight factor, which arise when two-magnons move together, is simply given as

$$\text{weight} [\text{---} \bullet \bullet \text{---}] \equiv N(p_1 + p_2)$$

Then, the tree-level hexagon form factor with two-magnon is given by

$$h(p_1, p_2) = \frac{\text{weight} [\text{---} \bullet \text{---}]}{\text{weight} [\text{---} \bullet \text{---}]} + S(p_1, p_2) \frac{\text{weight} [\text{---} \bullet \text{---}]}{\text{weight} [\text{---} \bullet \text{---}]}$$

Namely, the tree-level hexagon form factor with two-magnon is given by the sum over ordering with S-matrix for the two-magnon weight factors factor normalised one-magnon weight factors. Thus, the multi-magnon hexagon form factor can be written as:

$$h(p_1, \dots, p_M) = \sum_{\sigma \in P_M} \prod_{\substack{j < k \\ \sigma_k < \sigma_j}} S(p_{\sigma_j}, p_{\sigma_k}) \frac{N(p_1 + \dots + p_M)}{N(p_{\sigma_j})},$$

$$\left(\frac{N(p_1 + \dots + p_M)}{N(p_{\sigma_j})} = \frac{\text{weight} [\text{---} \bullet \bullet \text{---}]}{\text{weight} [\text{---} \bullet \text{---}]} \right)$$

Chapter 5

Complete method – integrability

In the context of the AdS₅/CFT₄ correspondence, one of the goals is surely to give a finite coupling solution. In this chapter, we explain a formalism which gives such result.

In the section 5.1, we discuss the three-point functions at finite coupling, which is so-called hexagon method [34].¹ The tree-level method, tailoring method, should be included into the hexagon method. In fact, these methods are deeply related to each other. Therefore, we start with the result in the section 4.2 and go to the discussion of the hexagon method.

In the section 5.2, we discuss a four-point functions at finite coupling, which is so-called hexagonalization [48, 49]. In particular, we consider the four-point functions of the BPS operators. Thus, we would like to see how to reproduce the results in section 3.2, which was the one-loop four-point functions of the BPS operators.

5.1 Structure constants at finite coupling

Let us first recall the result of the three-point functions at tree-level (4.65). Using the relation between the factor $h(u, v)$ and S-matrix (4.43), we immediately find that the (4.65) can be rewritten as

$$\mathcal{A}^{\text{tree}} = \sum_{\alpha \cup \bar{\alpha} = \{1, \dots, M\}} (-1)^{|\bar{\alpha}|} \prod_{j \in \bar{\alpha}} e^{ip_j^{\text{tree}} \ell_{12}} \prod_{\substack{j < k \\ j \in \bar{\alpha}, k \in \alpha}} S^{\text{tree}}(u_j, u_k) \mathcal{H}^{\text{tree}}(\alpha) H^{\text{tree}}(\bar{\alpha}), \quad (5.1)$$

$$\mathcal{H}^{\text{tree}}(\alpha) = \prod_{\substack{i < j \\ i, j \in \alpha}} h^{\text{tree}}(u_i, u_j), \quad \mathcal{H}^{\text{tree}}(\bar{\alpha}) = \prod_{\substack{i < j \\ i, j \in \bar{\alpha}}} h^{\text{tree}}(u_i, u_j), \quad (5.2)$$

where we added the subscript “tree” to the momentum, S-matrix and the function $h(u, v)$ in order to clarify that they are tree-level functions. Here, we try to replace the tree-level

¹The good review is for example [50]

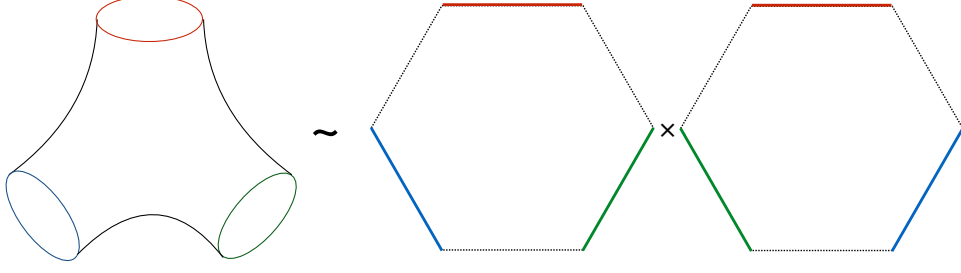


Figure 5.1: The pair of pants diagram is decomposed into two hexagons form factors.

factors by finite coupling functions as

$$\mathcal{A}^{\text{tree}} \rightarrow \mathcal{A}^{\text{finite}} : p_i^{\text{tree}} \rightarrow p_i^{\text{finite}}, S^{\text{tree}}(u_j, u_k) \rightarrow S^{\text{finite}}(u_j, u_k), \mathcal{H}^{\text{tree}}(\alpha) \rightarrow \mathcal{H}^{\text{finite}}(\alpha). \quad (5.3)$$

Immediately, we suggest asymptotic structure constants at finite coupling

$$C_{123}^{M_{\infty\infty}} = \frac{\mathcal{A}^{\text{finite}}}{\sqrt{\prod_{i<j} S^{\text{finite}}(u_i, u_j) \det \partial_{u_j} \phi_k^{\text{finite}}}}, \quad (5.4)$$

where p_i^{finite} is given by

$$e^{ip^{\text{finite}}(u)} = \frac{x(u + \frac{i}{2})}{x(u - \frac{i}{2})} \quad \text{with} \quad u = g\left(x + \frac{1}{x}\right), \quad (5.5)$$

and $S^{\text{finite}}(u, v)$ is the Beisert's S-matrix, see [7, 8]. The remained unknown factor is only $\mathcal{H}^{\text{finite}}(\alpha)$. Surely, we should add a factor occurred by loop correction. Such factor is known as a finite-size correction explained in subsection 5.1.5. In other words, the proposal (5.4) should be called asymptotic structure constants.² In what follows, we would like to suggest a solution from the symmetry and integrability argument.

Before we begin with the discussion, we comment the strong coupling description of the three-point functions. At the strong coupling, the three-point functions are depicted as the pair of pants diagram. Here, we try to decompose the pair of pants diagram into two hexagons in the similar way as the cutting in the tailoring method in figure 5.1. On the other hand, we consider two-magnons of the $\mathcal{A}^{\text{finite}}$ in (5.4):

$$\begin{aligned} \mathcal{A} &= \mathcal{H}(\{u_1, u_2\} = \alpha) \mathcal{H}(\{\} = \bar{\alpha}) - e^{ip_2 \ell_{12}} \mathcal{H}(\{u_1\} = \alpha) \mathcal{H}(\{u_2\} = \bar{\alpha}) \\ &\quad - S(p_1, p_2) e^{ip_1 \ell_{12}} \mathcal{H}(\{u_2\} = \alpha) \mathcal{H}(\{u_1\} = \bar{\alpha}) + e^{i(p_1 + p_2) \ell_{12}} \mathcal{H}(\{\} = \alpha) \mathcal{H}(\{u_1, u_2\} = \bar{\alpha}). \end{aligned} \quad (5.6)$$

Here, we remove the subscript “finite” due to illegibility. Assuming the existence of the finite coupling spin chain, the factors $\mathcal{H}(\alpha), \mathcal{H}(\bar{\alpha})$ in (5.6) seems to be interpreted as figure 5.2. In this picture, we assume that the $\mathcal{H}(\bar{\alpha})$ is a hexagon form factor with magnons, which is given by the decomposition of the pair of pants diagram. Notice that we ignored the remaining sign factor $(-1)^{|\alpha|}$, Because we can't mention anything until now.

²Of course, we cannot be denied any other correction.

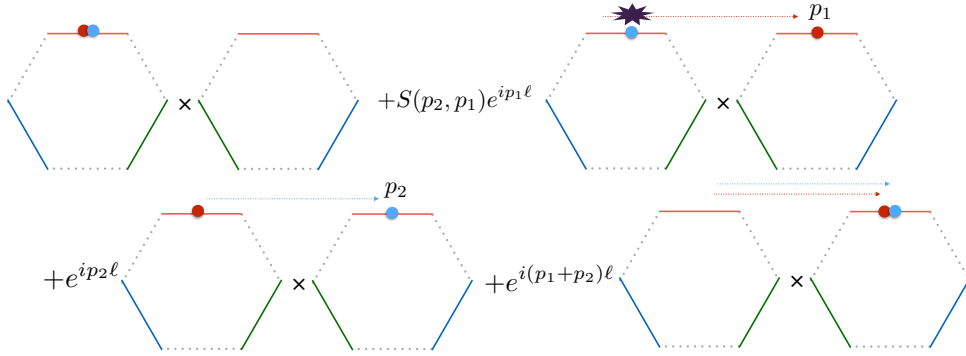


Figure 5.2: If we assume that the $\mathcal{H}(\bar{\alpha})$ is an object like a hexagon form factor, the $\mathcal{A}^{\text{strong}}$ can be interpreted as a movement of the magnon on the object.

5.1.1 Symmetry of the three-point functions

The symmetry of the $\mathcal{N} = 4$ SYM is $PSU(2, 2|4)$. Considering the correlation functions of $\mathcal{N} = 4$ SYM, the symmetry is broken. We first recall the symmetry of the two-point functions of the BPS operators

$$\langle \text{tr} Z^L(0) \text{tr} \bar{Z}^L(\infty) \rangle. \quad (5.7)$$

Choosing this vacuum, the correlator has the $SO(4)$ rotation for the R-symmetry in addition to $SO(4)$ rotation around the origin. Adding the fermionic part and central charges, Beisert proposed the centrally-extended $PSU(2|2)^2$ algebra. We write the generators as

$$\begin{aligned} \text{Lorentz} : & L_{\beta}^{\alpha}, \dot{L}_{\dot{\beta}}^{\dot{\alpha}}, & \text{R-symmetry} & R_b^a, \dot{R}_{\dot{b}}^{\dot{a}}, \\ \text{Supersymmetry} : & Q_b^{\alpha}, \dot{Q}_{\dot{b}}^{\dot{\alpha}}, & \text{Superconformal} : & S_{\beta}^a, \dot{S}_{\dot{\alpha}}^{\dot{a}}, \\ \text{Centralcharges} : & P, K, C. \end{aligned}$$

The central charges extend by the anti-commutators of the fermionic generators:

$$\begin{aligned} \{Q_a^{\alpha}, Q_b^{\beta}\} &= \epsilon^{\alpha\beta} \epsilon_{ab} P, \\ \{S_{\alpha}^a, S_{\beta}^b\} &= \epsilon^{ab} \epsilon_{\alpha\beta} K, \\ \{Q_a^{\alpha}, S_{\beta}^b\} &= \delta_{\beta}^{\alpha} R_b^a + \delta_a^b L_{\beta}^{\alpha} + \delta_a^b \delta_{\beta}^{\alpha} C. \end{aligned}$$

The symmetry of the three-point functions is less than the case of two-point functions. In the same way as the two-point functions, we start with the canonical configuration of the three-point functions. For example, we take

$$\begin{aligned} \mathcal{O}_1(0) &= \text{tr} Z^{L_1} |_{x_1=(0,0,0,0)}, \\ \mathcal{O}_2(1) &= \text{tr} \tilde{Z}^{L_2} |_{x_2=(1,0,0,0)}, \\ \mathcal{O}_3(\infty) &= \text{tr} \bar{Z}^{L_3} |_{x_3=(\infty,0,0,0)}. \end{aligned}$$

The boson symmetry part is $O(3)$ Lorentz symmetry³ and $O(3)$ R-symmetry⁴. It shows that it has the single $PSU(2|2)$ symmetry, which is the diagonal part of the $PSU(2|2)^2$ symmetry. We denote the generators of the diagonal $PSU(2|2)$ as follows:

$$\begin{aligned}\mathcal{L}^\alpha_\beta &= L^\alpha_\beta + \dot{L}^{\dot{\alpha}}_{\dot{\beta}}, & \mathcal{R}^a_b &= R^a_b + \dot{R}^{\dot{a}}_{\dot{b}} \\ \mathcal{Q}^\alpha_b &= Q^\alpha_b + i\epsilon^{\alpha\dot{\beta}}\epsilon_{ab}\dot{S}^{\dot{b}}_\beta, & \mathcal{S}^a_\alpha &= S^a_\alpha + \frac{i^{ab}}{\epsilon}\epsilon_{\alpha\dot{\beta}}\dot{Q}^{\dot{\beta}}_b.\end{aligned}\tag{5.8}$$

In addition, one central charge $\mathcal{P} \equiv P - K$ extend by the commutator between \mathcal{Q} and \mathcal{S} as follows

$$\begin{aligned}\{\mathcal{Q}^\alpha_a, \mathcal{Q}^\beta_b\} &= \epsilon^{\alpha\beta}\epsilon_{ab}\mathcal{P}, \\ \{\mathcal{S}^a_\alpha, \mathcal{S}^b_\beta\} &= -\epsilon^{ab}\epsilon_{\alpha\beta}\mathcal{P}, \\ \{\mathcal{Q}^\alpha_a, \mathcal{S}^b_\beta\} &= \delta^\alpha_\beta\mathcal{R}^a_b + \delta^b_a\mathcal{L}^\alpha_\beta.\end{aligned}$$

Therefore, the three-point functions, moreover the hexagon form factor, should be invariant under the above centrally-extended diagonal $PSU(2|2)$ symmetry.

5.1.2 Symmetry and hexagon form factor

From here, we consider the strong coupling region, and then we use the fact of the AdS_5/CFT_4 correspondence that the symmetries discussed above are equivalent to the one in the strong coupling. Furthermore, we introduce a hexagon vertex $\langle \mathcal{H} |$, and we assume that the function $\mathcal{H}(\alpha)$ is equal to the hexagon vertex contracted three spin chain states, which is the hexagon form factor:⁵

$$\mathcal{H}(\alpha) = \langle \mathcal{H} | (|\alpha\rangle \otimes |0\rangle \otimes |0\rangle).\tag{5.9}$$

Here, we introduce the notation: $\chi^{A\dot{A}} \in \alpha$, which is labeled by $PSU(2|2)^2$. The representations $\chi^{A\dot{A}} = \chi^A \otimes \dot{\chi}^{\dot{A}}$ are given by

$$\chi^A = (\phi^1, \phi^2, \psi^1, \psi^2), \quad \dot{\chi}^{\dot{A}} = (\dot{\phi}^{\dot{1}}, \dot{\phi}^{\dot{2}}, \dot{\psi}^{\dot{1}}, \dot{\psi}^{\dot{2}}),\tag{5.10}$$

where ϕ^a and ψ^α are bosonic and fermionic fields respectively. Furthermore, the excitation $\chi^{A\dot{A}}$ are related to the fields in $\mathcal{N} = 4$ SYM as follows:

$$\Phi^{1\dot{1}} = X, \quad \Phi^{1\dot{2}} = Y, \quad \Phi^{2\dot{1}} = \bar{Y}, \quad \Phi^{2\dot{2}} = -\bar{X},\tag{5.11}$$

$$\psi^\alpha \dot{\psi}^{\dot{\alpha}} = D^{\alpha\dot{\alpha}} Z, \quad \text{others} = \text{fermion},\tag{5.12}$$

where $\Phi^{a\dot{a}} \equiv \phi^a \dot{\phi}^{\dot{a}}$.

³The three operators can be arranged in a line. Then, we find that they are invariant under the rotation of the line in four-dimension.

⁴It is the rotation symmetry of the remained scalars ϕ^4, ϕ^5, ϕ^6 .

⁵The small consistency check of the ansatz is comparison with tailoring method in subsection 5.1.4.

The property of the hexagon vertex is only symmetry constraint as:

$$\langle \mathcal{H} | \mathcal{J} = 0, \quad J \in \{\mathcal{L}_\beta^\alpha, \mathcal{R}_b^a, \mathcal{Q}_b^\alpha, \mathcal{S}_\alpha^a\}. \quad (5.13)$$

Namely, the hexagon vertex should vanish by the generators of the centrally-extended diagonal $PSU(2|2)$ symmetry. Using this fact, we can consider the following identity:

$$0 = \langle \mathcal{H} | (\mathcal{J}|\alpha\rangle \otimes |0\rangle \otimes |0\rangle). \quad (5.14)$$

One-magnon state

We first calculate the identity for the case of the one-magnon state

$$0 = \langle \mathcal{H} | \mathcal{J} | \chi^{A\dot{A}} \rangle. \quad (5.15)$$

Here, we used the short hand notation. For example, we choose the generators of the R-symmetry \mathcal{R}_b^a and scalar excitation Φ^{ab} .

$$0 = \langle \mathcal{H} | \mathcal{R}_b^a | \Phi^{ab} \rangle. \quad (5.16)$$

By calculating the operation by \mathcal{R}_b^a , we have

$$\mathcal{R}_2^1 | \Phi^{2\dot{1}} \rangle = | \phi^1 \otimes \phi^{\dot{1}} \rangle, \quad (5.17)$$

$$\mathcal{R}_2^1 | \Phi^{2\dot{2}} \rangle = | \phi^1 \otimes \phi^{\dot{2}} \rangle + | \phi^2 \otimes \phi^{\dot{1}} \rangle. \quad (5.18)$$

Thus, we get

$$0 = \langle \mathcal{H} | \phi^1 \otimes \phi^{\dot{1}} \rangle, \quad (5.19)$$

$$\langle \mathcal{H} | \phi^1 \otimes \phi^{\dot{2}} \rangle = -\langle \mathcal{H} | \phi^2 \otimes \phi^{\dot{1}} \rangle. \quad (5.20)$$

They show that the one-scalar magnon hexagon form factor is determined up to a constant μ as⁶

$$\langle \mathcal{H} | \Phi^{ab} \rangle = -i\sqrt{\mu}\epsilon^{ab}. \quad (5.21)$$

Here, μ will be a measure factor. Using the other generators, we can determine the other one-magnon hexagon form factors as

$$\langle \mathcal{H} | \mathcal{D}^{\alpha\dot{\beta}} \rangle = \sqrt{\mu}\epsilon^{\alpha\dot{\beta}}, \quad (5.22)$$

$$\langle \mathcal{H} | \Psi^{\alpha\dot{a}} \rangle = 0. \quad (5.23)$$

In short, for the one-magnon the hexagon form factor with magnon $\chi^A \otimes \dot{\chi}^{\dot{A}}$ is given by the ϵ -tensor contraction up to normalization in figure 5.3:

$$\langle \mathcal{H} | \chi^{A\dot{A}} \rangle \propto \epsilon^{A\dot{A}}. \quad (5.24)$$

⁶The coefficients of the ϵ is just the convention.

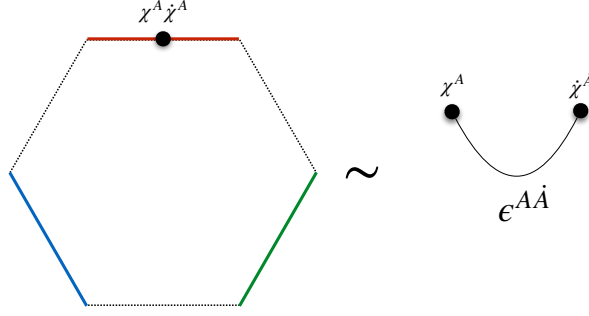


Figure 5.3: Hexagon form factor with one-magnon.

Two-magnon state

We next consider the two-magnon hexagon form factor. In the same way as the one-magnon hexagon form factors, we consider the following identities:

$$0 = \langle \mathcal{H} | \mathcal{J} | \chi^{A\dot{A}} \chi^{B\dot{B}} \rangle \otimes |0\rangle \otimes |0\rangle. \quad (5.25)$$

Calculating them, we have

$$\begin{aligned} \langle \mathcal{H} | \Phi_1^{a\dot{a}} \Phi_2^{b\dot{b}} \rangle &= \mathcal{A}_{12} \epsilon^{ab} \epsilon^{b\dot{a}} + \frac{1}{2} (\mathcal{A}_{12} - \mathcal{B}_{12}) \epsilon^{ab} \epsilon^{\dot{a}\dot{b}}, \\ \langle \mathcal{H} | \Phi_1^{a\dot{a}} \mathcal{D}_2^{\beta\dot{\beta}} \rangle &= \mathcal{G}_{12} \epsilon^{a\dot{a}} \epsilon^{\beta\dot{\beta}}, \quad \langle \mathcal{H} | \mathcal{D}_2^{\alpha\dot{\alpha}} \Phi_1^{b\dot{b}} \rangle = \mathcal{L}_{12} \epsilon^{\alpha\dot{\alpha}} \epsilon^{b\dot{b}}, \\ \langle \mathcal{H} | \mathcal{D}_1^{\alpha\dot{\alpha}} \mathcal{D}_2^{\beta\dot{\beta}} \rangle &= \mathcal{D}_{12} \epsilon^{ab} \epsilon^{b\dot{a}} + \frac{1}{2} (\mathcal{D}_{12} - \epsilon_{12}) \epsilon^{ab} \epsilon^{\dot{a}\dot{b}}, \\ \langle \mathcal{H} | \Psi_1^{a\dot{a}} \Psi_2^{b\dot{b}} \rangle &= \frac{1}{2} \mathcal{C}_{12} \epsilon^{ab} \epsilon^{\dot{a}\dot{b}}, \quad \langle \mathcal{H} | \Psi_1^{a\dot{a}} \Psi_2^{\beta\dot{\beta}} \rangle = \mathcal{H}_{12} \epsilon^{ab} \epsilon^{\beta\dot{\beta}}, \\ \langle \mathcal{H} | \Psi_1^{\alpha\dot{\alpha}} \Psi_2^{b\dot{b}} \rangle &= \mathcal{K}_{12} \epsilon^{b\dot{a}} \epsilon^{\alpha\dot{\beta}}, \quad \langle \mathcal{H} | \Psi_1^{\alpha\dot{\alpha}} \Psi_2^{\beta\dot{\beta}} \rangle = \frac{1}{2} \mathcal{F}_{12} \epsilon^{\dot{a}\dot{b}} \epsilon^{\alpha\beta}. \end{aligned} \quad (5.26)$$

The coefficients are also given by

$$\begin{aligned} \mathcal{A}_{12} &= h_{12} A_{12}, \quad \mathcal{B}_{12} = h_{12} B_{12}, \\ \mathcal{G}_{12} &= h_{12} N_2 G_{12}, \quad \mathcal{L}_{12} = h_{12} N_1 L_{12}, \\ \mathcal{D}_{12} &= -h_{12} N_1 N_2 C_{12}, \quad \epsilon_{12} = -h_{12} N_1 N_2 E_{12}, \\ \mathcal{C}_{12} &= -h_{12} N_1 N_2 z^{-1} C_{12}, \quad \mathcal{F}_{12} = -z h_{12} F_{12}, \\ \mathcal{K}_{12} &= h_{12} N_2 K_{12}, \quad \mathcal{H}_{12} = -h_{12} N_1 H_{12}. \end{aligned} \quad (5.27)$$

and

$$\begin{aligned}
A_{12} &= \frac{x_2^+ - x_1^-}{x_2^- - x_1^+}, \\
B_{12} &= \frac{x_2^+ - x_1^-}{x_2^- - x_1^+} \left(1 - 2 \frac{1 - g^2/2x_2^-x_1^+}{1 - g^2/2x_2^-x_1^-} \frac{x_2^+ - x_1^+}{x_2^- - x_1^-} \right), \\
C_{12} &= \frac{g^2\gamma_2\gamma_1}{\alpha x_2^-x_1^-} \frac{1}{1 - g^2/2x_2^-x_1^-} \frac{x_2^+ - x_1^+}{x_2^- - x_1^-}, \\
D_{12} &= -1, \\
E_{12} &= - \left(1 - 2 \frac{1 - g^2/2x_2^+x_1^-}{1 - g^2/2x_2^+x_1^+} \frac{x_2^- - x_1^-}{x_2^+ - x_1^+} \right), \\
F_{12} &= - \frac{2\alpha(x_2^+ - x_2^-)(x_1^+ - x_1^-)}{\gamma_2\gamma_1x_2^+x_1^+} \frac{1}{1 - g^2/2x_2^+x_1^+} \frac{x_2^- - x_1^-}{x_2^+ - x_1^+}, \\
G_{12} &= \frac{x_2^+ - x_1^+}{x_2^- - x_1^+}, \\
H_{12} &= \frac{\gamma_1}{\gamma_2} \frac{x_2^+ - x_2^-}{x_2^- - x_1^+}, \\
K_{12} &= \frac{\gamma_2}{\gamma_1} \frac{x_1^+ - x_1^-}{x_2^- - x_1^+}, \\
L_{12} &= \frac{x_1^- - x_1^+}{x_2^- - x_1^+}. \tag{5.28}
\end{aligned}$$

In fact, the results are completely match the Beisert's S-matrix up to unknown scalar factor h_{12} .⁷ In short, the two-magnon hexagon form factor is given by

$$\langle \mathcal{H} | \chi^{A_1 \dot{A}_1} \chi^{A_2 \dot{A}_2} \rangle = (-1)^{f_1 f_2} h_{12} \langle \chi_2^{A_2 \dot{A}_2} \chi_1^{A_1 \dot{A}_1} | \mathcal{S}_{12} | \chi_1^{A_1 \dot{A}_1} \chi_2^{A_2 \dot{A}_2} \rangle, \tag{5.29}$$

where \mathcal{S}_{12} is the Beisert's S-matrix [7, 8] in figure 5.4:

Multi-magnon conjecture

From the above lessons, we now propose the multi-magnon hexagon form factors. The form factors are composed two factors

$$\langle \mathcal{H} | \chi^{A_1 \dot{A}_1} \dots \chi^{A_M \dot{A}_M} \rangle = H_{\text{dyn}} H_{\text{mat}} \tag{5.30}$$

where H_{dyn} denotes the product of the scalar factor $h(u_i, u_j)$

$$H_{\text{dyn}} = \prod_{i < j} h(u_i, u_j), \tag{5.31}$$

⁷Strictly speaking, we take the $S_{12}^0 = 1$ in the Beisert's S-matrix.

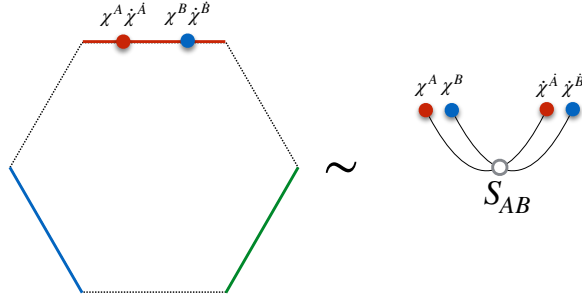


Figure 5.4: Hexagon form factor with two-magnon

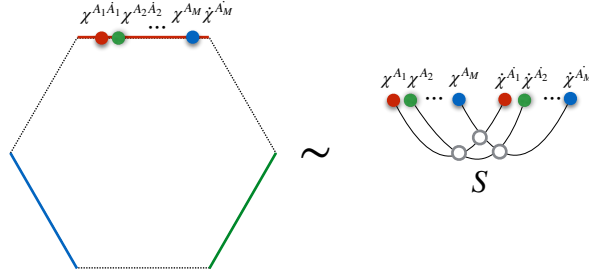


Figure 5.5: Hexagon form factor with multi-magnon

where we called the dynamics part. The H_{mat} denotes the matrix part determined by the Beisert's S-matrix:

$$H_{\text{mat}} = (-1)^\dagger \langle \chi_M^{A_M} \dots \chi_1^{A_1} | \mathcal{S} | \chi_1^{A_1} \dots \chi_M^{A_M} \rangle. \quad (5.32)$$

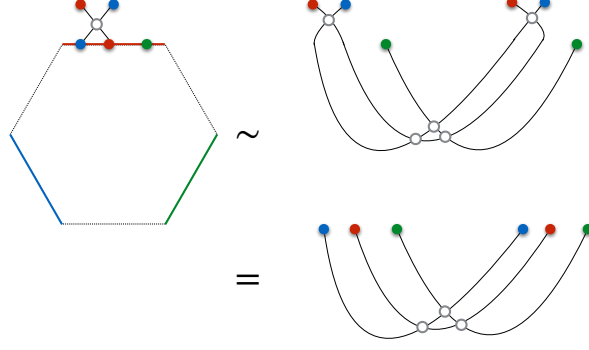
The matrix part can be fixed by the symmetry of the hexagon. Furthermore, the matrix part is depicted as figure 5.1.2. From the discussions so far, we find that the most parts of the hexagon form factor can be fixed only by the symmetry up to scalar factor. Although, we can determine the scalar factor (including the measure factors) by using the power of the integrability as well.

5.1.3 Integrability and hexagon form factor

In this subsection, we finally determine the scalar factor and measure factor, which is the dynamic part of the hexagon form factor. These factors can be fixed by integrability constraints which are Watson equation and decoupling equation.

Watson equation

Watson equation is known as one of the axioms of the form factor bootstrap [51, 52]. Thus, it is composed by the Yang-Baxter equation and Unitarity relation as

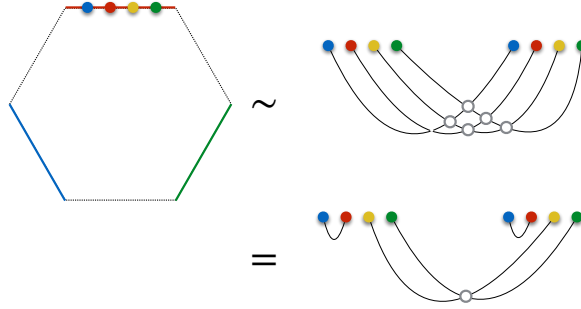


The equation is given by

$$\langle \mathcal{H} | (\mathbb{S}_{ii+1} - \mathbb{I}) | \cdots \chi_i^{A_i \dot{A}_i} \chi_{i+1}^{A_{i+1} \dot{A}_{i+1}} \cdots \rangle = 0. \quad (5.33)$$

decoupling equation

The decoupling equation says the decoupling of particle anti-particle pair⁸. Using the crossing relation and Yang-Baxter relation, the equation is depicted as



Thus, the equation is given by

$$-i \text{Res}_{u=v} [\langle \mathcal{H} | \chi(u) \chi(\bar{v}) \chi_1 \cdots \chi_M \rangle] = \langle \mathcal{H} | \chi_1 \cdots \chi_M \rangle. \quad (5.34)$$

Solutions

Solving these equations, Both the scalar factor and measure factor are given by

$$h(u, v) = \frac{x_u^- - x_v^-}{x_u^- - x_v^+} \frac{1 - 1/x_u^- x_v^+}{1 - 1/x_u^+ x_v^+} \frac{1}{\sigma(u, v)} \quad (5.35)$$

$$\mu(u) = \frac{(1 - 1/x^+ x^-)^2}{(1 - 1/(x^+)^2)(1 - 1/(x^-)^2)} \quad (5.36)$$

where $\sigma(u, v)$ is the Beisert-Eden-Staudacher (BES) dressing phase [53].

⁸In the context of the form factor, the anti-particle is given by the mirror transformation. In the section 5.1.5, we will explain in detail.

5.1.4 Three-point functions at tree-level

We now calculate the hexagon form factor at tree-level.

$$h^{YY}(u, v) = \frac{u - v}{u - v + i}. \quad (5.37)$$

In the case of two Y 's excitations, the hexagon form factor is given by

$$\langle \mathcal{H} | \Phi^{1\dot{2}} \Phi^{1\dot{2}} \rangle = \mathcal{A}_{12} \quad (5.38)$$

$$= h_{12} A_{12}. \quad (5.39)$$

The hexagon form factor is divided into two parts: the matrix part H_{mat} and the dynamics part H_{dyn} . The matrix part was given by the Beisert's S-matrix. In this case, the matrix part is A_{12} and the dynamical part is h_{12} . Each function is expanded at the weak coupling constant as follows:

$$A_{12} = \frac{u - v - i}{u - v + i} + \mathcal{O}(\lambda) \quad (5.40)$$

$$h_{12} = \frac{u - v}{u - v - i} + \mathcal{O}(\lambda) \quad (5.41)$$

Therefore, we could find that the result by the tailoring method (4.42) is reproduced from the weak coupling expansion of the hexagon form factor:

$$\langle \mathcal{H} | \Phi^{1\dot{2}} \Phi^{1\dot{2}} \rangle = \frac{u - v}{u - v + i} \quad (5.42)$$

$$= \mathcal{H}(u, v) \quad (5.43)$$

Even the other configurations, the ansatz (5.9) is corrected at tree-level.

5.1.5 Finite-size correction and mirror transformation

Until now, we have discussed the finite coupling expression of the three-point functions (5.2). Surely, the proposal could be reproduced the tree-level result given by the tailoring method. However, the formula is not still complete. Because, it has been known that there are corrections with dumping factor of the bridge lengths $e^{-\ell_{ij}}$ from the loop order. When the bridge lengths are small, the corrections of the dumping factors can't be ignored. Such correction is called *finite-size correction* [54–57]. Namely, the proposal (5.2) is available only when the all bridge lengths are long $\ell_{ij} \gg 1$ and the finite-size corrections are neglected.

In terms of the hexagon method, the finite-size corrections come from the gluing two hexagons by exchanging the mirror particles which live on the dashed edges of the hexagon form factor in figure 5.6

Then, we must calculate the hexagon form factors with mirror magnon. To do this, we here discuss how to get the mirror particles in terms of the (hexagon) form factor theory.

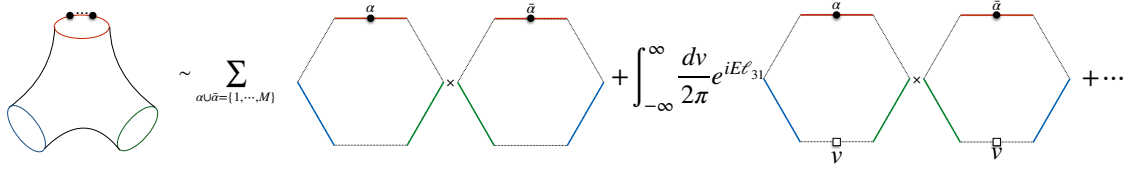


Figure 5.6: At the loop order, the structure constants receive the finite-size correction from the asymptotic result. Then, the correction is given by the gluing mirror edges. In other words it is given by a correction of mirror particles inserted in the glued edges.

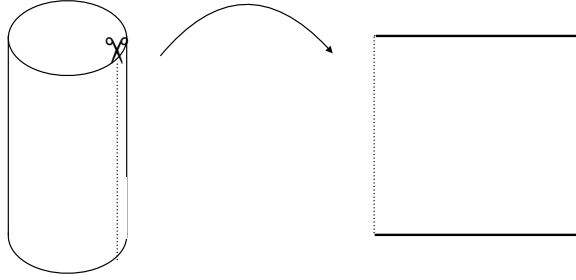


Figure 5.7: The square form factor is given by the cutting the cylinder.

Mirror transformation

Let us begin with the cylinder configuration, which is the two-point functions. Cutting the cylinder, we get the square form factor with two glued lines in figure 5.7. Then, we consider the energy and momentum of the magnon at finite coupling:

$$e^{ip} = \frac{x^+}{x^-}, \quad E = \frac{1}{2} \frac{1 + \frac{1}{x^+x^-}}{1 - \frac{1}{x^+x^-}}. \quad (5.44)$$

The Zhukowski variables were given by

$$x(u) = \frac{u + \sqrt{u^2 - 4g^2}}{2g}. \quad (5.45)$$

Here we defined as $x^\pm(u) \equiv x(u \pm \frac{i}{2})$. Since the Zhukowski variables have branch cuts $[-2g \pm i/2, 2g \pm i/2]$, we should understand the physical meaning when we pass through different sheets. It is simple to consider what happen by the analytic continuation. It is because when we pass through the branch cut, the variable become

$$x(u) \rightarrow \frac{1}{x(u)}. \quad (5.46)$$

Then, we define a mirror transformation which is the analytic continuation in the u -plane. Thus, $u^{2\gamma}$ means : we first pass through the branch cut $[-2g - i/2, 2g - i/2]$, after doing so we pass through the branch cut $[-2g + i/2, 2g + i/2]$ in figure 5.8. Then, the both

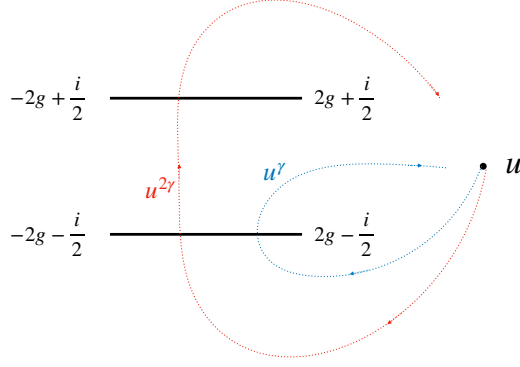


Figure 5.8: Mirror transformation is given by the crossing of the Zhukowski cut. When the magnon pass through the below cut $\pm 2g - i/2$, the magnon is mirror transformed once. On the other hand, When the magnon pass through the both cut $\pm 2g - i/2$ and $\pm 2g + i/2$, the magnon is mirror transformed twice.

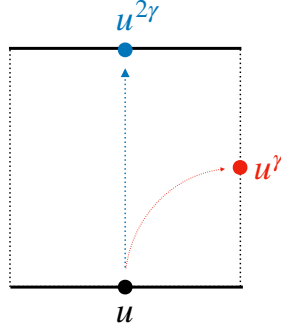


Figure 5.9: Under the twice mirror transformation, the in-coming particles are converted into out-going particles. On the other hand, the once mirror transformation corresponds to conversion into the mirror particle.

variables x^\pm are transformed to $1/x^\pm$. Thus, the momentum and energy also transform

$$2\gamma : p \rightarrow -p, \quad E \rightarrow -E. \quad (5.47)$$

It shows that the 2γ transformation convert the particles into anti-particles in figure 5.9. Thereby, it is just the crossing transformation.

On the other hand, if we consider the half-transformation of the crossing transformation, we path through only the branch cut $[-2g - i/2, 2g - i/2]$. Namely, the Zhukowski variables are transformed as

$$\gamma : x^+ \rightarrow 1/x^+, \quad x^- \rightarrow x^-. \quad (5.48)$$

Then, the particles are on the dashed line. In terms of such a particle, the space and time seems to be changed as figure 5.1.5, which is so-called *mirror transformation* [58, 59].

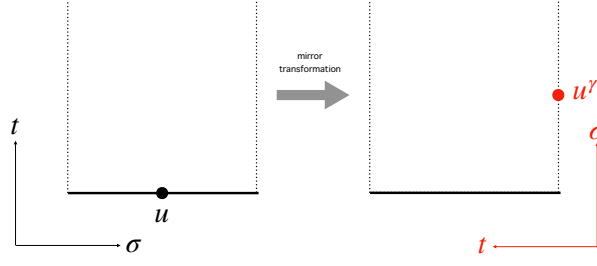


Figure 5.10: The mirror transformation means the double Wick rotation, which exchange space direction into time direction and vice verse.

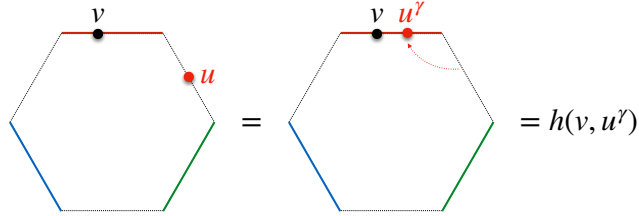
Furthermore, the particle is called mirror particles. Therefore, the mirror transformation lead to exchange between the momentum and energy [60, 61]

$$\gamma : p \rightarrow iE, \quad E \rightarrow -ip. \quad (5.49)$$

Furthermore, the transformation rules are as follows:

$$\begin{aligned} u \rightarrow u^\gamma : \quad x^+ &\rightarrow 1/x^+, & x^- &\rightarrow x^-, \\ u \rightarrow u^{2\gamma} : \quad x^+ &\rightarrow 1/x^+, & x^- &\rightarrow 1/x^-, \\ u \rightarrow u^{3\gamma} : \quad x^+ &\rightarrow 1/x^+, & x^- &\rightarrow x^-, \\ u \rightarrow u^{4\gamma} : \quad x^+ &\rightarrow x^+, & x^- &\rightarrow x^-. \end{aligned}$$

In the same way, the mirror particles on the hexagon form factor is defined by the mirror transformation:



Furthermore, the S-matrix of the mirror particles is also given by

$$S(u^\gamma, v^\gamma) = \frac{h(u^\gamma, v^\gamma)}{h(v^\gamma, u^\gamma)}. \quad (5.50)$$

5.2 Four-point functions and hexagon method

In this section, we calculate the four-point functions of the BPS operators at one-loop by extending the hexagon method. Thus, we would like to reproduce the perturbative result (3.6).

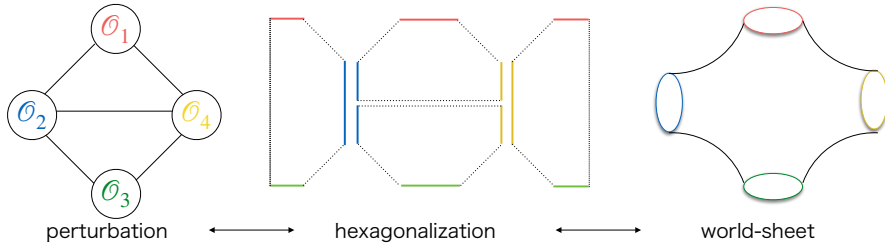


Figure 5.11: The most-left figure is in perturbative gauge theory realm, the middle figure is in hexagonalization realm and the most-right figure is in classical string theory realm.

The world-sheet diagram of the four-point functions is decomposed into four hexagons in figure 5.2. Since the BPS operator don't have any excitations, there are no magnons on the operator edge. Therefore, the one-loop correction comes from only the contributions of the mirror particles and gluing dashed edge:

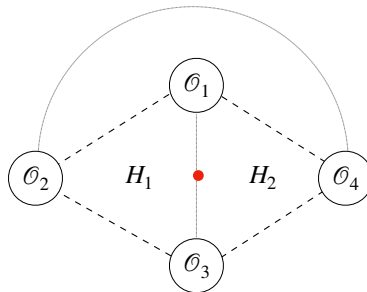
$$\text{1-loop dressed} = \int_{\square} \dots$$

5.2.1 Length two BPS operators

Let us consider the length two BPS operators. As discussed in section 1, the tree-level diagrams in this case are three disconnected diagrams and three connect diagrams. However, the disconnected diagrams have not correct power $1/N^{n-2}$. Therefore, we consider following connected diagrams:

$$d_{12}d_{23}d_{34}d_{41}, \quad d_{12}d_{13}d_{34}d_{24}, \quad d_{23}d_{13}d_{41}d_{24}. \quad (5.51)$$

In particular, we focus on one-mirror magnon on the zero-length edge between the operators \mathcal{O}_1 and \mathcal{O}_3 :



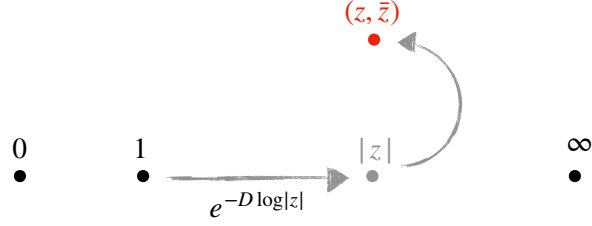


Figure 5.12: Using the conformal transformation, the operator \mathcal{O}_4 is located at the point written by the cross ratio (z, \bar{z}) .

As mentioned in section (5.1.5), the mirror contribution have the propagation factor $e^{iE\ell_{ij}}$. Then, the energy is a function of the coupling constant. Therefore, if we consider the mirror correction at the lower order of the coupling constants, we should put the mirror particles on the zero-bridge length $\ell_{ij} = 0$. For the other diagrams in (5.51), we can obtain by the replacement of the operators.

In order to reproduce the perturbative results, we should get the cross-ratio dependence and one-loop conformal integral from this mirror particle contribution. In what follows, we discuss how to glue the these hexagons for four-point functions.

5.2.2 Conformal transformation of the hexagon

We now recall the three-point functions with diagonal $PSU(2|2, 4)$ symmetry. When we consider the hexagon in terms of the symmetry, the operators were put on the canonical configuration. In the same way, we put a hexagon \mathcal{H}_1 on the canonical positions as follows:

$$\mathcal{O}_1 : x_1 = (0, 0, 0, 0), \quad \mathcal{O}_2 : x_2 = (1, 0, 0, 0), \quad \mathcal{O}_3 : x_3 = (\infty, 0, 0, 0). \quad (5.52)$$

On the other hand, the other hexagon with operator \mathcal{O}_4 should depend the cross ratios. Thus, the hexagon \mathcal{H}_2 is not canonical and is given by the conformal transformation (see figure 5.12)

$$e^{-D \log |z|} e^{iL\phi}, \quad (5.53)$$

where L and ϕ are combinations of the elements of the $PSU(2|2)^2$

$$L \equiv \frac{1}{2}(L^1_1 - L^2_2 - L^1_{\dot{1}} - L^2_{\dot{2}}), \quad e^{i\phi} \equiv \sqrt{\frac{z}{\bar{z}}}. \quad (5.54)$$

In the same argument, the R -symmetry part is also transformed as

$$e^{J \log |\alpha|} e^{iR\theta} \quad (5.55)$$

with

$$R \equiv \frac{1}{2}(R^1_1 - R^2_2 - R^1_{\dot{1}} - R^2_{\dot{2}}), \quad e^{i\theta} \equiv \sqrt{\frac{\alpha}{\bar{\alpha}}}. \quad (5.56)$$

	L	R
ψ^1	$+1/2$	0
ψ^2	$-1/2$	0
ϕ^1	0	$+1/2$
ϕ^2	0	$-1/2$

Table 5.1: Charges of the fundamental magnons

Combing them, the generator which is transformed \mathcal{H}_2 to \mathcal{H}_1 is given by

$$g \equiv e^{-D \log |z|} e^{iL\phi} e^{J \log |\alpha|} e^{iR\theta} \quad (5.57)$$

Thus, using the notation of the mirror momentum

$$\frac{D - J}{2} = E = i\tilde{p}, \quad (5.58)$$

we have

$$g = e^{-2i\tilde{p}_\psi \log |z|} e^{J_\psi \varphi} e^{iL_\psi \phi} e^{iR_\psi \theta} \quad (5.59)$$

with

$$e^\varphi = \left| \frac{\alpha}{z} \right|. \quad (5.60)$$

5.2.3 Gluing the hexagons

In order to glue the hexagons, the idea is that we first transform the hexagons to the canonical configuration and we second insert the complete basis:

$$\langle \mathcal{H}_1 | e^{i\tilde{E}\ell_{13}} | \mathcal{H}_2 \rangle \rightarrow \sum_{\psi} \langle \mathcal{H}_1 | \psi \rangle \langle \psi | e^{i\tilde{E}\ell_{13}} \tilde{g} | \psi \rangle \langle \psi | \mathcal{H}_1 \rangle. \quad (5.61)$$

where \tilde{g} is a generator of diagonal $PSU(2|2)$. The \sum_{ψ} means sum over rapidity, bound states and flavors. Then, the factor $\langle \mathcal{H}_1 | \psi \rangle$ is just the ordinary canonical hexagon form factor.

Here, referring the generator of $PSU(2|2)^2$, the generator \tilde{g} is given by

$$\tilde{g} = e^{-2i\tilde{p}_\psi \log |z|} e^{2J_\psi \varphi} e^{i\tilde{L}_\psi \phi} e^{i\tilde{R}_\psi \theta}. \quad (5.62)$$

where \tilde{L} and \tilde{R} is defined as

$$\tilde{L} \equiv \frac{1}{2}(L_1^1 - L_2^2), \quad \tilde{R} \equiv \frac{1}{2}(R_1^1 - R_2^2) \quad (5.63)$$

The charges of the left and right parts are given in table 5.1.

In the computation of (5.61), the non-trivial part is the trace of the generator \tilde{g} . We now compute the trace of the flavor part with bound state. In particular, we first treat the following part

$$\mathrm{tr}_a[(-1)^F e^{i\tilde{L}\phi+i\tilde{R}\theta}], \quad (5.64)$$

where a is bound state indices and F is a fermion number. The basis including the bound states which have been known as the a -th anti-symmetric representation are given by

$$|\psi_{\alpha_1} \cdots \psi_{\alpha_a}\rangle + \cdots, \quad |\phi_1 \psi_{\alpha_1} \cdots \psi_{\alpha_{a-1}}\rangle + \cdots, \quad (5.65)$$

$$|\phi_2 \psi_{\alpha_1} \cdots \psi_{\alpha_{a-1}}\rangle + \cdots, \quad |\phi_1 \phi_2 \psi_{\alpha_1} \cdots \psi_{\alpha_{a-2}}\rangle + \cdots, \quad (5.66)$$

with $\alpha_i = 1, 2$. Then, the trace of the flavors are given by

$$\mathrm{tr}_a[(-1)^F e^{i\phi\tilde{L}+i\theta\tilde{R}}] = (-1)^a \left(e^{ia\phi} \sum_{n=0}^a e^{-2in\phi} - 2 \cos \theta e^{i(a-1)\phi} \sum_{n=0}^{a-1} e^{-2in\phi} + e^{i(a-2)\phi} \sum_{n=0}^{a-2} e^{-2in\phi} \right) \quad (5.67)$$

$$= 2(-1)^a (\cos \phi - \cos \theta) \frac{\sin a\phi}{\sin \phi}. \quad (5.68)$$

Finally, we consider the J -charge factor⁹. Then, the result is modified as

$$\mathrm{tr}_a[(-1)^F e^{2\varphi J+i\phi\tilde{L}+i\theta\tilde{R}}] = 2(-1)^a (\cos \theta - \cosh \varphi \cos \theta) \frac{\sin a\phi}{\sin \phi}. \quad (5.69)$$

5.2.4 BPS four operators at one-loop

Using the result (5.69), the contributions of the gluing the hexagons are given by

$$\mathrm{int}_a^{1-3}(v) = \frac{2(\cos \theta - \cosh \varphi \cos \theta) \sin a\phi}{\sin \phi} \mu_a(v^\gamma) e^{-2i\tilde{p}(v) \log |z|} e^{-\tilde{E}\ell_{13}}. \quad (5.70)$$

We now set $\ell_{13} = 0$ and use the weak-coupling expansions of the measure factor

$$\mu_a(v^\gamma) = \frac{\lambda}{16\pi^2} \frac{a}{(v^2 + a^2/4)^2} + \mathcal{O}(g^4). \quad (5.71)$$

Then, the integrand is given by

$$\mathrm{int}_a^{1-3}(v) = \frac{2\lambda(\cos \theta - \cosh \varphi \cos \theta) \sin a\phi}{16\pi^2 \sin \phi} \frac{a}{(v^2 + a^2/4)^2} e^{-2iv \log |z|}. \quad (5.72)$$

⁹Due to the supersymmetry, it is known that the J -charge is shifted since the supercharges have $\pm 1/2$ J -charges: $|\psi\rangle \xrightarrow{Q,S} |Z^{\pm 1/2}\phi\rangle$, where Z called Z -marker and modify the difference of the J -charge.

Therefore, by summing over the bound states and rapidity, one mirror-magnon contribution on the edge between the hexagons \mathcal{H}_1 and \mathcal{H}_2 at one-loop is given by

$$\mathcal{M}_{z,\alpha} \equiv \sum_{a=1}^{\infty} \int \frac{dv}{2\pi} \text{int}_a(v) \quad (5.73)$$

$$= \frac{\lambda}{16\pi^2} [2(z + \bar{z}) - (\alpha^{-1} + \bar{\alpha}^{-1})(z\bar{z} + \alpha\bar{\alpha})] \Phi(z, \bar{z}). \quad (5.74)$$

Here, $\Phi(z, \bar{z})$ is the so-called one-loop conformal integral

$$\Phi(z, \bar{z}) = \frac{2\text{Li}_2(z) - 2\text{Li}_2(\bar{z}) + \log(z\bar{z}) \log \frac{1-z}{1-\bar{z}}}{z - \bar{z}}. \quad (5.75)$$

Using this result, we can reproduce the perturbative result. In particular, we consider the four-point functions of the BPS operators with length two. For the tree-level contraction $d_{12}d_{23}d_{34}d_{41}$, we get the following one-loop result:

In addition, the other contributions are given by the replacement of the space-time labels. Namely, the others are given by the transformations $z \rightarrow 1 - z$ and $z \rightarrow z/(z - 1)$. Therefore, the four-point function is given by

$$\begin{aligned} & \langle \mathcal{O}_1^{\text{BPS}(2)}(x_1) \mathcal{O}_2^{\text{BPS}(2)}(x_2) \mathcal{O}_3^{\text{BPS}(2)}(x_3) \mathcal{O}_4^{\text{BPS}(2)}(x_4) \rangle_{\text{one-loop}} \\ &= 2 \left(d_{12}d_{24}d_{34}d_{13} \mathcal{M}_{z,\alpha} + d_{13}d_{23}d_{24}d_{14} \mathcal{M}_{1-z,1-\alpha} + d_{12}d_{23}d_{34}d_{14} \mathcal{M}_{\frac{z}{z-1}, \frac{\alpha}{\alpha-1}} \right) \\ &= -\frac{\lambda}{8\pi^2} \tilde{R}_{1234} \Phi(z, \bar{z}). \end{aligned}$$

where \tilde{R}_{1234} is given by

$$\tilde{R}_{1234} = \frac{(z - \alpha)(z - \bar{\alpha})(\bar{z} - \alpha)(\bar{z} - \bar{\alpha})}{z\bar{z}(1 - z)(1 - \bar{z})} d_{13}^2 d_{24}^2. \quad (5.76)$$

The result completely match as the perturbation result (3.25).

5.2.5 Some developments of the hexagonalization

As a short comment, we would like to introduce some developments of hexagonalization. However, each content is highly technical to explain here, and we do not explain details.

For the three-point functions, the contributions of a few mirror magnons were calculated in [62–64]. For the four-point functions, the contributions of the multi-mirror magnons on one edge were sufficiently calculated in [65–68]. In addition, the non-planar correlator were also done in [69, 70].

Part III

Correlators of operators on the Wilson loop

Chapter 6

Maldacena-Wilson loop

6.1 Maldacena-Wilson loop

Wilson loop is a nonlocal quantity which stems from a very massive quark in the fundamental representation moving along the loop [71]. In $\mathcal{N} = 4$ SYM, however, there are no fields in the fundamental representation since the all fields in $\mathcal{N} = 4$ SYM belong to adjoint representation of the gauge group. In order to consider such a field in the context of the AdS₅/CFT₄ correspondence, one consider the $SU(N+1)$ $\mathcal{N} = 4$ SYM and construct a heavy W-boson by breaking gauge symmetry to $SU(N) \times U(1)$ [72].

After doing so, the Wilson loop in AdS₅/CFT₄ correspondence, which is often called the Maldacena-Wilson loop [73, 74], is introduced by

$$W(C) = \frac{1}{N} \text{tr} \mathbf{P} \exp \left[\oint_C d\tau (iA_\mu(x)\dot{x}^\mu + \phi_i(x)n^i|\dot{x}|) \right] \quad (6.1)$$

with $n^2 = 1$. The important role of the quantity is what the supersymmetry is partially remained, even though there is the Wilson loop [75]. Under the supersymmetry transformations of the gauge and scalar fields

$$\delta_\epsilon A_\mu = \bar{\Psi} \Gamma_\mu \epsilon, \quad \delta_\epsilon \phi(x) = \Gamma_i \epsilon, \quad (6.2)$$

the exponent of the Wilson loop become

$$\bar{\Psi} (i\Gamma_\mu \dot{x}^\mu(\tau) - \Gamma_i \theta^i |\dot{x}(\tau)|) \epsilon. \quad (6.3)$$

Due to the property of the gamma matrices $\{\Gamma^m, \Gamma^n\} = -2\eta^{mn}\mathbf{1}$, the square of the Dirac matrices $(i\Gamma_\mu \dot{x}^\mu(\tau) - \Gamma_i \theta^i |\dot{x}(\tau)|)^2$ equal to zero and half of the supersymmetry is remained. In addition, the case is occurred when the integrand is τ independent. This is only straight line case since $\dot{x}^\mu(\tau)$ is a constant. Thus, in the straight line configuration, the Wilson line operator is a BPS operator. Namely, it is independent of the coupling constant and

$$\langle W \rangle_{\text{line}} = 1. \quad (6.4)$$

On the other hand, when the path of the Wilson loop is not line, for example loop or rectangular, the expectation value has divergences. More generally, the Wilson line has a cusp, it has nontrivial divergences.

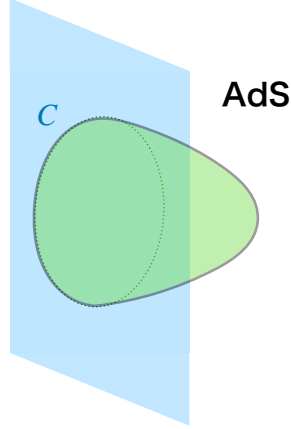


Figure 6.1: Wilson loop and minimal surface.

6.1.1 Wilson loop at the strong coupling

From the string in AdS point of view, the above discussion is corresponding to the configuration with a separated single D3-brane and N stacked D3-branes. In addition, an open string is stretched between them. Then, when we consider the infinite distance between a separated D3-brane and stacked D3-branes, the mass of the stretched open string become infinite corresponding to the heavy W-boson. In the AdS side the heavy open string interacted with closed string is propagated with the boundary condition characterized by the path C . Thereby, in the AdS/CFT correspondence the expectation value of the Wilson loop is given by the path integral of the string propagating with boundary on the path C :

$$\langle W \rangle = \int_{\partial X=C} \mathcal{D}X \exp \left(-\sqrt{\lambda} S[X] \right) \quad (6.5)$$

Here, X represents bosonic and fermionic coordinates. In particular, for the large λ case, the path integral is estimated by the area of the minimal surface bounded by the path C [76]:

$$\langle W \rangle \sim \exp \left(-\sqrt{\lambda} \times \text{area} \right) \quad (6.6)$$

Namely, the expectation value of the Wilson loop with path C is related to the minimal surface of the open string bounded by the path C in figure 6.1.

6.1.2 Wilson loop in perturbation theory

In the Wilson loop, the one-loop correction is given by

$$\langle W \rangle_C = 1 + \frac{\lambda}{16\pi^2} \oint_C d\tau_1 d\tau_2 \frac{|\dot{x}(\tau_1)| |\dot{x}(\tau_2)| - \dot{x}(\tau_1) \cdot \dot{x}(\tau_2)}{|x(\tau_1) - x(\tau_2)|^2} + \dots \quad (6.7)$$

The $|\dot{x}(\tau_1)||\dot{x}(\tau_2)|$ term in the integrand comes from the scalar exchange in the Wilson loop. Furthermore, the $\dot{x}(\tau_1) \cdot \dot{x}(\tau_2)$ term comes from the gauge field exchange.

We now take the line configuration, that is, $x(\tau) = (\tau, 0, 0, 0)$. In this case, the one-loop correction trivially vanishes. It's implied the BPS condition. On the other hand, for the case of the loop configuration, that is, $x(\tau) = (\cos \tau, \sin \tau, 0, 0)$, the denominator is written as

$$|x(\tau_1) - x(\tau_2)|^2 = 2(1 - \dot{x}(\tau_1) \cdot \dot{x}(\tau_2)). \quad (6.8)$$

Thus, the one-loop correction have nontrivial value

$$\oint_C d\tau_1 d\tau_2 \frac{|\dot{x}(\tau_1)||\dot{x}(\tau_2)| - \dot{x}(\tau_1) \cdot \dot{x}(\tau_2)}{|x(\tau_1) - x(\tau_2)|^2} = \frac{1}{2} \oint_C d\tau_1 d\tau_2 = \frac{(2\pi)^2}{2}. \quad (6.9)$$

Fortunately, thanks to the supersymmetry, the contribution other than the ladder diagrams are canceled out. Thereby, using the recursion relation of the ladder diagrams, we can solve the finite coupling result of the expectation value of the circle Wilson loop as follows [77, 78]:

$$\langle W \rangle_{\text{circ}} = \frac{2}{\sqrt{\lambda}} I_1(\sqrt{\lambda}), \quad (6.10)$$

where I_1 is modified the Bessel function. The leading order in large λ [72, 79] can be also given by

$$\langle W \rangle_{\text{circ}}^{\text{strong}} = e^\lambda. \quad (6.11)$$

6.2 Cusp and operator insertions in Wilson loop

In what follows, we basically consider the line configurations of the Wilson line, which is surely BPS configuration and the expectation value become trivial one. Then, we can consider the deformations of them. The deformations are to make cusps in the Wilson loop. Due to the existence of the cusps, the expectation values have several divergences which have an important meaning for physics [80–83].

We first introduce the geodesic cusp. Namely, two Wilson lines are meeting with angle ϕ in \mathbb{R}^4 . As a different point of view by using the conformal transformation, the two lines run along the time direction in $S^3 \times \mathbb{R}$, see figure 6.2. For $\phi = 0$, the cusp disappears and the configuration is infinity line, which is the BPS. On the other hand, for $\phi = \pi$, the two lines are very close. Expectation value of such a configuration is related as the potential of the quark antiquark pair.

The other deformation is realized by two different scalars coupled into Wilson loop, see figure 6.3. We now introduce the deformation parameter θ as an inner product of the two $SO(6)$ vectors $\vec{n}_1 \cdot \vec{n}_2 = \cos \theta$. For $\theta = 0$, the scalars coupled to each Wilson line are same scalar field, which is the BPS configuration. For $\theta = \pi$, the two vectors are orthogonal. It means that the two scalars are completely different scalars.

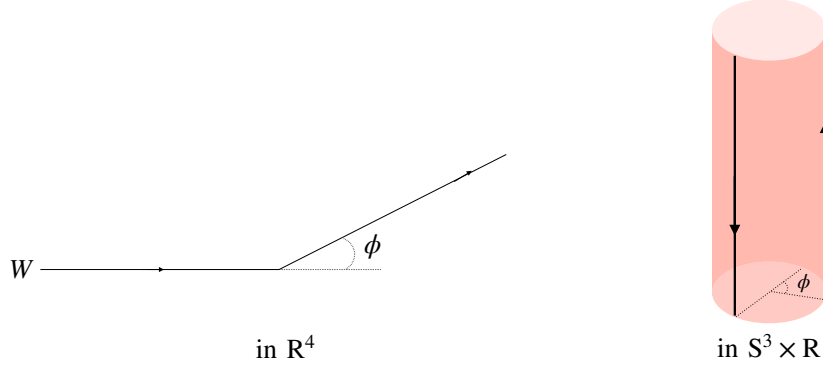


Figure 6.2: A cusped Wilson loop with the geodesic angle ϕ

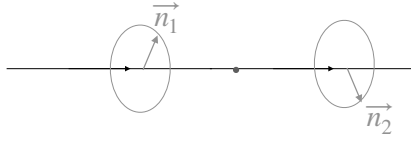


Figure 6.3: A cusped Wilson loop with the internal angle ϕ

As a further generalization, we can consider the operator insertion into the Wilson loop. While retaining the gauge invariance, we can insert local operators in the trajectory of the Wilson loop. In \mathbb{R}^4 , such a local operator shall be inserted at the cusp. In terms of $\mathbb{S}^3 \times \mathbb{R}$, the local operator is at past infinity and make the excitation of the Wilson loop, see figure 6.4. Furthermore, it will be corresponding to the excitation of the world sheet in AdS.

6.3 Set-up and notations

As mentioned in the section 6.1.2, the Maldacena-Wilson loop is given by

$$W(C) = \frac{1}{N} \text{tr} \mathbf{P} \exp \left[\oint_C d\tau (iA_\mu(x)\dot{x}^\mu + \Phi_i(x)n^i|\dot{x}|) \right]. \quad (6.12)$$

Using the non-local operator, the n -point functions of the operators inserted into the Wilson loop can be introduced by

$$\langle \mathcal{W}[\mathcal{O}_1(x_1) \cdots \mathcal{O}_n(x_n)] \rangle \equiv \left\langle \frac{1}{N} \text{Tr} \left[\mathbf{P} \left(\mathcal{O}_1(x_1) \cdots \mathcal{O}_n(x_n) e^{\oint_C (iA_\mu \dot{x}^\mu + \Phi_6 |\dot{x}|) ds} \right) \right] \right\rangle. \quad (6.13)$$

More explicitly, the one operator insertion of the corrector (6.13) can be written as

$$\langle W[\mathcal{O}] \rangle \equiv \left\langle \text{Tr} \left[\text{Pexp} \left(\int_{-\infty}^{\tau} d\tau' iA_\mu \dot{x}^\mu + \phi_i n^i |\dot{x}^\mu| \right) \underbrace{Z^L}_{\mathcal{O}} \text{Pexp} \left(\int_{\tau}^{\infty} d\tau'' iA_\mu \dot{x}^\mu + \phi_i \tilde{n}^i |\dot{x}^\mu| \right) \right] \right\rangle, \quad (6.14)$$

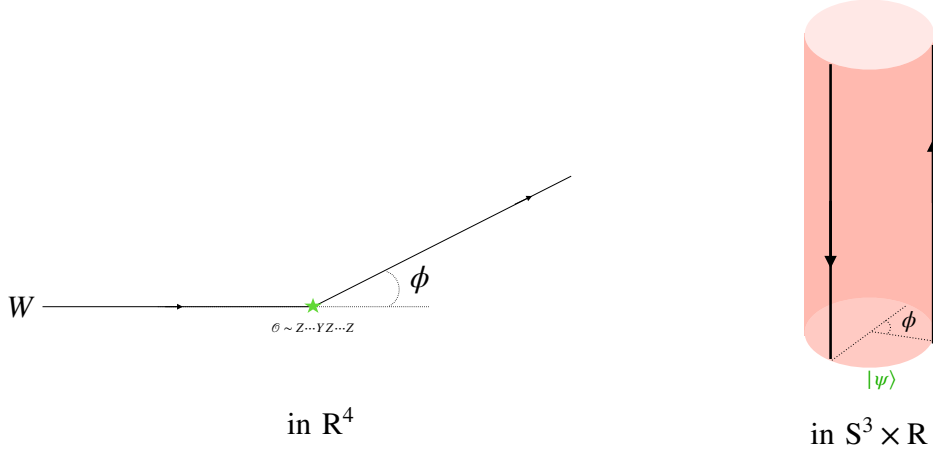


Figure 6.4: Operator inserted Wilson loop with geodesic cusp.

where Z is a complex scalar field.

Precisely speaking, to make contact with the defect CFT data, we should consider the *normalized* correlator which is obtained by dividing the correlator by the expectation value of the Wilson loop as [85, 112]

$$\langle\langle \mathcal{O}_1(x_1) \cdots \mathcal{O}_n(x_n) \rangle\rangle \equiv \frac{\langle \mathcal{W}[\mathcal{O}_1(x_1) \cdots \mathcal{O}_n(x_n)] \rangle}{\langle \mathcal{W} \rangle}. \quad (6.15)$$

For the straight-line Wilson loop, this manipulation is trivial since the expectation value of the Wilson loop is unity while for the circular Wilson loop it involves the division by the planar expectation value,

$$\langle \mathcal{W} \rangle_{\text{circle}} = \frac{2}{\sqrt{\lambda}} I_1(\sqrt{\lambda}), \quad (6.16)$$

with λ being the 't Hooft coupling constant $\lambda \equiv g_{\text{YM}}^2 N$. The spacetime dependence of these correlators is constrained by the $SL(2, R)$ symmetry [85]. For instance, the two- and the three-point functions are given by

$$\begin{aligned} \langle\langle \mathcal{O}_1(x_1) \mathcal{O}_2(x_2) \rangle\rangle &= n_{L_1} \delta_{L_1, L_2} \times (d_{12})^{L_1}, \\ \frac{\langle\langle \mathcal{O}_1(x_1) \mathcal{O}_2(x_2) \mathcal{O}_3(x_3) \rangle\rangle}{\sqrt{n_{L_1} n_{L_2} n_{L_3}}} &= \frac{c_{L_1, L_2, L_3}}{\sqrt{N}} \times (d_{12})^{\frac{L_{12|3}}{2}} (d_{23})^{\frac{L_{23|1}}{2}} (d_{31})^{\frac{L_{31|2}}{2}}, \end{aligned} \quad (6.17)$$

where N is the rank of the gauge group, $L_{ij|k} \equiv L_i + L_j - L_k$ and d_{ij} is the free-field Wick contraction which takes the following form for the straight-line Wilson loop:

$$d_{ij}|_{\text{straight line}} = \frac{\lambda}{8\pi^2} \frac{Y_i \cdot Y_j}{x_{ij}^2}, \quad x_{ij}^2 \equiv |x_i - x_j|^2. \quad (6.18)$$

The quantity c_{L_1, L_2, L_3} is the structure constant of the defect CFT while n_L is the normalization of the two-point function. For the circular Wilson loop, one just needs to replace d_{ij} with

$$d_{ij}|_{\text{circle}} = \frac{\lambda}{8\pi^2} \frac{Y_i \cdot Y_j}{(2 \sin \frac{\tau_i - \tau_j}{2})^2}, \quad (6.19)$$

where τ_i parametrizes the position of the insertion on the circle and ranges from 0 to 2π . Note that the two expressions (6.18) and (6.19) are related by the conformal transformation.

On the other hand, the four-point function

$$\frac{\langle\langle \mathcal{O}_1(x_1)\mathcal{O}_2(x_2)\mathcal{O}_3(x_3)\mathcal{O}_4(x_4) \rangle\rangle}{\sqrt{n_{L_1}n_{L_2}n_{L_3}n_{L_4}}} \equiv \frac{G_{L_1,L_2,L_3,L_4}}{N}, \quad (6.20)$$

is a nontrivial function of the cross ratios. To see this explicitly, we strip off the space-time (and the R-symmetry) dependence from G_{L_1,L_2,L_3,L_4} as

$$G_{L_1,L_2,L_3,L_4} = d_{12}^{\frac{L_1+L_2}{2}} d_{34}^{\frac{L_3+L_4}{2}} \left(\frac{d_{24}}{d_{14}}\right)^{\frac{L_2-L_1}{2}} \left(\frac{d_{13}}{d_{14}}\right)^{\frac{L_3-L_4}{2}} g_{L_1,L_2,L_3,L_4}(\chi, \alpha, \bar{\alpha}). \quad (6.21)$$

Then, the remaining quantity g_{L_1,L_2,L_3,L_4} depends only on the cross ratios.

Let us now make one important remark: In one-dimensional (defect) CFTs, one should be careful about the ordering of the operators since the correlators with different orderings are not related by a simple analytic continuation even in the Euclidean kinematics. This is in marked contrast to the higher-dimensional CFTs in which one can continuously move one operator around another to reach a different configuration. In terms of the conformal cross ratio, the different orderings correspond to different ranges of χ as¹

$$\{2134\} : \chi \in [-\infty, 0], \quad \{1234\} : \chi \in [0, 1], \quad \{1324\} : \chi \in [1, \infty], \quad (6.22)$$

where $\{ijkl\}$ signifies the correlator with the operator ordering $\mathcal{O}_i\mathcal{O}_j\mathcal{O}_k\mathcal{O}_l$. Thus the above statement translates to the fact that the correlators with different values of χ are not simply related by the analytic continuation. In the rest of this paper, to avoid any possible confusions arising from this point, we always consider the correlators in the ordering $\{1234\}$. In other words, we always assume that the cross ratio χ takes the value between 0 and 1.

¹These are all possible orderings in the presence of the parity invariance.

Chapter 7

BPS operators – perturbation

In this chapter, we compute two-, three- and four-point functions of BPS operators up to one loop from perturbation theory.

As a set-up, we use the Maldacena-Wilson loop that mentioned in section 6.3. In this chapter, we, however, choose a specific scalar field coupled to Wilson loop to six-direction ϕ^6 :

$$W(C) = \frac{1}{N} \text{tr} \mathbf{P} \exp \left[\oint_C d\tau (iA_\mu(x)\dot{x}^\mu + \phi_6(x)|\dot{x}|) \right]. \quad (7.1)$$

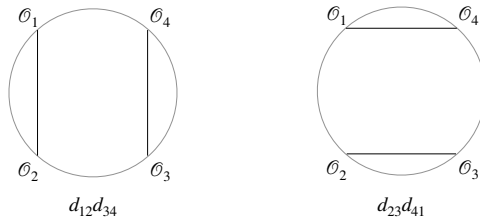
Instead, the BPS operator we consider in this chapter, don't include the scalar ϕ^6 :

$$\mathcal{O}_i^{\text{BPS}(L_i)}(x_i) = (Y_i \cdot \phi^i)^{L_i}(x_i),$$

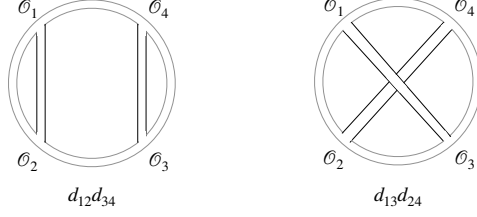
where Y^i satisfy $Y_6 = 0$ and $\sum_{i=1}^5 Y^i Y^i = 0$. In this configuration, there are no direct propagators between the BPS operators and Wilson loop.

7.1 Four-point functions at tree-level

As a warm up, let us consider the most trivial case, which has all the operator lengths one. Then, it has two contraction patterns:

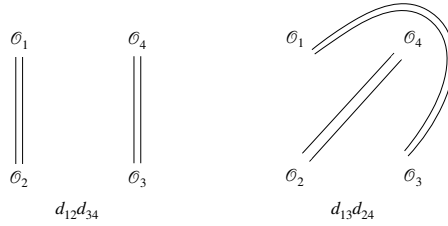


Here. we would like to mention that the contraction $d_{13}d_{24}$ are not dominant in this Wilson loop correlator since such contraction is suppressed in the large N limit. By using the double line notation, we can easily see the fact as:



In the left picture, the number of unicursal lines are four. On the other hand, the number of unicursal lines are two in the right picture. This shows that the contraction $d_{13}d_{24}$ become a non-planar correction in the large N theory.

Here it may be bit interesting to recall the single trace operator case. Because, the cross contraction $d_{13}d_{24}$ were dominant for the that case, for instance in the double line notation:



The above figure states that the number of unicursal lines of the contraction $d_{12}d_{34}$ are same with the one of the $d_{13}d_{24}$. More precisely, if there is a boundary such as the Wilson loop, the location of the operators are fixed and they have only contraction with the nearest neighbor operators. On the other hand, if there are no such boundaries, we should take into account the permutations of the operators. For that reason, the cross contraction is also dominant in the single trace operator case even the large N theory. This is one of the important differences between the “open”(with boundary) and “closed”(without boundary) operators theory.

The next simple examples are cases in which all the operators have length two and three, and then one have following contraction patterns.

$$\text{length two: } d_{12}^2 d_{34}^2, d_{12} d_{34} d_{23} d_{41}, d_{23}^2 d_{41}^2.$$

$$\text{length three: } d_{12}^3 d_{34}^3, d_{12}^2 d_{34}^2 d_{23} d_{41}, d_{12} d_{34} d_{23}^2 d_{41}^2, d_{23}^3 d_{41}^3.$$

It is easy to find that the tree-level diagrams of all the operator length L can be simply written as follows

$$\text{length } L : d_{12}^{L-x} d_{34}^{L-x} d_{14}^x d_{23}^x, \quad x = [0, \dots, L]. \quad (7.2)$$

Namely, the tree-level diagrams of the correlators of the operators with boundary arranged in a low with one-dimensional parameter x , see in figure 7.1. Also here, we can mention the relation with the tree-level diagrams of the single trace operators.

Let us recall the tree-level diagrams in section 3.1, the contractions were arranged in triangle as

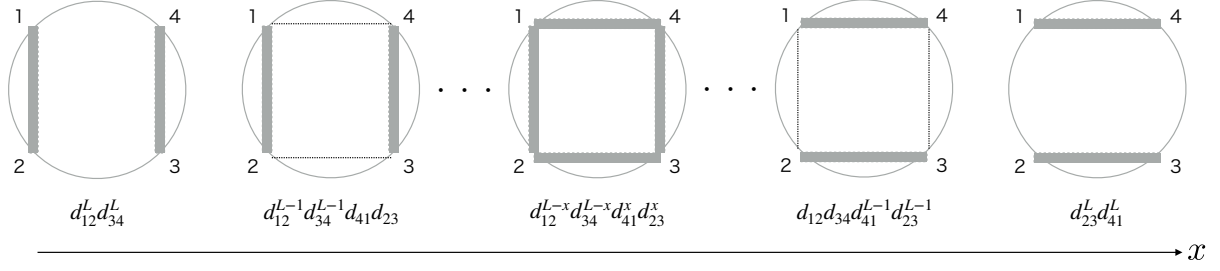


Figure 7.1: Tree-level four-point correlators which have all same operator lengths. The tree-level diagrams are on the one-parameter.

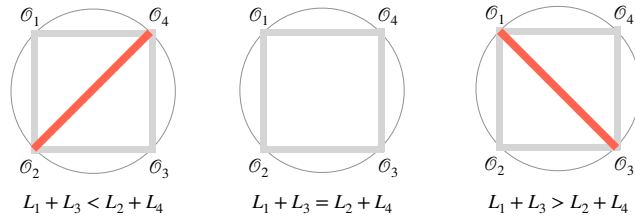
$$\begin{array}{ccc}
 d_{12}^L d_{34}^L & \cdots & d_{23}^L d_{41}^L \\
 & \ddots & \ddots \\
 & & d_{13}^L d_{24}^L
 \end{array}$$

Briefly, by using the double-parameters, they are summarized as

$$d_{12}^{L-x-y} d_{34}^{L-x-y} d_{14}^x d_{23}^x d_{13}^y d_{24}^y, \quad x = [0, \dots, L-y], \quad y = [0, \dots, L]. \quad (7.3)$$

Namely, the tree-level diagrams of the operators on the defect are simply given by a sub-multiplet, such as $y = 0$, of the cases without the defect.

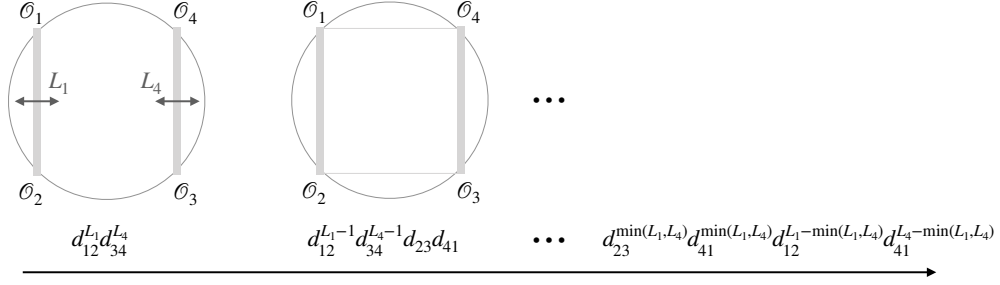
In this section, we try to generalize to the correlator with the operator lengths (L_1, L_2, L_3, L_4) . First of all, we divide the diagrams into three cases: $L_1 + L_3 = L_2 + L_4$, $L_1 + L_3 < L_2 + L_4$, and $L_1 + L_3 > L_2 + L_4$, which corresponds whether there are cross contractions, d_{13} or d_{24} , or not:



If we can get the correlator for the case of $L_1 + L_3 = L_2 + L_4$, the other cases are easily obtained by simple extensions. Therefore, we first consider the only $L_1 + L_3 = L_2 + L_4$ case in what follows.

Case $L_1 = L_2$ and $L_3 = L_4$ in Case $L_1 + L_3 = L_2 + L_4$

We further divide the diagrams and first consider the case of $L_1 = L_2$ and $L_3 = L_4$. The most-left contraction in the one-parameter diagrams is written as the $d_{12}^{L_1} d_{34}^{L_4}$. Then, the one-parameter is continued until that the lengths either ℓ_{12} or ℓ_{34} vanishes. Namely the diagram of the end of the one-parameter, which is at the most-right diagram, are characterized as $\min(L_1, L_4)$ such as



Therefore, for the case of $L_1 = L_2$ and $L_3 = L_4$, the diagrams are given by

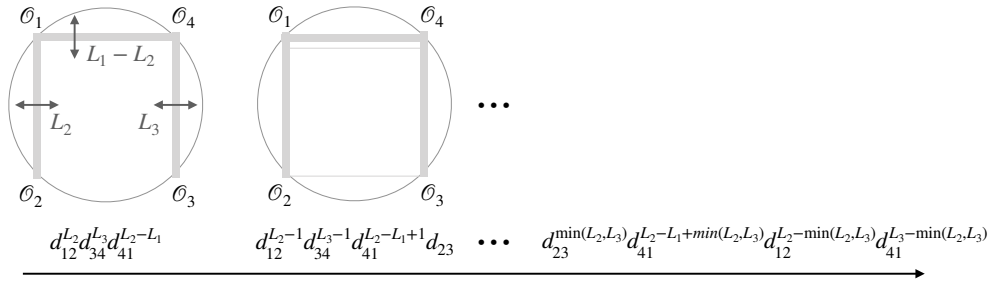
$$d_{12}^{L_1-x} d_{34}^{L_4-x} d_{23}^x d_{41}^x, \quad x = [0, \dots, \min(L_1, L_4)], \quad (7.4)$$

where we defined the function $\min(L_i, L_j)$ as follows:

$$\min(L_i, L_j) = \begin{cases} L_j & L_i \geq L_j \\ L_i & L_i < L_j \end{cases}. \quad (7.5)$$

Case $L_1 > L_2$ and $L_3 < L_4$ in Case $L_1 + L_3 = L_2 + L_4$

Secondly we consider the case of $L_1 > L_2$ and $L_3 < L_4$. In this case, the most-left contraction become $d_{12}^{L_2} d_{34}^{L_3} d_{41}^{L_1-L_2}$. In addition, by using the same one-parameter argument with the case of $L_1 = L_2$ and $L_3 = L_4$, the diagrams are written as

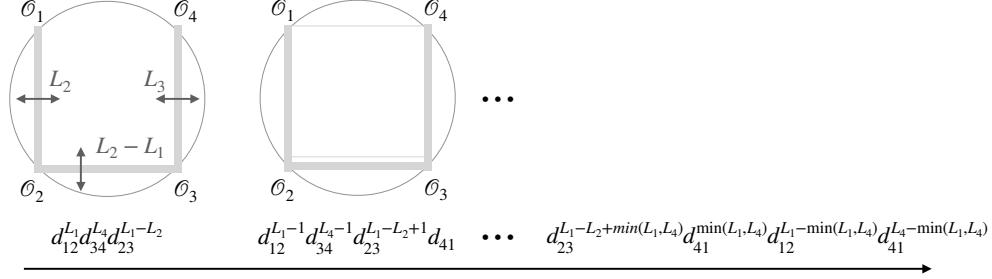


Therefore, for the case of $L_1 > L_2$ and $L_3 < L_4$, the diagrams are given by

$$d_{12}^{L_2-x} d_{34}^{L_3-x} d_{23}^x d_{41}^{L_2-L_1+x}, \quad x = [0, \dots, \min(L_2, L_3)]. \quad (7.6)$$

Case $L_1 < L_2$ and $L_3 > L_4$ in Case $L_1 + L_3 = L_2 + L_4$

Lastly, we consider the case of $L_1 < L_2$ and $L_3 > L_4$. The diagrams of this case are also parametrized as



Therefore, for the case of $L_1 < L_2$ and $L_3 > L_4$, the diagrams are given by

$$d_{12}^{L_1 - x} d_{34}^{L_4 - x} d_{41}^x d_{23}^{L_1 - L_2 + x}, \quad x = [0, \dots, \min(L_1, L_4)]. \quad (7.7)$$

Case $L_1 + L_3 = L_2 + L_4$: gathering three-pieces

By gathering three cases (7.4), (7.6) and (7.7), we can put together as

$$d_{12}^{\min(L_1, L_2) - x} d_{34}^{\min(L_3, L_4) - x} d_{41}^{\max(0, L_2 - L_1) + x} d_{23}^{\max(0, L_1 - L_2) + x} \quad (7.8)$$

$$\text{with } x = [0, \dots, \min(L_1, L_2, L_3, L_4)].$$

Case $L_1 + L_3 < L_2 + L_4$ and Case $L_1 + L_3 > L_2 + L_4$

In this cases, the diagrams have additional cross contractions. Such cross contractions have the following bridge lengths:

$$\ell_{13} \equiv \frac{1}{2}(L_1 + L_3 - L_2 - L_4), \quad \ell_{24} \equiv \frac{1}{2}(L_2 + L_4 - L_1 - L_3).$$

By taking into account these corrections to (7.8), we can write down tree-level contractions of the three-point functions of the BPS operators as follows:

$$\mathbf{H}_x^{L_1, L_2, L_3, L_4} \equiv d_{12}^{\min(\tilde{L}_1, \tilde{L}_2) - x} d_{34}^{\min(\tilde{L}_3, \tilde{L}_4) - x} d_{41}^{\max(0, \tilde{L}_2 - \tilde{L}_1) + x} d_{23}^{\max(0, \tilde{L}_1 - \tilde{L}_2) + x} d_{13}^{\max(0, \ell_{13})} d_{24}^{\max(0, \ell_{24})} \quad (7.9)$$

$$\text{with } x = [0, \dots, \min(\tilde{L}_1, \tilde{L}_2, \tilde{L}_3, \tilde{L}_4)],$$

where

$$\tilde{L}_1 = L_1 - \max(0, \ell_{13}), \quad \tilde{L}_3 = L_3 - \max(0, \ell_{13}),$$

$$\tilde{L}_2 = L_2 - \max(0, \ell_{24}), \quad \tilde{L}_4 = L_4 - \max(0, \ell_{24}).$$

Notice that the left-most diagrams, which is $\mathbf{H}_0^{L_1, L_2, L_3, L_4}$, have diagrams in figure 7.2.

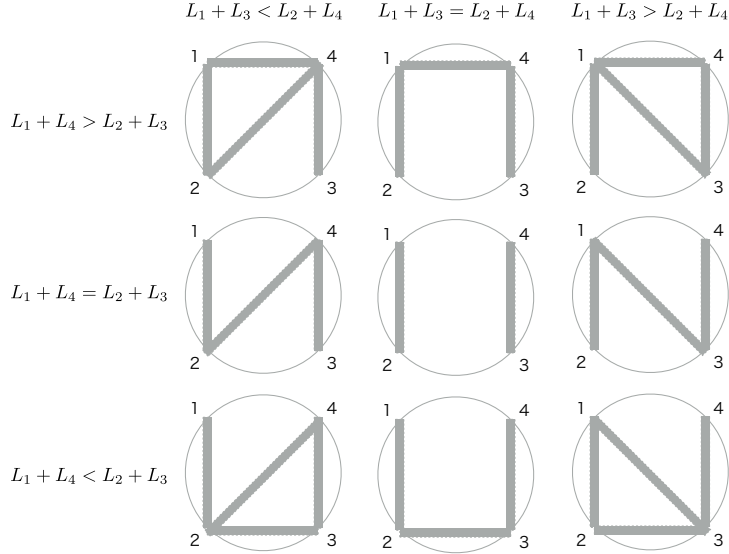


Figure 7.2: The left-most diagrams in the one-parameter, which is $\mathbf{H}_0^{L_1, L_2, L_3, L_4}$.

7.2 One-loop correlation functions of the BPS operators on the Wilson loop

In this section, we calculate the one-loop correlation functions of the BPS operators on the Wilson loop. Then, the one-loop diagrams are divided into two cases: whether the one-loop diagrams are contracting with the Wilson loop boundary or not. The cases of not contracting with the Wilson loop boundary has same diagrams with the correlation functions of the single trace operators in the section 3.2. However, each coefficient of the functions the we consider here is slightly different from the one of the single trace operators due to the boundary.

7.2.1 One-loop insertion formulas without Wilson loop boundary

Basic one-loop dressed diagrams not contracting with the Wilson loop in $\mathcal{N} = 4$ SYM are self-energy, gluon exchange and quartic scalar vertex diagrams in figure 7.3. First of all, the self-energy, which is two-body diagrams, has the same contribution with the case of the single trace operator such as

$$\text{self}_{12} = \frac{\lambda}{8\pi^2} \left(-2 \log \frac{x_{21}}{\epsilon} - 2 \right). \quad (7.10)$$

On the other hand, the other four-body diagrams should be added 1/2 factors from the result of the G_{1234} and S_{1234} . Roughly speaking, the gluon propagator in $G_{1234}^{\text{boundary}}$ and scalar quartic interaction in $S_{1234}^{\text{boundary}}$ can be contracted only at inside of the four-

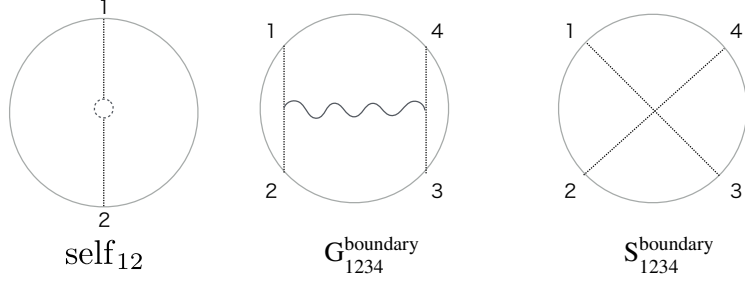


Figure 7.3: Basic one-loop diagrams on the Wilson loop boundary

$$\frac{1}{2}\text{CI}_{123}d_{12}d_{23} = \frac{1}{4} \left[\begin{array}{c} \text{Diagram 1} \\ \text{Diagram 2} \end{array} \right] + \begin{array}{c} \text{Diagram 3} \\ \text{Diagram 4} \end{array}$$

Figure 7.4: Corner diagrams on the Wilson loop boundary

operators.¹ Therefore, we have

$$\text{G}_{1234}^{\text{boundary}} = \frac{1}{2}\text{G}_{1234}, \quad \text{S}_{1234}^{\text{boundary}} = \frac{1}{2}\text{S}_{1234}. \quad (7.11)$$

Thus, the corner interaction with boundary in figure 7.4 has also half contribution as

$$\text{CI}_{123}^{\text{boundary}} d_{12}d_{23} \equiv \frac{1}{2}\text{CI}_{123}d_{12}d_{23} = \left[\frac{1}{4}(\text{self}_{12} + \text{self}_{23}) + \text{G}_{1223}^{\text{boundary}} \right] d_{12}d_{23} + \text{S}_{1223}^{\text{boundary}}. \quad (7.12)$$

Furthermore, the D_{1234} -function is also given by

$$\begin{aligned} \frac{1}{2}D_{1234} &= \left(\text{G}_{1234}^{\text{boundary}} - \frac{1}{2}\text{CI}_{12,43} \right) d_{12}d_{34} + \left(\text{G}_{4123}^{\text{boundary}} - \frac{1}{2}\text{CI}_{14,23} \right) d_{14}d_{23} + \text{S}_{1234}^{\text{boundary}} \\ &= \frac{\lambda}{32\pi^2} \Phi(z, \bar{z}) (2d_{13}d_{24} - ((1-z) + (1-\bar{z}))d_{14}d_{23} - (z + \bar{z})d_{12}d_{34}). \end{aligned} \quad (7.13)$$

7.2.2 One-loop insertion formulas with Wilson loop boundary

We next calculate the one-loop insertion formulas contracting with the Wilson loop boundary. In the Lagrangian of $\mathcal{N} = 4$, such contractions are occurred only through the scalar-scalar-gauge vertex and the gauge field comes from the Wilson loop. In what follows, we calculate the line configurations for all diagrams.

¹On the other hand, the diagrams without boundary, G_{1234} and S_{1234} , include the contribution that contracted at the out side of the four-operators. More rigorously, we can see the $1/2$ factor from the difference of the trace of the gauge group.

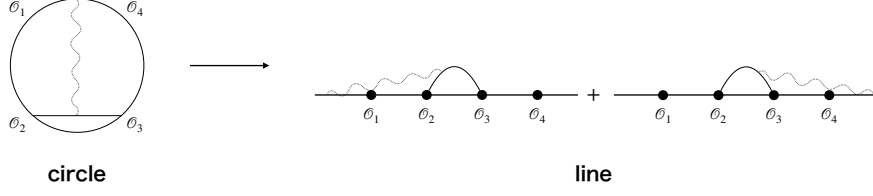


Figure 7.5: Four-point boundary diagrams $T_{23,14}$

It is useful to first introduce the four-point boundary diagram in figure 7.5. The diagram in the straight line configuration is given by

$$\begin{aligned}
T_{23,14}d_{23} \equiv & \int_{-\infty}^{x_1} d\tau \left\langle \text{Tr}[\mathcal{A}(\tau)\Phi_2(x_2)\Phi_3(x_3)] \left(\frac{2i}{g_{\text{YM}}^2} \int d^4x \text{Tr}\{\partial_\mu\phi(x)[A_\mu(x),\phi(x)]\} \right) \right\rangle \\
& + \int_{x_4}^{\infty} d\tau \left\langle \text{Tr}[\Phi_2(x_2)\Phi_3(x_3)\mathcal{A}(\tau)] \left(\frac{2i}{g_{\text{YM}}^2} \int d^4x \text{Tr}\{\partial_\mu\phi(x)[A_\mu(x),\phi(x)]\} \right) \right\rangle.
\end{aligned} \tag{7.14}$$

where $\Phi_i \equiv n_i \cdot \phi$, $i = (1, 2, 3, 4)$ and $\mathcal{A} \equiv A_\mu \dot{x}^\mu$. By calculating them, we get

$$\begin{aligned}
T_{23,14} = & \frac{\lambda}{8\pi^2} \left(-4\zeta(2) + 2\zeta(2)\text{Li}_R \left[\frac{x_{21}}{x_{31}} \right] + 2\zeta(2)\text{Li}_R \left[\frac{x_{43}}{x_{42}} \right] \right) \\
& - \frac{1}{3}(\text{CI}_{123}^{\text{boundary}} - \text{CI}_{231}^{\text{boundary}} + \text{CI}_{234}^{\text{boundary}} - \text{CI}_{324}^{\text{boundary}}).
\end{aligned} \tag{7.15}$$

The function $\text{Li}_R[x] \equiv \frac{6}{\pi^2}(\text{Li}_2[x] + \frac{1}{2} \log x \log(1-x))$ is so-called Roger's Dilogarithm, which has a ‘‘crossing’’ like property:

$$\text{Li}_R[x] + \text{Li}_R[1-x] = 1. \tag{7.16}$$

Thus, the other four-body diagram in figure 7.6 is given by

$$\begin{aligned}
T_{14,23} = & \frac{\lambda}{8\pi^2} \left(8\zeta(2) + 2\zeta(2)\text{Li}_R \left[\frac{x_{43}}{x_{31}} \right] + 2\zeta(2)\text{Li}_R \left[\frac{x_{21}}{x_{42}} \right] \right) \\
& - \frac{1}{3}(\text{CI}_{341}^{\text{boundary}} - \text{CI}_{413}^{\text{boundary}} + \text{CI}_{412}^{\text{boundary}} - \text{CI}_{142}^{\text{boundary}}).
\end{aligned} \tag{7.17}$$

Notice that we must be careful that the diagram $T_{23,14}$ is not simply related to the diagram $T_{14,23}$ by the rotation of the space-time. The difference comes from whether the gluon propagator go to infinity or not. Although it may seem strange, there are no problem. It is Because it is no reason that the diagram has rotation property at the each diagrammatic level. In fact, there is the rotation property at the correlator level.

We next calculate the three-body diagrams in figure 7.7. Such diagrams are given by collapsed limit of the space-time points from the four-body diagram $T_{23,14}$ and $T_{14,23}$.

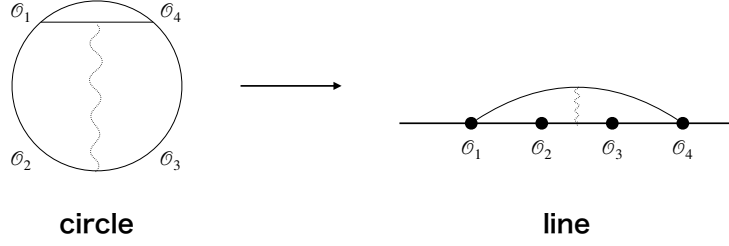


Figure 7.6: Four-point boundary diagrams $T_{14,23}$

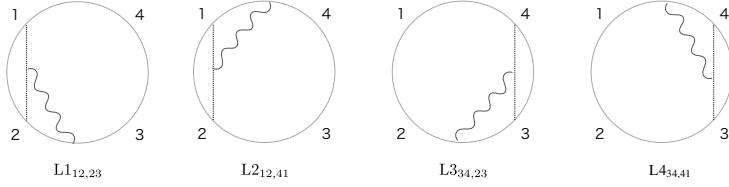


Figure 7.7: Three-point basic boundary diagrams

Then, we use the point-splitting regularization since the diagrams have divergence. For instance, the $L_{12,23}$ is given as follows:

$$L_{434,41} = \lim_{x \rightarrow 4+\epsilon} T_{34,x1}. \quad (7.18)$$

In the same way, by calculating the other diagrams, we obtain ²

$$L_{12,23} = \frac{\lambda}{8\pi^2} \left(\frac{1}{2} - 2\zeta(2) + \frac{1}{2} \log \frac{x_{21}}{\epsilon} + 2\zeta(2) \text{Li}_R \left[\frac{x_{21}}{x_{31}} \right] \right) + \frac{1}{3} (\text{CI}_{123}^{\text{boundary}} - \text{CI}_{312}^{\text{boundary}}),$$

$$L_{212,41} = \frac{\lambda}{8\pi^2} \left(\frac{1}{2} - 2\zeta(2) + \frac{1}{2} \log \frac{x_{21}}{\epsilon} - 2\zeta(2) \text{Li}_R \left[\frac{x_{21}}{x_{41}} \right] \right) + \frac{1}{3} (\text{CI}_{412}^{\text{boundary}} - \text{CI}_{124}^{\text{boundary}}),$$

$$L_{334,23} = \frac{\lambda}{8\pi^2} \left(\frac{1}{2} - 2\zeta(2) + \frac{1}{2} \log \frac{x_{43}}{\epsilon} + 2\zeta(2) \text{Li}_R \left[\frac{x_{43}}{x_{42}} \right] \right) + \frac{1}{3} (\text{CI}_{234}^{\text{boundary}} - \text{CI}_{243}^{\text{boundary}}),$$

$$L_{434,41} = \frac{\lambda}{8\pi^2} \left(\frac{1}{2} - 2\zeta(2) + \frac{1}{2} \log \frac{x_{43}}{\epsilon} - 2\zeta(2) \text{Li}_R \left[\frac{x_{43}}{x_{41}} \right] \right) + \frac{1}{3} (\text{CI}_{341}^{\text{boundary}} - \text{CI}_{431}^{\text{boundary}}).$$

Furthermore, the two-body diagrams in fig (7.8) are given by the further limit and we have

$$\text{DK}_{12} \equiv \frac{\lambda}{8\pi^2} \left(1 + 2\zeta[2] + \log \frac{x_{12}}{\epsilon} \right), \quad (7.19)$$

$$\text{DK}_{21} \equiv \frac{\lambda}{8\pi^2} \left(1 - 4\zeta[2] + \log \frac{x_{12}}{\epsilon} \right). \quad (7.20)$$

²The pictures are written as the circle configuration for simplicity. However, the equations are line configuration results. As a consistency check, we directly calculate the three-body diagrams, and we saw that these results are exactly match.

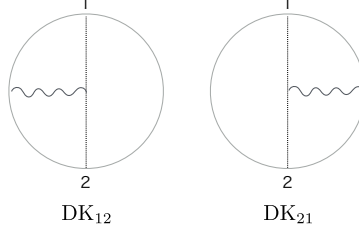


Figure 7.8: Two-point basic boundary diagrams

It is useful to combine some diagrams to make cross ratio functions without divergence:

$$\begin{aligned}
\mathbf{L}_{12,34} &\equiv (\mathbf{L}_{12,23} + \mathbf{L}_{212,41} + \mathbf{L}_{34,23} + \mathbf{L}_{434,41}) + \frac{1}{2}\text{self}_{12} + \frac{1}{2}\text{self}_{34} \\
&= \frac{\lambda}{8\pi^2} (-8\zeta(2) + 2\zeta(2)\text{Li}_R[z]) - \text{CI}_{12,43}^{\text{boundary}}, \tag{7.21}
\end{aligned}$$

$$\begin{aligned}
\mathbf{Table}_{1234} &\equiv (\mathbf{L}_{212,41} + \mathbf{L}_{434,41} + \mathbf{T}_{23,14}) + \text{CI}_{123}^{\text{boundary}} + \text{CI}_{234}^{\text{boundary}} + \frac{1}{4}\text{self}_{12} + \frac{1}{4}\text{self}_{34} \\
&= \frac{\lambda}{8\pi^2} (-8\zeta(2) + 2\zeta(2)\text{Li}_R[z]) - \text{CI}_{14,23}^{\text{boundary}} \tag{7.22}
\end{aligned}$$

$$\begin{aligned}
\mathbf{B}_{12} &= \text{DK}_{12} + \frac{1}{2}\text{self}_{12} \\
&= \frac{\lambda}{8\pi^2} (2\zeta(2)), \tag{7.23}
\end{aligned}$$

$$\begin{aligned}
\mathbf{B}'_{12} &= \text{DK}_{21} + \frac{1}{2}\text{self}_{12} \\
&= \frac{\lambda}{8\pi^2} (-4\zeta(2)). \tag{7.24}
\end{aligned}$$

Then, we used the five-term relation for the Rogers Dilogarithm

$$\text{Li}_R[x] + \text{Li}_R[y] - \text{Li}_R\left[\frac{x(1-y)}{1-xy}\right] - \text{Li}_R\left[\frac{y(1-x)}{1-xy}\right] - \text{Li}_R[xy] = 0. \tag{7.25}$$

7.3 One-loop correlation functions

7.3.1 Two- and three-point functions

By using the one-loop insertion formulas discussed above, we would like to calculate the one-loop correlation functions. We first consider the two-point functions with the operator length L . Then, there are a lot of one-loop diagrams:

$$(L-1) \text{S}_{1221}^{\text{boundary}}, (L-1) \text{G}_{1221}^{\text{boundary}}, L \text{self}_{12}, \text{DK}_{12}, \text{DK}_{21}. \tag{7.26}$$

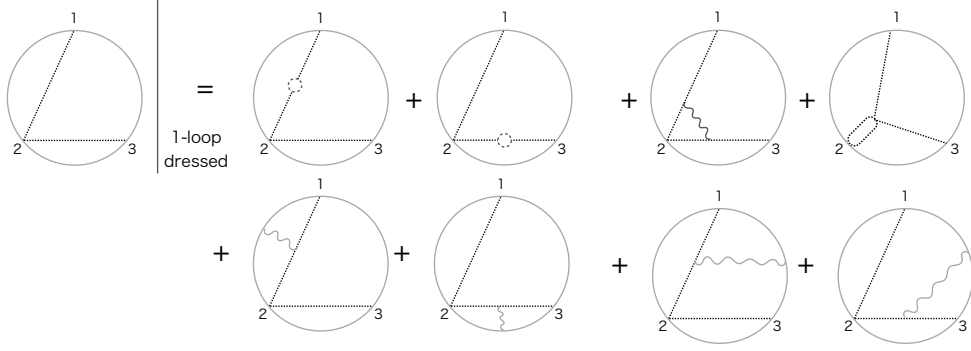


Figure 7.9: One-loop dressed diagram with zero-bridge length

Using the explicit form of the functions of S_{1223} and G_{1221} in appendix A, we find

$$S_{1221}^{\text{boundary}} + G_{1221}^{\text{boundary}} + \text{self}_{12} = 0. \quad (7.27)$$

Then, the remaining diagrams are only \mathbf{B}_{12} and \mathbf{B}'_{12} . Namely, the two-point functions are given by

$$\langle\langle \mathcal{O}_1^{\text{BPS}(L)} \mathcal{O}_1^{\text{BPS}(L)} \rangle\rangle_{1\text{-loop}} = (\mathbf{B}_{12} + \mathbf{B}'_{12}) d_{12}^L = -\frac{\lambda}{8\pi^2} 2\zeta(2) d_{12}^L. \quad (7.28)$$

Notice that the two-point function of the BPS operators on the Wilson loop doesn't vanish unlike one of the single-trace BPS operators.³

Next, we calculate the three-point functions in the same way as the two-point functions. The difference is what the three-point functions have two-type contractions at the tree-level whether there is a zero-bridge length. The case which there is a zero-bridge length, has one-loop dressed diagrams in figure 7.9. Using the property (7.27), we have

$$\begin{aligned} & \frac{\langle\langle \mathcal{O}_1^{\text{BPS}(L_1)}(x_1) \mathcal{O}_2^{\text{BPS}(L_2)}(x_2) \mathcal{O}_3^{\text{BPS}(L_3)}(x_3) \rangle\rangle_{\ell_{13}=0}}{\sqrt{n_1 n_2 n_3}} \Big|_{1\text{-loop}} \\ &= \left[\text{CI}_{123}^{\text{boundary}} + \mathbf{B}_{12} + \mathbf{B}_{23} + \mathbf{L}_{12,31} + \frac{\lambda}{8\pi^2} 3\zeta(2) \right] d_{12}^{\ell_{12}} d_{23}^{\ell_{23}} = \frac{\lambda}{8\pi^2} \zeta(2) d_{12}^{\ell_{12}} d_{23}^{\ell_{23}}. \end{aligned} \quad (7.29)$$

The last term in the bracket, which is the $\frac{\lambda}{8\pi^2} 3\zeta(2)$, is the normalization term from the two-point functions. The other diagram, which is the triangle diagram, become

$$\begin{aligned} & \frac{\langle\langle \mathcal{O}_1^{\text{BPS}(L_1)}(x_1) \mathcal{O}_2^{\text{BPS}(L_2)}(x_2) \mathcal{O}_3^{\text{BPS}(L_3)}(x_3) \rangle\rangle_{\ell_{ij} \neq 0}}{\sqrt{n_1 n_2 n_3}} \Big|_{1\text{-loop}} \\ &= \left[\text{CI}_{123}^{\text{boundary}} + \text{CI}_{231}^{\text{boundary}} + \text{CI}_{312}^{\text{boundary}} + \mathbf{B}_{12} + \mathbf{B}_{23} + \mathbf{B}'_{31} + \frac{\lambda}{8\pi^2} 3\zeta(2) \right] d_{12}^{\ell_{12}} d_{23}^{\ell_{23}} d_{31}^{\ell_{31}} \\ &= \frac{\lambda}{8\pi^2} 3\zeta(2) d_{12}^{\ell_{12}} d_{23}^{\ell_{23}} d_{31}^{\ell_{31}}, \end{aligned} \quad (7.30)$$

³Surely, the anomalous dimensions vanish.

Unified two-type three-point functions, we can write as

$$\frac{\langle\langle \mathcal{O}_1^{\text{BPS}(L_1)}(x_1) \mathcal{O}_2^{\text{BPS}(L_2)}(x_2) \mathcal{O}_3^{\text{BPS}(L_3)}(x_3) \rangle\rangle}{\sqrt{n_1 n_2 n_3}} \Big|_{1\text{-loop}} = \frac{\lambda}{8\pi^2} (3 - 2\delta_{\ell_{ij}}) \zeta(2) d_{12}^{\ell_{12}} d_{23}^{\ell_{23}} d_{31}^{\ell_{31}}, \quad (7.31)$$

where $\delta_{\ell_{ij}}$ is Kronecker delta functions and defied as follows:

$$\delta_{\ell_{ij}} = \begin{cases} 1 & \ell_{ij} = 0 \\ 0 & \ell_{ij} \neq 0 \end{cases}. \quad (7.32)$$

7.3.2 Four-point functions

Let us calculate the four-point functions. As a form up, we firstly consider the four-point functions with all operator lengths are one $L_1 = L_2 = L_3 = L_4 = 1$. The one-loop diagrams not contracting with the Wilson loop part is given by

$$\left(\begin{array}{c} \text{Diagram 1} \\ \text{Diagram 2} \end{array} \right) \Big|_{\text{not contracting with Wilson loop}} = \frac{1}{2} D_{1234} + \text{CI}_{12,43}^{\text{boundary}} d_{12} d_{34} + \text{CI}_{14,23}^{\text{boundary}} d_{41} d_{23}.$$

In addition, The one-loop diagrams contracting with the Wilson loop parts given by

$$\begin{aligned} \left(\begin{array}{c} \text{Diagram 3} \\ \text{Diagram 4} \end{array} \right) \Big|_{\text{contracting with Wilson loop}} &= (\mathbf{L}_{12,34} + \mathbf{B}_{12} + \mathbf{B}_{34} - \text{norm}) d_{12} d_{34} \\ &= \left(\frac{\lambda}{8\pi^2} 2\zeta(2) \text{Li}_R[z] - \text{CI}_{12,43}^{\text{boundary}} \right) d_{12} d_{34}. \end{aligned} \quad (7.33)$$

$$\left(\begin{array}{c} \text{Diagram 5} \\ \text{Diagram 6} \end{array} \right) \Big|_{\text{contracting with Wilson loop}} = \left(\frac{\lambda}{8\pi^2} 2\zeta(2) \text{Li}_R[1-z] - \text{CI}_{14,23}^{\text{boundary}} \right) d_{23} d_{41}.$$

By combing them, all the corner interactions are canceled with each other and we get

$$\begin{aligned} &\frac{\langle\langle \mathcal{O}_1^{\text{BPS}(1)}(x_1) \mathcal{O}_2^{\text{BPS}(1)}(x_2) \mathcal{O}_3^{\text{BPS}(1)}(x_3) \mathcal{O}_4^{\text{BPS}(1)}(x_4) \rangle\rangle}{\sqrt{n_1 n_2 n_3 n_4}} \Big|_{1\text{-loop}} \\ &= \frac{1}{2} D_{1234} + \frac{\lambda}{8\pi^2} 2\zeta(2) \text{Li}_R[z] d_{12} d_{34} + \frac{\lambda}{8\pi^2} 2\zeta(2) \text{Li}_R[1-z] d_{23} d_{41} \end{aligned} \quad (7.34)$$

In the same argument, by collecting the appropriate one-loop insertion formulas, the

four-point functions of the length L operators is given by ⁴

$$\begin{aligned}
& \frac{\langle\langle \mathcal{O}_1^{\text{BPS}(L)}(x_1) \mathcal{O}_2^{\text{BPS}(L)}(x_2) \mathcal{O}_3^{\text{BPS}(L)}(x_3) \mathcal{O}_4^{\text{BPS}(L)}(x_4) \rangle\rangle}{\sqrt{n_1 n_2 n_3 n_4}} \Big|_{1\text{-loop}} \\
&= \frac{1}{2} D_{1234} \langle \mathcal{O}_1^{\text{BPS}(L_1-1)} \mathcal{O}_2^{\text{BPS}(L_2-1)} \mathcal{O}_3^{\text{BPS}(L_3-1)} \mathcal{O}_4^{\text{BPS}(L_4-1)} \rangle_{\text{tree}} \\
&+ \frac{\lambda}{8\pi^2} 6\zeta(2) \left(\sum_{x=1}^{L-1} \text{H}_x^{L,L,L,L} \right) \\
&+ \frac{\lambda}{8\pi^2} 2\zeta(2) \text{Li}_R[z] \text{H}_0^{L,L,L,L} + \frac{\lambda}{8\pi^2} 2\zeta(2) \text{Li}_R[1-z] \text{H}_L^{L,L,L,L} \tag{7.35}
\end{aligned}$$

The first term is the same with the one-loop four-point functions of the single trace operators up to 1/2 factor. The other terms come from the existence of the Wilson loop boundary.

Next we consider the $(L_1 + L_4 < L_2 + L_3)$ and $(L_1 + L_4 > L_2 + L_3)$ cases in no cross, $\ell_{13} = \ell_{24} = 0$, condition $(L_1 + L_3 \neq L_2 + L_4)$. In this case, the difference from the (7.35) is only the contribution from the left-(right)-most diagrams. Then the diagrams are given by

$$\begin{aligned}
& \left(\begin{array}{c} \text{Diagram 1} \\ \text{Diagram 2} \end{array} \right) \Big|_{\text{contracting with Wilson loop}} = \frac{\lambda}{8\pi^2} (2\zeta(2) + 2\zeta(2) \text{Li}_R[z]) \text{H}_0^{L_1, L_2, L_3, L_4} \\
& \quad - \text{CI}_{12,43}^{\text{boundary}} \text{H}_0^{L_1, L_2, L_3, L_4} . \\
& \left(\begin{array}{c} \text{Diagram 3} \\ \text{Diagram 4} \end{array} \right) \Big|_{\text{contracting with Wilson loop}} = \frac{\lambda}{8\pi^2} (2\zeta(2) + 2\zeta(2) \text{Li}_R[1-z]) \text{H}_L^{L_1, L_2, L_3, L_4} \\
& \quad - \text{CI}_{14,23}^{\text{boundary}} \text{H}_L^{L_1, L_2, L_3, L_4} .
\end{aligned}$$

Therefore, by adding the (7.35), the four-point functions with $(L_1 + L_3 \neq L_2 + L_4)$ are

⁴Notice that the tree-level contribution is denoted as $\langle \mathcal{O}_1^{\text{BPS}(L)}(x_1) \mathcal{O}_2^{\text{BPS}(L)}(x_2) \mathcal{O}_3^{\text{BPS}(L)}(x_3) \mathcal{O}_4^{\text{BPS}(L)}(x_4) \rangle = \sum_{x=0}^L \text{H}_x^{L,L,L,L}$

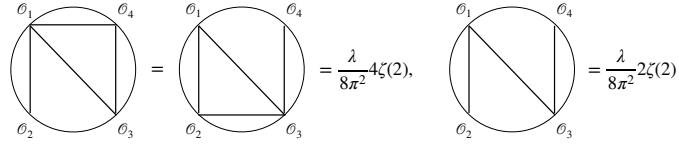
given by

$$\begin{aligned}
& \frac{\langle\langle \mathcal{O}_1^{\text{BPS}(L_1)}(x_1) \mathcal{O}_2^{\text{BPS}(L_2)}(x_2) \mathcal{O}_3^{\text{BPS}(L_3)}(x_3) \mathcal{O}_4^{\text{BPS}(L_4)}(x_4) \rangle\rangle_{\ell_{13}=\ell_{24}=0}}{\sqrt{n_1 n_2 n_3 n_4}} \Big|_{1\text{-loop}} \\
&= \frac{1}{2} D_{1234} \langle \mathcal{O}_1^{\text{BPS}(L_1-1)} \mathcal{O}_2^{\text{BPS}(L_2-1)} \mathcal{O}_3^{\text{BPS}(L_3-1)} \mathcal{O}_4^{\text{BPS}(L_4-1)} \rangle_{\text{tree}} \\
&+ \frac{\lambda}{8\pi^2} 6\zeta(2) \left(\sum_{x=1}^{\min(L_1, L_2, L_3, L_4)-1} \mathbb{H}_x^{L_1, L_2, L_3, L_4} \right) \\
&+ \frac{\lambda}{8\pi^2} (2\zeta(2)(\delta_{\ell_{14}} + \delta_{\ell_{23}} - 2\delta_{\ell_{14}} \cdot \delta_{\ell_{23}}) + 2\zeta(2)\text{Li}_R[z]) \mathbb{H}_0^{L_1, L_2, L_3, L_4} \\
&+ \frac{\lambda}{8\pi^2} (2\zeta(2)(\delta_{\ell_{12}} + \delta_{\ell_{34}} - 2\delta_{\ell_{12}} \cdot \delta_{\ell_{34}}) + 2\zeta(2)\text{Li}_R[1-z]) \mathbb{H}_L^{L_1, L_2, L_3, L_4}, \tag{7.36}
\end{aligned}$$

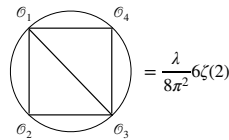
It shows that if it is $\ell_{14} = \ell_{23} = 0$ ($L_1 + L_4 = L_2 + L_3$), the single $\zeta(2)$ for the leftmost vanish and it has $2\zeta(2)\text{Li}_R[z]$. On the other hand, if it is $\ell_{14} = 0$ or $\ell_{23} = 0$ ($L_1 + L_4 \neq L_2 + L_3$), the leftmost become $2\zeta(2) + 2\zeta(2)\text{Li}_R[z]$.

Lastly we consider the most general four-point functions, which has cross contractions. By using the one-loop insertion formulas, the four-point functions with cross contraction has following contributions:

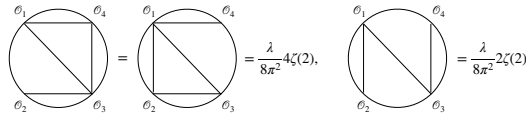
Left-most



Middle



Right-most



From the lessons of above and the one-loop insertion formulas, we can see the following statement for the general four-point functions.

1. If the four-point functions have cross contractions, there are no $\frac{1}{2}D_{1234}$ functions since four-body diagrams cannot contribute.
2. The Left-(and Right-)most diagrams receive the contributions of the zeta function $\zeta(2)$ in respect to the number of the zero-bridge lengths: If the number of the zero-bridge lengths is one, it has $\frac{\lambda}{8\pi^2}4\zeta(2)$. On the other hand, If the number of the zero-bridge lengths is two, it has $\frac{\lambda}{8\pi^2}2\zeta(2)$.

Therefore we have

$$\begin{aligned}
& \frac{\langle\langle \mathcal{O}_1^{\text{BPS}(L_1)}(x_1)\mathcal{O}_2^{\text{BPS}(L_2)}(x_2)\mathcal{O}_3^{\text{BPS}(L_3)}(x_3)\mathcal{O}_4^{\text{BPS}(L_4)}(x_4)\rangle\rangle_{\ell_{13}\neq 0 \text{ or } \ell_{24}\neq 0}}{\sqrt{n_1n_2n_3n_4}} \Big|_{1\text{-loop}} \\
&= \frac{\lambda}{8\pi^2}6\zeta(2) \left(\sum_{x=1}^{\min(L_1,L_2,L_3,L_4)-1} \mathbf{H}_x^{L_1,L_2,L_3,L_4} \right) \\
&+ \frac{\lambda}{8\pi^2}(2\zeta(2)(1 + \delta_{\ell_{14}} + \delta_{\ell_{23}} - 2\delta_{\ell_{14}} \cdot \delta_{\ell_{23}}))\mathbf{H}_0^{L_1,L_2,L_3,L_4} \\
&+ \frac{\lambda}{8\pi^2}(2\zeta(2)(1 + \delta_{\ell_{12}} + \delta_{\ell_{34}} - 2\delta_{\ell_{12}} \cdot \delta_{\ell_{34}}))\mathbf{H}_L^{L_1,L_2,L_3,L_4}. \tag{7.37}
\end{aligned}$$

Summing up the results (7.36) and (7.37), we finally have the complete form of the one-loop four-point functions of the BPS-operators as follows:

$$\begin{aligned}
& \frac{\langle\langle \mathcal{O}_1^{\text{BPS}(L_1)}(x_1)\mathcal{O}_2^{\text{BPS}(L_2)}(x_2)\mathcal{O}_3^{\text{BPS}(L_3)}(x_3)\mathcal{O}_4^{\text{BPS}(L_4)}(x_4)\rangle\rangle}{\sqrt{n_1n_2n_3n_4}} \Big|_{1\text{-loop}} \\
&= \frac{1}{2}D_{1234}\delta_{\ell_{13}} \cdot \delta_{\ell_{24}} \left(\sum_{x=0}^{\min(\tilde{L}_1,\tilde{L}_2,\tilde{L}_3,\tilde{L}_4)} \mathbf{H}_x^{L_1,L_2,L_3,L_4} \right) + \frac{\lambda}{8\pi^2}6\zeta(2) \left(\sum_{x=1}^{\min(\tilde{L}_1,\tilde{L}_2,\tilde{L}_3,\tilde{L}_4)-1} \mathbf{H}_x^{L_1,L_2,L_3,L_4} \right) \\
&+ \frac{\lambda}{8\pi^2}(2\zeta(2)(1 - \delta_{\ell_{13}} \cdot \delta_{\ell_{24}} + \delta_{\ell_{14}} + \delta_{\ell_{23}} - 2\delta_{\ell_{14}} \cdot \delta_{\ell_{23}}) + 2\zeta(2)\text{Li}_R[z])\mathbf{H}_0^{L_1,L_2,L_3,L_4} \\
&+ \frac{\lambda}{8\pi^2}(2\zeta(2)(1 - \delta_{\ell_{13}} \cdot \delta_{\ell_{24}} + \delta_{\ell_{12}} + \delta_{\ell_{34}} - 2\delta_{\ell_{12}} \cdot \delta_{\ell_{34}}) + 2\zeta(2)\text{Li}_R[1 - z])\mathbf{H}_L^{L_1,L_2,L_3,L_4} \tag{7.38}
\end{aligned}$$

Chapter 8

Zero-length operators – perturbation

In this chapter, we study the three-point functions of zero-length operators inserted into the Wilson loop. Such a zero-length operator is constructed as follows

$$\mathcal{O}^{\text{DCO}} : Z^L \xrightarrow{L \rightarrow 0} \text{DCO},$$

where the DCO means the *defect changing operator*. It is because insertion of the zero-length operator into the Wilson loop merely change the polarization of the R-symmetry of the $SO(6)$ scalars as

$$W[\mathcal{O}^{\text{DCO}}] \equiv \text{trP} \left[\exp \left(\int_{-\infty}^{\tau} d\tau' iA_{\mu} \dot{x}^{\mu} + \phi_i n^i |\dot{x}^{\mu}| \right) \underbrace{\text{DCO}}_{\mathcal{O}^{\text{DCO}}} \left(\int_{\tau}^{\infty} d\tau'' iA_{\mu} \dot{x}^{\mu} + \phi_i \tilde{n}^i |\dot{x}^{\mu}| \right) \right]. \quad (8.1)$$

The main topic of this chapter is the three-point functions of the DCO's. Then, the Wilson loop has three-type scalars. To characterized these three scalars, we introduce the 6-dimensional unit vector n_{ij} , see figure 8.1. Namely, the three-point functions of the DCOs are written as

$$\begin{aligned} & \langle\langle \mathcal{O}_1^{\text{DCO}}(t_1) \mathcal{O}_2^{\text{DCO}}(t_2) \mathcal{O}_3^{\text{DCO}}(t_3) \rangle\rangle \\ & \equiv \langle \text{Tr} \left[\text{Pexp} \left(\int_{-\infty}^{t_1} d\tau iA_{\mu} \dot{x}^{\mu} + \phi_i n_{31}^i |\dot{x}^{\mu}| \right) \text{Pexp} \left(\int_{t_1}^{t_2} d\tau iA_{\mu} \dot{x}^{\mu} + \phi_i n_{12}^i |\dot{x}^{\mu}| \right) \right. \\ & \quad \left. \text{Pexp} \left(\int_{t_2}^{t_3} d\tau iA_{\mu} \dot{x}^{\mu} + \phi_i n_{23}^i |\dot{x}^{\mu}| \right) \text{Pexp} \left(\int_{t_3}^{\infty} d\tau iA_{\mu} \dot{x}^{\mu} + \phi_i n_{31}^i |\dot{x}^{\mu}| \right) \right] \rangle. \end{aligned} \quad (8.2)$$

Notice that the inner product of the unit vectors are often written in terms of the angle θ_i as

$$\cos \theta_1 \equiv n_{31} \cdot n_{12}, \quad \cos \theta_2 \equiv n_{12} \cdot n_{23}, \quad \cos \theta_3 \equiv n_{23} \cdot n_{31}. \quad (8.3)$$

In order to calculate and extract the structure constants of the three-point functions up to two-loop, we should first calculate the two-point functions and determine the normalization. We perform them in section 8.1 and see what the known anomalous dimensions in

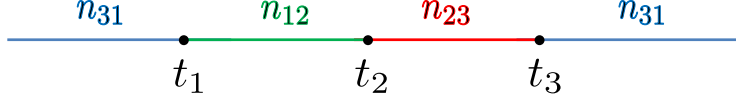


Figure 8.1: The DCOs are located at $t_i, i = (1, 2, 3)$. The each blue, green and red segment show the each Wilson loop coupled scalar with the polarization n_{31} , n_{12} and n_{31} respectively.

the literature [80] are reproduced. Next we compute the three-point functions at two-loop in section 8.2. After doing so, we discuss a theory in the ladder limit whose contributions are only ladder diagrams rather than other interactive diagrams. In the ladder limit, the structure constants are evaluated at finite coupling by solving the SD-equation.

8.1 Two-point functions at two loops

8.1.1 One loop

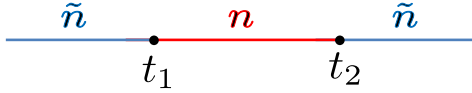


Figure 8.2: Two-point function of DCO's. The DCOs are located at t_1 and t_2

The two-point functions of DCOs are of the following form, see also figure 8.2:

$$\begin{aligned} \langle\langle \mathcal{O}_1^{\text{DCO}}(t_1) \mathcal{O}_2^{\text{DCO}}(t_2) \rangle\rangle &\equiv \langle \text{Tr} \left[\text{Pexp} \left(\int_{-\infty}^{t_1} d\tau iA_\mu \dot{x}^\mu + \phi_i \tilde{n}^i |\dot{x}^\mu| \right) \right. \\ &\quad \left. \text{Pexp} \left(\int_{t_1}^{t_2} d\tau iA_\mu \dot{x}^\mu + \phi_i n^i |\dot{x}^\mu| \right) \text{Pexp} \left(\int_{t_2}^{\infty} d\tau iA_\mu \dot{x}^\mu + \phi_i \tilde{n}^i |\dot{x}^\mu| \right) \right] \rangle. \end{aligned} \quad (8.4)$$

In the perturbative computation, we have to expand the exponentials in (8.4) and take the contractions them with the vertices in $\mathcal{N}=4$ SYM. Then the result should depend on the inner product $n \cdot \tilde{n}$.

At the one-loop level, there are no vertices contribution in $\mathcal{N} = 4$ SYM. Since the Wilson loop include both the gauge field and scalar field, we use the following single propagators:

$$\text{Gauge propadeter} : -\frac{\lambda}{8\pi^2} \frac{1}{\tau_{12}^2}, \quad \text{Scalar propadeter} : (n_1 \cdot n_2) \frac{\lambda}{8\pi^2} \frac{1}{\tau_{12}^2}, \quad (8.5)$$

The extra minus sign for gluons comes from factors of i in the exponentials in (8.4). As is clear from (8.5), the contributions from the gauge field and the scalar field cancel out if $n_1 = n_2$ and $n_1 \cdot n_2 = 1$, which is the BPS configuration explained in previous chapter.



Figure 8.3: Two-point function of DCOs at one-loop. Owing to the cancellation between gluon propagator and scalar propagator, the survived diagrams are only propagators connecting two different segments of the Wilson loop.

The remained diagrams are propagators connecting two segments with different polarizations n_i , see figure 8.3. Then, we must be careful of the UV divergence when we compute such diagrams. We introduce a point-splitting regularization by cutting out a small circle $\epsilon/2$ around the DCO's and we have

$$\langle\langle \mathcal{O}_1^{\text{DCO}}(t_1) \mathcal{O}_2^{\text{DCO}}(t_2) \rangle\rangle_{1\text{-loop}} = \frac{\lambda(n \cdot \tilde{n} - 1)}{8\pi^2} \left(\int_{-\infty}^{t_1^-} d\tau_1 \int_{t_1^+}^{t_2^-} d\tau_2 \frac{1}{\tau_{12}^2} + \int_{t_1^+}^{t_2^-} d\tau_1 \int_{t_2^+}^{\infty} d\tau_2 \frac{1}{\tau_{12}^2} \right), \quad (8.6)$$

with $t_i^\pm = t_i \pm \epsilon/2$. Using the following integration formula

$$\int_d^c d\tau_1 \int_b^a d\tau_2 \frac{1}{\tau_{12}^2} = \log \frac{(a-c)(b-d)}{(a-d)(b-c)}, \quad (8.7)$$

we can easily evaluate as

$$\langle\langle \mathcal{O}_1^{\text{DCO}}(t_1) \mathcal{O}_2^{\text{DCO}}(t_2) \rangle\rangle_{1\text{-loop}} = \frac{\lambda(n \cdot \tilde{n} - 1)}{4\pi^2} \log \frac{t_{12}}{\epsilon} + O(\epsilon). \quad (8.8)$$

Comparing the weak coupling expansions with (2.24), we can determine the one-loop normalization $a^{(1)}$ and the anomalous dimension $\gamma^{(1)}$ as

$$a^{(1)} = 0, \quad \gamma^{(1)} = \frac{1 - n_1 \cdot n_2}{8\pi^2}. \quad (8.9)$$

The result for $\gamma^{(1)}$ of course matches the one in the literature [80]. Furthermore, we find that the one-loop normalization $a^{(1)}$ vanishes in our set-up.

8.1.2 Two loops

Next we compute the two-point functions of DCO's at two-loop. At two loop order, there are three types diagrams; the ladder, the vertex and the self-energy diagrams. Below sub-subsections, we evaluate them one by one.

Ladder diagrams

We first consider the ladder diagrams, which consist only of propagators. In the similar manner as the one-loop computations in the previous subsection, the cancellation between the scalars and the gluons occurs.

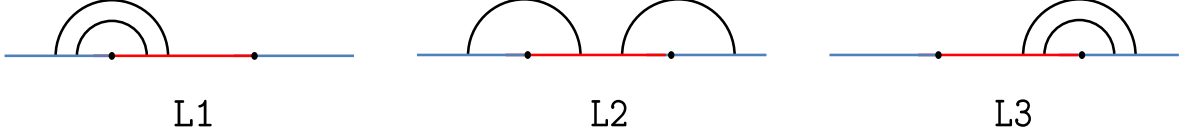


Figure 8.4: Ladder diagrams that contribute to the two-point function at two loops. Here, thick black curves represent either a scalar propagator or a gluon propagator.

Thus only non-zero diagrams are the ones depicted in figure 8.4, which are given by

$$\begin{aligned}
L1 &= \left(\frac{(n_1 \cdot n_2 - 1)\lambda}{8\pi^2} \right)^2 \int_{-\infty}^{t_1^-} d\tau_1 \int_{\tau_1}^{t_1^-} d\tau_2 \int_{t_1^+}^{t_2^-} d\tau_3 \int_{\tau_3}^{t_2^-} d\tau_4 \frac{1}{\tau_{14}^2} \frac{1}{\tau_{23}^2}, \\
L2 &= \left(\frac{(n_1 \cdot n_2 - 1)\lambda}{8\pi^2} \right)^2 \int_{-\infty}^{t_1^-} d\tau_1 \int_{t_1^+}^{t_2^-} d\tau_2 \int_{\tau_2}^{t_2^-} d\tau_3 \int_{t_2^+}^{\infty} d\tau_4 \frac{1}{\tau_{12}^2} \frac{1}{\tau_{34}^2}, \\
L3 &= \left(\frac{(n_1 \cdot n_2 - 1)\lambda}{8\pi^2} \right)^2 \int_{t_1^+}^{t_2^-} d\tau_1 \int_{\tau_1}^{t_2^-} d\tau_2 \int_{t_2^+}^{\infty} d\tau_3 \int_{\tau_3}^{\infty} d\tau_4 \frac{1}{\tau_{14}^2} \frac{1}{\tau_{23}^2}.
\end{aligned} \tag{8.10}$$

Thus, we have

$$\begin{aligned}
L1 = L3 &= \left(\frac{(n_1 \cdot n_2 - 1)\lambda}{8\pi^2} \right)^2 \left[\frac{\pi^2}{6} - \log \frac{t_{21}}{\epsilon} + \frac{1}{2} \left(\log \frac{t_{21}}{\epsilon} \right)^2 \right] + O(\epsilon), \\
L2 &= \left(\frac{(n_1 \cdot n_2 - 1)\lambda}{8\pi^2} \right)^2 \left[-\frac{\pi^2}{6} + \left(\log \frac{t_{21}}{\epsilon} \right)^2 \right] + O(\epsilon).
\end{aligned} \tag{8.11}$$

Summing three terms, we get

$$L \equiv L1 + L2 + L3 = \left(\frac{(n_1 \cdot n_2 - 1)\lambda}{8\pi^2} \right)^2 \left[\frac{\pi^2}{6} - 2 \log \frac{t_{21}}{\epsilon} + 2 \left(\log \frac{t_{21}}{\epsilon} \right)^2 \right]. \tag{8.12}$$

Vertex diagrams

We second consider the diagrams which contain one interaction vertex. Written explicitly, they arise from the Wick contraction of the following terms:

$$\begin{aligned}
&\frac{i^3}{3!} \int d\tau_1 d\tau_2 d\tau_3 \left\langle \text{Tr P}[\mathcal{A}(\tau_1)\mathcal{A}(\tau_2)\mathcal{A}(\tau_3)] \left(\frac{2i}{g_{\text{YM}}^2} \int d^4x \text{Tr} \{ \partial_\mu A_\nu(x) [A_\mu(x), A_\nu(x)] \} \right) \right\rangle \\
&+ \frac{i}{2!1!} \int d\tau_1 d\tau_2 d\tau_3 \left\langle \text{Tr P}[\Phi_1(\tau_1)\Phi_2(\tau_2)\mathcal{A}(\tau_3)] \left(\frac{2i}{g_{\text{YM}}^2} \int d^4x \text{Tr} \{ \partial_\mu \phi(x) [A_\mu(x), \phi(x)] \} \right) \right\rangle.
\end{aligned}$$

Here $\mathcal{A} \equiv A_\mu \dot{x}^\mu$ and $\Phi_i \equiv (\phi \cdot n_i) |\dot{x}|$ with $n_{1,2}$.

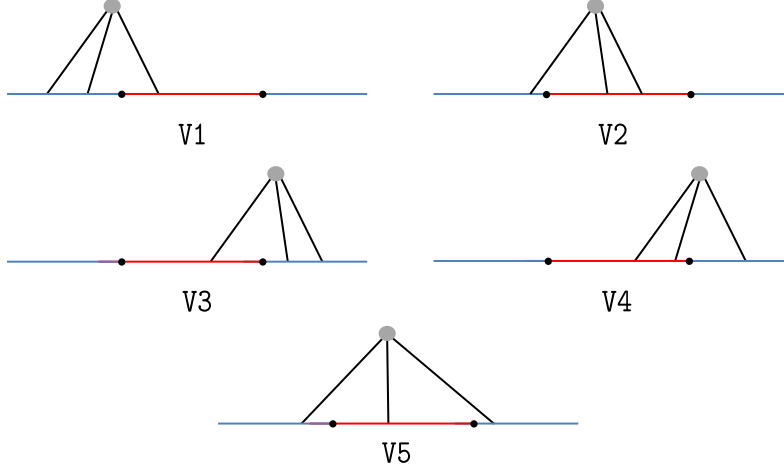


Figure 8.5: The interaction vertex diagrams for two-loop diagrams. Each black line can be either scalar propagator or gluon propagator.

Let us focus on the diagram V1 in figure 8.5. The contribution in the diagram V1 include the three different terms of the scalar-scalar-gauge vertex by the path-ordering:

$$\begin{aligned}
& i \int_{\substack{\tau_1, \tau_2 \in [-\infty, t_1] \\ \tau_1 < \tau_2}} d\tau_1 d\tau_2 \int_{\tau_3 \in [t_1, t_2]} d\tau_3 [\langle \text{Tr} (\mathcal{A}(\tau_3) \Phi_2(\tau_2) \Phi_2(\tau_1)) \rangle \\
& + \langle \text{Tr} (\Phi_1(\tau_3) \mathcal{A}(\tau_2) \Phi_2(\tau_1)) \rangle + \langle \text{Tr} (\Phi_1(\tau_3) \Phi_2(\tau_2) \mathcal{A}(\tau_1)) \rangle] .
\end{aligned} \tag{8.13}$$

Here $\Phi_i \equiv n_i \cdot \phi$, $i = (1, 2)$, and we did not write the interaction vertex for brevity. Among these three terms, since two scalars are in the same segment $[-\infty, t_1]$, $n_2 \cdot n_2 = 1$, the first term does not contribute to the final answer. On the other hand, from the second term we get

$$(\text{second term}) = -\frac{\lambda^2 (n \cdot \tilde{n})}{4(4\pi^2)^3} \int_{\substack{\tau_1, \tau_2 \in [-\infty, t_1] \\ \tau_1 < \tau_2}} d\tau_1 d\tau_2 \int_{\tau_3 \in [t_1, t_2]} d\tau_3 (-\partial_{\tau_1} Y_{123} + \partial_{\tau_3} Y_{123}) , \tag{8.14}$$

with (see Appendix A for more details)

$$Y_{123} \left(\equiv \int \frac{d^4 x_5}{x_{15}^2 x_{25}^2 x_{35}^2} \right) = -2\pi^2 \left(\frac{\log |\tau_{12}|}{\tau_{13} \tau_{23}} + \frac{\log |\tau_{13}|}{\tau_{12} \tau_{32}} + \frac{\log |\tau_{23}|}{\tau_{21} \tau_{31}} \right) . \tag{8.15}$$

In (8.14), the term $-\partial_{\tau_1} Y_{123}$ comes from the contraction with the interaction $\int d^4 x \text{Tr}(\partial_\mu \phi A_\mu \phi)$ while the term $\partial_{\tau_3} Y_{123}$ comes from the contraction with $-\int d^4 x \text{Tr}(\partial_\mu \phi \phi A_\mu)$. Similarly the third term (8.13) yields¹

$$(\text{third term}) = -\frac{\lambda^2 (n \cdot \tilde{n})}{4(4\pi^2)^3} \int_{\substack{\tau_1, \tau_2 \in [-\infty, t_1] \\ \tau_1 < \tau_2}} d\tau_1 d\tau_2 \int_{\tau_3 \in [t_1, t_2]} d\tau_3 (-\partial_{\tau_3} Y_{123} + \partial_{\tau_2} Y_{123}) . \tag{8.16}$$

¹Here $-\partial_{\tau_3} Y_{123}$ comes from the contraction with $\int d^4 x \text{Tr}(\partial_\mu \phi A_\mu \phi)$ while $\partial_{\tau_2} Y_{123}$ comes from the contraction with $-\int d^4 x \text{Tr}(\partial_\mu \phi \phi A_\mu)$.

Adding up the two terms, (8.14) and (8.16), and also the contributions from the three-gauge vertex, we arrive at the following result for the diagram V1:

$$V1 = -\frac{\lambda^2(n_1 \cdot n_2 - 1)}{4(4\pi^2)^3} \int_{-\infty}^{t_1^-} d\tau_1 \int_{-\infty}^{t_1^-} d\tau_2 \int_{t_1^+}^{t_2^-} d\tau_3 \epsilon(\tau_1 - \tau_2) \partial_{\tau_1} Y_{123}. \quad (8.17)$$

Here we used the permutation symmetry of Y_{123} , $Y_{123} = Y_{213}$ etc., to simplify the result and $\epsilon(x) \equiv \theta(x) - \theta(-x)$ with $\theta(x)$ being the step function.

By performing the similar analysis, we arrive at the following results for other diagrams:

$$\begin{aligned} V2 &= -\frac{\lambda^2(n_1 \cdot n_2 - 1)}{4(4\pi^2)^3} \int_{-\infty}^{t_1^-} d\tau_1 \int_{t_1^+}^{t_2^-} d\tau_2 \int_{t_1^+}^{t_2^-} d\tau_3 \epsilon(\tau_2 - \tau_3) \partial_{\tau_2} Y_{123}, \\ V3 &= -\frac{\lambda^2(n_1 \cdot n_2 - 1)}{4(4\pi^2)^3} \int_{t_1^+}^{t_2^-} d\tau_1 \int_{t_2^+}^{\infty} d\tau_2 \int_{t_2^+}^{\infty} d\tau_3 \epsilon(\tau_2 - \tau_3) \partial_{\tau_2} Y_{123}, \\ V4 &= -\frac{\lambda^2(n_1 \cdot n_2 - 1)}{4(4\pi^2)^3} \int_{t_1^+}^{t_2^-} d\tau_1 \int_{t_1^+}^{t_2^-} d\tau_2 \int_{t_2^+}^{\infty} d\tau_3 \epsilon(\tau_1 - \tau_2) \partial_{\tau_1} Y_{123}, \\ V5 &= -\frac{\lambda^2(n_1 \cdot n_2 - 1)}{4(4\pi^2)^3} \int_{-\infty}^{t_1^-} d\tau_1 \int_{t_1^+}^{t_2^-} d\tau_2 \int_{t_2^+}^{\infty} d\tau_3 (\partial_{\tau_1} Y_{123} - \partial_{\tau_3} Y_{123}). \end{aligned} \quad (8.18)$$

To proceed, we perform the integration by parts to each contribution and rewrite them using $\partial_x \epsilon(x) = 2\delta(x)$ as

$$\begin{aligned} V1 &= -\frac{\lambda^2(n_1 \cdot n_2 - 1)}{4(4\pi^2)^3} \left[\int_{-\infty}^{t_1^-} d\tau_2 \int_{t_1^+}^{t_2^-} d\tau_3 Y_{t_1^- 23} - 2 \int_{-\infty}^{t_1^-} d\tau_1 \int_{-\infty}^{t_1^-} d\tau_2 \int_{t_1^+}^{t_2^-} d\tau_3 \delta(\tau_1 - \tau_2) Y_{123} \right] \\ &= -\frac{\lambda^2(n_1 \cdot n_2 - 1)}{4(4\pi^2)^3} \left[\int_{-\infty}^{t_1^-} d\tau_2 \int_{t_1^+}^{t_2^-} d\tau_3 Y_{t_1^- 23} - 2 \int_{-\infty}^{t_1^-} d\tau_2 \int_{t_1^+}^{t_2^-} d\tau_3 Y_{223} \right]. \end{aligned} \quad (8.19)$$

We thus get

$$\begin{aligned} V &\equiv V1 + V2 + V3 + V4 + V5 = \\ &= -\frac{\lambda^2(n_1 \cdot n_2 - 1)}{4(4\pi^2)^3} \left[\int_{-\infty}^{t_1^-} d\tau_2 \int_{t_1^+}^{t_2^-} d\tau_3 \left(Y_{t_1^- 23} + Y_{t_1^+ 23} + Y_{t_2^- 23} + Y_{t_2^+ 23} \right) \right. \\ &\quad + \int_{t_1^+}^{t_2^-} d\tau_2 \int_{t_2^+}^{\infty} d\tau_3 \left(Y_{t_1^- 23} + Y_{t_1^+ 23} + Y_{t_2^- 23} + Y_{t_2^+ 23} \right) \\ &\quad \left. - 2 \int_{-\infty}^{t_1^-} d\tau_2 \int_{t_1^+}^{t_2^-} d\tau_3 (Y_{223} + Y_{233}) - 2 \int_{t_1^+}^{t_2^-} d\tau_2 \int_{t_2^+}^{\infty} d\tau_3 (Y_{223} + Y_{233}) \right]. \end{aligned} \quad (8.20)$$



Figure 8.6: The self-energy diagrams that contribute to the two-loop two-point function. The sum of these two diagrams is given by (8.22).

Self-energy diagrams

We next compute the self-energy diagrams, see figure 8.6. The one-loop correlation of the scalar propagators were introduced in the section 3.8. We here recall them as

$$\begin{aligned} \mu \text{ --- } \text{---} \text{---} \text{---} \nu &= \frac{\lambda \delta^{ac} \delta^{bd} \delta_{\mu\nu}}{2} (Y_{223} + Y_{233}), \\ i \text{ --- } \text{---} \text{---} \text{---} j &= -\frac{\lambda \delta^{ac} \delta^{bd} \delta_{ij}}{2} (Y_{223} + Y_{233}). \end{aligned} \quad (8.21)$$

Here again $\delta^{ac} \delta^{bd}$ is the color factor. Using them, the contribution if the self-energy diagrams are given by

$$\mathbf{S} = -\frac{\lambda^2 (n_1 \cdot n_2 - 1)}{2(4\pi^2)^3} \left[\int_{-\infty}^{t_1^-} d\tau_2 \int_{t_1^+}^{t_2^-} d\tau_3 (Y_{223} + Y_{233}) + \int_{t_1^+}^{t_2^-} d\tau_2 \int_{t_2^+}^{\infty} d\tau_3 (Y_{223} + Y_{233}) \right]. \quad (8.22)$$

Surprisingly, the contribution from the self-energy diagrams cancels the divergent terms in the vertex diagrams (8.20).

Using the expression for Y_{123} (8.15), one can straightforwardly evaluate the remaining integral² to get

$$\mathbf{V} + \mathbf{S} = -2(n_1 \cdot n_2 - 1) \left(\frac{\lambda}{8\pi^2} \right)^2 \left(\frac{\pi^2}{3} \log \frac{t_{21}}{\epsilon} + 3\zeta(3) \right). \quad (8.23)$$

Final result

Summing up all the contributions: the ladder (8.12) and the vertex and self-energy (8.23), we finally get the two-point function of DCO's at two loop:

$$\begin{aligned} \langle\langle \mathcal{O}_1^{\text{DCO}}(t_1) \mathcal{O}_2^{\text{DCO}}(t_2) \rangle\rangle_{2\text{-loop}} &= \left(\frac{\lambda}{8\pi^2} \right)^2 \left[(n_1 \cdot n_2 - 1)^2 \left(\frac{\pi^2}{6} - 2 \log \frac{t_{21}}{\epsilon} + 2 \left(\log \frac{t_{21}}{\epsilon} \right)^2 \right) \right. \\ &\quad \left. - 2(n_1 \cdot n_2 - 1) \left(\frac{\pi^2}{3} \log \frac{t_{21}}{\epsilon} + 3\zeta(3) \right) \right]. \end{aligned} \quad (8.24)$$

²In terms of polylogarithms.



Figure 8.7: The one-loop diagrams with the coefficient $(n_{12} \cdot n_{23} - 1)$ for the three-point functions. The result of the computation is given in (8.27).

By comparing the weak coupling expansion of the two-point function (2.28), one can finally obtain the two-loop anomalous dimension $\gamma_j^{(2)}$ and the constant term $a_j^{(2)}$ as follows:

$$a^{(2)} = \frac{1}{(8\pi^2)^2} \left[\frac{\pi^2}{12} (n_1 \cdot n_2 - 1)^2 - 3\zeta(3)(n \cdot \tilde{n} - 1) \right], \quad (8.25)$$

$$\gamma^{(2)} = \frac{1}{(8\pi^2)^2} \left[(n_1 \cdot n_2 - 1)^2 + \frac{\pi^2}{3} (n \cdot \tilde{n} - 1) \right]. \quad (8.26)$$

The result for $\gamma^{(2)}$ matches the one in the literature [80] again.

8.2 Three-point functions at two loop

In this section, we calculate the three-point functions of DCO's.

8.2.1 One loop

At one-loop level, the three-point functions have three patterns: the coefficients are $(n_{12} \cdot n_{23} - 1)$, $(n_{23} \cdot n_{31} - 1)$ and $(n_{31} \cdot n_{12} - 1)$. However, we only focus on the diagrams with the $(n_{12} \cdot n_{23} - 1)$ in figure 8.7. It is because other diagrams are obtained by the permutation of the operator labels. The diagram of figure 8.7 can straightforwardly be evaluated as

$$\frac{\lambda(n_{12} \cdot n_{23} - 1)}{8\pi^2} \int_{t_1^+}^{t_2^-} d\tau_1 \int_{t_2^+}^{t_3^-} d\tau_2 \frac{1}{\tau_{12}^2} = \frac{\lambda(n_{12} \cdot n_{23} - 1)}{8\pi^2} \log \frac{t_{21} t_{32}}{t_{31} \epsilon}. \quad (8.27)$$

By taking into account the symmetrization, the one-loop result become

$$\langle\langle \mathcal{O}_1^{\text{DCO}}(t_1) \mathcal{O}_2^{\text{DCO}}(t_2) \mathcal{O}_3^{\text{DCO}}(t_3) \rangle\rangle_{1\text{-loop}} = \frac{\lambda}{8\pi^2} \sum_{\{i,j,k\}} (n_{ij} \cdot n_{jk} - 1) \log \left| \frac{t_{ij} t_{jk}}{t_{ki} \epsilon} \right|, \quad (8.28)$$

where the sum is over $\{i, j, k\} = \{1, 2, 3\}, \{2, 3, 1\}, \{3, 1, 2\}$. Comparing with the weak coupling expansion given in (2.28), one can read off the one-loop anomalous dimension and the one-loop structure constant as³

$$\gamma_j^{(1)} = \frac{(1 - n_{ij} \cdot n_{jk})}{8\pi^2}, \quad c_{123}^{(1)} = 0.$$

As expected the result for the anomalous dimension matches the previous result (8.9). This also shows that the one-loop structure constant is exactly zero.

³Here we already used the fact that the one-loop normalization $a^{(1)}$ vanishes in our scheme. See (8.9).

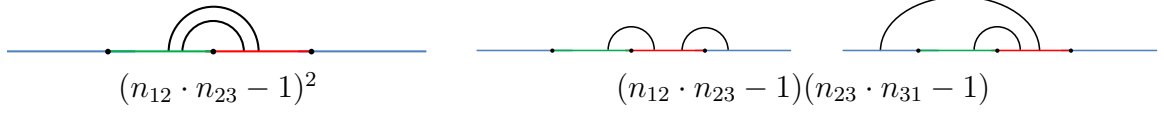


Figure 8.8: The two-loop ladder diagrams. The left diagram produces the term proportional to $(n_{12} \cdot n_{23} - 1)^2$ while the right two diagrams produce the term proportional to $(n_{12} \cdot n_{23} - 1)(n_{23} \cdot n_{31} - 1)$.

8.2.2 Two loop

At the two-loop order, there are three-types of the diagrams in the same way as the two-point functions: ladder, self-energy and vertex.

Ladder diagrams

In the ladder diagrams, we only focus on the diagrams with $(n_{12} \cdot n_{23} - 1)^2$ and $(n_{12} \cdot n_{23} - 1)(n_{23} \cdot n_{31} - 1)$ in figure 8.8. Then, the diagram with $(n_{12} \cdot n_{23} - 1)^2$ can be evaluated as

$$\begin{aligned} & \left(\frac{(n_{12} \cdot n_{23} - 1)\lambda}{8\pi^2} \right)^2 \int_{t_1^+}^{t_2^-} d\tau_1 \int_{\tau_1}^{t_2^-} d\tau_2 \int_{t_2^+}^{t_3^-} d\tau_3 \int_{\tau_3}^{t_3^-} d\tau_4 \frac{1}{\tau_{14}^2} \frac{1}{\tau_{23}^2} \\ & = \left(\frac{(n_{12} \cdot n_{23} - 1)\lambda}{8\pi^2} \right)^2 \left[\frac{\pi^2}{6} - \log \left| \frac{t_{12}t_{23}}{t_{31}\epsilon} \right| + \frac{1}{2} \left(\log \left| \frac{t_{12}t_{23}}{t_{31}\epsilon} \right| \right)^2 \right]. \end{aligned} \quad (8.29)$$

Next the diagram with $(n_{12} \cdot n_{23} - 1)(n_{23} \cdot n_{31} - 1)$ is given by

$$\begin{aligned} & (n_{12} \cdot n_{23} - 1)(n_{23} \cdot n_{31} - 1) \left(\frac{\lambda}{8\pi^2} \right)^2 \left[\int_{t_1^+}^{t_2^-} d\tau_1 \int_{t_2^+}^{t_3^-} d\tau_2 \int_{\tau_2}^{t_3^-} d\tau_3 \int_{t_3^+}^{\infty} d\tau_4 \frac{1}{\tau_{12}^2} \frac{1}{\tau_{34}^2} \right. \\ & \quad \left. + \int_{-\infty}^{t_1^-} d\tau_1 \int_{t_1^+}^{t_2^-} d\tau_2 \int_{t_2^+}^{t_3^+} d\tau_3 \int_{\tau_3}^{t_3^+} d\tau_4 \frac{1}{\tau_{14}^2} \frac{1}{\tau_{23}^2} \right] \\ & = -(n_{12} \cdot n_{23} - 1)(n_{23} \cdot n_{31} - 1) \left(\frac{\lambda}{8\pi^2} \right)^2 \left(\frac{\pi^2}{6} - \log \left| \frac{t_{12}t_{23}}{t_{31}\epsilon} \right| \log \left| \frac{t_{23}t_{31}}{t_{12}\epsilon} \right| \right). \end{aligned} \quad (8.30)$$

Self-energy and vertex diagrams

Next we consider the self-energy and vertex diagrams. In the three-point functions case, the divergence parts are canceled each other. Therefore, the relevant terms are only finite part of the vertex diagrams in figure 8.9. However, since the computations are tedious task, we devote the detail of the computation to Appendix C. We present only the final result here:

$$-(n_{12} \cdot n_{23} - 1) \left(\frac{\lambda}{8\pi^2} \right)^2 \left(3\zeta(3) + \frac{\pi^2}{3} \log \left| \frac{t_{12}t_{23}}{t_{31}\epsilon} \right| \right). \quad (8.31)$$

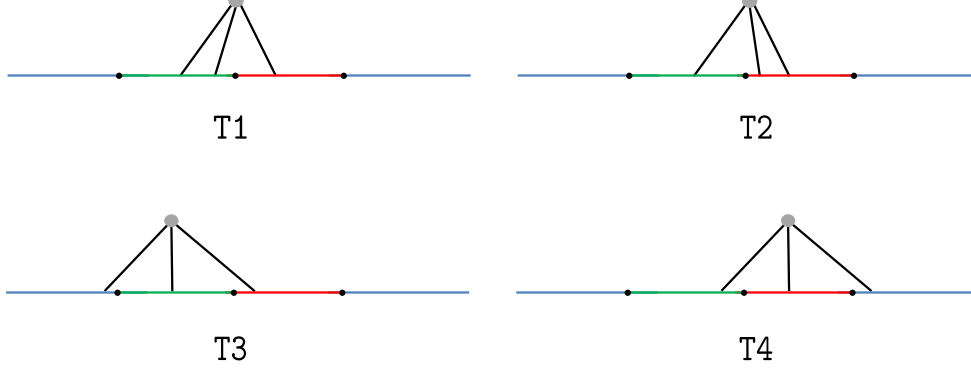


Figure 8.9: The two-loop diagram with one interaction vertex for the three-point functions. Notice that the each diagram produce the single $(n_{12} \cdot n_{23} - 1)$.

The result

Adding and symmetrizing them, we get the two-loop three-point functions as

$$\begin{aligned}
& \langle\langle \mathcal{O}_1^{\text{DCO}}(t_1) \mathcal{O}_2^{\text{DCO}}(t_2) \mathcal{O}_3^{\text{DCO}}(t_3) \rangle\rangle_{2\text{-loop}} = \\
& \left(\frac{\lambda}{8\pi^2} \right)^2 \sum_{\{i,j,k\}} \left[(n_{ij} \cdot n_{jk} - 1)^2 \left(\frac{\pi^2}{6} - \log \left| \frac{t_{ij} t_{jk}}{t_{ki} \epsilon} \right| + \frac{1}{2} \left(\log \left| \frac{t_{ij} t_{jk}}{t_{ki} \epsilon} \right| \right)^2 \right) \right. \\
& - (n_{ij} \cdot n_{jk} - 1)(n_{jk} \cdot n_{ki} - 1) \left(\frac{\pi^2}{6} - \log \left| \frac{t_{ij} t_{jk}}{t_{ki} \epsilon} \right| \log \left| \frac{t_{jk} t_{ki}}{t_{ij} \epsilon} \right| \right) \\
& \left. - (n_{ij} \cdot n_{jk} - 1) \left(3\zeta(3) + \frac{\pi^2}{3} \log \frac{t_{ij} t_{jk}}{t_{ki} \epsilon} \right) \right]. \tag{8.32}
\end{aligned}$$

Here, the $\sum_{\{i,j,k\}}$ means the sum over $\{i, j, k\} = \{1, 2, 3\}, \{2, 1, 3\}, \{3, 1, 2\}$.

Comparing (8.32) with the weak-coupling expansion (2.28) and using the two-point functions result, we can read off the two-loop anomalous dimension and the two-loop structure constant as follows:

$$\gamma_j^{(2)} = \frac{1}{(8\pi^2)^2} \left[(n_{ij} \cdot n_{jk} - 1)^2 + \frac{\pi^2}{3} (n_{ij} \cdot n_{jk} - 1) \right], \tag{8.33}$$

$$c_{123}^{(2)} = \frac{1}{(8\pi^2)^2} \frac{\pi^2}{12} \sum_{\{i,j,k\}} \left[(n_{ij} \cdot n_{jk} - 1)^2 - 2(n_{ij} \cdot n_{jk} - 1)(n_{jk} \cdot n_{ki} - 1) \right]. \tag{8.34}$$

As expected, the result for the two-loop anomalous dimension matches with the previous paper [80].

8.3 Three-point functions in the ladders limit

In this section, we consider a ladders limit. In this limit, the only specific diagrams survive and one can resum them by solving the Schwinger-Dyson equation (SD-equation). We



Figure 8.10: The ladder diagram.

perform such a resummation for the computation of the structure constant of DCOs as we explain below.

8.3.1 Set-up

The ladders limit is a double scaling limit: the 't Hooft coupling constant λ goes to zero while the angle θ , between the neighboring polarizations ($\cos \theta \equiv n_1 \cdot n_2$), goes to imaginary negative infinity:

$$\lambda \rightarrow 0, \quad (n_1 \cdot n_2) \rightarrow \infty \text{ with } \tilde{\lambda} \equiv \frac{\lambda(n_1 \cdot n_2)}{2} : \text{ fixed.} \quad (8.35)$$

Since $n_1 \cdot n_2$ sent to infinity, all the diagrams which contain gluon propagators or interaction vertices disappear in the limit. The only diagrams that survive are the ones which have scalar propagators connecting the two segments, which called ladder diagrams (See figure 8.10.). It is because the coefficients of the ladder diagram is $(n_1 \cdot n_2)^{\sharp}$ of order of loop. On the other hand, the diagrams that vanish here have $(n_1 \cdot n_2)^{\sharp}$ of order of loop $^{-1}$

The three-point function has three polarizations and we thus have three different angles $\cos \theta_i = n_{ij} \cdot n_{jk}$, $i = (1, 2, 3)$. We can therefore define three rescaled couplings⁴

$$\tilde{\lambda}_i \equiv \frac{\cos \theta_i \lambda}{2} \quad (i = 1, 2, 3). \quad (8.36)$$

Here, there are various different limits whether $\tilde{\lambda} = 0$ or $\tilde{\lambda} \neq 0$, depending on how we scale θ_i 's, in figure 8.11.

The simplest case among them is the limit in which one of the angle, say $\cos \theta_2$, sent to infinity while the others are kept finite. In this limit, the rescaled coupling constants become following configurations:

$$C_{123}^{\circ\circ\circ}, \quad \text{Case I : } \tilde{\lambda}_1 = \tilde{\lambda}_3 = 0, \quad \tilde{\lambda}_2 \neq 0, \quad (8.37)$$

The survive ladder diagrams are the connected two neighboring segments of \mathcal{O}_2 . In what follows, the operators whose effective coupling is zero, are called *trivial operators* such as \mathcal{O}_1 and \mathcal{O}_3 in this case. On the other hand, the operator \mathcal{O}_2 with non-vanishing effective coupling is a nontrivial operator.

The next simplest limit is the following limit,

$$C_{123}^{\bullet\bullet\circ}, \quad \text{Case II : } \tilde{\lambda}_1 \neq 0, \quad \tilde{\lambda}_2 \neq 0, \quad \tilde{\lambda}_3 = 0. \quad (8.38)$$

⁴See (8.3) for definitions of θ_i 's

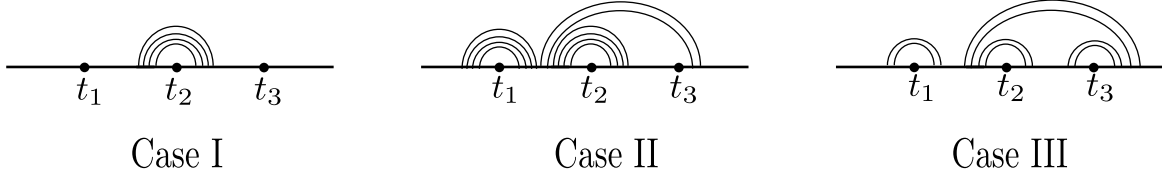


Figure 8.11: From the left diagrams to right diagrams, each structure constant are Case I, the Case II and the Case III.

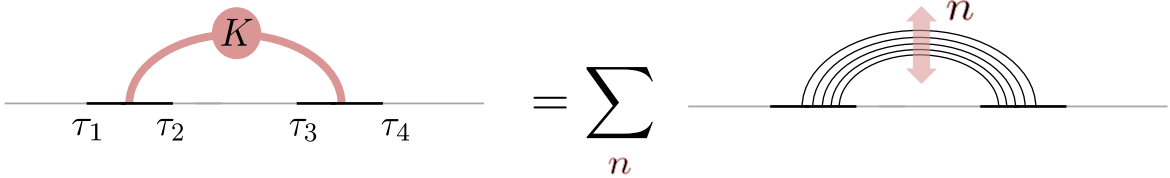


Figure 8.12: The bridge-kernel is defined as a sum over all the ladder diagrams.

The structure constants have two trivial DCOs, \mathcal{O}_1 , \mathcal{O}_2 , and one nontrivial DCO, \mathcal{O}_3 . Lastly, the most complicated structure constant case is in the following limit:

$$C_{123}^{\bullet\bullet\bullet}, \quad \text{Case III} : \tilde{\lambda}_1 \neq 0, \quad \tilde{\lambda}_2 \neq 0, \quad \tilde{\lambda}_3 \neq 0. \quad (8.39)$$

These three cases are discussed in subsections 8.3.4-8.3.6.

8.3.2 Bridge kernel and the SD-equation

In order to compute the ladder resummed diagrams, we first introduce a building block. It is defined as a sum over all the ladder diagrams see also figure 8.12 and we call the *bridge-kernel* $K(\tau_1, \tau_2|\tau_3, \tau_4)$.

The SD-equation of the bridge-kernel $K(\tau_1, \tau_2|\tau_3, \tau_4)$ is shown in figure 8.13 and given by

$$K(\tau_1, \tau_2|\tau_3, \tau_4) = 1 + \int_{\tau_1}^{\tau_2} ds \int_{\tau_3}^{\tau_4} dt P(t-s)K(\tau_1, s|t, \tau_4), \quad (8.40)$$

where $P(x) = \frac{\tilde{\lambda}}{4\pi^2} \frac{1}{x^2}$ is a scalar propagator connecting the two segments between $[\tau_1, \tau_2]$ and $[\tau_3, \tau_4]$. Then, we differentiate in respect to the variables τ_1 and τ_2 and derive a differential equation for the bridge-kernel as follows:

$$\partial_{\tau_2} \partial_{\tau_3} K = -P(\tau_3 - \tau_2)K. \quad (8.41)$$

Furthermore, for simplicity, we here use the one-dimensional cross ratio

$$z = \frac{\tau_{12}\tau_{34}}{\tau_{13}\tau_{24}}. \quad (8.42)$$



Figure 8.13: The SD-equation satisfied by the bridge-kernel K .

Using the variable, cross ratio, we can rewrite⁵ bridge-kernel (8.41) as a differential equation of the variable z :

$$\left[z(1-z)\frac{d^2}{dz^2} + (1-z)\frac{d}{dz} - \frac{\tilde{\lambda}}{4\pi^2(1-z)} \right] K(z) = 0. \quad (8.43)$$

Since this is a second-order differential equation, there are two linearly independent solutions⁶. Imposing the boundary condition which is $K(z=0) = 1$ (or equivalently $K|_{\tau_1 \rightarrow \tau_2} = K|_{\tau_3 \rightarrow \tau_4} = 1$), we can get correct solution. As a result, the bridge-kernel is given by the hypergeometric function

$$K(z) = (1-z)^{-\Omega} {}_2F_1(-\Omega, -\Omega, 1; z), \quad (8.44)$$

with

$$\Omega = \frac{1}{2} \left(-1 + \sqrt{1 + \frac{\tilde{\lambda}}{\pi^2}} \right). \quad (8.45)$$

Using the bridge-kernel, we compute a physically important quantity which we call the *vertex function* $\Gamma_\epsilon(S, T)$. Roughly speaking, the function is given by the limit $\tau_2 \rightarrow \tau_3$ in the bridge-kernel, see in figure 8.14. However, since such a quantity has UV divergence, one has to be cut off to regularize such divergence. Then, we introduce the point-splitting cut off in the same way as the two loop calculation in the previous section. Thus, the precise definition is given by

$$\Gamma_\epsilon(S, T) \equiv K(-S, -\epsilon/2 | \epsilon/2, T) = K\left(\frac{(S - \frac{\epsilon}{2})(T - \frac{\epsilon}{2})}{(S + \frac{\epsilon}{2})(T + \frac{\epsilon}{2})}\right) \quad (8.46)$$

Notice that from the differential equation of the bridge-kernel (8.41) the vertex function $\Gamma_\epsilon(S, T)$ also satisfies the following differential equation

$$\partial_S \partial_T \Gamma_\epsilon(S, T) = P(S+T) \Gamma_\epsilon(S, T), \quad (8.47)$$

From the bridge-kernel written by the hyper geometric function, we can calculate the ϵ expansion in the region $S, T \gg \epsilon$,

$$\Gamma_\epsilon(S, T) = \frac{A(\Omega)}{\epsilon^\Omega} \left(\frac{1}{S} + \frac{1}{T} \right)^{-\Omega} + O(\epsilon), \quad A(\Omega) = \frac{\Gamma(2\Omega + 1)}{\Gamma(\Omega + 1)^2}. \quad (8.48)$$

Then, we define the leading term of the ϵ as

⁵To rewrite the differential equation, we used $\partial_{\tau_2} = -\tau_{14}/(\tau_{12}\tau_{24}) \partial_z$ and $\partial_{\tau_3} = \tau_{14}/(\tau_{13}\tau_{34}) \partial_z$

⁶The other (incorrect) solution is $(1-z)^{-\Omega} [{}_2F_1^*(-\Omega, -\Omega, 1; z) + \log z {}_2F_1(-\Omega, -\Omega, 1; z)]$, with ${}_2F_1^*(a, b, c; z) = (\partial_a + \partial_b + 2\partial_c) {}_2F_1^*(a, b, c; z)$.

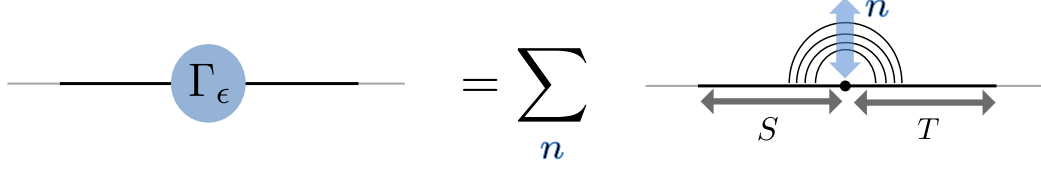


Figure 8.14: The vertex function. is defined as a sum of diagrams whose end-points are in $[-S, -\epsilon/2]$ and $[\epsilon/2, T]$ and the ϵ is a cut off parameter by point-splitting regularization.

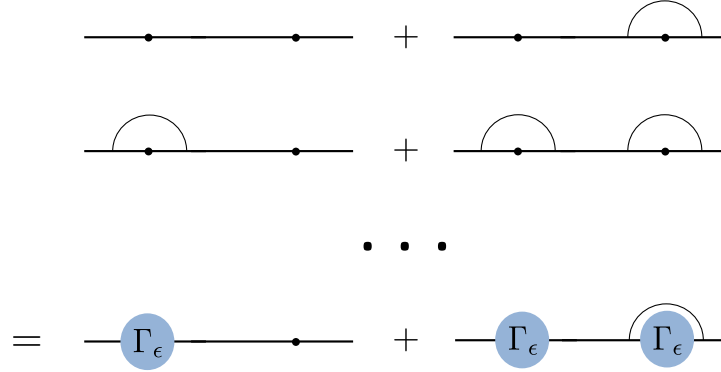


Figure 8.15: The resummation of the ladder diagrams for the two-point function. The left diagram, which has single vertex functions will be denoted as **Single**. On the other hand, the right diagram, which has double vertex functions will be denoted as **Double**.

$$\Gamma_{\text{IR}}(S, T) \equiv \frac{A(\Omega)}{\epsilon^\Omega} \left(\frac{1}{S} + \frac{1}{T} \right)^{-\Omega}.$$

As discussed in appendix D, there is an intriguing relation between the vertex function and the solutions to the Schrödinger equation.

8.3.3 Two-point functions and renormalization

In this subsection, we calculate the two-point functions of DCO's for the ladder resummed diagrams and determine the renormalization to calculate the three-point functions.

Using the vertex functions introduced the previous subsection, the two-point functions are in figure 8.15. The contributions of the two-point functions come from two parts: single vertex operator and double vertex operators

$$\begin{aligned} \text{Single} &= \Gamma_\epsilon(\infty, \tau_{21}), \\ \text{Double} &= \int_{\tau_1^+}^{\tau_2^-} ds \int_{\tau_2^+}^{\infty} dt \Gamma_\epsilon(\infty, s - \tau_1) P(t - s) \Gamma_\epsilon(\tau_2 - s, t - \tau_2). \end{aligned} \quad (8.49)$$

In advance, we state the important comment: for the contribution **single**, the order of the ϵ become **Single** $\sim \epsilon^{-\Omega}$. On the other hand, the **Double** has the order **Double** $\sim \epsilon^{-2\Omega}$.

Therefore, in the $\epsilon \rightarrow 0$ limit, the diagrams **Double** are relevant, rather than **Single**. In what follows, we check the fact and determine the renormalization from the diagrams **Double**.

We easily find that using the Γ_{IR} , the divergence part of the **Single** is evaluated as

$$\mathbf{Single} \sim \Gamma_{\text{IR}}(\infty, \tau_{21}) = \left(\frac{\tau_{21}}{\epsilon}\right)^\Omega. \quad (8.50)$$

The second diagram can be written as

$$\mathbf{Double} = \int_{\tau_1^+}^{\tau_2^-} ds \int_{\tau_2^+}^{\infty} dt \Gamma_\epsilon(\infty, s - \tau_1) (-\partial_s \partial_t) \Gamma_\epsilon(\tau_2 - s, t - \tau_2) \quad (8.51)$$

Here, we used the differential equation (8.47). Thus, computing the total derivative and the fact $\Gamma_\epsilon(*, \epsilon/2) = K(u)|_{u=0} = 0$, we get

$$- \int_{\tau_1^+}^{\tau_2^-} ds \Gamma_\epsilon(\infty, s - \tau_1) \partial_s \Gamma_\epsilon(\tau_2 - s, \infty) \quad (8.52)$$

Unlike the first contribution, there is a priori no reason to expect that Γ_ϵ can be approximated by Γ_{IR} in (8.52) since the arguments of Γ_ϵ can be of order $O(\epsilon)$. Nevertheless, it turns out that the leading singular piece in the limit $\epsilon \ll 1$ can be computed by replacing Γ_ϵ with Γ_{IR} .⁷ Replacing the vertex operators Γ_ϵ with Γ_{IR} , the diagram **Double** become straightforward:

$$\begin{aligned} \mathbf{Double} &\stackrel{\epsilon \ll 1}{\equiv} - \left(\frac{A(\Omega)}{\epsilon^\Omega}\right)^2 \int_{\tau_1}^{\tau_2} ds (s - \tau_1)^\Omega \partial_s (\tau_2 - s)^\Omega = \left(\frac{A(\Omega)}{\epsilon^\Omega}\right)^2 \Omega \int_0^1 d\bar{s} \bar{s}^\Omega (1 - \bar{s})^{\Omega-1} \\ &= \frac{\Gamma(2\Omega + 1) |\tau_{12}|^{2\Omega}}{\Gamma(\Omega + 1)^2 \epsilon^{2\Omega}}. \end{aligned} \quad (8.54)$$

In the second equality, we changed the variable as $\bar{s} = (s - \tau_1)/(\tau_1 - \tau_2)$. Furthermore, in the last equality we used the property of the Beta function

$$B(a, b) \equiv b \int_0^1 d\bar{s} \bar{s}^a (1 - \bar{s})^{b-1} = \frac{\Gamma(a + 1) \Gamma(b)}{\Gamma(a + b + 1)}. \quad (8.55)$$

Therefore we get the two-point functions of the bare DCO's for ladder diagrams as

$$\langle \mathcal{O}^{B, \text{DCO}}(\tau_1) \mathcal{O}^{B, \text{DCO}}(\tau_2) \rangle \stackrel{\epsilon \ll 1}{\equiv} \frac{\Gamma(2\Omega + 1) |\tau_{12}|^{2\Omega}}{\Gamma(\Omega + 1)^2 \epsilon^{2\Omega}}. \quad (8.56)$$

⁷Roughly speaking, this is because the difference between Γ_ϵ and Γ_{IR} ,

$$\Gamma_{\text{UV}} \equiv \Gamma_\epsilon - \Gamma_{\text{IR}}, \quad (8.53)$$

is of order $\epsilon \Gamma_{\text{IR}}$ whenever the arguments are $O(1)$ while it is of $O(1)$ only when the arguments are in a small interval of length ϵ near the origin. Therefore the contribution from Γ_{UV} is always $O(\epsilon)$ smaller than the contribution from Γ_{IR} . See Appendix E for more detailed arguments.

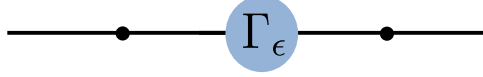


Figure 8.16: The three-point functions for the Case I.

Through the definition of the renormalized operator $\mathcal{O} = Z^{-1/2}\mathcal{O}^B$, the renormalized two-point function has a following canonical form:

$$\langle \mathcal{O}^{\text{DCO}}(\tau_1)\mathcal{O}^{\text{DCO}}(\tau_2) \rangle = Z^{-1}\langle \mathcal{O}, \text{DCO}(\tau_1)\mathcal{O}, \text{DCO}(\tau_2) \rangle = \frac{1}{|\tau_{12}|^{2\Delta}}. \quad (8.57)$$

Therefore, by comparing (8.56) with (8.57), we can get the conformal dimension and the renormalization factor of the DCO as follows:

$$\Delta(\tilde{\lambda}) = -\Omega, \quad Z(\tilde{\lambda}) = \frac{A(\Omega)}{\epsilon^{2\Omega}}. \quad (8.58)$$

As expected, the result for the conformal dimension matches the result in the literature [81]. Finally, we defined the renormalized vertex function Γ^R for later discussions as

$$\Gamma^R(S, T) \equiv \lim_{\epsilon \rightarrow 0} Z^{-1/2}\Gamma_{\text{IR}}(S, T) = \sqrt{A(\Omega)} \left(\frac{1}{S} + \frac{1}{T} \right)^{-\Omega}. \quad (8.59)$$

8.3.4 Case I: one nontrivial and two trivial DCOs

We now compute the three-point function of one nontrivial DCO and two trivial DCOs, see figure 8.16. In the figure, a nontrivial operator is in the middle and the structure constants are $C_{123}^{\circ\bullet\circ}$. Here and in what follows, the symbols \circ and \bullet signify a trivial DCO and a nontrivial DCO respectively. On the other hand, the others, for example $C_{123}^{\bullet\circ\circ}$, whose nontrivial operator is in the most-left, can be obtained as the same value with $C_{123}^{\circ\bullet\circ}$. Therefore, we only consider the $C_{123}^{\circ\bullet\circ}$ case. Thus, the configuration is easily given by the single vertex function as follows:

$$\begin{aligned} \langle \mathcal{O}_1^{\text{DCO}\circ}(\tau_1)\mathcal{O}_2^{\text{DCO}\bullet}(\tau_2)\mathcal{O}_3^{\text{DCO}\circ}(\tau_3) \rangle &= \Gamma^R(\tau_{21}, \tau_{32}) = \frac{C_{123}^{\circ\bullet\circ}}{\tau_{21}^{-\Omega}\tau_{32}^{-\Omega}\tau_{31}^{\Omega}}, \\ C_{123}^{\circ\bullet\circ} &= \sqrt{A(\Omega)} = \frac{\Gamma(2\Omega + 1)^{1/2}}{\Gamma(\Omega + 1)}. \end{aligned} \quad (8.60)$$

At weak coupling of the effective coupling constant $\tilde{\lambda}$, the result can be expanded from (8.45) as

$$C_{123}^{\circ\bullet\circ} = 1 + \frac{\pi^2}{12} \left(\frac{\tilde{\lambda}}{4\pi^2} \right)^2 - \left(\frac{\pi^2}{6} + \zeta(3) \right) \left(\frac{\tilde{\lambda}}{4\pi^2} \right)^3 + O(\tilde{\lambda}^4). \quad (8.61)$$

The result up to two loops reproduces the perturbative result for the ladder diagrams in the previous section. At strong coupling ($\tilde{\lambda} \gg 1$), on the other hand, the result



Figure 8.17: The structure constant $C_{123}^{\bullet\circ\circ}$, which is in Case I. The structure constants $C_{123}^{\circ\bullet\circ}$ are given by the two diagrams unlike the $C_{123}^{\circ\circ\bullet}$ in figure 8.16.

exponentiates and is given by

$$\ln C_{123}^{\circ\bullet\circ} \sim \frac{\sqrt{\tilde{\lambda}}}{2\pi} \ln 2. \quad (8.62)$$

On the other hand, we can compute the structure constant $C_{123}^{\bullet\circ\circ}$. As shown in figure 8.17, we have

$$\frac{C_{123}^{\bullet\circ\circ}}{\tau_{21}^{-\Omega} \tau_{32}^{\Omega} \tau_{31}^{-\Omega}} = \Gamma^R(\infty, \tau_{21}) + \underbrace{\frac{\tilde{\lambda}}{4\pi^2} \int_{\tau_1}^{\tau_2} ds \int_{\tau_3}^{\infty} dt \frac{\Gamma^R(\infty, s - \tau_1) K(s, \tau_2 | \tau_3, t)}{(t - s)^2}}_{(*)}. \quad (8.63)$$

Using the differential equation of the SD-equation (8.41), and boundary condition $K(*, *' | x, x) = 1$, the integration can be evaluated in appendix F and we obtain the expected result

$$C_{123}^{\bullet\circ\circ} = C_{123}^{\circ\bullet\circ} = \sqrt{A(\Omega)}. \quad (8.64)$$

8.3.5 Case II: two nontrivial and one trivial DCOs

Next we calculate the structure constant for Case II. Since the operators have two nontrivial conformal dimensions $\Delta_i = -\Omega_i$, the structure constant have following form:

$$\langle \mathcal{O}_1^{\text{DCO}\bullet}(\tau_1) \mathcal{O}_2^{\text{DCO}\bullet}(\tau_2) \mathcal{O}_3^{\text{DCO}\circ}(\tau_3) \rangle = \frac{C_{123}^{\bullet\bullet\circ}}{\tau_{21}^{-\Omega_1 - \Omega_2} \tau_{32}^{\Omega_1 - \Omega_2} \tau_{31}^{-\Omega_1 + \Omega_2}}. \quad (8.65)$$

The diagrams of Case II is in 8.3.3. The diagrams also include two patterns: single vertex functions and double vertex functions. However, in the same argument as the Case I, the relevant diagrams are just with a maximal number of vertex functions.

The renormalized three-point function is given by

$$\begin{aligned} \langle \mathcal{O}_1^{\text{DCO}\bullet} \mathcal{O}_2^{\text{DCO}\bullet} \mathcal{O}_3^{\text{DCO}\circ} \rangle &= \int_{\tau_1}^{\tau_2} ds \int_{\tau_2}^{\tau_3} dt \int_{-\infty}^{\tau_1} du \int_{\tau_1}^s dv (-\partial_u \partial_v) \Gamma_1^R(\tau_1 - u, v - \tau_1) \\ &\quad \times K_1(v, s | \tau_3, \infty) (-\partial_s \partial_t) \Gamma_2^R(\tau_2 - s, t - \tau_2). \end{aligned} \quad (8.66)$$

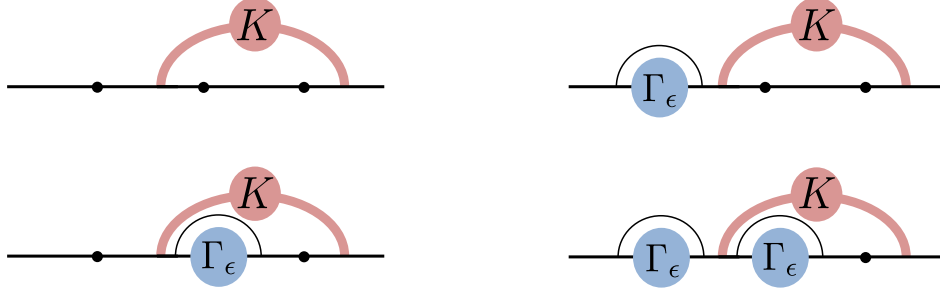


Figure 8.18: The three-point functions for Case II have four diagrams. However, the most dominant contribution in the limit $\epsilon \rightarrow 0$ is only double vertex functions.

Here we used the SD-equation (8.41). In (8.66), the integral of u can be easily computed. Thus, the integral of v is just the same with (8.63)

$$\int_{\tau_1}^s dv \partial_v \Gamma_1^R(\infty, v - \tau_1) K_1(v, s | \tau_3, \infty) = \tau_{31}^{\Omega_1} \left(\frac{s - \tau_1}{\tau_3 - s} \right)^{\Omega_1} \sqrt{A(\Omega_1)} \quad (8.67)$$

Therefore, (8.66) become

$$\begin{aligned} \langle \mathcal{O}_1^{\text{DCO}} \bullet \mathcal{O}_2^{\text{DCO}} \bullet \mathcal{O}_3^{\text{DCO}} \rangle &= \tau_{31}^{\Omega_1} \sqrt{A(\Omega_1)} \int_{\tau_1}^{\tau_2} ds \int_{\tau_2}^{\tau_3} dt \left(\frac{s - \tau_1}{\tau_3 - s} \right)^{\Omega_1} (-\partial_s \partial_t) \Gamma_2^R(\tau_2 - s, t - \tau_2) \\ &= -\tau_{31}^{\Omega_1} \tau_{32}^{\Omega_2} \sqrt{A(\Omega_1) A(\Omega_2)} \int_{\tau_1}^{\tau_2} ds \left(\frac{s - \tau_1}{\tau_3 - s} \right)^{\Omega_1} \partial_s \left(\frac{\tau_2 - s}{\tau_3 - s} \right)^{\Omega_2}. \end{aligned} \quad (8.68)$$

The last integral can be done explicitly⁸ by performing the following change of variables, which amounts to performing the Möbius transformation $(\tau_1, \tau_2, \tau_3) \rightarrow (0, 1, \infty)$:

$$\bar{s} = \frac{s - \tau_1}{s - \tau_3} \frac{\tau_2 - \tau_3}{\tau_2 - \tau_1}. \quad (8.69)$$

As a result, we finally get the two nontrivial structure constant

$$C_{123}^{\bullet\bullet\bullet} = \sqrt{A(\Omega_1) A(\Omega_2)} I(\Omega_1, \Omega_2) = \frac{\Gamma(2\Omega_1 + 1)^{1/2} \Gamma(2\Omega_2 + 1)^{1/2}}{\Gamma(\Omega_1 + \Omega_2 + 1)}. \quad (8.70)$$

Surely, setting the $\Omega_2 = 0$, we can reproduce the $C_{123}^{\bullet\bullet\bullet}$. Weak coupling expansion of the result is

$$C_{123}^{\bullet\bullet\bullet} = 1 + \frac{(\tilde{\lambda}_1 - \tilde{\lambda}_2)^2}{192\pi^2} + \frac{(\tilde{\lambda}_1 - \tilde{\lambda}_2)^2 (\tilde{\lambda}_1 + \tilde{\lambda}_2) (\pi^2 + 6\zeta(3))}{384\pi^6} + O(\tilde{\lambda}^4), \quad (8.71)$$

whereas at strong coupling we have

$$\ln C_{123}^{\bullet\bullet\bullet} \sim \Omega_1 \ln \frac{2\Omega_1}{\Omega_1 + \Omega_2} + \Omega_2 \ln \frac{2\Omega_2}{\Omega_1 + \Omega_2}, \quad \Omega_i \sim \frac{\sqrt{\tilde{\lambda}_i}}{2\pi}. \quad (8.72)$$

The result at two loops at weak coupling matches the ladder contribution to the perturbative result given in section 8.2.

⁸The integral reduces to the integral for $I(a, b)$ given in (8.55).

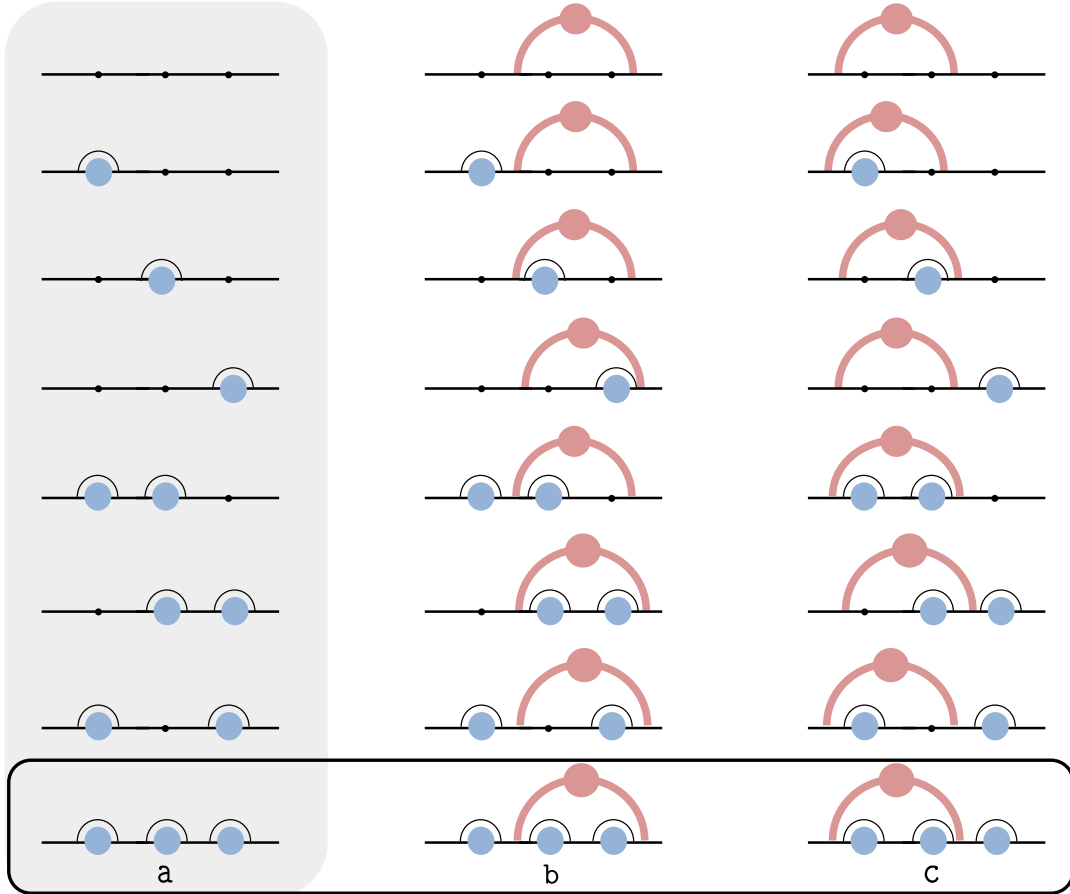


Figure 8.19: The three-point functions for Case III. It seems that there are a lot of diagrams. However, in the same argument as the previous cases, the dominant diagrams in the limit $\epsilon \rightarrow 0$ are only triple vertex diagrams.

8.3.6 Case III: three nontrivial DCOs

In this subsection, we compute the most general three-point functions of DCOs,

$$\langle \mathcal{O}_1^{\text{DCO}\bullet}(\tau_1) \mathcal{O}_2^{\text{DCO}\bullet}(\tau_2) \mathcal{O}_3^{\text{DCO}\bullet}(\tau_3) \rangle = \frac{C_{123}^{\bullet\bullet\bullet}}{\tau_{21}^{-\Omega_1 - \Omega_2 + \Omega_3} \tau_{32}^{-\Omega_2 - \Omega_3 + \Omega_1} \tau_{31}^{-\Omega_3 - \Omega_1 + \Omega_2}}. \quad (8.73)$$

As shown in figure 8.19, there are 24 diagrams for the Case III. However, only three diagrams which are a, b and c in figure 8.19, are relevant diagrams since they contain a maximal number of vertex functions. 8.3.3.

We first consider the diagram **b** and given by

$$\begin{aligned}
\mathbf{b} &= \int_{\tau_1}^{\tau_2} ds \int_{\tau_2}^{\tau_3} dt \int_{\tau_3}^{\infty} du \int_t^{\tau_3} dv \int_{-\infty}^{\tau_1} dw \int_{\tau_1}^s dx K(x, s|u, \infty) \\
&\quad \times (-\partial_w \partial_x) \Gamma^R(w - \tau_1, x - \tau_1) (-\partial_s \partial_t) \Gamma^R(\tau_2 - s, t - \tau_2) (-\partial_u \partial_v) \Gamma^R(\tau_3 - v, u - \tau_3) \\
&= \prod_{i=1}^3 \sqrt{A(\Omega_i)} \int_{\tau_1}^{\tau_2} ds \int_{\tau_2}^{\tau_3} dt \int_{\tau_3}^{\infty} du \left(\frac{(s - \tau_1)(u - \tau_1)}{u - s} \right)^{\Omega_1} \\
&\quad \times (-\partial_s \partial_t) \left(\frac{(\tau_2 - s)(t - \tau_2)}{t - s} \right)^{\Omega_2} \partial_u \left(\frac{(\tau_3 - t)(u - \tau_3)}{u - t} \right)^{\Omega_3}.
\end{aligned} \tag{8.74}$$

Then, performing the integration by parts for the variable u , we get the contribution of the diagram **a** as a surface term:

$$\mathbf{b} = -\mathbf{a} + I_2, \tag{8.75}$$

with

$$\begin{aligned}
\mathbf{a} &= (-1) \times \int_{\tau_1}^{\tau_2} ds \int_{\tau_2}^{\tau_3} dt \int_t^{\tau_3} du \int_{\tau_3}^{\infty} dv \Gamma^R(\infty, s - \tau_1) (-\partial_s \partial_t) \Gamma^R(\tau_2 - s, t - \tau_2) \\
&\quad \times (-\partial_u \partial_v) \Gamma^R(\tau_3 - u, v - \tau_3) \\
&= \prod_{i=1}^3 \sqrt{A(\Omega_i)} \int_{\tau_1}^{\tau_2} ds \int_{\tau_2}^{\tau_3} dt (s - t)^{\Omega_1} (-\partial_s \partial_t) \left(\frac{(\tau_2 - s)(t - \tau_2)}{t - s} \right)^{\Omega_2} (\tau_3 - t)^{\Omega_3}
\end{aligned} \tag{8.76}$$

and

$$\begin{aligned}
I_2 &= \prod_{i=1}^3 \sqrt{A(\Omega_i)} \int_{\tau_1}^{\tau_2} ds \int_{\tau_2}^{\tau_3} dt \int_{\tau_3}^{\infty} du (-\partial_u) \left(\frac{(s - \tau_1)(u - \tau_1)}{u - s} \right)^{\Omega_1} \\
&\quad \times (-\partial_s \partial_t) \left(\frac{(\tau_2 - s)(t - \tau_2)}{t - s} \right)^{\Omega_2} \left(\frac{(\tau_3 - t)(u - \tau_3)}{u - t} \right)^{\Omega_3}.
\end{aligned} \tag{8.77}$$

The contribution from the diagram **c** can be evaluated in a similar manner and the result reads

$$\begin{aligned}
\mathbf{c} &= \prod_{i=1}^3 \sqrt{A(\Omega_i)} \int_{\tau_1}^{\tau_2} ds \int_{\tau_2}^{\tau_3} dt \int_{-\infty}^{\tau_1} du (-\partial_u) \left(\frac{(s - \tau_1)(u - \tau_1)}{u - s} \right)^{\Omega_1} \\
&\quad \times (-\partial_s \partial_t) \left(\frac{(\tau_2 - s)(t - \tau_2)}{t - s} \right)^{\Omega_2} \left(\frac{(\tau_3 - t)(u - \tau_3)}{u - t} \right)^{\Omega_3}.
\end{aligned} \tag{8.78}$$

Summing up three contributions, we get

$$\langle \mathcal{O}_1^\bullet \mathcal{O}_2^\bullet \mathcal{O}_3^\bullet \rangle = \mathbf{a} + \mathbf{b} + \mathbf{c} = I_2 + \mathbf{c} \tag{8.79}$$

To further proceed, we perform the following change of variables,

$$\bar{s} = \frac{\tau_{23} s - \tau_1}{\tau_{21} s - \tau_3}, \quad \bar{t} = \frac{\tau_{31} t - \tau_2}{\tau_{32} t - \tau_1}, \quad \bar{u} = \frac{\tau_{12} u - \tau_3}{\tau_{13} u - \tau_2}. \tag{8.80}$$

After doing so, the three-point function have the following simple form:

$$C_{123}^{\bullet\bullet\bullet} = \left(\prod_{i=1}^3 \sqrt{A(\Omega_i)} \right) \times J, \quad (8.81)$$

$$J \equiv - \int_0^1 d\bar{s} \int_0^1 d\bar{t} \int_0^1 d\bar{u} \partial_{\bar{u}} [g(\bar{u}, \bar{s})^{-\Omega_1}] \partial_{\bar{s}} [g(\bar{s}, \bar{t})^{-\Omega_2}] \partial_{\bar{t}} [g(\bar{t}, \bar{u})^{-\Omega_3}].$$

with $g(x, y) \equiv (1-x)^{-1} + y^{-1} - 1$. The integral J can be evaluated explicitly. The tedious expression is in Appendix G.

Then, the weak coupling expansion of the effective coupling $\tilde{\lambda}$ is given by

$$C_{123}^{\bullet\bullet\bullet} = 1 + \frac{1}{192\pi^2} \left(\sum_i^3 \tilde{\lambda}_i^2 - 2 \sum_{i<j} \tilde{\lambda}_i \tilde{\lambda}_j \right) + \frac{\pi^2 + 6\zeta(3)}{384\pi^6} \left(\sum_{i=1}^3 \tilde{\lambda}_i^3 - \sum_{i<j} (\tilde{\lambda}_i^2 \tilde{\lambda}_j + \tilde{\lambda}_i \tilde{\lambda}_j^2) \right) + \frac{\pi^2 - 3 - 6\zeta(3)}{192\pi^6} \tilde{\lambda}_1 \tilde{\lambda}_2 \tilde{\lambda}_3 + \mathcal{O}(\tilde{\lambda}^4). \quad (8.82)$$

We can explicitly check the result with the two-loop calculation in section 8.2. Furthermore, when we take the limits $\tilde{\lambda}_i$, we can reproduce the results in the previous subsections.

In order to evaluate the strong coupling expansion ($\tilde{\lambda}_i \gg 1$), we use the saddle-point approximation of the integral J ,

$$J = \int_0^1 d\bar{s} \int_0^1 d\bar{t} \int_0^1 d\bar{u} e^{f(\bar{s}, \bar{t}, \bar{u})}, \quad (8.83)$$

$$f(\bar{s}, \bar{t}, \bar{u}) = -\Omega_1 \log g(\bar{u}, \bar{s}) - \Omega_2 \log g(\bar{s}, \bar{t}) - \Omega_3 \log g(\bar{t}, \bar{u}) + O(\ln \tilde{\lambda}).$$

By analyzing the saddle-point approximation of J , that is $\partial_{\bar{s}} g = \partial_{\bar{t}} g = \partial_{\bar{u}} g = 0$, we find the two solutions. However, the relevant solution for the integral, which is inside the integration region is given by

$$(\bar{s}^*, \bar{t}^*, \bar{u}^*) = \left(\frac{\Omega_1}{\Omega_1 + \Omega_2}, \frac{\Omega_2}{\Omega_2 + \Omega_3}, \frac{\Omega_3}{\Omega_3 + \Omega_1} \right). \quad (8.84)$$

At the saddle point $(\bar{s}^*, \bar{t}^*, \bar{u}^*)$, we get the strong coupling expansions as follows:

$$\ln C_{123}^{\bullet\bullet\bullet} \sim \Omega_1 \log \frac{2\Omega_1}{\Omega_1 + \Omega_2 + \Omega_3} + \Omega_2 \log \frac{2\Omega_2}{\Omega_1 + \Omega_2 + \Omega_3} + \Omega_3 \log \frac{2\Omega_3}{\Omega_1 + \Omega_2 + \Omega_3}. \quad (8.85)$$

Chapter 9

Non-BPS operators – perturbation and integrability

In this chapter, we calculate the three-point functions of non-BPS operators inserted into the Wilson loop. In the same way as the single trace operators, first of all, we choose the following state:

$$\mathcal{O}_1 : Z^{L_1}, \quad \mathcal{O}_2 : \bar{Z}^{L_1}, \quad \mathcal{O}_3 : \tilde{Z}^{L_3} = (Z + \bar{Z} + Y - \bar{Y})^{L_3}. \quad (9.1)$$

Furthermore, we insert the another complex scalar Y as an excitation. Then, we used the total scalars $\phi^i, i = (1, 2, 3, 4)$ in the operators. On the other hand, we have a choice what the scalar coupled to the Wilson loop is. If we choose the Wilson loop scalar as the same scalar of the operators, there are direct contractions between the operator and Wilson loop:



Furthermore, if we take the $\phi^i, i = (1, 2, 3, 4)$ scalar in the Wilson loop, such a configuration can't be BPS even if the operators are ordinary vacuums state (9.1). For the other choices, the Wilson loop scalar is ϕ^5 or ϕ^6 , there are not direct contracting diagrams and it becomes BPS state when the operators are (9.1). Therefore, the choice of the Wilson loop scalar is very important. In this chapter, we ordinarily choose the Wilson loop coupled to the scalar ϕ^6 as follows:

$$W = \exp \left[\int d\tau (iA_\mu \dot{x}^\mu + \phi_6 |\dot{x}^\mu|) \right], \quad (9.2)$$

In the section 9.1, we first explain the open spin chain under the coordinate Bethe ansatz. Next, in the section 9.2 we calculate the structure constants by using the tailoring method.

9.1 Open spin-chain and wave functions

In our set up, the one-loop anomalous dimension is corresponding to the eigenvalue of the $XXX_{1/2}$ open spin-chain Hamiltonian [85]. Thus, the open spin-chain Hamiltonian introduced in [86] is given by

$$\mathcal{H}_{\text{open}} = \sum_{k=1}^{L-1} (I_{k,k+1} - P_{k,k+1}) + C_1(I - Q_1^{\phi_6}) + C_L(I - Q_L^{\phi_6}), \quad (9.3)$$

where $I_{k,k+1}$ is the identity operator in flavor-space and $P_{k,k+1}$ is the permutation operator which switches two scalars at site k and at site $k+1$ each other. Here, the operators $Q_1^{\phi_6}$ and $Q_L^{\phi_6}$ appear since we chose the scalar in the Wilson loop as ϕ_6 . As a result, $Q_1^{\phi_6}$ and $Q_L^{\phi_6}$ are defined as¹

$$\begin{aligned} Q_1^{\phi_6} |\phi_6 \cdots\rangle &= 0, & Q_1^{\phi_6} |Z \cdots\rangle &= |Z \cdots\rangle, \\ Q_L^{\phi_6} |\cdots \phi_6\rangle &= 0, & Q_L^{\phi_6} |\cdots Z\rangle &= |\cdots Z\rangle. \end{aligned} \quad (9.4)$$

The coefficients C_1 and C_L determine the boundary condition of the Bethe wave function. For example, if the excitations are the Y scalar, the boundary coefficients are given as $C_1 = C_L = 0$ and the wave function satisfies the Neumann boundary condition. On the other hand, the excitations include the ϕ_6 scalar, the boundary coefficients C_1 and C_L become non-zero. In fact, the boundary coefficients depend on the contraction between the operator and Wilson loop.

9.1.1 One-magnon

Let us begin by giving the explicit form of the open spin-chain state for a few number of magnons in our conventions. The eigenfunction for one-magnon $|\Psi_{\text{open}}^{(1)}\rangle$ is defined as

$$\mathcal{H}_{\text{open}} |\Psi_{\text{open}}^{(1)}\rangle = E^{(1)} |\Psi_{\text{open}}^{(1)}\rangle. \quad (9.5)$$

Then, the Bethe state is written as

$$\begin{aligned} |\Psi_{\text{open}}^{(1)}\rangle &= \sum_{1 \leq x \leq L} \psi_{\text{open}}^{(1)}(x) |Z \cdots Z \overset{x}{\downarrow} Y Z \cdots Z\rangle, \\ \psi_{\text{open}}^{(1)}(x) &= A'(p) \left(\mathcal{A}(x, p) + e^{2ipL} B_L(p) \mathcal{A}(x, -p) \right) \quad \text{with} \quad B_L(p) = -\frac{e^{-ip} - (1 - C_L)}{1 - (1 - C_L)e^{-ip}}, \end{aligned} \quad (9.6)$$

where $A'(p)$ is a normalization factor of the wave function. The propagation factor is defined as $\mathcal{A}(x, p) \equiv e^{ip(x-\frac{1}{2})}$. Notice that the factor is half-step shifted, such feature is first mentioned in [88]. The wave function can be interpreted as a dynamical processes on the spin chain coordinate, see also figure 9.1. The details of the wave function are analyzed in appendix H.

¹The notation was introduced in [87]. In addition, although we shall not introduce the computations, we actually have calculated the $SO(6)$ Hamiltonian by evaluating all Feynman diagrams, and could check that the result is written as the above form.

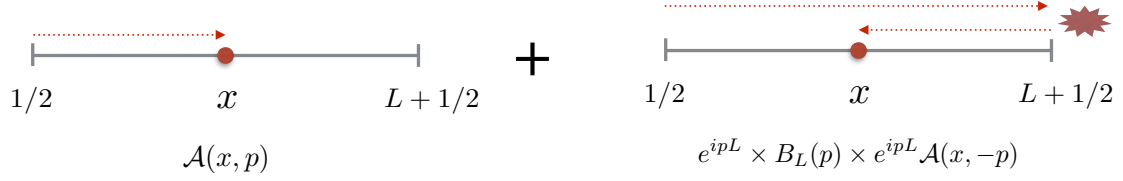


Figure 9.1: The first term $\mathcal{A}(x, p)$ in the wave function (H.2) shows that the magnon is propagated from the site at $1/2$ to the site at x . The second term $e^{2ipL} B_L(p) \mathcal{A}(x, -p)$ is factorized to $e^{ipL} B_L(p) e^{ipL} \mathcal{A}(x, -p)$. It shows that the magnon first go to the other boundary at $L + 1/2$ and reflected denoted by boundary factor $B_L(p)$. After doing so, the magnon return back to the site at x .

9.1.2 Two-magnon

Next the two-magnon eigenfunction is given by

$$\mathcal{H}_{\text{open}} |\Psi_{\text{open}}^{(2)}\rangle = E^{(2)} |\Psi_{\text{open}}^{(2)}\rangle. \quad (9.7)$$

The Bethe ansatz state for the two-magnon is

$$|\Psi_{\text{open}}^{(2)}\rangle = \sum_{1 \leq x_1 < x_2 \leq L} \psi_{\text{open}}^{(2)}(x_1, x_2) |Z \cdots Z \overset{x_1}{\downarrow} Y Z \cdots Z \overset{x_2}{\downarrow} Y Z\rangle,$$

$$\begin{aligned} \psi_{\text{open}}^{(2)}(x_1, x_2) / A'(p_1, p_2) &= f(x_1, p_1; x_2, p_2) + e^{2ip_2L} B_L(p_2) f(x_1, p_1; x_2, -p_2) \\ &+ S(p_2, p_1) S(-p_2, p_1) e^{2ip_1L} B_L(p_1) f(x_1, -p_1; x_2, p_2) \\ &+ S(p_2, p_1) S(-p_2, p_1) e^{2i(p_1+p_2)L} B_L(p_1) B_L(p_2) f(x_1, -p_1; x_2, -p_2), \end{aligned} \quad (9.8)$$

where $A'(p_1, p_2)$ is a normalization factor. Note that the S -matrix for $SU(2)$ sector is given as

$$S(p_2, p_1) = \frac{u - v - i}{u - v + i},$$

where $u = \cot \frac{p_1}{2}$ and $v = \cot \frac{p_2}{2}$ are ordinary rapidity notations. Notice that the S -matrix is the same with the closed spin chain's one and has the following property:

$$S(-p_j, p_i) = S(-p_i, p_j).$$

The factor $f(x_1, p_1; x_2, p_2)$ is defined as

$$f(x_1, p_1; x_2, p_2) \equiv \mathcal{A}(x_1, p_1) \mathcal{A}(x_2, p_2) + S(p_2, p_1) \mathcal{A}(x_1, p_2) \mathcal{A}(x_2, p_1), \quad (9.9)$$

The terms are just the summation over the permutations property, which appear in the closed spin chain system. The dynamical processes of the two-magnon wave function are

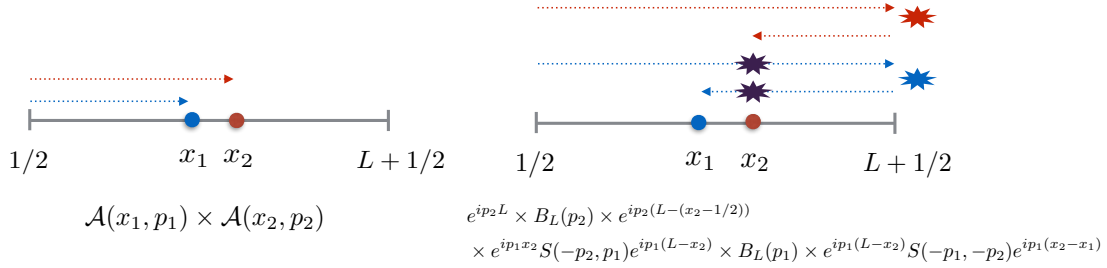


Figure 9.2: For the first term $\mathcal{A}(x_1, p_1)\mathcal{A}(x_2, p_2)$, the red magnon first go to site x_2 . After doing so, the blue magnon go to the site x_1 . For the final term, each red and blue magnon go to the other boundary and return back to the site x_2 and x_1 respectively after reflecting by the boundary. Then, the ordering of the positions of the magnons are changed each other. By taking account into such contribution, we add the S-matrix factors appropriately.

understood as in figure 9.2.² In the two-magnon wave functions (9.8), we found that the wave function is basically constructed by the summation over the sign flipping terms of $f(x_1, p_1; x_2, p_2)$ as follows:

$$f(x_1, p_1; x_2, p_2), f(x_1, -p_1; x_2, p_2), f(x_1, p_1; x_2, -p_2), f(x_1, -p_1; x_2, -p_2). \quad (9.10)$$

In addition, because of the scatterings of the magnons, we must insert the boundary coefficient, S-matrix factor and propagation factors such as $e^{2ip_1 L} B_L(p_1) S(p_2, p_1) S(-p_2, p_1)$. Such a factors are inserted when the sign of the momentum p_l is flipped. For multi-magnon case, the factor is generalized as

$$e^{2ip_l L} B_L(p_l) \prod_{k>l} S(p_k, p_l) S(-p_k, p_l). \quad (9.11)$$

Based on these systematic constructions, we can find the multi-magnon open spin chain wave function.

9.1.3 Multi-magnon

The M -magnon wave function can be decomposed into two parts: summation over the sign flipping terms with appropriate factors and summation over the permutation. Thereby it

²For intuitive understanding, it may be better to rewrite the S-matrix factor $S(p_2, p_1) S(-p_2, p_1)$ as $S(p_2, p_1) S(-p_1, p_2)$.

is written down:

$$\psi_{\text{open}}^{(M)} = \sum_{\mathbf{P}_+ \cup \mathbf{P}_- = \{1, \dots, M\}} \underbrace{\left[\prod_{l \in \mathbf{P}_-} (e^{2ip_l L}) \prod_{k > l} S(p_k, p_l) S(-p_k, p_l) \right]}_{\text{summation over the sign flipping terms with appropriate factors}} f(\hat{p}_1, \dots, \hat{p}_M),$$

$$f(\hat{p}_1, \dots, \hat{p}_M) \equiv \underbrace{\sum_{\sigma_1 \neq \dots \neq \sigma_M} \prod_{\substack{j < k \\ \sigma_k < \sigma_j}} S(\hat{p}_{\sigma_j}, \hat{p}_{\sigma_k})}_{\text{summation over the permutation}} \prod_{m=1}^M \mathcal{A}(x_m, \hat{p}_{\sigma_m}), \quad (9.12)$$

where \hat{p}_i is defined as

$$\hat{p}_i = \begin{cases} p_i & i \in \mathbf{P}_+ \\ -p_i & i \in \mathbf{P}_- \end{cases}. \quad (9.13)$$

Notice that the $f(\hat{p}_1, \dots, \hat{p}_M)$ in the wave functions is the same with the closed spin chain wave function.

9.2 Structure constants and the hexagon form factor

Using the open spin chain wave functions discussed above, we now calculate the structure constants at tree-level by using the tailoring method. Surprisingly, the hexagon form factors, which are introduced in the structure constants of the single trace operators, appear as a fundamental block.

9.2.1 A nontrivial operator with one-magnon : $C_{123}^{Y_{\circ\circ}}$

We first consider the following configurations

$$\mathcal{O}_1 : \sum_x Z^x Y Z^{L_1 - (x+1)}, \quad \mathcal{O}_2 : \bar{Z}^{L_2}, \quad \mathcal{O} : \tilde{Z}^{L_3}. \quad (9.14)$$

According to the ordinary tailoring method explained in section 4.2, we first do mapping, cutting and flipping and we have

$$\begin{aligned} \mathcal{O}_1 &\rightarrow |\dots Z \dots\rangle_1 \otimes \sum_x \psi_{\text{open}}^{(1)} \langle \dots Z Y Z \dots |, \\ \mathcal{O}_2 &\rightarrow |\dots \bar{Z} \dots\rangle_2 \otimes \langle \dots \bar{Z} \dots |, \\ \mathcal{O}_3 &\rightarrow |\dots \tilde{Z} \dots\rangle_3 \otimes \langle \dots \tilde{Z} \dots |. \end{aligned}$$

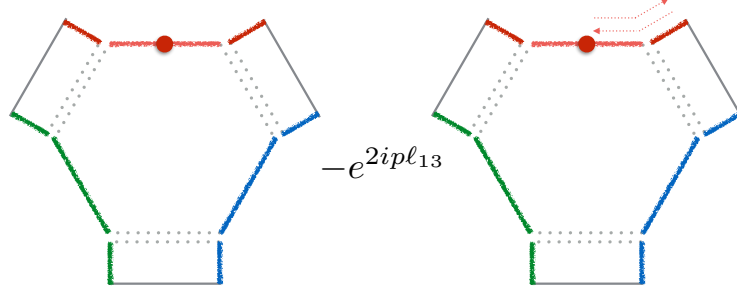


Figure 9.3: The first term means that a magnon is located at the start point ℓ_{12} , which is shifted by the normalization. The second term has the propagation factor $e^{2ip\ell_{13}}$. It shows that the magnon is propagated to the right-boundary and return back to the start point.

Contracting them, the structure constants are given by

$$C_{123}^{1\circ\circ} \propto \sum_{x_2=\ell_{12}+1}^{L_1} \psi_{\text{open}}^{(1)}(x). \quad (9.15)$$

The summation of the propagator $\mathcal{A}(x, p)$ in the wave function becomes

$$\sum_{x_2=\ell_{12}+1}^{L_1} \mathcal{A}(x, p) = \mathcal{M}(p)(e^{ip\ell_{12}} - e^{ipL_1}), \quad (9.16)$$

where the factor $\mathcal{M}(p) \equiv (e^{-i\frac{p}{2}} - e^{i\frac{p}{2}})^{-1}$ obeys a useful identity $\mathcal{M}(p) = -\mathcal{M}(-p)$. Therefore, we get

$$\begin{aligned} C_{123}^{1\circ\circ} &\propto \mathcal{M}(p)(e^{ip\ell_{12}} - e^{2ipL_1}e^{-ip\ell_{12}}) \\ &= \mathcal{M}_{\ell_{12}}(p)(1 - e^{2ip\ell_{13}}), \quad \mathcal{M}_{\ell_{12}}(p) \equiv \mathcal{M}(p)e^{ip\ell_{12}} \end{aligned} \quad (9.17)$$

Then, we defined the normalization including the exponent of the bridge length $e^{ip\ell_{12}}$. It means that we should interpret as the start point of the magnon is changed to the point ℓ_{12} , rather than $1/2$.

9.2.2 A nontrivial operator with two-magnon : $C_{123}^{Y^2\circ\circ}$

Next we consider the case of a nontrivial operator with two excitations as follows:

$$\mathcal{O}_1 : \sum_{x<y} Z^x Y Z^{y-(x+1)} Y Z^{L_1-(y+1)}, \quad \mathcal{O}_2 : \bar{Z}^{L_2}, \quad \mathcal{O} : \tilde{Z}^{L_3}. \quad (9.18)$$

Then, the structure constants become

$$C_{123}^{Y^2\circ\circ} \propto \sum_{1 \leq x_1 < x_2 \leq L_1} \psi_{\text{open}}^{(2)}(x_1, x_2) = \sum_{x_1=\ell_{12}+1}^{L_1} \sum_{x_2=x_1+1}^{L_1} \psi_{\text{open}}^{(2)}(x_1, x_2). \quad (9.19)$$

Notice that we extend the summation range because the contribution of $x_1 = L_1$ becomes zero. The summation of the product of the propagators $\mathcal{A}(x_1, p_1)\mathcal{A}(x_2, p_2)$ in the two-magnon wave function $\psi_{\text{open}}^{(2)}$ is written as

$$\begin{aligned} & \sum_{1 \leq x_1 < x_2 \leq L_1} \mathcal{A}(x_1, p_1)\mathcal{A}(x_2, p_2) \\ &= \mathcal{M}(p_1)\mathcal{M}(p_2) \left\{ \frac{i+2v}{2(u+v)} e^{i(p_1+p_2)\ell_{12}} - e^{ip_2 L_1} e^{ip_1 \ell_{12}} + \left(-\frac{i+2v}{2(u+v)} + 1 \right) e^{i(p_1+p_2)L_1} \right\}. \end{aligned} \quad (9.20)$$

Here, there are nontrivial factors $\frac{i+2v}{2(u+v)}$. Such factors come from the geometric series and we can give the appropriate expression in the same way as the three-point functions of the closed string in section 4.2.

Next we substitute the result (9.20) in the two-magnon wave function (9.8) and we get the structure constant as follows:

$$\begin{aligned} C_{123}^{Y^2\circ\circ} &\propto \mathcal{M}_{\ell_{12}}(p_1)\mathcal{M}_{\ell_{12}}(p_2) \left\{ \frac{u-v}{i+u-v} - S(p_2, p_1)S(-p_2, p_1) e^{2ip_1 \ell_{13}} \frac{-u-v}{i-u-v} \right. \\ &\quad \left. - e^{2ip_2 \ell_{13}} \frac{u+v}{i+u+v} + S(p_2, p_1)S(-p_2, p_1) e^{2i(p_1+p_2)\ell_{13}} \frac{-u+v}{i-u+v} \right\}. \end{aligned} \quad (9.21)$$

Here, we obtained nontrivial factors, i.e. $\frac{u-v}{i+u-v}$. Actually, this factor is known as the hexagon form factor, which is introduced in the three-point functions of the closed string, at tree-level

$$h_{YY}(u, v) = \frac{u-v}{i+u-v} + \mathcal{O}(g).$$

As an another case, we calculate the structure constants $C_{123}^{YY\circ}$ in appendix K

9.2.3 A nontrivial operator with M -magnon : $C_{123}^{YM\circ\circ}$

By doing similar tasks, we would like to get the structure constants for the multi-magnon. The wave function for the multi-magnon is naively written as

$$\sum_{x_1 < \dots < x_M} \psi_{\text{open}}^{(M)}(x_1, \dots, x_M). \quad (9.22)$$

From a few magnons lessons, we expect that the summation of positions for the multi-magnon wave function should be obtained by summing the hexagon form factor over all patterns such as flipping momentum signs with the negative weight. To justify the above statement, we prove the following two lemmas:

1. Bridge length dependent terms : the bridge length dependent terms such as $e^{i(p_1+\dots+p_M)\ell_{12}}$ produce the multi-magnon hexagon form factors.
2. Bridge length independent terms : The others terms which are independent of the bridge length, completely vanish.

1. Multi-magnon hexagon form factor

We first focus on the sum over the permutation parts of the multi-magnon wave function (9.12):

$$\begin{aligned} & \sum_{x_1 < \dots < x_M} f(p_1, \dots, p_M) \\ &= \sum_{x_1 < \dots < x_M} \sum_{\sigma_1 \neq \dots \neq \sigma_M} \prod_{\substack{\sigma_k < \sigma_j \\ j < k}} S(p_{\sigma_j}, p_{\sigma_k}) \mathcal{A}(x_1, p_{\sigma_1}) \cdots \mathcal{A}(x_M, p_{\sigma_M}). \end{aligned} \quad (9.23)$$

As the above summation for a few number of magnons is relatively manageable, it is given in appendix I. The evaluation of the equation is the similar to the closed spin chain case. In fact, we start to recall the relation between the S -matrix and the hexagon form factor:

$$S(u, v) = \frac{h(v, u)}{h(u, v)}. \quad (9.24)$$

By using this, the product of S -matrices can be transformed as

$$\prod_{\substack{\sigma_k < \sigma_j \\ j < k}} S(p_{\sigma_j}, p_{\sigma_k}) = \left(\prod_{\substack{\sigma_k < \sigma_j \\ j < k}} h(u_{\sigma_k}, u_{\sigma_j}) \right) \left(\prod_{\substack{\sigma_k < \sigma_j \\ j < k}} \frac{1}{h(u_{\sigma_j}, u_{\sigma_k})} \right). \quad (9.25)$$

Using the same discussion with the closed case, we therefore can be rewritten the summation (9.23) as

$$h(u_1, \dots, u_M) \sum_{\sigma_1 \neq \dots \neq \sigma_M} \left(\prod_{j < k} \frac{1}{h(u_{\sigma_j}, u_{\sigma_k})} \right) \sum_{x_1 < \dots < x_M} \mathcal{A}(x_1, p_{\sigma_1}) \cdots \mathcal{A}(x_M, p_{\sigma_M}). \quad (9.26)$$

Then, we used the following identity:

$$h(u_1, \dots, u_M) = \prod_{j < k} h(u_j, u_k), \quad (9.27)$$

Because the multi-magnon hexagon form factor can be decomposed by the two-magnon hexagon form factor.

The remaining part is the summation over the positions for the multi-product of the propagation factors

$$\sum_{x_1 < \dots < x_M} \mathcal{A}(x_1, p_{\sigma_1}) \cdots \mathcal{A}(x_M, p_{\sigma_M}), \quad (9.28)$$

$$\begin{aligned}
\sum_{x=\ell_{12}}^{L_1} \sum_{y=x+1}^{L_1} \underbrace{\text{---} \overbrace{\ell_{12} \quad \color{blue}{\bullet} \quad \color{red}{\bullet} \quad \dots \quad \color{green}{\bullet}}^{x \quad y}}_{e^{ip_1 x} e^{i(p_2 + \dots + p_M) y}} &= g^{(2-M)(p)} \underbrace{\text{---} \overbrace{\ell_{12} \quad \color{blue}{\bullet} \quad \color{red}{\bullet} \quad \dots \quad \color{green}{\bullet}}^x}_{e^{i(p_1 + \dots + p_M) x}} + \dots \\
&\quad \underbrace{\hspace{10em}}_{\text{irrelevant}} \\
g^{(2-M)(p)} \sum_{x=\ell_{12}}^{L_1} \underbrace{\text{---} \overbrace{\ell_{12} \quad \color{blue}{\bullet} \quad \color{red}{\bullet} \quad \dots \quad \color{green}{\bullet}}^x}_{\ell_{12}} &= g^{(2-M)(p)} g^{(1-M)(p)} \underbrace{\text{---} \overbrace{\ell_{12} \quad \color{red}{\bullet} \quad \color{green}{\bullet}}^{\ell_{12}}}_{e^{i(p_1 + \dots + p_M) \ell_{12}}} + \dots
\end{aligned}$$

Figure 9.4: Let us consider the summation of the positions for a magnon at site x and $M - 1$ magnon at site y . We first sum over the position y . From this, we get a nontrivial function $g^{(2-M)} = \frac{1}{e^{-i(p_2 + \dots + p_M)} - 1}$. After doing so, we sum over the position x and get the further factor $g^{(1-M)} = \frac{1}{e^{-i(p_1 + \dots + p_M)} - 1}$. Thereby, the coefficients of the $e^{i(p_1 + \dots + p_M)}$ become the product of the $g^{(2-M)}$ and $g^{(1-M)}$.

which is easily evaluated by geometric series. For one- and two-magnon cases, they respectively become

$$\begin{aligned}
\sum_x \mathcal{A}(x, p) &= e^{-\frac{i}{2}p} \frac{1}{e^{-ip} - 1} e^{ip\ell_{12}} + \dots, \\
\sum_{x_1 < x_2} \mathcal{A}(x_1, p_1) \mathcal{A}(x_2, p_2) &= e^{-\frac{i}{2}(p_1 + p_2)} \frac{1}{e^{-ip_2} - 1} \frac{1}{e^{-i(p_2 + p_1)} - 1} e^{i(p_1 + p_2)\ell_{12}} + \dots
\end{aligned}$$

Then, we would expect the summation for the multi-magnon wave function

$$\sum_{x_1 < \dots < x_M} \mathcal{A}(x_1, p_1) \dots \mathcal{A}(x_M, p_M) = \prod_{k=1}^M e^{-\frac{i}{2}p_k} \prod_{j=1}^M \frac{1}{e^{-i\sum_{k=j}^M p_k} - 1} e^{i(p_1 + \dots + p_M)\ell_{12}} + \dots \quad (9.29)$$

Pictorially, the geometric series in the summation can be sketched in figure 9.4.

From above argument the summation (9.23) becomes

$$\prod_{k=1}^M e^{-\frac{i}{2}p_k} \left(\prod_{s < t} h(u_s, u_t) \right) \sum_{\sigma_1 \neq \dots \neq \sigma_M} \left(\prod_{j < k} \frac{1}{h(u_{\sigma_j}, u_{\sigma_k})} \right) \prod_{n=1}^M \frac{1}{e^{-i\sum_{m=n}^M p_m} - 1} e^{i(p_1 + \dots + p_M)\ell_{12}} + \dots \quad (9.30)$$

We finally prove the following relations :

$$F(p_1, \dots, p_M) = \prod_{k=1}^M i \left(u_k + \frac{i}{2} \right), \quad (9.31)$$

$$F(p_1, \dots, p_M) \equiv \sum_{\sigma_1 \neq \dots \neq \sigma_M} \left(\prod_{j < k} \frac{1}{h(u_{\sigma_j}, u_{\sigma_k})} \right) \prod_{n=1}^M \frac{1}{e^{-i \sum_{m=n}^M p_m} - 1}, \quad (9.32)$$

by mathematical induction. First, relating $F(p_1)$ for the $M = 1$ case is trivially found. Next, we assume that the relation holds for $M - 1$ case. Then, we extract the expression $F(p_1, \dots, \check{p}_j, \dots, p_M)$ where the j -th excitation does not contribute :

$$F(p_1, \dots, p_M) = \frac{1}{e^{-i \sum_{k=1}^M p_k} - 1} \sum_{j=1}^M \left(\prod_{k \neq j} \frac{1}{h(u_k, u_j)} \right) F(p_1, \dots, \check{p}_j, \dots, p_M). \quad (9.33)$$

We finally have

$$F(p_1, \dots, p_M) = \frac{1}{e^{-i \sum_{k=1}^M p_k} - 1} \sum_{j=1}^M \left(\prod_{k \neq j} \frac{1}{h(u_k, u_j)} \right) \frac{\prod_{k=1}^M i(u_k + 1/2)}{i(u_j + 1/2)}. \quad (9.34)$$

Here, the expression

$$\frac{1}{e^{-i \sum_{k=1}^M p_k} - 1} \sum_{j=1}^M \left(\prod_{k \neq j} \frac{1}{h(u_k, u_j)} \right) \frac{1}{i(u_j + 1/2)} \quad (9.35)$$

can be handled by introducing a residue integral which is given as

$$\oint \frac{dz}{2\pi i} \frac{1}{z} \left(\prod_{k=1}^M \frac{u_k - z - i/2}{u_k - z + i/2} - 1 \right), \quad (9.36)$$

where the integrand has poles at $z = 0$ and $z = u_k + i/2$. Picking up the pole at $z = 0$, we get

$$\oint_{z=0} \frac{dz}{2\pi i} \frac{1}{z} \left(\prod_{k=1}^M \frac{u_k - z - i/2}{u_k - z + i/2} - 1 \right) = e^{-i \sum_{k=1}^M p_k} - 1. \quad (9.37)$$

Otherwise, from the other poles, we have

$$\oint_{z=u_k+i/2} \frac{dz}{2\pi i} \frac{1}{z} \left(\prod_{k=1}^M \frac{u_k - z - i/2}{u_k - z + i/2} - 1 \right) = \sum_{j=1}^M \left(\prod_{k \neq j} \frac{1}{h(u_k, u_j)} \right) \frac{1}{i(u_j + 1/2)}. \quad (9.38)$$

From those, we could completely get the following relation :

$$F(p_1, \dots, p_M) = \prod_{k=1}^M i \left(u_k + \frac{i}{2} \right) \quad (9.39)$$

$$= \prod_{k=1}^M \frac{1}{e^{-i p_k} - 1}. \quad (9.40)$$

Thus, the summation (9.23) becomes

$$\sum_{x_1 < \dots < x_M} \sum_{\sigma_1 \neq \dots \neq \sigma_M} \prod_{\substack{\sigma_k < \sigma_j \\ j < k}} S(p_{\sigma_j}, p_{\sigma_k}) \mathcal{A}(x_1, p_{\sigma_1}) \cdots \mathcal{A}(x_M, p_{\sigma_M}) \quad (9.41)$$

$$= \prod_{k=1}^M \mathcal{M}(p_k) \prod_{j < k} h(u_j, u_k) e^{i(p_1 + \dots + p_M) \ell_{12}} + \dots \quad (9.42)$$

2. Bridge length independent terms

Next we prove the second lemma, which is for the terms which have exponent of the spin-chain length, $e^{i(p_1 + \dots + p_M)L_1}$. As a more simpler case, we explain a few magnon case in appendix J for helping to understand.³ By applying the result of the multi-magnon hexagon form factor, the summation (9.22) for the wave function with Neumann boundary condition is given by:

$$\begin{aligned} & \sum_{x_1 < \dots < x_M} \psi_{\text{open}}^{(M)}(x_1, \dots, x_M) / \prod_{i=1}^M \mathcal{M}(p_i) \\ &= \sum_{\mathbf{P}_+ \cup \mathbf{P}_- = \{1, \dots, M\}} \left[\prod_{k \in \mathbf{P}_-} (-e^{2ip_k L}) \prod_{l < k} S(p_k, p_l) S(-p_k, p_l) \right] \prod_{i < j} h(\hat{p}_i, \hat{p}_j) e^{i(\hat{p}_1 + \dots + \hat{p}_M)L_1} + \dots \end{aligned} \quad (9.43)$$

First of all, the propagation factor can be trivially picked out:

$$e^{i(p_1 + \dots + p_M)L} \sum_{\mathbf{P}_+ \cup \mathbf{P}_- = \{1, \dots, M\}} \left[\prod_{k \in \mathbf{P}_-} (-) \prod_{l < k} S(p_k, p_l) S(-p_k, p_l) \right] \prod_{i < j} h(\hat{p}_i, \hat{p}_j) + \dots \quad (9.44)$$

By dividing the factor such as

$$\prod_{l < k} h(p_l, p_k) \prod_{l < k} h(p_l, -p_k), \quad (9.45)$$

the leading term (p_1, \dots, p_M) becomes

$$\begin{aligned} & e^{i(p_1 + \dots + p_M)L} \prod_{l < k} h(p_l, p_k) \prod_{l < k} h(p_l, -p_k) \left(\frac{1}{\prod_{l < k} h(p_l, p_k) \prod_{l < k} h(p_l, -p_k)} \prod_{i < j} h(p_i, p_j) \right) \\ &= e^{i(p_1 + \dots + p_M)L} \prod_{l < k} h(p_l, p_k) \prod_{l < k} h(p_l, -p_k) \left(\prod_{l < k} \frac{1}{h(p_l, -p_k)} \right). \end{aligned} \quad (9.46)$$

³For a naive discussion, when we consider the case, for example $\ell_{12} = 0$, $\ell_{13} \neq 0$ and $\ell_{23} \neq 0$, the structure constants don't have any non-trivial factors because the Bethe state can't contract with other states. This shows that the structure constants are independent for the spin chain length L_i .

On the other hand, the next to leading term which is the term for $p_1 \rightarrow -p_1$ is written as

$$\begin{aligned}
& - e^{i(p_1+\dots+p_M)L} \prod_{l<k} h(p_l, p_k) \prod_{l<k} h(p_l, -p_k) \\
& \times \left(\frac{1}{\prod_{l<k} h(p_l, p_k) \prod_{l<k} h(p_l, -p_k)} \prod_{l<k} S(p_k, p_l) S(-p_k, p_l) \prod_{i=1}^M h(-p_1, p_i) \prod_{1 \neq i < j}^M h(p_i, p_j) \right) \\
& = - e^{i(p_1+\dots+p_M)L} \prod_{l<k} h(p_l, p_k) \prod_{l<k} h(p_l, -p_k) \left(\prod_k \frac{1}{h(p_1, p_k)} \prod_{1 \neq l < k} \frac{1}{h(p_l, -p_k)} \right), \quad (9.47)
\end{aligned}$$

where the expression in brackets is just the negative k part of (9.46). Generally, the equation (9.44) becomes

$$e^{i(p_1+\dots+p_M)L} \prod_{l<k} h(p_l, p_k) \prod_{l<k} h(p_l, -p_k) \sum_{P_+ \cup P_- = \{1, \dots, M\}} \left[\prod_{k \in P_-} (-) \right] \prod_{l<k} \frac{1}{h(\hat{p}_l, -\hat{p}_k)}. \quad (9.48)$$

From this, we shall show that

$$G(p_i) \equiv \sum_{P_+ \cup P_- = \{1, \dots, M\}} \left[\prod_{k \in P_-} (-) \right] \prod_{l<k} \frac{1}{h(\hat{p}_l, -\hat{p}_k)} = 0 \quad (9.49)$$

by investigating the poles. The function $G(p_i)$ has poles at $u_i = \pm u_k$ because of

$$\frac{1}{h(u, v)} = 1 + \frac{i}{u - v}. \quad (9.50)$$

However, these poles are irrelevant since the residues of such poles become zero. Now let us move to the pole at $\hat{p}_m = \hat{p}_n$, ($n < m$). Then we can simply show that the residue is

$$\begin{aligned}
& \sum_{P_+ \cup P_- = \{1, \dots, M\} / \{m, n\}} \left[\prod_{k \in P_-} (-) \right] \Big|_{\hat{p}_m \rightarrow \hat{p}_n}^{\text{res}} \left(\prod_{n \neq i < m} \frac{1}{h(\hat{p}_i, \pm \hat{p}_m)} \prod_{m < j} \frac{1}{h(\pm \hat{p}_m, \hat{p}_j)} \frac{1}{h(\pm \hat{p}_n, \pm \hat{p}_m)} \right) \\
& + \prod_{i < n \neq m} \frac{1}{h(\hat{p}_i, \pm \hat{p}_n)} \prod_{n < j} \frac{1}{h(\pm \hat{p}_n, \hat{p}_j)} \frac{1}{h(\pm \hat{p}_m, \pm \hat{p}_n)} \\
& = 0. \quad (9.51)
\end{aligned}$$

Therefore, the function $G(p_i)$ does not have any poles. Thus, the remaining one is determined by the $u \rightarrow \infty$ behavior. Since it trivially becomes zero such as

$$G(u_i \rightarrow \infty) = \underbrace{1 - 1 + 1 - 1 + \dots}_{2M \text{ terms}} = 0, \quad (9.52)$$

we showed that the function $G(p_i)$ is precisely zero. This fact means that the summation of the spin-chain length dependent terms doesn't contribute to the structure constants.

As a result, we can write down the final result for the multi-magnon structure constants at tree-level as

$$\begin{aligned}
C_{123}^{Y^M \circ\circ} |_{\text{tree}} &\propto \prod_{i=1}^M \mathcal{M}(p_i) e^{i(p_1 + \dots + p_M) \ell_{12}} \\
&\times \sum_{\mathbb{P}_+ \cup \mathbb{P}_- = \{1, \dots, M\}} \left[\prod_{k \in \mathbb{P}_-} (-e^{2ip_k \ell_{13}}) \prod_{l < k} S(p_k, p_l) S(-p_k, p_l) \right] \prod_{i < j} h_{YY}^{\text{tree}}(\hat{p}_i, \hat{p}_j)
\end{aligned} \tag{9.53}$$

We would like to emphasize that the structure constants depend on only the exponential of the bridge length terms and the hexagon form factor, which is the same with the closed string case, naturally appears.

Chapter 10

Complete method – integrability

In this chapter, we would like to suggest the finite coupling correlators of the open strings or operators inserted into the Wilson loop. In the section 10.1, we conjecture a finite coupling structure constants naively, following the original hexagon paper [34]. After doing so, we suggest a more refined form in section 10.2. It is because the conjecture in section 10.1 is slightly different from the one-loop perturbative results. The accuracy of the result in section 10.2 was supported at higher loops by using the recent developed localization techniques [90].

10.1 Conjecture for finite coupling structure constants

In the previous chapter, the result of tree-level structure constants are given by

$$\begin{aligned}
 C_{123}^{YM\infty}|_{\text{tree}} &\propto \prod_{i=1}^M \mathcal{M}(p_i) e^{i(p_1^{\text{tree}} + \dots + p_M^{\text{tree}})\ell_{12}} \\
 &\times \sum_{\mathbf{P}_+ \cup \mathbf{P}_- = \{1, \dots, M\}} \left[\prod_{k \in \mathbf{P}_-} (-e^{2ip_k^{\text{tree}}\ell_{13}}) \prod_{l < k} S^{\text{tree}}(p_k, p_l) S^{\text{tree}}(-p_k, p_l) \right] \prod_{i < j} h_{YY}^{\text{tree}}(\hat{p}_i, \hat{p}_j),
 \end{aligned} \tag{10.1}$$

with

$$\hat{p}_i = \begin{cases} p_i & i \in \mathbf{P}_+ \\ -p_i & i \in \mathbf{P}_- \end{cases}. \tag{10.2}$$

Then, in the same argument of three-point functions of the closed strings in section 5.1, we replace the tree-level quantities to finite coupling functions:

$$C_{123}|_{\text{tree}} \rightarrow C_{123}|_{\text{finite}} : p_i^{\text{tree}} \rightarrow p_i^{\text{finite}}, \quad S^{\text{tree}}(u, v) \rightarrow S^{\text{finite}}(u, v), \quad h^{\text{tree}}(u, v) \rightarrow h^{\text{finite}}(u, v).$$

In addition, by inserting the reflection amplitude $B(p)$ at finite coupling given in [83, 89] and correct norm explained in appendix L, we propose the structure constants at finite coupling¹

$$\left(\frac{C_{123}^{M\circ\circ}}{C_{123}^{\circ\circ\circ}}\right)^2 \stackrel{?}{=} \frac{(e^{i(p_1+\dots+p_M)\ell_{12}}\mathcal{K})^2}{\det(\partial_{u_i}\phi_j) \prod_{i<j} S(p_j, p_i) e^{i(p_1+\dots+p_M)L_1}}, \quad (10.3)$$

where the denominator is a norm part by a product of S -matrices times the open-chain version of Gaudin norm factor which is a determinant of differential ϕ defined from

$$e^{i\phi_j} \equiv e^{2ip_j L_1} \prod_{k \neq j} S(u_k, u_j) B_L(p_j) S(-u_k, u_j) B_1(-p_j) \quad (10.4)$$

with respect to rapidity variables u_i (not the momentum), and by the propagation factor for the length of the operator \mathcal{O}_1 . Also, we define

$$\mathcal{K} = \sum_{P_+ \cup P_- = \{1, \dots, M\}} \left[\prod_{k \in P_-} (-e^{2ip_k \ell_{13}} B_L(p_k)) \prod_{l < k} S(p_k, p_l) S(-p_k, p_l) \right] \mathcal{H}(p), \quad (10.5)$$

where $\mathcal{H}(p) \equiv \prod_{i < j} h_{YY}(\hat{p}_i, \hat{p}_j)$.

We now give some comments for this result. First, we here recall the result of the three-point functions of the closed string (5.2):

$$\mathcal{A}^{\text{closed}} = \sum_{\alpha \cup \bar{\alpha} = \{1, \dots, M\}} (-1)^{|\bar{\alpha}|} \prod_{j \in \bar{\alpha}} e^{ip_j \ell_{12}} \prod_{\substack{j < k \\ j \in \bar{\alpha}, k \in \alpha}} S(u_j, u_k) \mathcal{H}(\alpha) H(\bar{\alpha}) \quad (10.6)$$

The closed sting version is written as the sum over partitions and there are two hexagons. On the other hand, comparing the results, the open sting version has one hexagon and sum over the sign flipped momentum by the reflection amplitude. Pictorially, the three-point function of operators inserted on the Wilson loop is implemented by a hexagonal object. Cutting the three seams, the hexagonal object can be described by one hexagon with three mirror edges contracted by the boundary states $|B\rangle$, see figure 10.1.

In the case of two magnon, the above expression is simply written as

$$\begin{aligned} \mathcal{K}^{(2)} &= h_{YY}(u, v) - S(p_2, p_1) S(-p_2, p_1) B_L(p_1) e^{2ip_1 \ell_{13}} h_{YY}(-u, v) \\ &\quad - B_L(p_2) e^{2ip_2 \ell_{13}} h_{YY}(u, -v) + S(p_2, p_1) S(p_1, -p_2) B_L(p_1) B_L(p_2) e^{2i(p_1+p_2)\ell_{13}} h_{YY}(-u, -v). \end{aligned} \quad (10.7)$$

It shows that *the structure constant is given by the summation over the sign flipping hexagon form factor with negative sign and appropriate factors related dynamical processes of the magnons*. Furthermore, the two-magnon structure constants at finite coupling is depicted in figure 10.2.

¹The meaning of question mark ? is explained in the next section.

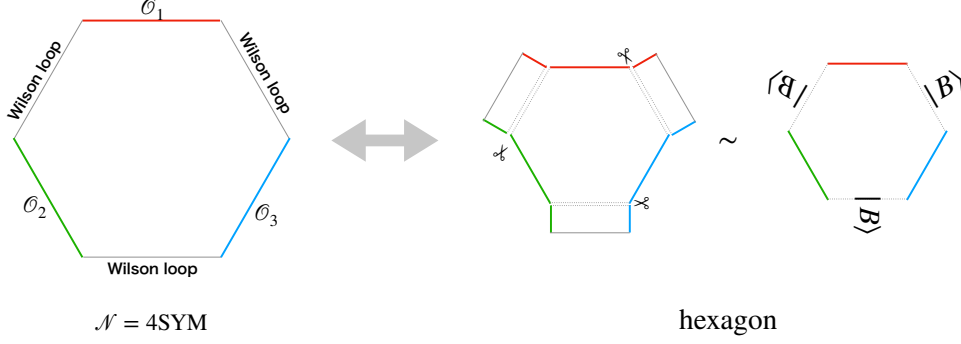


Figure 10.1: In the $\mathcal{N} = 4$ SYM, the configuration can be pictorially written as a hexagon. In the hexagon method of open string attached D-brane, we cut the world sheet and make one hexagon and three square like figures. Then, we identify the three square like figures are boundary states.

10.2 Hexagonalization and the perturbation

In this section, we would like to predict the hexagonalization data from the perturbation. In advance, we mention the summary of the relations between the hexagonalization and perturbation method in the subsection 10.2.1. After doing so, we explicitly see how to predict the hexagonalization data from the perturbation in subsection 10.2.2.

10.2.1 Summary of the hexagonalization and perturbation

One interesting (and perhaps peculiar) outcome of our analysis is that the integrability computation does not give the normalized correlator $\langle\langle * \rangle\rangle$, which is the result (10.3). It rather corresponds to the ratio of the correlators on the circular Wilson loop,

$$\text{Hexagonalization} = \frac{\langle \mathcal{W}[\mathcal{O}_1 \cdots \mathcal{O}_m] \rangle_{\text{circle}}}{\prod_{k=1}^m \sqrt{\langle \mathcal{W}[\mathcal{O}_k \mathcal{O}_k] \rangle'_{\text{circle}}}}, \quad (10.8)$$

where $\langle \mathcal{W}[\mathcal{O}_k \mathcal{O}_k] \rangle'_{\text{circle}}$ denotes the space-time independent part of the two-point function on the circular loop; namely $\langle \mathcal{W}[\mathcal{O}_k \mathcal{O}_k] \rangle'_{\text{circle}} = n_{L_k} \times \langle \mathcal{W} \rangle_{\text{circle}}$. In terms of normalized correlators, the conjecture (10.8) can be rewritten as

$$\text{Hexagonalization} = (\langle \mathcal{W} \rangle_{\text{circle}})^{\frac{2-m}{2}} \frac{\langle\langle \mathcal{O}_1 \cdots \mathcal{O}_m \rangle\rangle}{\sqrt{\prod_{k=1}^m n_k}}. \quad (10.9)$$

Although we do not have a strong argument as to why the hexagonalization computes the correlators on the circle rather than the normalized correlators, we check this conjecture explicitly for the three- and four-point functions at one loop.

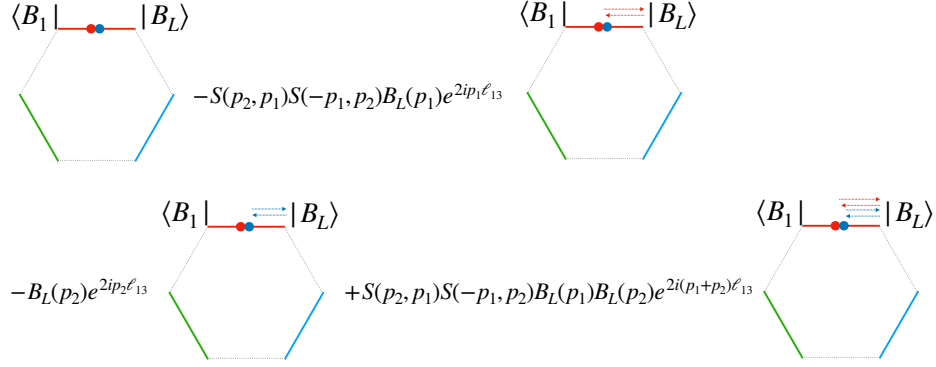


Figure 10.2: The red and blue magnons on the hexagon form factors give the hexagon form factors $h_{YY}(u, v)$. Then, the four terms shows the propagating process on the edge of the hexagon form factor and boundary states.

10.2.2 Hexagonalization data from the one-loop correlators

Assembling some 1-loop BPS correlation functions, we shall try to predict hexagonalization data, which should also be calculated from integrability method. Because, in our conjecture, the BPS correlation functions are given by summing of hexagonalization data with having mirror-magnon on the gluing edge. In fact, by counting the power of the coupling constant, there are three-type hexagon data related up to three mirror-magnon, as long as we consider the 1-loop calculation by the perturbation. The aim in this section is to read the three hexagonalization data from the 1-loop BPS correlation functions.

As a beginning step to be good at but including essences, let us consider the three three-point functions whether it has a zero-bridge lengths or not. The 1-loop results are given by

$$\frac{\langle\langle \mathcal{O}_1^{\text{BPS}(2)}(x_1) \mathcal{O}_2^{\text{BPS}(2)}(x_2) \mathcal{O}_3^{\text{BPS}(2)}(x_3) \rangle\rangle}{\sqrt{n_1 n_2 n_3}} \Big|_{1\text{-loop}} = \frac{\lambda}{8\pi^2} 3\zeta(2) d_{12} d_{23} d_{31}, \quad (10.10)$$

$$\frac{\langle\langle \mathcal{O}_1^{\text{BPS}(2)}(x_1) \mathcal{O}_2^{\text{BPS}(1)}(x_2) \mathcal{O}_3^{\text{BPS}(1)}(x_3) \rangle\rangle}{\sqrt{n_1 n_2 n_3}} \Big|_{1\text{-loop}} = \frac{\lambda}{8\pi^2} \zeta(2) d_{12} d_{31}. \quad (10.11)$$

The first shape with one triangle and three objects like crescent moon has all non-zero bridge length. On the other hand, the second shape has zero bridge length. The difference, in terms of the hexagonalization, shows a mirror magnon on the gluing edge between the boundary state and the hexagon in figure 10.3. As mentioned the original hexagonalization paper, only single-particle states on zero-length bridges can contribute at 1-loop. However it is curious why the three-point function of the first shape has non-zero value since it cannot have any contribution from hexagonalization method. We find that it implies that the hexagonalization data are related to the perturbation results divided by the expectation value of the Wilson loop. Namely, the three-point functions divided by the

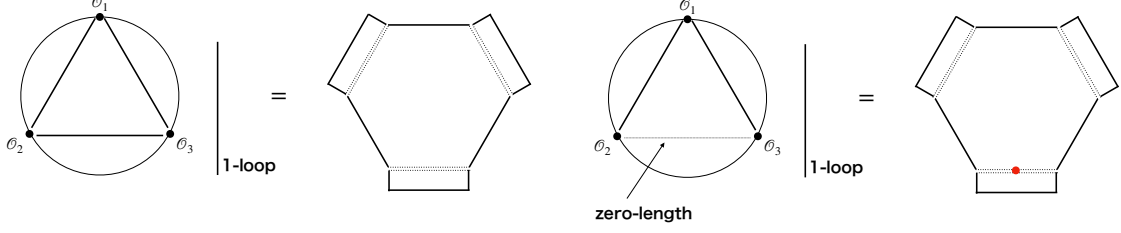


Figure 10.3: The left figure is the $\langle\langle \mathcal{O}_1^{\text{BPS}(2)}(x_1) \mathcal{O}_2^{\text{BPS}(2)}(x_2) \mathcal{O}_3^{\text{BPS}(2)}(x_3) \rangle\rangle$. The right correlator is $\langle\langle \mathcal{O}_1^{\text{BPS}(2)}(x_1) \mathcal{O}_2^{\text{BPS}(1)}(x_2) \mathcal{O}_3^{\text{BPS}(1)}(x_3) \rangle\rangle$, which have zero-bridge length.

one with the appropriate power become

$$(\langle\mathcal{W}\rangle_{\text{circle}})^{-\frac{1}{2}} \frac{\langle\langle \mathcal{O}_1^{\text{BPS}(2)}(x_1) \mathcal{O}_2^{\text{BPS}(2)}(x_2) \mathcal{O}_3^{\text{BPS}(2)}(x_3) \rangle\rangle}{\sqrt{n_1 n_2 n_3}} \Big|_{1\text{-loop}} = 0, \quad (10.12)$$

$$(\langle\mathcal{W}\rangle_{\text{circle}})^{-\frac{1}{2}} \frac{\langle\langle \mathcal{O}_1^{\text{BPS}(2)}(x_1) \mathcal{O}_2^{\text{BPS}(1)}(x_2) \mathcal{O}_3^{\text{BPS}(1)}(x_3) \rangle\rangle}{\sqrt{n_1 n_2 n_3}} \Big|_{1\text{-loop}} = \frac{\lambda}{8\pi^2} (-2\zeta(2)) d_{12} d_{31}. \quad (10.13)$$

In the second line, the coefficient $\frac{\lambda}{8\pi^2} (-2\zeta(2))$ should be reproduced by a hexagonalization data in hexagonalization method which has one mirror-magnon on the gluing edge between hexagon and boundary state,

$$= -2 \frac{\lambda}{8\pi^2} \zeta(2). \quad (10.14)$$

Considering a next beginning step is a four-point function with the operator length $L_1 = 5, L_2 = L_3 = L_4 = 3$ and $L_1 = 4, L_2 = L_3 = L_4 = 2$. The tree-level diagrams are in figure 10.4. They are given by

$$\frac{\langle\langle \mathcal{O}_1^{\text{BPS}(5)}(x_1) \mathcal{O}_2^{\text{BPS}(3)}(x_2) \mathcal{O}_3^{\text{BPS}(3)}(x_3) \mathcal{O}_4^{\text{BPS}(3)}(x_4) \rangle\rangle}{\sqrt{n_1 n_2 n_3 n_4}} \Big|_{1\text{-loop}}$$

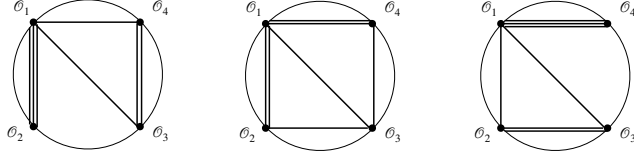
$$= \frac{\lambda}{8\pi^2} 4\zeta(2) d_{12}^3 d_{34}^2 d_{41} d_{13} + \frac{\lambda}{8\pi^2} 6\zeta(2) d_{12}^2 d_{23} d_{34} d_{41}^2 d_{13} + \frac{\lambda}{8\pi^2} 4\zeta(2) d_{12} d_{23}^2 d_{41}^3 d_{13}, \quad (10.15)$$

$$\frac{\langle\langle \mathcal{O}_1^{\text{BPS}(4)}(x_1) \mathcal{O}_2^{\text{BPS}(2)}(x_2) \mathcal{O}_3^{\text{BPS}(2)}(x_3) \mathcal{O}_4^{\text{BPS}(2)}(x_4) \rangle\rangle}{\sqrt{n_1 n_2 n_3 n_4}} \Big|_{1\text{-loop}}$$

$$= \frac{\lambda}{8\pi^2} 4\zeta(2) d_{12}^2 d_{34} d_{41} d_{13} + \frac{\lambda}{8\pi^2} 4\zeta(2) d_{12} d_{23} d_{41}^2 d_{13}. \quad (10.16)$$

We found that the $4\zeta(2)$ terms come from the tree-level diagrams with zero-bridge lengths. It implies that the contributions in terms of the hexagonalization came from the one-mirror

length : (5,3,3,3)



length : (4,2,2,2)

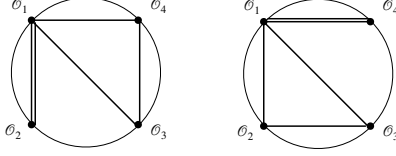


Figure 10.4: The tree-level diagram of the correlator $\langle\langle \mathcal{O}_1^{\text{BPS}(5)}(x_1)\mathcal{O}_2^{\text{BPS}(3)}(x_2)\mathcal{O}_3^{\text{BPS}(3)}(x_3)\mathcal{O}_4^{\text{BPS}(3)}(x_4) \rangle\rangle$ and $\langle\langle \mathcal{O}_1^{\text{BPS}(4)}(x_1)\mathcal{O}_2^{\text{BPS}(2)}(x_2)\mathcal{O}_3^{\text{BPS}(2)}(x_3)\mathcal{O}_4^{\text{BPS}(2)}(x_4) \rangle\rangle$.

particle between the hexagon and boundary state. On the other hand, the existence of the $6\zeta(2)$ term is not so good. Because we cannot see the well interpretation in the hexagonalization theory. It is also implied that we should divided by the expectation value of the Wilson loop. For the four-point function, it is turned out well by divided by $(\langle\mathcal{W}\rangle_{\text{circle}})^{-1}$. Then we have

$$\begin{aligned} & (\langle\mathcal{W}\rangle_{\text{circle}})^{-1} \frac{\langle\langle \mathcal{O}_1^{\text{BPS}(5)}(x_1)\mathcal{O}_2^{\text{BPS}(3)}(x_2)\mathcal{O}_3^{\text{BPS}(3)}(x_3)\mathcal{O}_4^{\text{BPS}(3)}(x_4) \rangle\rangle}{\sqrt{n_1 n_2 n_3 n_4}} \Big|_{1\text{-loop}} \\ &= \frac{\lambda}{8\pi^2} (-2\zeta(2)) d_{12}^3 d_{34}^2 d_{41} d_{13} + \frac{\lambda}{8\pi^2} (-2\zeta(2)) d_{12} d_{23}^2 d_{41}^3 d_{13}, \end{aligned} \quad (10.17)$$

$$\begin{aligned} & (\langle\mathcal{W}\rangle_{\text{circle}})^{-1} \frac{\langle\langle \mathcal{O}_1^{\text{BPS}(4)}(x_1)\mathcal{O}_2^{\text{BPS}(2)}(x_2)\mathcal{O}_3^{\text{BPS}(2)}(x_3)\mathcal{O}_4^{\text{BPS}(2)}(x_4) \rangle\rangle}{\sqrt{n_1 n_2 n_3 n_4}} \Big|_{1\text{-loop}} \\ &= \frac{\lambda}{8\pi^2} (-2\zeta(2)) d_{12}^2 d_{34} d_{41} d_{13} + \frac{\lambda}{8\pi^2} (-2\zeta(2)) d_{12} d_{23} d_{41}^2 d_{13}. \end{aligned} \quad (10.18)$$

We now call each hexagonalization data which have mirror-magnon on the bottom, right, up, left edge between the hexagon and the boundary states to **HBbottom**, **HBright**, **HBup** and **HBlleft** respectively, see figure 10.5. Using these notations, in our conjecture, the each equation (10.17) and (10.18) would be respectively equal to

$$(10.17) = (\mathbf{HBbottom}) d_{12}^3 d_{34}^2 d_{41} d_{13} + (\mathbf{HBright}) d_{12} d_{23}^2 d_{41}^3 d_{13},$$

$$(10.18) = (\mathbf{HBbottom}) d_{12}^2 d_{34} d_{41} d_{13} + (\mathbf{HBright}) d_{12} d_{23} d_{41}^2 d_{13}.$$

By solving two simultaneous equations, we have the hexagonalization data:

$$(\mathbf{HBbottom}) = (\mathbf{HBright}) = -2 \frac{\lambda}{8\pi^2} \zeta(2).$$

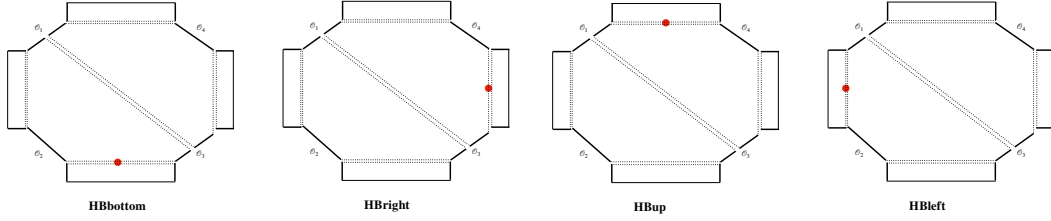


Figure 10.5: The one-mirror particle on both the hexagon form factor and boundary state.

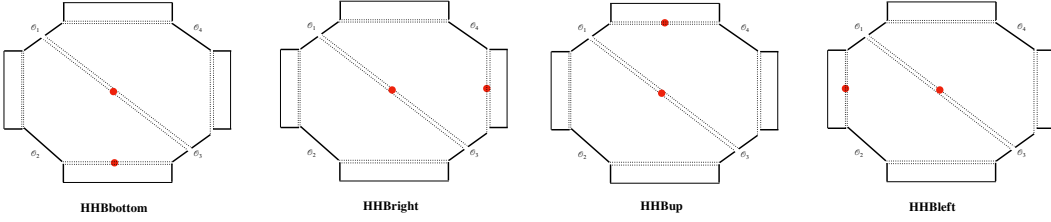


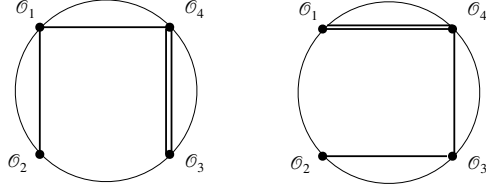
Figure 10.6: The two-mirror particle on two hexagon form factors and boundary state.

In the same way, we can get other hexagonalization data which have mirror-magnon on the up and left edge between the hexagon and the boundary states², **HBup** and **HLeft**. They also have same value $\mathbf{HBup}=\mathbf{HLeft}=-2\frac{\lambda}{8\pi^2}\zeta(2)$. We can see that these values are the same with the three-point function (10.14). From these facts, we find that the hexagonalization data with one-magnon on the edge gluing between the hexagon and the boundary state will be $-2\frac{\lambda}{8\pi^2}\zeta(2)$.

More hexagonalization data with two-mirror magnon defined in 10.6 can be predicted from other 1-loop four-point functions. For example, we consider the four-point functions with $L_1 = 2, L_2 = 1, L_3 = 2, L_4 = 3$ and $L_1 = 3, L_2 = 2, L_3 = 3, L_4 = 4$ in 10.7:

²In this case, for example, we consider the four-point functions with the operator length $L_1 = L_2 = L_3 = 3, L_4 = 5$ and $L_1 = L_2 = L_3 = 2, L_4 = 4$.

length : (2,1,2,3)



length : (3,2,3,4)

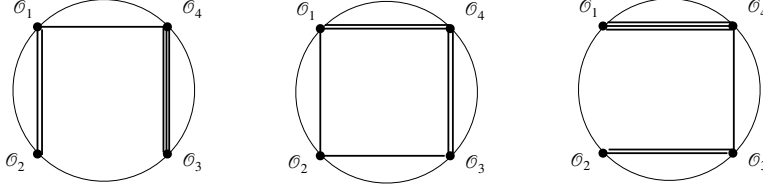


Figure 10.7: Tree-level diagrams of correlator $\langle\langle \mathcal{O}_1^{\text{BPS}(2)}(x_1)\mathcal{O}_2^{\text{BPS}(1)}(x_2)\mathcal{O}_3^{\text{BPS}(2)}(x_3)\mathcal{O}_4^{\text{BPS}(3)}(x_4) \rangle\rangle$ and $\langle\langle \mathcal{O}_1^{\text{BPS}(3)}(x_1)\mathcal{O}_2^{\text{BPS}(2)}(x_2)\mathcal{O}_3^{\text{BPS}(3)}(x_3)\mathcal{O}_4^{\text{BPS}(4)}(x_4) \rangle\rangle$

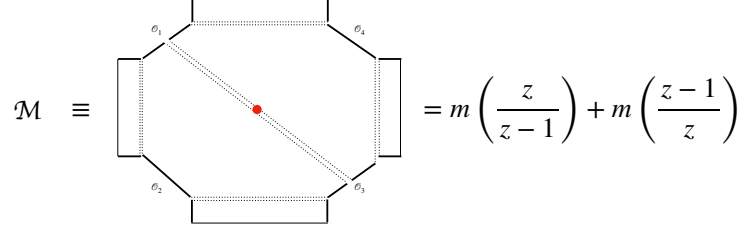
$$\begin{aligned}
& (\langle\mathcal{W}\rangle_{\text{circle}})^{-1} \frac{\langle\langle \mathcal{O}_1^{\text{BPS}(2)}(x_1)\mathcal{O}_2^{\text{BPS}(1)}(x_2)\mathcal{O}_3^{\text{BPS}(2)}(x_3)\mathcal{O}_4^{\text{BPS}(3)}(x_4) \rangle\rangle}{\sqrt{n_1 n_2 n_3 n_4}} \Big|_{1\text{-loop}} \\
&= \frac{1}{2} D_{1234} d_{34} d_{41} \\
&+ \frac{\lambda}{8\pi^2} (-4\zeta(2) + 2\zeta(2)\text{Li}_R[z]) d_{12} d_{34}^2 d_{41} + \frac{\lambda}{8\pi^2} (-4\zeta(2) + 2\zeta(2)\text{Li}_R[1-z]) d_{23} d_{34} d_{41}^2.
\end{aligned} \tag{10.19}$$

$$\begin{aligned}
& (\langle\mathcal{W}\rangle_{\text{circle}})^{-1} \frac{\langle\langle \mathcal{O}_1^{\text{BPS}(3)}(x_1)\mathcal{O}_2^{\text{BPS}(2)}(x_2)\mathcal{O}_3^{\text{BPS}(3)}(x_3)\mathcal{O}_4^{\text{BPS}(4)}(x_4) \rangle\rangle}{\sqrt{n_1 n_2 n_3 n_4}} \Big|_{1\text{-loop}} \\
&= \frac{1}{2} D_{1234} (d_{12} d_{34}^2 d_{41} + d_{23} d_{34} d_{41}^2) \\
&+ \frac{\lambda}{8\pi^2} (-4\zeta(2) + 2\zeta(2)\text{Li}_R[z]) d_{12}^2 d_{34}^3 d_{41} + \frac{\lambda}{8\pi^2} (-4\zeta(2) + 2\zeta(2)\text{Li}_R[1-z]) d_{23}^2 d_{34} d_{41}^3.
\end{aligned} \tag{10.20}$$

In the hexagonalization picture, the equations (10.19) and (10.20) should be equal to

$$\begin{aligned}
(10.19) &= \mathcal{M}(d_{12} d_{34}^2 d_{41} + d_{23} d_{34} d_{41}^2) \\
&+ (\mathbf{HHBbottom} + \mathbf{HBbottom}) d_{12} d_{34}^2 d_{41} + (\mathbf{HHBleft} + \mathbf{HBleft}) d_{23} d_{34} d_{41}^2, \\
(10.20) &= \mathcal{M}(d_{12}^2 d_{34}^3 d_{41} + d_{12} d_{23} d_{34}^2 d_{41}^2 + d_{23}^2 d_{34} d_{41}^3) \\
&+ (\mathbf{HHBbottom} + \mathbf{HBbottom}) d_{12}^2 d_{34}^3 d_{41} + (\mathbf{HHBleft} + \mathbf{HBleft}) d_{23}^2 d_{34} d_{41}^3,
\end{aligned}$$

where $\mathcal{M} = m\left(\frac{z}{z-1}\right) + m\left(\frac{z-1}{z}\right)$, $m \equiv \frac{\lambda}{16\pi^2} \frac{(z+\bar{z}) - (\alpha+\bar{\alpha})}{2} \Phi(z, \bar{z})$ is the one-mirror particle contribution between hexagon form factors calculated in section 5.2, see figure 10.8. Then,



$$\mathcal{M} \equiv m\left(\frac{z}{z-1}\right) + m\left(\frac{z-1}{z}\right)$$

Figure 10.8: The one-mirror particle on the hexagons.

the D_{1234} function can be also written in terms of the $m(z)$ as

$$D_{1234} = m\left(\frac{z}{z-1}\right) d_{23}d_{41} + m\left(\frac{z-1}{z}\right) d_{12}d_{34}.$$

Since we have already known the \mathcal{M} , **HBbottom** and **HBleft**, by solving the equations for the unknown hexagonalization data **HHBbottom** and **HHBleft**, we get

$$(\mathbf{HHBbottom}) = m\left(\frac{1}{1-z}\right) - \frac{\lambda}{8\pi^2} 2\zeta(2) \text{Li}_R[1-z],$$

$$(\mathbf{HHBleft}) = m\left(\frac{1}{z}\right) - \frac{\lambda}{8\pi^2} 2\zeta(2) \text{Li}_R[z].$$

From the other four-point functions, we find

$$\mathbf{HHBbottom} = \mathbf{HHBup} \text{ and } \mathbf{HHBleft} = \mathbf{HHBright}.$$

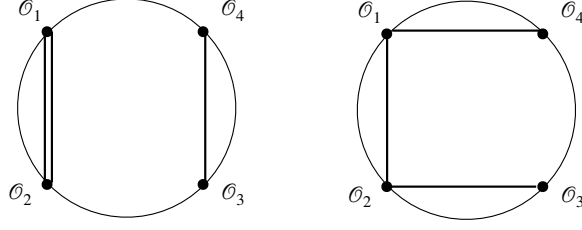
Finally, we consider the four-point functions with $L_1 = L_2 = 2, L_3 = L_4 = 1$ and $L_1 = 2, L_2 = 1, L_3 = 1, L_4 = 2$ in (10.9):

$$\begin{aligned} & (\langle \mathcal{W} \rangle_{\text{circle}})^{-1} \frac{\langle \langle \mathcal{O}_1^{\text{BPS}(2)}(x_1) \mathcal{O}_2^{\text{BPS}(2)}(x_2) \mathcal{O}_3^{\text{BPS}(1)}(x_3) \mathcal{O}_4^{\text{BPS}(1)}(x_4) \rangle \rangle}{\sqrt{n_1 n_2 n_3 n_4}} \Big|_{1\text{-loop}} \\ &= \frac{1}{2} D_{1234} d_{12} + \frac{\lambda}{8\pi^2} (-6\zeta(2) + 2\zeta(2) \text{Li}_R[z]) d_{12}^2 d_{34} + \frac{\lambda}{8\pi^2} (-4\zeta(2) + 2\zeta(2) \text{Li}_R[1-z]) d_{12} d_{23} d_{41}, \end{aligned} \quad (10.21)$$

$$\begin{aligned} & (\langle \mathcal{W} \rangle_{\text{circle}})^{-1} \frac{\langle \langle \mathcal{O}_1^{\text{BPS}(2)}(x_1) \mathcal{O}_2^{\text{BPS}(1)}(x_2) \mathcal{O}_3^{\text{BPS}(1)}(x_3) \mathcal{O}_4^{\text{BPS}(2)}(x_4) \rangle \rangle}{\sqrt{n_1 n_2 n_3 n_4}} \Big|_{1\text{-loop}} \\ &= \frac{1}{2} D_{1234} d_{41} + \frac{\lambda}{8\pi^2} (-4\zeta(2) + 2\zeta(2) \text{Li}_R[z]) d_{12} d_{34} d_{41} + \frac{\lambda}{8\pi^2} (-6\zeta(2) + 2\zeta(2) \text{Li}_R[1-z]) d_{23} d_{41}^2. \end{aligned} \quad (10.22)$$

In the hexagonalization picture, they include the hexagon data with three-mirror particle in figure 10.10. The each correlators (10.21) and (10.22) should be equal to

length : (2,2,1,1)



length : (2,1,1,2)

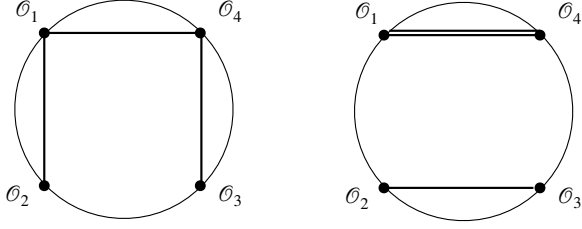


Figure 10.9: Tree-level diagrams of correlator $\langle\langle \mathcal{O}_1^{\text{BPS}(2)}(x_1) \mathcal{O}_2^{\text{BPS}(2)}(x_2) \mathcal{O}_3^{\text{BPS}(1)}(x_3) \mathcal{O}_4^{\text{BPS}(1)}(x_4) \rangle\rangle$ and $\langle\langle \mathcal{O}_1^{\text{BPS}(2)}(x_1) \mathcal{O}_2^{\text{BPS}(1)}(x_2) \mathcal{O}_3^{\text{BPS}(1)}(x_3) \mathcal{O}_4^{\text{BPS}(2)}(x_4) \rangle\rangle$

$$\begin{aligned}
 (10.21) &= \mathcal{M}(d_{12}^2 d_{34} + d_{12} d_{23} d_{41}) \\
 &+ (\mathbf{BHHBvertical} + \mathbf{HHBdown} + \mathbf{HHBup} + \mathbf{HBdown} + \mathbf{HBup}) d_{12}^2 d_{34} \\
 &+ (\mathbf{HHBright} + \mathbf{HBright}) d_{12} d_{23} d_{41},
 \end{aligned}$$

$$\begin{aligned}
 (10.22) &= \mathcal{M}(d_{12} d_{34} d_{41} + d_{23} d_{41}^2) \\
 &+ (\mathbf{BHHBhorizon} + \mathbf{HHBleft} + \mathbf{HHBright} + \mathbf{HBleft} + \mathbf{HBright}) d_{23} d_{41}^2 \\
 &+ (\mathbf{HHBdown} + \mathbf{HBdown}) d_{12} d_{34} d_{41}.
 \end{aligned}$$

By solving the equations, we get

$$\begin{aligned}
 (\mathbf{BHHBvertical}) &= -m \left(\frac{1}{1-z} \right) + \frac{\lambda}{8\pi^2} 2\zeta(2) \text{Li}_R[1-z], \\
 (\mathbf{BHHBhorizon}) &= -m \left(\frac{1}{z} \right) + \frac{\lambda}{8\pi^2} 2\zeta(2) \text{Li}_R[z].
 \end{aligned}$$

The result is just the opposite signs of $\mathbf{HHBbottom}$ and $\mathbf{HHBleft}$ respectively.

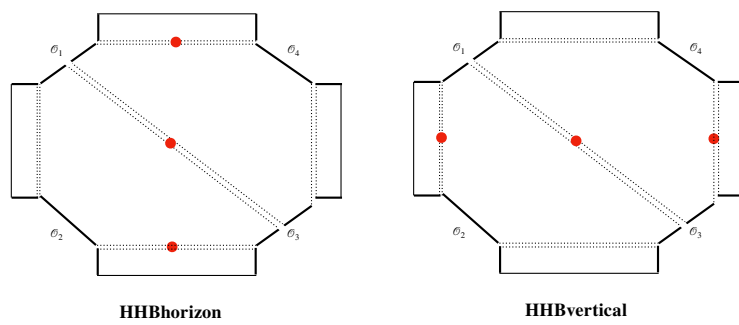


Figure 10.10: The three-mirror particle on two hexagon form factors and two boundary states.

Part IV

Conclusions and future directions

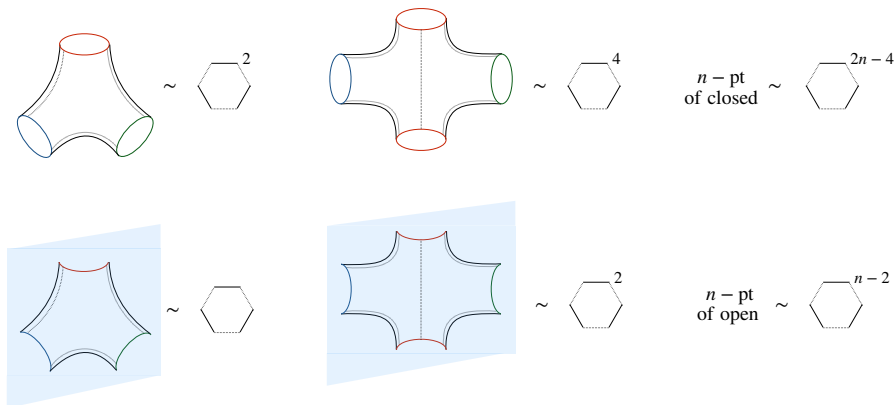
Chapter 11

Conclusions

The main topic of this thesis was to study the correlation functions of the $\mathcal{N} = 4$ SYM in the $\text{AdS}_5/\text{CFT}_4$ correspondence. Among them, we mentioned three directions of the notable topics in the introduction of chapter 1. In what follows, we indicate conclusions and discussions of the each paragraphs.

Closed string and open string

In the section 10.1, we proposed the asymptotic structure constants on the Wilson loop at finite coupling by using the hexagon method, and the result was (10.3). As a result, the structure constants were given by the hexagon form factor and three boundary states. Furthermore, the hexagon form factor in our studies was the same as the one introducing in original closed string correlators. Our proposal was reminiscent of the KLT relation between open and closed string tree-level amplitudes in flat space [102]. Actually, the number of hexagons for the correlators on the Wilson loop was precisely half the number for the correlators of single trace operators:



Of course, the analogy is more complicated, rather than KLT relation. Although, it will be interesting what we try to do more clearly the analogy and study the folklore $(\text{closed string}) = (\text{open string})^2$ in the future work.

Open string correlator and finite-size corrections

In section 8.2, we calculated the three-point functions of DCOs on the Wilson loop at two-loop. All calculations were performed by perturbation method. In terms of the hexagon method, the two-loop results should correspond a lot of mirror particles on the hexagon form factor and boundary state. It was a great advantage of studying DCOs that we could get such contributions from the perturbation. In addition, it may be further value that one could perform perturbative computation for the contribution corresponding to mirror particle. It is because the information of the mirror particles seems rather less than “physical” magnons which is in ordinary integrable spin chain system such as coordinate (and algebraic) Bethe ansatz, Bethe ansatz equation and so on. In other words, I want to know *what is a Hamiltonian of the mirror particle* if it exists. I hope to discover the similar argument with the paper by Minahan and Zarembo for mirror particles.

In the section 8.3, by solving the SD-equations, we calculated the ladder resummed diagrams for the three-point functions of the DCOs at finite coupling. Recently, some calculable resummed diagrams models with dual bulk theory have been studied, for instance SYK model [103–108] and fishnet model [109–111]. As a next step for studying our model, it is interesting to understand the AdS dual of the ladders limit, that is, “tensionless string”.

In the section 10.2, we predicted the hexagonalization data from the perturbative computation. Thereby, we found the correct relation between the hexagonalization and perturbation (10.8). Moreover, if we try to calculate hexagonalization data corresponding to the predictions, it is highly technical and difficult problem. Although, the future work is surely to reproduce the data from integrability-based computation.

Perturbation and hexagonalization

In the subsection 4.2.2, we shortly commented how to reproduce the hexagon form factor from the tailoring method. The result was sum over ordering with S-matrix for normalized multi-magnon weight factors occurred when the magnons move together. As a natural question, it is interesting to extend the higher-loop. Then, we will need the two-loop wave function of the spin chain, and the geometric sum will be generalized

$$\sum_x e^{ipx} \rightarrow ?. \quad (11.1)$$

On the other hand, the hexagon form factor was identified with hexagon vertex contracted spin chain states (5.9) as

$$\mathcal{H}(\alpha) = \langle \mathcal{H}(|\alpha\rangle \otimes |0\rangle \otimes |0\rangle). \quad (11.2)$$

However, we do not sure how to understand the relation between the weight factors and hexagon vertex formalism.

Chapter 12

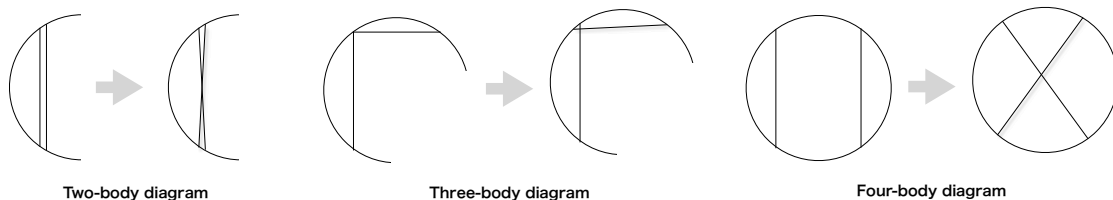
Future directions

12.1 Higher rank sector

In the section 9.2, we calculate the non-BPS structure constants of $SU(2)$ sector by using the tailoring method. As a natural extension, to calculate the higher rank sector is open problem.¹ For example, if we consider an excitation including ϕ_6 , which is the same scalar with the one coupled to Wilson loop, we must consider the contraction between the operators and Wilson loop even the tree-level diagram. Then, due to the boundary reflection matrix, the excitation will be mixing at the boundary. Therefore, the extension for the general excitation is not so easy problem.

12.2 $1/N$ correction

In this thesis, we discuss the correlation functions of the BPS operators by using the perturbative method. Then, to study the $1/N$ correction is not so hopeless problem. Because, since the $1/N$ correction is comes from only the traces of the gauge group, the fundamental one-loop insertion formulas can be used continuously. Furthermore, the tree-level diagrams including $1/N$ can be easily written down by dressed three parts:



By calculating them, we will predict the hexagonalization data for $1/N$.

¹The $SL(2)$ and the diagonal $SO(6)$ sector were already calculated in unpublished note.

12.3 Hexagonalization of multi-magnon

In the section 10.2, we predicted the hexagonalization data from the perturbation. However, the direct calculation from the hexagonalization is so complicated but not a hopeless problem.

As an interesting comment, we would like to see the “relations” between the mirror-particles. the one-mirror magnon on the both two hexagons are given by the one-loop conformal integral:²

$$\Phi(z) = \frac{-(1-z)\log(1-z)^2 - \log z^2}{z(1-z)} \quad (12.1)$$

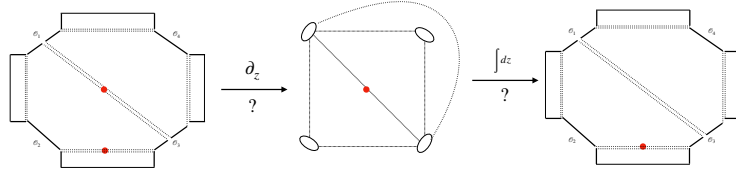
On the other hand, the one-mirror magnon on the between hexagon from factor and boundary state had roughly $\zeta(2)$ contribution, which is given by the integration $\Phi(z)$ with respect to z :

$$\int_0^{\infty} \Phi(z) dz = 8\zeta(2). \quad (12.2)$$

Furthermore, the two-magnons on the two hexagons and one boundary state was given by the Roger’s Dilogarithm. Thus, the derivative of the Roger’s Dilogarithm times $\zeta(2)$ is equal to the one-loop conformal integral:

$$\frac{d}{dz} (\zeta(2)\text{Li}_R[z]) = \Phi(z) \quad (12.3)$$

Namely, these mirror particle contributions may relate as follows:



It is interesting to clarify these mirror particle contributions.

12.4 Application to higher spin holography

It may be useful to apply the hexagon decomposition method to other theories. For example, as a simple integrable CFT model, there is the three-dimensional $O(N)$ vector model as free boson (fermion) theory. The theory is trivially integrable since it is a free theory. The simplest dual gauge invariant operator is given by the bi-fundamental operator. The operator would map to a sort of open spin-chain with only two sites. Furthermore, this

²As a simple discussion, we noted the one-dimensional one-loop conformal integral, which is defined as $\Phi(z) \lim_{\bar{z} \rightarrow z} \Phi(z, \bar{z})$

theory has an attractive property, so-called 3d-bosonization [91, 92]. The boson theory and a fermion theory can be interchanged by the Chern-Simons coupling constants. How this information is realized in the hexagon framework would be an interesting question. The AdS dual description of this model is the Vasiliev's higher spin theory which is defined as a bulk theory [93–96]. The coupling to Chern-Simons amounts to changing the boundary condition on the Vasiliev side. On the other hand, the hexagon method is based on the world-sheet formalism, since the hexagon is basically obtained by the cutting the world-sheet. Therefore, if we can express the three-point function of the three dimensional $O(N)$ vector model in terms of the hexagon method, it may give a useful hint for the world-sheet formulation of the higher spin theory.

Part V
Appendix

Appendix A

Basic integrals

Here we introduce basic integrals following [97], which appear in the perturbative computation. The fundamental integrals are defined by

$$I_{12} = \frac{1}{(2\pi)^2 x_{12}^2}, \quad (\text{A.1})$$

$$Y_{123} = \int d^4\omega I_{1\omega} I_{2\omega} I_{3\omega}, \quad (\text{A.2})$$

$$X_{1234} = \int d^4\omega I_{1\omega} I_{2\omega} I_{3\omega} I_{4\omega}, \quad (\text{A.3})$$

$$H_{12,34} = \int d^4u d^4v I_{1u} I_{2u} I_{uv} I_{3v} I_4. \quad (\text{A.4})$$

The third integral is the so-called 1-loop conformal integral and can be evaluated explicitly [98] as

$$X_{1234} = \frac{\pi^2 \Phi(z, \bar{z})}{(2\pi)^8 x_{13}^2 x_{24}^2}, \quad \Phi(z, \bar{z}) \equiv \frac{2\text{Li}_2(z) - 2\text{Li}_2(\bar{z}) + \log z \bar{z} \log \frac{1-z}{1-\bar{z}}}{z - \bar{z}}, \quad (\text{A.5})$$

where z and \bar{z} are the usual conformal cross ratios:

$$z\bar{z} = \frac{x_{12}^2 x_{34}^2}{x_{13}^2 x_{24}^2}, \quad (1-z)(1-\bar{z}) = \frac{x_{14}^2 x_{23}^2}{x_{13}^2 x_{24}^2}. \quad (\text{A.6})$$

The second integral can be evaluated using X_{1234} as

$$Y_{123} = \lim_{x_4 \rightarrow \infty} (2\pi)^2 x_4^2 X_{1234} = \frac{\pi^2 \Phi(z', \bar{z}')}{(2\pi)^6 x_{13}^2}, \quad (\text{A.7})$$

with

$$z'\bar{z}' = \frac{x_{12}^2}{x_{13}^2}, \quad (1-z')(1-\bar{z}') = \frac{x_{23}^2}{x_{13}^2}. \quad (\text{A.8})$$

When all external points are on a single line, these integrals further simplify to

$$\begin{aligned} X_{1234}|_{\text{line}} &= -\frac{2\pi^2}{(2\pi)^8} \left(\frac{\log(|\tau_{12}\tau_{34}|)}{\tau_{13}\tau_{24}\tau_{14}\tau_{23}} + \frac{\log(|\tau_{13}\tau_{24}|)}{\tau_{12}\tau_{34}\tau_{14}\tau_{32}} + \frac{\log(|\tau_{14}\tau_{23}|)}{\tau_{12}\tau_{43}\tau_{13}\tau_{42}} \right), \\ Y_{123}|_{\text{line}} &= -\frac{2\pi^2}{(2\pi)^6} \left(\frac{\log|\tau_{12}|}{\tau_{13}\tau_{23}} + \frac{\log|\tau_{13}|}{\tau_{12}\tau_{32}} + \frac{\log|\tau_{23}|}{\tau_{21}\tau_{31}} \right), \end{aligned} \quad (\text{A.9})$$

where τ_i 's are the positions of the external points on the line and $\tau_{ij} = \tau_i - \tau_j$. The fourth integral is accompanied by derivative in the calculation of the Feynman one-loop diagram as

$$F_{12,34} = \frac{(\partial_1 - \partial_2) \cdot (\partial_3 - \partial_4) H_{12,34}}{I_{12}I_{34}} = \frac{X_{1234}}{I_{13}I_{24}} - \frac{X_{1234}}{I_{14}I_{23}} + G_{1,34} - G_{2,34} + G_{3,12} - G_{4,12}, \quad (\text{A.10})$$

$$G_{1,34} = \frac{Y_{134}}{I_{14}} - \frac{Y_{134}}{I_{13}}. \quad (\text{A.11})$$

When any two points are collided, the integrals become divergent. Such a value is useful to calculate the two- and three-point functions at one-loop. Therefore, we further note the results in the point-splitting regularization

$$\begin{aligned} Y_{112} &= Y_{122} = -\frac{1}{16\pi^2} \left(\ln \frac{\epsilon^2}{x_{12}^2} - 2 \right) I_{12}, \\ X_{1123} &= -\frac{1}{16\pi} I_{12}I_{13} \left(\ln \frac{\epsilon^2 x_{23}^2}{x_{12}^2 x_{31}^2} - 2 \right), \\ F_{12,13} &= -\frac{1}{16\pi^2} \left(\ln \frac{\epsilon^2}{x_{23}^2} - 2 \right) + Y_{123} \left(\frac{1}{I_{12}} + \frac{1}{I_{13}} - \frac{2}{I_{23}} \right), \\ X_{1122} &= -\frac{1}{8\pi^2} I_{12}^2 \left(\ln \frac{\epsilon^2}{x_{12}^2} - 1 \right), \\ F_{12,12} &= -\frac{1}{8\pi^2} I_{12}^2 \left(\ln \frac{\epsilon^2}{x_{12}^2} - 3 \right). \end{aligned}$$

Finally, the fundamental one-loop diagrams are written as

$$\text{self}_{12} = \frac{\lambda}{8\pi^2} \left(-2 \log \frac{x_{21}}{\epsilon} - 2 \right), \quad (\text{A.12})$$

$$G_{1234} = \left[\frac{\lambda}{16\pi^2} \Phi(z, \bar{z}) ((1-z)(1-\bar{z}) - 1) + C_{12,43} \right], \quad (\text{A.13})$$

$$S_{1234} = \frac{\lambda}{16\pi^2} \Phi(z, \bar{z}) (2d_{13}d_{24} - (1-z)(1-\bar{z})d_{23}d_{41} - z\bar{z}d_{12}d_{34}) \quad (\text{A.14})$$

Appendix B

Three-point functions with double-magnon states at tree-level

$$C_{123}^{XX\circ}$$

We first consider the three-point functions of the two non-BPS operators with each excitation X or \bar{X} and one BPS operator as following:

$$\mathcal{O}_1 = \text{Tr}[Z^{L_1-1}X], \quad \mathcal{O}_2 = \text{Tr}[\bar{Z}^{L_2-1}\bar{X}], \quad \mathcal{O}_3 = \text{Tr}[\tilde{Z}^{L_3}], \quad (\text{B.1})$$

where we recall definition of the scalars

$$Z = \phi_1 + i\phi_2, \quad Y = \phi_3 + i\phi_4, \quad X = \phi_5 + i\phi_6, \quad (\text{B.2})$$

$$\tilde{Z} = Z + \bar{Z} + Y - \bar{Y}. \quad (\text{B.3})$$

Also, the notation \bar{Z}, \bar{Y} and \bar{X} are complex conjugate of Z, Y and X respectively. In this set up, while the excitation X of operator \mathcal{O}_1 is only contracting with the excitation \bar{X} of operator \mathcal{O}_2 , see figure B.1.

In order to systematically calculate the structure constants, we go on spin chain system. First of all, the operators are mapped to the each ‘‘spin chains’’ with magnon as follows:

$$\mathcal{O}_1 \rightarrow |p\rangle_1 = \sum_x e^{ipx} |\dots ZXZ \dots\rangle_1,$$

$$\mathcal{O}_2 \rightarrow |q\rangle_2 = \sum_x e^{iqx} |\dots \bar{Z}\bar{X}\bar{Z} \dots\rangle_2,$$

$$\mathcal{O}_3 \rightarrow |0\rangle_3 = |\dots \tilde{Z} \dots\rangle_3.$$

Next, these ‘‘spin chains’’ states are decomposed into two states. Then we must be careful

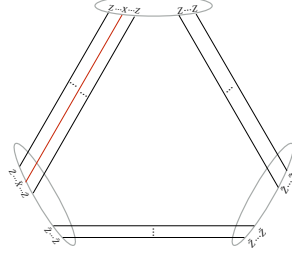


Figure B.1: $C^{X\bar{X}^{\circ}}$

of range of the excitations X and \bar{X}

$$\mathcal{O}_1 \rightarrow \sum_{x=1}^{\ell_{12}} e^{ipx} |\cdots ZXZ \cdots\rangle_1 \otimes |\cdots Z \cdots\rangle_1,$$

$$\mathcal{O}_2 \rightarrow |\cdots \bar{Z} \cdots\rangle_2 \otimes \sum_{x=\ell_{12}+1}^{L_2} e^{iqx} |\cdots \bar{Z}\bar{X}\bar{Z} \cdots\rangle_2,$$

$$\mathcal{O}_3 \rightarrow |\cdots \tilde{Z} \cdots\rangle_3 \otimes |\cdots \tilde{Z} \cdots\rangle_3.$$

Also, we define a flipping operation which is merely change from the bra state to ket state and act the flipping operator to the right side states

$$\mathcal{O}_1 \rightarrow \sum_{x=1}^{\ell_{12}} e^{ipx} |\cdots ZXZ \cdots\rangle_1 \otimes {}_1\langle \cdots Z \cdots|,$$

$$\mathcal{O}_2 \rightarrow |\cdots \bar{Z} \cdots\rangle_2 \otimes \sum_{x=\ell_{12}+1}^{L_2} e^{iqx} {}_2\langle \cdots \bar{Z}\bar{X}\bar{Z} \cdots|,$$

$$\mathcal{O}_3 \rightarrow |\cdots \tilde{Z} \cdots\rangle_3 \otimes {}_3\langle \cdots \tilde{Z} \cdots|.$$

Finally, by contracting the states like in fig, the structure constants are given by

$$C_{123}^{X\bar{X}^{\circ}} \propto \sum_{x=1}^{\ell_{12}} e^{ipx+iq(L_1-x+1)}. \quad (\text{B.4})$$

Calculating the geometric sum, we finally have

$$C_{123}^{X\bar{X}^{\circ}} \propto \mathcal{N}(p)\mathcal{N}(q) \frac{-i}{u-v} (1 + e^{ip\ell_{31}} e^{iq\ell_{12}}). \quad (\text{B.5})$$

Then, we got the nontrivial factor $-i/(u-v)$. The factor is interpreted as a weight factor, when two magnons are propagated as a mass:

$$\sum_x \text{Diagram} = \mathcal{N}(p)\mathcal{N}(q) \frac{-i}{u-v} \left\{ \text{Diagram}_1 - \text{Diagram}_2 \right\}$$

Thus, the factor is just the tree-level hexagon form factor

$$h_{X|\bar{X}}(u, v) = h_{X\bar{X}}(v^{2\gamma}, u) = -\frac{i}{u-v} + \mathcal{O}(g). \quad (\text{B.6})$$

Finally, the asymptotic structure constants at finite coupling in this set-up is given by

$$\mathcal{A}^{\text{finite}} = h_{X|\bar{X}}^{\text{finite}}(u, v)(1 - e^{ip\ell_{31}} e^{iq\ell_{12}}). \quad (\text{B.7})$$

Notice that, the one-particle hexagon form factor for X excitation is zero: $h_X(u) = 0$ by (5.21).

Appendix C

Vertex and self-energy diagrams for the three-point functions

In this appendix, we explain the contributions from the vertex diagrams and self-energy diagrams for three-point functions at two-loop. Then, the diagrams are divided into three-parts: the coefficients have $(n_{12} \cdot n_{23} - 1)$, $(n_{23} \cdot n_{31} - 1)$, and $(n_{31} \cdot n_{12} - 1)$. However, we explicitly write down the $(n_{12} \cdot n_{23} - 1)$ diagrams. Because, the others are obtained by the replacement of the operator.

The vertex diagrams are listed in figure 8.9 and we have

$$\begin{aligned}
 \text{T1} &= -\frac{\lambda^2(n_{12} \cdot n_{23} - 1)}{4(4\pi^2)^3} \int_{t_1^+}^{t_2^-} d\tau_1 \int_{t_1^+}^{t_2^-} d\tau_2 \int_{t_2^+}^{t_3^-} d\tau_3 \epsilon(\tau_1 - \tau_2) \partial_{\tau_1} Y_{123} + (\text{perm.}), \\
 \text{T2} &= -\frac{\lambda^2(n_{12} \cdot n_{23} - 1)}{4(4\pi^2)^3} \int_{t_1^+}^{t_2^-} d\tau_1 \int_{t_2^+}^{t_3^-} d\tau_2 \int_{t_2^+}^{t_3^-} d\tau_3 \epsilon(\tau_2 - \tau_3) \partial_{\tau_2} Y_{123} + (\text{perm.}), \\
 \text{T3} &= -\frac{\lambda^2(n_{12} \cdot n_{23} - 1)}{4(4\pi^2)^3} \int_{-\infty}^{t_1^-} d\tau_1 \int_{t_1^+}^{t_2^-} d\tau_2 \int_{t_2^+}^{t_3^-} d\tau_3 (\partial_{\tau_2} Y_{123} - \partial_{\tau_3} Y_{123}) + (\text{perm.}), \\
 \text{T4} &= -\frac{\lambda^2(n_{12} \cdot n_{23} - 1)}{4(4\pi^2)^3} \int_{t_1^+}^{t_2^-} d\tau_1 \int_{t_2^+}^{t_3^-} d\tau_2 \int_{t_2^+}^{\infty} d\tau_3 (\partial_{\tau_1} Y_{123} - \partial_{\tau_2} Y_{123}) + (\text{perm.}).
 \end{aligned} \tag{C.1}$$

Calculating them, some integrals produce the divergent terms. However, fortunately, these terms are completely canceled by the self-energy diagrams in the same way as the

two-point functions. Therefore, the remained finite terms are given by

$$\begin{aligned}
\mathbb{T}|_{\text{finite}} = & -\frac{\lambda^2(n_{12} \cdot n_{23} - 1)}{4(4\pi^2)^3} \left[\int_{t_1^+}^{t_2^-} d\tau_2 \int_{t_2^+}^{t_3^-} d\tau_3 \left(Y_{t_2^- 23} + Y_{t_1^+ 23} + Y_{t_3^- 23} + Y_{t_2^+ 23} \right) \right. \\
& + \int_{-\infty}^{t_1^-} d\tau_2 \int_{t_2^+}^{t_3^-} d\tau_3 (Y_{t_2^- 23} - Y_{t_1^+ 23}) + \int_{-\infty}^{t_1^-} d\tau_2 \int_{t_1^+}^{t_2^-} d\tau_3 (Y_{t_2^+ 23} - Y_{t_3^- 23}) \\
& \left. + \int_{t_2^+}^{t_3^-} d\tau_2 \int_{t_3^+}^{\infty} d\tau_3 (Y_{t_2^- 23} - Y_{t_1^+ 23}) + \int_{t_1^+}^{t_2^-} d\tau_2 \int_{t_3^+}^{\infty} d\tau_3 (Y_{t_2^+ 23} - Y_{t_3^- 23}) \right]. \tag{C.2}
\end{aligned}$$

Thus, performing the integration, we get

$$\mathbb{T}|_{\text{finite}} = -(n_{12} \cdot n_{23} - 1) \left(\frac{\lambda}{8\pi^2} \right)^2 \left(3\zeta(3) + \frac{\pi^2}{3} \log \left| \frac{t_{12} t_{23}}{t_{31} \epsilon} \right| \right). \tag{C.3}$$

Appendix D

Excited states and conformal descendants

In this appendix, we explain the relation between the vertex function Γ_ϵ and the Schrödinger equation in [81,99]. In particular, we clarify the physical meaning of the wave functions of the Schrödinger equation by showing that they correspond to the three-point functions of DCOs, and that the excited states of the Schrödinger equation correspond to conformal descendants.

For this purpose, let us quickly review how the Schrödinger equation comes about from the differential equation for Γ_ϵ (8.47). To begin with, we rewrite the equation in terms of the “radial coordinate”¹

$$S = \exp(-x + y), \quad T = \exp(x + y), \quad (\text{D.1})$$

to get

$$\left[-\frac{1}{4}(\partial_x^2 - \partial_y^2) - \frac{\tilde{\lambda}}{4\pi^2} \frac{1}{(2 \cosh x)^2} \right] \Gamma_\epsilon = 0. \quad (\text{D.2})$$

Physically this rewriting corresponds to considering the theory on $R \times S^3$: x describes the (Euclidean) time difference of the two endpoints while y corresponds to the time of the “center of mass”. Then, assuming the form of the solution to be

$$\Gamma_\epsilon = \sum_N c_N e^{\Omega_N y} \Psi_N(x), \quad (\text{D.3})$$

one can reduce the differential equation (D.2) to the following one-dimensional Schrödinger equation:

$$\left[-\frac{d^2}{dx^2} - \frac{\tilde{\lambda}}{4\pi^2} \frac{1}{\cosh^2 x} \right] \Psi_N(x) = -\Omega_N^2 \Psi_N(x). \quad (\text{D.4})$$

¹If we instead rewrite the equation in terms of the coordinates $s = S + T$ and $t = S - T$, one arrives at the “conformal quantum mechanics” [100]; the Schrödinger equation with the inverse square potential. This description, however, is not very useful for our purpose and we will not discuss it here.

The Schrödinger equation with this potential (called the Pöschl-Teller potential) has the $SL(2, \mathbb{R})$ symmetry² and is known to be exactly solvable. This can be seen explicitly by the change of the variable

$$z = \frac{1}{1 + e^x}, \quad (\text{D.5})$$

which maps the problem to the hypergeometric differential equation.

By using the explicit form of Γ_ϵ shown in (8.46), one can determine which wave functions appear in the expansion (D.3). The result turns out to be given by a sum of two families of solutions³

$$\Gamma_\epsilon = \sum_{n=0}^{\infty} c_n e^{\Omega^{(n)} y} \Psi_n(x) + \sum_{n=0}^{\infty} \tilde{c}_n e^{\tilde{\Omega}^{(n)} y} \tilde{\Psi}_n(x) \quad (\text{D.7})$$

with

$$\begin{aligned} \Omega^{(n)} &= \Omega - n, & \tilde{\Omega}^{(n)} &= -\Omega - n - 1, \\ \Psi_n(z) &= (z(1-z))^{\frac{\Omega^{(n)}}{2}} {}_2F_1(\Omega^{(n)} - \Omega, \Omega^{(n)} + \Omega + 1, 1 + \Omega^{(n)}; z), \\ \tilde{\Psi}_n(z) &= (z(1-z))^{\frac{\tilde{\Omega}^{(n)}}{2}} {}_2F_1(\tilde{\Omega}^{(n)} - \Omega, \tilde{\Omega}^{(n)} + \Omega + 1, 1 + \tilde{\Omega}^{(n)}; z). \end{aligned} \quad (\text{D.8})$$

These solutions have several interesting properties. First, they are the only solutions to (D.4) for which the hypergeometric function reduces to a polynomial. Second, the first family of solutions with $n < \Omega$ decay at $x = \pm\infty$ and correspond to the bound states of the Schrödinger equation (D.4), as discussed in [81]. Note also that, to reconstruct Γ_ϵ , one needs to include “unphysical solutions” which blow up at $x = \pm\infty$, in addition to such bound state solutions. Although it might seem counter-intuitive, it has natural interpretation in terms of the OPE in the defect CFT as we see below.

To see this, recall that the vertex function is obtained as a limit of the four-point ladder kernel $\Gamma_\epsilon(S, T) \equiv K(-S, -\epsilon/2 | \epsilon/2, T)$. A crucial observation is that the ladder kernel itself can be interpreted as a certain four-point function of (trivial) DCOs,

$$\Gamma_\epsilon(S, T) = K(-S, -\epsilon/2 | \epsilon/2, T) = \langle \mathcal{O}_1^\circ(-S) \mathcal{O}_2^\circ(-\epsilon/2) \mathcal{O}_3^\circ(\epsilon/2) \mathcal{O}_4^\circ(T) \rangle, \quad (\text{D.9})$$

and the limit $\epsilon \rightarrow 0$ corresponds to the OPE limit where \mathcal{O}_2 and \mathcal{O}_3 approach. Using the OPE, one can replace the product of \mathcal{O}_2 and \mathcal{O}_3 with an infinite sum⁴,

$$\mathcal{O}_2^\circ(-\epsilon/2) \mathcal{O}_3^\circ(\epsilon/2) = \sum_{\tilde{\mathcal{O}}} \epsilon^{\Delta_{\tilde{\mathcal{O}}}} c_{23\tilde{\mathcal{O}}} \tilde{\mathcal{O}}(0). \quad (\text{D.10})$$

²The difference from the usual conformal quantum mechanics [100] lies in that the “dilatation generator” of the $SL(2, \mathbb{R})$ is identified not with the Hamiltonian itself but with its square root. See for instance [101].

³As in the main text Ω is defined by

$$\Omega(\tilde{\lambda}) = \frac{1}{2} \left[-1 + \sqrt{1 + \frac{\tilde{\lambda}}{\pi^2}} \right]. \quad (\text{D.6})$$

⁴Here we used the fact that the trivial DCOs have zero conformal dimensions.

Here the sum on the right hand side is over both primaries and descendants, and $c_{23\tilde{\mathcal{O}}}$ denotes the structure constant. Using this OPE inside the four-point function (D.9), we get the following infinite-sum representation for the vertex function

$$\Gamma_\epsilon(S, T) = \sum_{\tilde{\mathcal{O}}} \epsilon^{\Delta_{\tilde{\mathcal{O}}}} c_{23\tilde{\mathcal{O}}} \langle \mathcal{O}_1^\circ(-S) \tilde{\mathcal{O}}(0) \mathcal{O}_4^\circ(T) \rangle. \quad (\text{D.11})$$

Let us now compare this sum with the sum over wave functions (D.7). To do so, one has to know the behavior of $\langle \mathcal{O}_1^\circ(-S) \tilde{\mathcal{O}}(0) \mathcal{O}_4^\circ(T) \rangle$ (both for primaries and descendants) and express it in terms of the x and y coordinates. When $\tilde{\mathcal{O}}$ is primary, the behavior of the three-point function is well-known⁵,

$$\langle \mathcal{O}_1^\circ(-S) \tilde{\mathcal{O}}_{\text{primary}}(0) \mathcal{O}_4^\circ(T) \rangle \propto \left(\frac{S+T}{ST} \right)^\Delta. \quad (\text{D.12})$$

On the other hand, the behavior for the descendants can be computed by differentiation as

$$\langle \mathcal{O}_1^\circ(-S) \partial^n \tilde{\mathcal{O}}_{\text{primary}}(0) \mathcal{O}_4^\circ(T) \rangle \propto \left(\frac{S+T}{ST} \right)^\Delta \sum_{k=0}^n \binom{n}{k} (-1)^k (\Delta)_k (\Delta)_{n-k} \frac{1}{S^k T^{n-k}}, \quad (\text{D.13})$$

with $(x)_k$ being the Pochhammer symbol. Re-expressing this in terms of x and y , we obtain

$$\begin{aligned} (\text{D.13}) &= e^{-(\Delta+n)y} (e^x + e^{-x})^{\Delta+n} \sum_{k=0}^n \binom{n}{k} (-1)^k (\Delta)_k (\Delta)_{n-k} e^{2kx} (1 + e^{-2x})^{-n} \\ &= e^{-(\Delta+n)y} (z(1-z))^{-\frac{\Delta+n}{2}} \left[\sum_{k=0}^n \binom{n}{k} (-1)^k (\Delta)_k (\Delta)_{n-k} z^{n-k} (1-z)^k \right]. \end{aligned} \quad (\text{D.14})$$

In the second line, we further rewrote it in terms of $z = 1/(1 + e^x)$. The polynomial in the bracket turns out to be summed into a hypergeometric function ${}_2F_1(-n, 1 - 2\Delta - n, 1 - \Delta - n, z)$. We thus get the expression

$$\begin{aligned} &\langle \mathcal{O}_1^\circ(-S) \partial^n \tilde{\mathcal{O}}_{\text{primary}}(0) \mathcal{O}_4^\circ(T) \rangle \\ &\propto e^{-(\Delta+n)y} (z(1-z))^{-\frac{\Delta+n}{2}} {}_2F_1(-n, 1 - 2\Delta - n, 1 - \Delta - n, z). \end{aligned} \quad (\text{D.15})$$

With the identifications $\Delta = -\Omega$ and $\Delta = 1 + \Omega$, this coincides with $e^{\Omega n y} \Psi_n$ and $e^{\tilde{\Omega} n y} \tilde{\Psi}_n$ in (D.8) respectively. We can therefore interpret the sum (D.7) really as the OPE expansion and the wave functions are identified with the three-point functions:

$$\begin{aligned} \Gamma_\epsilon &= \sum_{X=\text{DCO,shadow}} \sum_{n=0}^{\infty} \epsilon^{\Delta_X+n} c_{X,n} \langle \mathcal{O}_1^\circ(-S) \partial^n \mathcal{O}_X^\bullet(0) \mathcal{O}_4^\circ(T) \rangle, \\ \langle \mathcal{O}_1^\circ(-S) \partial^n \mathcal{O}_{\text{DCO}}^\bullet(0) \mathcal{O}_4^\circ(T) \rangle &\leftrightarrow e^{\Omega n y} \Psi_n, \\ \langle \mathcal{O}_1^\circ(-S) \partial^n \mathcal{O}_{\text{shadow}}^\bullet(0) \mathcal{O}_4^\circ(T) \rangle &\leftrightarrow e^{\tilde{\Omega} n y} \tilde{\Psi}_n. \end{aligned} \quad (\text{D.16})$$

⁵For the sake of brevity, below we omit writing the subscript $\tilde{\mathcal{O}}$ in $\Delta_{\tilde{\mathcal{O}}}$.

Here $\mathcal{O}_{\text{DCO}}^\bullet$ is a nontrivial DCO, which we studied in the main text, and $\mathcal{O}_{\text{shadow}}^\bullet$ is its *shadow* operator⁶, which has dimension $\Delta_{\text{shadow}} = 1 - \Delta_{\text{DCO}} = 1 + \Omega$. This provides a clear physical interpretation of the wave functions for the Schrödinger equation (D.4).

⁶In unitary CFTs, the shadow operators do not usually show up in the spectrum since they are often below the unitarity bound. However, the possibility of having both an operator and its shadow in the spectrum is not totally ruled out. In fact, it is known that some long-range CFTs have such a spectrum.

Appendix E

Contribution from the integral of Γ_{UV}

In this appendix, we show that, in the $\epsilon \rightarrow 0$ limit, the integrals involving the vertex function Γ_ϵ can be approximated by replacing Γ_ϵ with its IR counterpart, Γ_{IR} . More precisely the goal is to show that the ratio between the contributions from Γ_{UV} and Γ_{IR} is given as follows:

$$\frac{\int ds \int dt \Gamma_{UV}(s, t) f(s, t)}{\int ds \int dt \Gamma_{IR}(s, t) f(s, t)} \leq O(\epsilon \log \epsilon) \xrightarrow{\epsilon \rightarrow 0} 0. \quad (\text{E.1})$$

Here $f(s, t)$ denotes the rest of the integrand, which may contain other vertex functions, propagators and the ladder kernels K .

For this purpose, it is convenient to split the vertex function in a slightly different way as follows:

$$\begin{aligned} \Gamma_\epsilon(u) &= \tilde{\Gamma}_{IR}(u) + \tilde{\Gamma}_{UV}(u), \\ \tilde{\Gamma}_{IR}(u) &= \frac{A(\Omega)}{(1-u)^\Omega}. \end{aligned} \quad (\text{E.2})$$

Since the ratio $(\Gamma_{IR} - \tilde{\Gamma}_{IR})/\Gamma_{IR}$ is always of order $O(\epsilon)$ (regardless of their arguments), it is enough to show (E.1) for $\tilde{\Gamma}_{IR}$ and $\tilde{\Gamma}_{UV}$.

Now, let us estimate the maximal value of $\tilde{\Gamma}_{UV}$. In all the examples studied in the main text, the cross ratio $u = \frac{(S-\epsilon/2)(T-\epsilon/2)}{(S+\epsilon/2)(T+\epsilon/2)}$ takes values in $[0, 1 - \epsilon/C]^1$ with a $O(1)$ positive constant C . In this region, the UV vertex $\tilde{\Gamma}_{UV}$ monotonically decreases in u for $\Omega \leq 1$ while it monotonically increases in u for $\Omega > 1^2$. Therefore, the maximal absolute value of the UV vertex is given by

$$\max |\tilde{\Gamma}_{UV}(u)| = \begin{cases} |1 - A(\Omega)| & (= |\tilde{\Gamma}_{UV}(0)|) & \text{for } \Omega \leq 1 \\ O(\epsilon^{1-\Omega}) & (= |\tilde{\Gamma}_{UV}(1 - \epsilon/C)|) & \text{for } \Omega > 1 \end{cases}. \quad (\text{E.3})$$

¹ u can reach 1 only when $S = T = \infty$. However, we never encounter an integral whose integration regions both extend to infinity.

²One can easily verify this by using the definitions of the vertex functions (8.46) and (E.2), and the series expansion of the hypergeometric function.

Hence, the integral of $\tilde{\Gamma}_{UV}$ can be bounded from above as follows:

$$\int ds \int dt \tilde{\Gamma}_{UV}(s, t) f(s, t) \leq \frac{\tilde{C}}{\epsilon^{\Omega-1}} \int ds \int dt f(s, t). \quad (\text{E.4})$$

In all the cases encountered in the main text, the integral of $f(s, t)$ can produce at most logarithmic divergences³ $\int ds \int dt (s-t)^{-2} \sim \log \epsilon$. We thus have

$$\int ds \int dt \tilde{\Gamma}_{UV}(s, t) f(s, t) \leq O\left(\frac{\log \epsilon}{\epsilon^{\Omega-1+|f|}}\right), \quad (\text{E.5})$$

where $\epsilon^{-|f|}$ is the singularity contained already in the integrand, $f \sim O(\epsilon^{-|f|})$.

On the other hand, since $\tilde{\Gamma}_{IR} \sim \epsilon^{-\Omega} \times k(s, t)$ with $k(s, t)$ being the $O(1)$ function, we can easily estimate its integral as

$$\int ds \int dt \tilde{\Gamma}_{IR}(s, t) f(s, t) \geq O\left(\frac{1}{\epsilon^{\Omega+|f|}}\right). \quad (\text{E.6})$$

Combining (E.5) and (E.6), we get the estimation (E.1) for $\tilde{\Gamma}_{UV}$ and $\tilde{\Gamma}_{IR}$.

³This inverse square behavior comes from a propagator contained in $f(s, t)$.

Appendix F

Explicit calculation of the $C_{123}^{\bullet\circ\circ}$ in (8.63)

In this chapter, we explicitly calculate the following integral

$$\frac{C_{123}^{\bullet\circ\circ}}{\tau_{21}^{-\Omega}\tau_{32}^{\Omega}\tau_{31}^{-\Omega}} = \Gamma^R(\infty, \tau_{21}) + \frac{\tilde{\lambda}}{4\pi^2} \int_{\tau_1}^{\tau_2} ds \int_{\tau_3}^{\infty} dt \frac{\Gamma^R(\infty, s - \tau_1) K(s, \tau_2 | \tau_3, t)}{(t - s)^2}. \quad (\text{F.1})$$

Using the SD-equation and performing the t integral, we get

$$\frac{C_{123}^{\bullet\circ\circ}}{\tau_{21}^{-\Omega}\tau_{32}^{\Omega}\tau_{31}^{-\Omega}} = \equiv \int_{\tau_1}^{\tau_2} ds \partial_s \Gamma^R(\infty, s - \tau_1) K(s, \tau_2 | \tau_3, \infty). \quad (\text{F.2})$$

Thus, by substituting the explicit form of the bridge kernel K , we have

$$\frac{C_{123}^{\bullet\circ\circ}}{\tau_{21}^{-\Omega}\tau_{32}^{\Omega}\tau_{31}^{-\Omega}} = \frac{\sqrt{A(\Omega)}}{\tau_{32}^{\Omega}} \int_{\tau_1}^{\tau_2} ds \partial_s [(s - \tau_1)^{\Omega}] (\tau_3 - s)^{\Omega} {}_2F_1\left(-\Omega, -\Omega, 1; \frac{\tau_2 - s}{\tau_3 - s}\right). \quad (\text{F.3})$$

Furthermore, we perform the following change of variables:

$$x = \frac{s - \tau_2}{s - \tau_3} \frac{\tau_1 - \tau_3}{\tau_1 - \tau_2}, \quad (\text{F.4})$$

and use the identity ${}_2F_1(a, b, c; z) = (1 - z)^{-a-b+c} {}_2F_1(c - a, c - b, c; z)$ to get

$$\frac{C_{123}^{\bullet\circ\circ}}{\tau_{21}^{-\Omega}\tau_{32}^{\Omega}\tau_{31}^{-\Omega}} = \Omega \sqrt{A(\Omega)} \tau_{21}^{\Omega} (1 - \alpha) \int_0^1 dx (1 - x)^{\Omega-1} {}_2F_1(\Omega + 1, \Omega + 1, 1; \alpha x), \quad (\text{F.5})$$

with $\alpha = \tau_{21}/\tau_{32}$. To proceed, we rewrite ${}_2F_1$ using the integral representation as

$${}_2F_1(\Omega + 1, \Omega + 1, 1; \alpha x) = \frac{1}{\Gamma(\Omega + 1)\Gamma(-\Omega)} \int_0^1 dy y^{\Omega} (1 - y)^{-\Omega-1} (1 - y\alpha x)^{-\Omega-1}. \quad (\text{F.6})$$

One can then perform the x integral to get¹

$$\frac{C_{123}^{\bullet\circ\circ}}{\tau_{21}^{-\Omega}\tau_{32}^{\Omega}\tau_{31}^{-\Omega}} = \frac{\sqrt{A(\Omega)} \tau_{21}^{\Omega} (1 - \alpha)}{\Gamma(\Omega + 1)\Gamma(-\Omega)} \int_0^1 dy y^{\Omega} (1 - y)^{-\Omega-1} (1 - \alpha y)^{-1}. \quad (\text{F.7})$$

¹Here we used the integral expression for the hypergeometric function and the identity ${}_2F_1(a, 1, a; z) = (1 - z)^{-1}$.

This is again a hypergeometric integral and we can compute it as follows:

$$\frac{C_{123}^{\bullet\circ\circ}}{\tau_{21}^{-\Omega}\tau_{32}^{\Omega}\tau_{31}^{-\Omega}} = \sqrt{A(\Omega)}\tau_{21}^{\Omega}(1-\alpha) {}_2F_1(1, \Omega+1, 1; \alpha) . \quad (\text{F.8})$$

Finally, using the identity ${}_2F_1(1, \Omega+1, 1; \alpha) = (1-\alpha)^{-\Omega-1}$, we arrive at

$$\frac{C_{123}^{\bullet\circ\circ}}{\tau_{21}^{-\Omega}\tau_{32}^{\Omega}\tau_{31}^{-\Omega}} = \frac{\sqrt{A(\Omega)}}{\tau_{21}^{-\Omega}\tau_{32}^{\Omega}\tau_{31}^{-\Omega}} . \quad (\text{F.9})$$

Appendix G

An infinite sum representation for

$$C_{123}^{\bullet\bullet\bullet}$$

In this appendix, we perform the integral of the structure constants (8.81). As a result, we can see the infinite-sum representation, rather than integral representation.

First we perform the change of variables as follows:

$$x = \frac{1 - \bar{u}}{1 - (1 - \bar{s})\bar{u}}, \quad y = 1 - (1 - \bar{s})\bar{u}, \quad z = \frac{1 - \bar{t}}{1 - (1 - \bar{u})\bar{t}}. \quad (\text{G.1})$$

Here the Jacobean is given by $\frac{y}{(1-xyz)^2}$. Then we have

$$J = \prod_{i=1}^3 \Omega_i \int_0^1 dx \int_0^1 dy \int_0^1 dz x^{\Omega_1-1} y^{\Omega_1} z^{\Omega_3-1} \quad (\text{G.2})$$

$$(1-x)^{\Omega_1+1} (1-y)^{\Omega_2-1} (1-z)^{\Omega_2+1} (1-xy)^{-(\Omega_1+\Omega_2-\Omega_3+1)} (1-yz)^{-(\Omega_2+1)}.$$

The integrals of x and z yield the hypergeometric functions,

$$J = \prod_{i=1}^3 \Omega_i \int_0^1 dy y^{\Omega_1} (1-y)^{\Omega_2-1} \frac{\Gamma(\Omega_3)\Gamma(\Omega_2+2)}{\Gamma(\Omega_2+\Omega_3+2)} {}_2F_1(\Omega_3, \Omega_2+1, \Omega_2+\Omega_3+2; y) \quad (\text{G.3})$$

$$\times \frac{\Gamma(\Omega_1)\Gamma(\Omega_1+2)}{\Gamma(2\Omega_1+2)} {}_2F_1(\Omega_1, \Omega_1+\Omega_2-\Omega_3+1, 2\Omega_1+2; y).$$

Using the series expansion of the hypergeometric function, the y integral is also calculated. After doing so, using the Euler integral representation for the generalized hypergeometric function

$${}_3F_2 \left(\begin{matrix} \alpha_1, \alpha_2, \alpha_3 \\ \beta_1, \beta_2 \end{matrix}; z \right) = \frac{\Gamma(\beta_1)\Gamma(\beta_2)}{\Gamma(\alpha_1)\Gamma(\beta_1-\alpha_1)\Gamma(\alpha_2)\Gamma(\beta_2-\alpha_2)} \quad (\text{G.4})$$

$$\times \int_0^1 ds \int_0^1 dt s^{\alpha_1-1} (1-s)^{\beta_1-\alpha_1-1} t^{\alpha_2-1} (1-t)^{\beta_2-\alpha_2-1} (1-zst)^{-\alpha_3},$$

we finally obtain the infinite-sum representation of the structure constants

$$\begin{aligned}
C_{123}^{\bullet\bullet\bullet} &= \prod_{k=1}^3 \sqrt{A(\Omega_k)} \frac{\Gamma(\Omega_1 + 1)^2 \Gamma(\Omega_1 + 2) \Gamma(\Omega_2 + 1) \Gamma(\Omega_2 + 2) \Gamma(\Omega_3 + 1)}{\Gamma(2\Omega_1 + 2) \Gamma(\Omega_2 + \Omega_3 + 2) \Gamma(\Omega_1 + \Omega_2 + 1)} \\
&\times \sum_{k=0}^{\infty} \frac{(\Omega_3)_k (\Omega_2 + 1)_k}{(\Omega_2 + \Omega_3 + 2)_k k!} \frac{(\Omega_1 + 1)_k}{(\Omega_1 + \Omega_2 + 1)_k} {}_3F_2 \left(\begin{matrix} \Omega_1, \Omega_1 + \Omega_2 - \Omega_3 + 1, \Omega_1 + k + 1 \\ 2\Omega_1 + 2, \Omega_1 + \Omega_2 + k + 1 \end{matrix}; 1 \right).
\end{aligned} \tag{G.5}$$

Appendix H

Open spin chain wave functions

In this appendix, we discuss the wave functions of the open spin chain in Coordinate Bethe ansatz.

H.1 One-magnon

We first recall the eigenfunction equation and wave function ansatz

$$\mathcal{H}_{\text{open}}|\Psi_{\text{open}}^{(1)}\rangle = E^{(1)}|\Psi_{\text{open}}^{(1)}\rangle. \quad (\text{H.1})$$

The Bethe state is written as

$$|\Psi_{\text{open}}^{(1)}\rangle = \sum_{1 \leq x \leq L} \psi_{\text{open}}^{(1)}(x) |Z \cdots Z \overset{x}{\downarrow} Y Z \cdots Z\rangle,$$

$$\psi_{\text{open}}^{(1)}(x) = A'(p) \left(\mathcal{A}(x, p) + e^{2ipL} B_L(p) \mathcal{A}(x, -p) \right) \quad \text{with} \quad B_L(p) = -\frac{e^{-ip} - (1 - C_L)}{1 - (1 - C_L)e^{-ip}}, \quad (\text{H.2})$$

The wave function of $x = 1, L$ and others satisfy following constraint:

$$E^{(1)}\psi_{\text{open}}(1) = (1 + C_1)\psi_{\text{open}}(1) - \psi_{\text{open}}(2), \quad (\text{H.3})$$

$$E^{(1)}\psi_{\text{open}}(x) = 2\psi(x) - \psi_{\text{open}}(x - 1) - \psi_{\text{open}}(x + 1), \quad (\text{H.4})$$

$$E^{(1)}\psi_{\text{open}}(L) = (1 + C_L)\psi_{\text{open}}(L) - \psi_{\text{open}}(L - 1). \quad (\text{H.5})$$

Furthermore, we take the following general boundary conditions:

$$\psi_{\text{open}}(0) = (1 - C_1)\psi_{\text{open}}(1), \quad \psi_{\text{open}}(L + 1) = (1 - C_L)\psi_{\text{open}}(L) \quad (\text{H.6})$$

Thus the Bethe equation become

$$1 = e^{2ipL} B_1(-p) B_L(p) \quad (\text{H.7})$$

where $B_1(p)$ and $B_L(p)$ are defined as

$$\begin{aligned} B_1(p) &\equiv -e^{-ip} \frac{A(-p)}{A(p)} = -\frac{e^{-ip} - (1 - C_1)}{1 - (1 - C_1)e^{-ip}}, \\ B_L(p) &\equiv -e^{-ip} e^{-2ipL} \frac{A(-p)}{A(p)} = -\frac{e^{ip} - (1 - C_L)}{1 - (1 - C_L)e^{ip}}. \end{aligned} \quad (\text{H.8})$$

H.2 Two-magnon

Next for two-magnon wave functions, the eigenfunction equation become

$$\begin{aligned} E^{(2)}\psi_{\text{open}}(1, x_2) &= (1 + C_1)\psi_{\text{open}}(1, x_2) + 2\psi_{\text{open}}(1, x_2) - \psi_{\text{open}}(2, x_2) \\ &\quad - \psi_{\text{open}}(1, x_2 - 1) - \psi_{\text{open}}(1, x_2 + 1), \end{aligned} \quad (\text{H.9})$$

$$\begin{aligned} E^{(2)}\psi_{\text{open}}(x_1, x_2) &= 4\psi_{\text{open}}(x_1, x_2) - \psi_{\text{open}}(x_1 - 1, x_2) - \psi_{\text{open}}(x_1 + 1, x_2) \\ &\quad - \psi_{\text{open}}(x_1, x_2 - 1) - \psi_{\text{open}}(x_1, x_2 + 1), \end{aligned} \quad (\text{H.10})$$

$$E^{(2)}\psi_{\text{open}}(x_1, x_1 + 1) = 2\psi_{\text{open}}(x_1, x_1 + 1) - \psi_{\text{open}}(x_1 - 1, x_1 + 1) - \psi_{\text{open}}(x_1, x_2 + 2), \quad (\text{H.11})$$

$$\begin{aligned} E^{(2)}\psi_{\text{open}}(x_1, L) &= (1 + C_L)\psi_{\text{open}}(x_1, L) + 2\psi_{\text{open}}(x_1, L) - \psi_{\text{open}}(x_1, L - 1) \\ &\quad - \psi_{\text{open}}(x_1 + 1, L) - \psi_{\text{open}}(x_1 - 1, L). \end{aligned} \quad (\text{H.12})$$

We have the boundary conditions as follows:

$$\psi_{\text{open}}(0, x_2) = (1 - C_1)\psi_{\text{open}}(1, x_2), \quad \psi_{\text{open}}(x_1, L + 1) = (1 - C_L)\psi_{\text{open}}(x_1, L) \quad (\text{H.13})$$

The constraints (H.10) and (H.11) for the bulk wave functions give the following equation :

$$0 = 2\psi_{\text{open}}(x_1, x_1 + 1) - \psi_{\text{open}}(x_1 + 1, x_1 + 1) - \psi_{\text{open}}(x_1, x_1). \quad (\text{H.14})$$

By solving the equation, we obtain the bulk S -matrix

$$S(p_2, p_1) = \frac{u - v - i}{u - v + i}, \quad (\text{H.15})$$

The S -matrix is completely same with the closed spin chain system. Finally, the Bethe equation for two-magnon is given as

$$1 = e^{-2iLp_2} B_1(p_2) B_L(-p_2) S(p_2, p_1) S(p_2, -p_1). \quad (\text{H.16})$$

In the literature [86], the wave functions have another notation. we comment on these relation. In [86], the wave function was written as

$$\begin{aligned} \psi_{\text{open}} &= A(p_1, p_2) e^{i(p_1 x_1 + p_2 x_2)} - A(-p_1, p_2) e^{-i(p_1 x_1 - p_2 x_2)} - A(p_1, -p_2) e^{i(p_1 x_1 - p_2 x_2)} \\ &\quad + A(-p_1, -p_2) e^{-i(p_1 x_1 + p_2 x_2)} - A(p_2, p_1) e^{i(p_2 x_1 + p_1 x_2)} + A(p_2, -p_1) e^{-i(p_2 x_1 - p_1 x_2)} \\ &\quad + A(-p_2, p_1) e^{i(p_2 x_1 - p_1 x_2)} - A(-p_2, -p_1) e^{-i(p_2 x_1 + p_1 x_2)}. \end{aligned}$$

It is useful to introduce the half-step shift which means that the first and the last sites are the ‘ 1/2-th ’ and the ‘ $L + 1/2$ -th ’ sites respectively.

$$\begin{aligned}\psi_{\text{open}}^{(2)} &= A'(p_1, p_2)e^{i(p_1(x_1 - \frac{1}{2}) + p_2(x_2 - \frac{1}{2}))} - A'(-p_1, p_2)e^{-i(p_1(x_1 - \frac{1}{2}) - p_2(x_2 - \frac{1}{2}))} \\ &\quad - A'(p_1, -p_2)e^{i(p_1(x_1 - \frac{1}{2}) - p_2(x_2 - \frac{1}{2}))} + A'(-p_1, -p_2)e^{-i(p_1(x_1 - \frac{1}{2}) + p_2(x_2 - \frac{1}{2}))} \\ &\quad - A'(p_2, p_1)e^{i(p_2(x_1 - \frac{1}{2}) + p_1(x_2 - \frac{1}{2}))} + A'(p_2, -p_1)e^{i(p_2(x_1 - \frac{1}{2}) - p_1(x_2 - \frac{1}{2}))} \\ &\quad + A'(-p_2, p_1)e^{-i(p_2(x_1 - \frac{1}{2}) - p_1(x_2 - \frac{1}{2}))} - A'(-p_2, -p_1)e^{-i(p_2(x_1 - \frac{1}{2}) + p_1(x_2 - \frac{1}{2}))}\end{aligned}$$

where

$$A'(p_1, p_2) = e^{\frac{i}{2}p_1 + \frac{i}{2}p_2} A(p_1, p_2).$$

By using the Bethe equation, bulk and boundary S -matrices $S(p_j, p_i) = \frac{A(p_j, p_i)}{A(p_i, p_j)}$, $B_L(p_1) = -e^{-ip_1} e^{-2ip_1 L} \frac{A(p_2, -p_1)}{A(p_2, p_1)}$ and $B_L(p_2) = -e^{-ip_2} e^{-2ip_2 L} \frac{A(p_1, -p_2)}{A(p_1, p_2)}$ ¹, we get our notation

$$\begin{aligned}\psi_{\text{open}}^{(2)}(x_1, x_2)/A'(p_1, p_2) &= \\ g(x_1, p_1; x_2, p_2) &+ S(p_2, p_1)S(-p_2, p_1)e^{2ip_1 L} B_L(p_1)g(x_1, -p_1; x_2, p_2) \\ &+ e^{2ip_2 L} B_L(p_2)g(x_1, p_1; x_2, -p_2) + S(p_2, p_1)S(-p_2, p_1)e^{2i(p_1 + p_2)L} B_L(p_1)B_L(p_2)g(x_1, -p_1; x_2, -p_2)\end{aligned}$$

where the function $g(x_1, p_1; x_2, p_2)$ is defined as

$$g(x_1, p_1; x_2, p_2) \equiv \mathcal{A}(x_1, p_1)\mathcal{A}(x_2, p_2) + S(p_2, p_1)\mathcal{A}(x_1, p_2)\mathcal{A}(x_2, p_1).$$

¹ $B_1(p_1) = -e^{-ip_1} \frac{A(-p_1, p_2)}{A(p_1, p_2)}$ and $B_1(p_2) = -e^{-ip_2} \frac{A(-p_2, p_1)}{A(p_2, p_1)}$

Appendix I

Multi-magnon hexagon form factor

In section 9.2.3, we explained the multi-magnon structure constant by using the tailoring method. As a result, we got the multi-magnon hexagon form factor. However, these arguments are quite tedious. Therefore in this appendix, we express again for a few magnon case.

For the most simple case, which have one-magnon, the sum over positions of the propagation factor become

$$\begin{aligned} \sum_{x_1=\ell_{12}+1}^{L_1} \mathcal{A}(x, p) &= e^{-\frac{i}{2}p} \frac{1}{e^{-ip} - 1} e^{ip\ell_{12}} + \dots \\ &= \mathcal{M}(p)h(u)e^{ip\ell_{12}} + \dots \end{aligned} \quad (\text{I.1})$$

Here $h(u)$ is the one-magnon hexagon form factor.

Next for two-magnon case, we have

$$\begin{aligned} &\sum_{x_1=\ell_{12}+1}^{L_1} \sum_{x_2=x_1+1}^{L_1} \left(\mathcal{A}(x_1, p_1)\mathcal{A}(x_2, p_2) + S(p_2, p_1)\mathcal{A}(x_1, p_2)\mathcal{A}(x_2, p_1) \right) \\ &= e^{-\frac{i}{2}(p_1+p_2)}h(p_1, p_2) \\ &\left(\frac{1}{h(p_1, p_2)} \frac{1}{e^{-ip_2} - 1} \frac{1}{e^{-i(p_2+p_1)} - 1} + \frac{1}{h(p_2, p_1)} \frac{1}{e^{-ip_1} - 1} \frac{1}{e^{-i(p_2+p_1)} - 1} \right) e^{i(p_1+p_2)\ell_{12}} + \dots \\ &= \mathcal{M}(p_1)\mathcal{M}(p_2)h(u_1, u_2)e^{i(p_1+p_2)\ell_{12}} + \dots, \end{aligned} \quad (\text{I.2})$$

where in the second line we used the property $S(v, u) = \frac{h(u, v)}{h(v, u)}$ and the terms in bracket become $\frac{1}{(e^{-ip_1}-1)(e^{-ip_2}-1)}$. Also in this case, we could get the two-magnon hexagon form factor from the geometric sum.

Next for three-magnon case, it is bit difficult and we start with

$$\begin{aligned}
& \sum_{x_1=\ell_{12}+1}^{L_1} \sum_{x_2=x_1+1}^{L_1} \sum_{x_3=x_2+1}^{L_1} \left(\mathcal{A}(x_1, p_1) \mathcal{A}(x_2, p_2) \mathcal{A}(x_3, p_3) + S(p_2, p_1) \mathcal{A}(x_1, p_2) \mathcal{A}(x_2, p_1) \mathcal{A}(x_3, p_3) \right) \\
& + S(p_3, p_2) \mathcal{A}(x_1, p_1) \mathcal{A}(x_2, p_3) \mathcal{A}(x_3, p_2) + S(p_3, p_1) \mathcal{A}(x_1, p_3) \mathcal{A}(x_2, p_2) \mathcal{A}(x_3, p_1) \\
& + S(p_2, p_1) S(p_3, p_1) \mathcal{A}(x_1, p_2) \mathcal{A}(x_2, p_3) \mathcal{A}(x_3, p_1) + S(p_3, p_2) S(p_3, p_1) \mathcal{A}(x_1, p_3) \mathcal{A}(x_2, p_1) \mathcal{A}(x_3, p_2),
\end{aligned} \tag{I.3}$$

where we used the following property of the summation

$$\begin{aligned}
& \sum_{x_1=\ell_{12}+1}^{L_1} \sum_{x_2=x_1+1}^{L_1} \sum_{x_3=x_2+1}^{L_1} \mathcal{A}(x_1, p_1) \mathcal{A}(x_2, p_2) \mathcal{A}(x_3, p_3) \\
& = e^{-\frac{i}{2}(p_1+p_2+p_3)} \frac{1}{e^{-ip_3} - 1} \frac{1}{e^{-i(p_3+p_2)} - 1} \frac{1}{e^{-i(p_3+p_2+p_1)} - 1} e^{i(p_1+p_2+p_3)\ell_{12}} + \dots
\end{aligned} \tag{I.4}$$

For the bridge length dependent terms, we have

$$\begin{aligned}
& e^{-\frac{i}{2}(p_1+p_2+p_3)} h(p_1, p_2) h(p_1, p_3) h(p_2, p_3) \\
& \left\{ \frac{\mathcal{M}(p_1, p_2, p_3)}{h(p_1, p_2) h(p_2, p_3) h(p_1, p_3)} + \frac{\mathcal{M}(p_2, p_1, p_3)}{h(p_2, p_1) h(p_1, p_3) h(p_2, p_3)} + \frac{\mathcal{M}(p_1, p_3, p_2)}{h(p_1, p_2) h(p_1, p_3) h(p_3, p_2)} \right. \\
& \left. + \frac{\mathcal{M}(p_3, p_2, p_1)}{h(p_1, p_2) h(p_3, p_1) h(p_2, p_3)} + \frac{\mathcal{M}(p_2, p_3, p_1)}{h(p_2, p_1) h(p_3, p_1) h(p_2, p_3)} + \frac{\mathcal{M}(p_3, p_1, p_2)}{h(p_1, p_2) h(p_3, p_2) h(p_3, p_1)} \right\}.
\end{aligned} \tag{I.5}$$

Using the identity

$$M(p_1, p_2, p_3) = \frac{\mathcal{M}(p_2, p_3)}{e^{-i(p_1+p_2+p_3)} - 1}, \tag{I.6}$$

we get

$$\begin{aligned}
& e^{-\frac{i}{2}(p_1+p_2+p_3)} h(p_1, p_2) h(p_1, p_3) h(p_2, p_3) \frac{1}{e^{-i(p_1+p_2+p_3)}} \\
& \left\{ \left(\frac{\mathcal{M}(p_2, p_3)}{h(p_2, p_3)} + \frac{\mathcal{M}(p_3, p_2)}{h(p_3, p_2)} \right) \frac{1}{h(p_1, p_2) h(p_1, p_3)} + \left(\frac{\mathcal{M}(p_1, p_2)}{h(p_1, p_2)} + \frac{\mathcal{M}(p_2, p_1)}{h(p_2, p_1)} \right) \frac{1}{h(p_3, p_1) h(p_3, p_2)} \right. \\
& \left. + \left(\frac{\mathcal{M}(p_1, p_3)}{h(p_1, p_3)} + \frac{\mathcal{M}(p_3, p_1)}{h(p_3, p_1)} \right) \frac{1}{h(p_2, p_3) h(p_2, p_1)} \right\}.
\end{aligned} \tag{I.7}$$

By mathematical induction, we have

$$\begin{aligned}
& e^{-\frac{i}{2}(p_1+p_2+p_3)} h(p_1, p_2) h(p_1, p_3) h(p_2, p_3) \frac{1}{e^{-i(p_1+p_2+p_3)}} \frac{1}{(e^{-ip_1} - 1)(e^{-ip_2} - 1)(e^{-ip_3} - 1)} \\
& \left\{ \frac{e^{-ip_1} - 1}{h(p_1, p_2) h(p_1, p_3)} + \frac{e^{-ip_3} - 1}{h(p_3, p_1) h(p_3, p_2)} + \frac{e^{-ip_2} - 1}{h(p_2, p_3) h(p_2, p_1)} \right\}.
\end{aligned} \tag{I.8}$$

Finally, by using the following residue integral

$$\oint \frac{dz}{2\pi i} \frac{1}{z} \left(\prod_{k=1}^3 \frac{u_k - z - i/2}{u_k - z + i/2} - 1 \right), \quad (\text{I.9})$$

we find the relation

$$\frac{1}{e^{-i(p_1+p_2+p_3)}} = \frac{e^{-ip_1} - 1}{h(p_1, p_2)h(p_1, p_3)} + \frac{e^{-ip_3} - 1}{h(p_3, p_1)h(p_3, p_2)} + \frac{e^{-ip_2} - 1}{h(p_2, p_3)h(p_2, p_1)}. \quad (\text{I.10})$$

Therefore we get the following expression for three-particle hexagon form factor :

$$\mathcal{M}(p_1)\mathcal{M}(p_2)\mathcal{M}(p_3)h(u_1, u_2, u_3). \quad (\text{I.11})$$

From these lessons, we would be able to expect the multi-magnon hexagon form factor as follows:

$$\begin{aligned} & h_{YY}(u_1, \dots, u_M) \\ &= \frac{1}{\mathcal{M}(p_1) \cdots \mathcal{M}(p_1)} \sum_{x_1 < \cdots < x_M} \sum_{\sigma_1 \neq \cdots \neq \sigma_M} \prod_{\substack{\sigma_k < \sigma_j \\ j < k}} S(p_{\sigma_k}, p_{\sigma_j}) \prod_{l=1}^M \mathcal{A}(x_l, p_{\sigma_l}). \end{aligned} \quad (\text{I.12})$$

Appendix J

Bridge length independent terms

In section 9.2.3, we found that the bridge length independent terms (9.43) are irrelevant. In this appendix, we write down the same arguments but for two- and three-magnon cases.

First let us consider the case of two-magnon. The bridge length independent terms in the calculation of the sum over the positions of wave functions are given by

$$\begin{aligned} & \sum \psi^{(2)}(x_1, x_2) / \mathcal{M}(p_1) \mathcal{M}(p_2) e^{i(p_1+p_2)L} |_{\ell_{ij} \text{ independent}} \\ & = h(u_1, u_2) - S(u_2, u_1) S(-u_2, u_1) h(-u_1, u_2) - h(u_1, -u_2) + S(u_2, u_1) S(-u_2, u_1) h(-u_1, -u_2), \end{aligned} \quad (\text{J.1})$$

which can be straightforwardly rewritten as

$$h(u_1, u_2) h(u_1, -u_2) \left(\frac{1}{h(u_1, -u_2)} - \frac{1}{h(-u_1, -u_2)} - \frac{1}{h(u_1, u_2)} + \frac{1}{h(-u_1, u_2)} \right). \quad (\text{J.2})$$

Although it seems that we have poles at $u_1 = \pm u_2$, their residues are all zero:

$$\text{res}_{u \rightarrow v} \left(\frac{1}{h(u_1, \pm u_2)} + \frac{1}{h(-u_1, \mp u_2)} \right) = i - i = 0. \quad (\text{J.3})$$

This shows that all the poles at $u_1 = \pm u_2$ are spurious poles. After doing so, we only focus on the no-pole part, rigorously $u \rightarrow \infty$ behavior. By taking account into the inverse of the hexagon form factor is written as

$$\frac{1}{h(u, v)} = 1 + \frac{i}{u - v},$$

we can say that the $u \rightarrow \infty$ behavior is also canceled with each other. Namely, the the spin chain length dependent terms for two-magnon are exactly zero.

For the three-magnon case, the terms are given by

$$\begin{aligned}
& \sum \psi^{(3)}(x_1, x_2, x_3) / \mathcal{M}(u_1) \mathcal{M}(u_2) \mathcal{M}(u_3) \mathcal{M}(u_3) e^{i(p_1+p_2+p_3)L} \Big|_{\ell_{i,j} \text{ independent}} \\
&= h(u_1, u_2, u_3) - h(u_1, u_2, -u_3) \\
&- S(u_2, u_1) S(-u_2, u_1) S(u_3, u_1) S(-u_3, u_1) \{h(-u_1, u_2, u_3) - h(-u_1, u_2, -u_3)\} \\
&- S(u_3, u_2) S(-u_3, u_2) \{h(u_1, -u_2, u_3) - h(u_1, -u_2, -u_3)\} \\
&+ S(u_3, u_2) S(-u_3, u_2) S(u_2, u_1) S(-u_2, u_1) S(u_3, u_1) S(-u_3, u_1) \{h(-u_1, -u_2, u_3) - h(-u_1, -u_2, -u_3)\}.
\end{aligned}$$

By taking $\prod_{i < j} h(u_i, u_j) h(u_i, -u_j)$ in front of whole expression, we could obtain

$$\begin{aligned}
& h(u_2, u_3) h(u_2, -u_3) h(u_1, u_2) h(u_1, -u_2) h(u_1, u_3) h(u_1, -u_3) \\
& \left(\frac{1}{h(u_1, u_2) h(u_1, -u_3) h(u_3, u_2)} - \frac{1}{h(u_1, u_2) h(u_1, u_3) h(-u_3, u_2)} \right. \\
& - \frac{1}{h(-u_1, u_2) h(-u_1, -u_3) h(u_3, u_2)} + \frac{1}{h(-u_1, u_2) h(-u_1, u_3) h(-u_3, u_2)} \\
& - \frac{1}{h(u_1, -u_2) h(u_1, -u_3) h(u_3, -u_2)} + \frac{1}{h(u_1, -u_2) h(u_1, u_3) h(-u_3, -u_2)} \\
& \left. + \frac{1}{h(-u_1, -u_2) h(-u_1, -u_3) h(u_3, -u_2)} - \frac{1}{h(-u_1, -u_2) h(-u_1, u_3) h(-u_3, -u_2)} \right). \quad (\text{J.4})
\end{aligned}$$

Similarly, this expression appears to have poles at $u_1 = \pm u_2, u_1 = \pm u_3$ and $u_2 = \pm u_3$. However, the residues are zero again:

$$\begin{aligned}
& \text{res}_{u_1 \rightarrow \pm u_2} \left(\frac{1}{h(u_1, \pm u_2) h(u_1, -u_3) h(u_3, \pm u_2)} - \frac{1}{h(u_1, \pm u_2) h(u_1, u_3) h(-u_3, \pm u_2)} \right. \\
& \quad \left. + \frac{1}{h(-u_1, \mp u_2) h(-u_1, -u_3) h(u_3, \mp u_2)} - \frac{1}{h(-u_1, \mp u_2) h(-u_1, u_3) h(-u_3, \mp u_2)} \right) = 0, \\
& \text{res}_{u_1 \rightarrow \pm u_3} \left(\frac{1}{h(u_1, u_2) h(u_1, \pm u_3) h(\mp u_3, u_2)} - \frac{1}{h(u_1, -u_2) h(u_1, \pm u_3) h(\mp u_3, -u_2)} \right. \\
& \quad \left. + \frac{1}{h(-u_1, u_2) h(-u_1, \mp u_3) h(\pm u_3, u_2)} - \frac{1}{h(-u_1, -u_2) h(-u_1, \mp u_3) h(\pm u_3, -u_2)} \right) = 0, \\
& \text{res}_{u_2 \rightarrow \pm u_3} \left(\frac{1}{h(u_1, u_2) h(u_1, \mp u_3) h(\pm u_3, u_2)} - \frac{1}{h(-u_1, u_2) h(-u_1, \mp u_3) h(\pm u_3, u_2)} \right. \\
& \quad \left. + \frac{1}{h(u_1, -u_2) h(u_1, \pm u_3) h(\mp u_3, -u_2)} - \frac{1}{h(-u_1, -u_2) h(-u_1, \pm u_3) h(\mp u_3, -u_2)} \right) = 0.
\end{aligned}$$

Through the same argument as the two-magnon case, we can say that the contributions of the $u \rightarrow \infty$ behavior are canceled with each other. Therefore the spin chain length dependent terms for the three-magnon are exactly zero.

Appendix K

Two nontrivial operators with one-magnon : $C_{123}^{YY^\circ}$

In this appendix, we calculate another configuration which has two-magnons on each different spin chains. Specifically, we consider the following configuration:

$$\mathcal{O}_1 : \sum_x Z^x Y Z^{L_1 - (x+1)}, \quad \mathcal{O}_2 : \sum_x \bar{Z}^x \bar{Y} \bar{Z}^{L_2 - (x+1)}, \quad \mathcal{O}_3 : \tilde{Z}^{L_3}$$

With this configuration, there exist two possible ways to contract local operators together for obtaining the structure constant :

$$\begin{aligned} C_{123}^{YY^\circ} &= C_{123}^{\text{direct}} + C_{123}^{\text{indirect}}, \\ C_{123}^{\text{direct}} &\propto \sum_{x=1}^{\ell_{12}} \psi_{\text{open}}^{(1)}(x, p_1) \psi_{\text{open}}^{(1)}(L_2 - x + 1, p_2), \\ C_{123}^{\text{indirect}} &\propto \sum_{x=\ell_{12}+1}^{L_1} \psi_{\text{open}}^{(1)}(x, p_1) \sum_{y=1}^{\ell_{23}} \psi_{\text{open}}^{(1)}(y, p_2). \end{aligned} \quad (\text{K.1})$$

Here we decomposed into two part:direct and indirect. These contributions are represented in figure K.1. The summation of the propagators in C_{123}^{direct} and in $C_{123}^{\text{indirect}}$ are respectively calculated as

$$\sum_{x=1}^{\ell_{12}} \mathcal{A}(x, p_1) \mathcal{A}(L_2 - x + 1, p_2) = \mathcal{M}(p_1) \mathcal{M}(p_2) \frac{i}{u - v} (e^{ip_2 L_2} - e^{ip_1 \ell_{12}} e^{ip_2 \ell_{23}}), \quad (\text{K.2})$$

$$- \sum_{x=\ell_{12}+1}^{L_1} \mathcal{A}(x, p_1) \sum_{y=1}^{\ell_{23}} \mathcal{A}(y, p_2) = -\mathcal{M}(p_1) \mathcal{M}(p_2) (e^{ip_1 \ell_{12}} - e^{ip_1 L_1}) (1 - e^{ip_2 \ell_{23}}). \quad (\text{K.3})$$

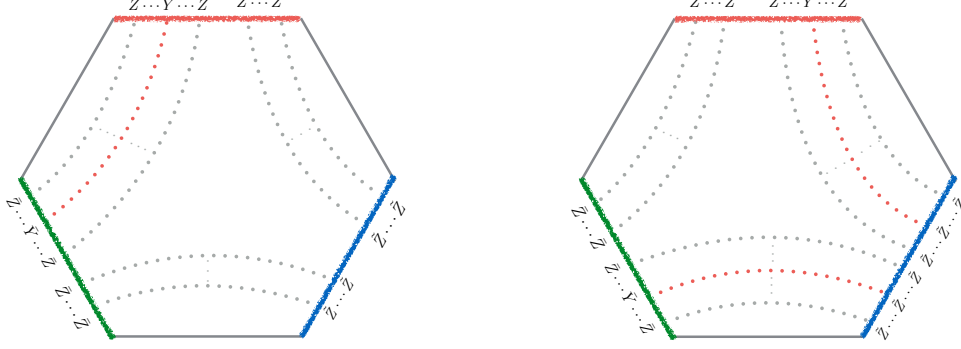


Figure K.1: C_{123}^{direct} and $C_{123}^{\text{indirect}}$

By adding the two parts, we have

$$C_{123}^{YY^\circ} \propto \mathcal{M}_{\ell_{12}}(p_1)\mathcal{M}_{\ell_{23}}(p_2) \left[\frac{u-v-i}{u-v} - e^{2ip_1\ell_{13}} \frac{-u-v-i}{-u-v} - e^{2ip_2\ell_{12}} \frac{u+v-i}{u+v} + e^{2ip_1\ell_{13}} e^{2ip_2\ell_{12}} \frac{-u+v-i}{-u+v} \right], \quad (\text{K.4})$$

Even here, there are nontrivial factors, which came from the geodesic summation i.e. $\frac{u-v-i}{u-v}$. In the same way as the structure constant $C_{123}^{Y^2\circ\circ}$, the nontrivial factors are just the tree-level hexagon form factor. However, in this case, the nontrivial factors in the $C_{123}^{YY^\circ}$ are surely different. Because, the hexagon form factors that appear here should be defined by the mirror transformation twice. Namely,

$$h_{Y|Y}(v|u) = h_{YY}(u^{2\gamma}, v) \frac{u-v-i}{u-v} + \mathcal{O}(g). \quad (\text{K.5})$$

Thus the result (K.4) can also generalized to the finite coupling conjecture as (see figure K.2)

$$C_{123}^{YY^\circ} \propto \mathcal{M}_{\ell_{12}}(p_1)\mathcal{M}_{\ell_{23}}(p_2) \left[h_{Y|Y}(v|u) - e^{2ip_1\ell_{13}} h_{Y|Y}(v|-u) - e^{2ip_2\ell_{12}} h_{Y|Y}(-v|u) + e^{2ip_1\ell_{13}} e^{2ip_2\ell_{12}} h_{Y|Y}(-v|-u) \right] \quad (\text{K.6})$$

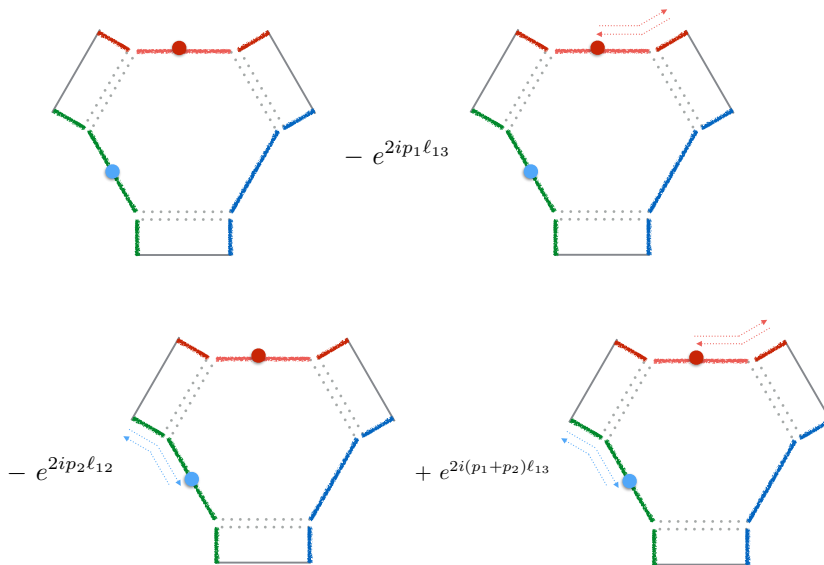


Figure K.2: By appropriate propagation factors $e^{2ip_1\ell_{13}}$ and $e^{2ip_2\ell_{12}}$, the each terms can be interpreted as the each magnon with (p_1, p_2) , $(-p_1, p_2)$, $(p_1, -p_2)$ and $(-p_1, -p_2)$ lived on the hexagon.

Appendix L

On norms of structure constants for open string

Here we would like to mention the norm of the structure constant for open strings. In ordinary, the correct structure constants including normalizations at tree-level are given by

$$\left(\frac{C_{123}^{M\circ\circ}}{C_{123}^{\circ\circ\circ}}\right)^2 = \frac{1}{\mathcal{N}^{(M)}} \left(\sum_{\ell_{12}+1 \leq x_1 < \dots < x_M \leq L_1} \psi_{\text{open}}^{(M)}(x_1, \dots, x_M) \right)^2,$$

where

$$\mathcal{N}^{(M)} = \sum_{1 \leq x_1 < \dots < x_M \leq L_1} (\psi_{\text{open}}^{(M)})^{\mathfrak{f}} \psi_{\text{open}}^{(M)},$$

where subscript \mathfrak{f} is the flipping operation introduced in [45].

In this appendix, we specifically calculate for one- and two-magnon norm. After doing so, we see that the result is given by the Gaudin norm for open spin chain system. By using the lessons, we try to suggest the multi-magnon norm.

Let us start with recalling the one-magnon wave function:

$$\psi_{\text{open}}^{(1)}(x) = e^{ip(x-\frac{1}{2})} + e^{2ipL} e^{-ip(x-\frac{1}{2})}.$$

By flipping operation it can be easily found that $\mathfrak{f} : \psi_{\text{open}}^{(1)} \rightarrow e^{ipL} (\psi_{\text{open}}^{(1)})^*$.¹ Notice that we found a curious property of the open spin chain wave function that the conjugated wave function is the exactly same with the original wave function for the one-magnon : $(\psi_{\text{open}}^{(1)})^* = \psi_{\text{open}}^{(1)}$. By computing the summation of the square of the wave function, we can get the following identity for the norm $\mathcal{N}^{(1)}$:

$$\mathcal{N}^{(1)} = (\mathcal{M}(p))^2 (\partial_u \phi), \tag{L.1}$$

¹For the closed spin chain, the operation is slightly different such as $(\psi_{\text{closed}}^{(1)})^{\mathfrak{f}} = e^{ip(L+1)} \psi_{\text{closed}}^{(1)}$.

where the derivative is performed for the rapidity variable and ϕ is defined from the Bethe Yang equation for open spin-chain :

$$e^{i\phi} = e^{2ipL}. \quad (\text{L.2})$$

Furthermore, remember that the factor $\mathcal{M}(p)$ came from the main part of the structure constant.

For two-magnon case, the wave function is written by

$$\begin{aligned} \psi_{\text{open}}^{(2)}(x_1, x_2) = & g(x_1, p_1; x_2, p_2) + S(p_2, p_1)S(-p_2, p_1)e^{2ip_1L}g(x_1, -p_1; x_2, p_2) \\ & + e^{2ip_2L}g(x_1, p_1; x_2, -p_2) + S(p_2, p_1)S(-p_2, p_1)e^{2i(p_1+p_2)L}g(x_1, -p_1; x_2, -p_2), \end{aligned}$$

where

$$g(x_1, p_1; x_2, p_2) \equiv \mathcal{A}(x_1, p_1)\mathcal{A}(x_2, p_2) + S(p_2, p_1)\mathcal{A}(x_1, p_2)\mathcal{A}(x_2, p_1).$$

The flipping operation can be written again by the original wave function such as $\mathbf{f} : \psi_{\text{open}}^{(2)} \rightarrow e^{i(p_1+p_2)L}S(p_2, p_1)(\psi_{\text{open}}^{(2)})^*$ and $(\psi_{\text{open}}^{(2)})^* = S(p_1, p_2)S(p_1, -p_2)e^{-2i(p_1+p_2)L}\psi_{\text{open}}^{(2)}$. Thus, we can expect the general magnon case

$$\mathbf{f} : \psi_{\text{open}}^{(M)} \rightarrow (\psi_{\text{open}}^{(M)})^* \prod_{i < j} S(p_j, p_i)e^{i(p_1+\dots+p_M)L},$$

and

$$(\psi_{\text{open}}^{(M)})^* = \prod_{i < j} S(p_i, p_j)S(p_i, -p_j)e^{-2i(p_1+\dots+p_2)L}\psi_{\text{open}}^{(M)}.$$

From the summation for the wave function, we can obtain the norm for open spin-chain :

$$\sum_{1 \leq x_1 < x_2 \leq L_1} (\psi_{\text{open}}^{(2)})^* \psi_{\text{open}}^{(2)} = (\mathcal{M}(p_1)\mathcal{M}(p_2))^2 \det(\partial_{u_i}\phi_j). \quad (\text{L.3})$$

Here, the determinant $\det(\partial_{u_i}\phi_j)$ is known as the Gaudin norm [46, 47], where the ϕ_j is defined from the Bethe-Yang equation for the open spin-chain such as²

$$\begin{aligned} e^{i\phi_1} &= e^{2ip_1L_1}S(p_2, p_1)S(-p_2, p_1), \\ e^{i\phi_2} &= e^{2ip_2L_1}S(p_1, p_2)S(-p_1, p_2). \end{aligned}$$

Therefore, the norm $\mathcal{N}^{(2)}$ can be given in terms of the Gaudin norm :

$$\mathcal{N}^{(2)} = (\mathcal{M}(p_1)\mathcal{M}(p_2))^2 \det(\partial_{u_i}\phi_j)S(p_2, p_1)e^{i(p_1+p_2)L}. \quad (\text{L.4})$$

We finally expect that the norm for the multi-magnon is given as

$$\mathcal{N}^{(M)} = \left(\prod_i \mathcal{M}(p_i) \right)^2 \det(\partial_{u_i}\phi_j) \prod_{i < j} S(p_j, p_i)e^{i(p_1+\dots+p_M)L}. \quad (\text{L.5})$$

We emphasize that we checked validity of (L.5) by numerically solving the Bethe ansatz equations.

²We have $B(p) = 1$ in our basis.

Bibliography

- [1] J. M. Maldacena, “The Large N limit of superconformal field theories and supergravity,” *Int. J. Theor. Phys.* **38**, 1113 (1999) [*Adv. Theor. Math. Phys.* **2**, 231 (1998)] [hep-th/9711200](#).
- [2] N. Beisert et al., “Review of AdS/CFT Integrability: An Overview,” [hep-th/1012.3982](#).
- [3] I. Bena, J. Polchinski and R. Roiban, “Hidden symmetries of the $\text{AdS}_5 \times \text{S}^5$ superstring,” *Phys. Rev. D* **69**, 046002 (2004), [hep-th/0305116](#).
- [4] N. Beisert, V. A. Kazakov, K. Sakai and K. Zarembo, “The Algebraic curve of classical superstrings on $\text{AdS}_5 \times \text{S}^5$,” *Commun. Math. Phys.* **263**, 659 (2006), [hep-th/0502226](#).
- [5] N. Gromov and P. Vieira, “The $\text{AdS}_5 \times \text{S}^5$ superstring quantum spectrum from the algebraic curve,” *Nucl. Phys. B* **789**, 175 (2008) [hep-th/0703191](#).
- [6] J. A. Minahan and K. Zarembo, “The Bethe ansatz for $\mathcal{N} = 4$ super Yang-Mills,” *JHEP* **0303**, 013 (2003) [hep-th/0212208](#).
- [7] N. Beisert, “The $\text{su}(2|2)$ Dynamic S-matrix,” *Adv. Theor. Math. Phys.* **12**, 945 (2008) [hep-th/0511082](#).
- [8] N. Beisert, “The Analytic Bethe Ansatz for a Chain with Centrally Extended $\text{su}(2|2)$ Symmetry,” *J. Stat. Mech.* **0701**, P017 (2007) [hep-th/0610017](#).
- [9] R. A. Janik, “The $\text{AdS}_5 \times \text{S}^5$ superstring worldsheet S-matrix and crossing symmetry,” *Phys. Rev. D* **73**, 086006 (2006) [hep-th/0603038](#).
- [10] N. Beisert, R. Hernandez and E. Lopez, “A Crossing-Symmetric Phase for $\text{AdS}_5 \times \text{S}^5$ Strings,” *JHEP* **0611**, 070 (2006) [hep-th/0609044](#).
- [11] N. Beisert, B. Eden and M. Staudacher, “Transcendentality and Crossing,” *Stat. Mech.* **0701**, P021 (2007) [hep-th/0610251](#).
- [12] N. Beisert and M. Staudacher, “Long-range $\text{psu}(2,2|4)$ Bethe Ansatzes for gauge theory and strings,” *Nucl. Phys. B* **727**, 1 (2005) [hep-th/0504190](#).

- [13] N. Gromov, V. Kazakov, S. Leurent and D. Volin, “Quantum spectral curve for arbitrary state/operator in AdS₅/CFT₄,” JHEP 1509 (2015) 187 [hep-th/405.4857](#).
- [14] C. Marboe, V. Velizhanin and D. Volin, “Six-loop anomalous dimension of twist-two operators in planar $\mathcal{N} = 4$ SYM theory,” JHEP 1507 (2015) 084 [hep-th/1412.4762](#).
- [15] K. Zarembo, “Holographic three-point functions of semiclassical states,” JHEP **1009** (2010) 030 [hep-th/1008.1059](#).
- [16] M. S. Costa, R. Monteiro, J. E. Santos and D. Zoakos, “On three-point correlation functions in the gauge/gravity duality,” JHEP **1011** (2010) 141 [hep-th/1008.1070](#).
- [17] R. A. Janik and A. Wereszczynski, “Correlation functions of three heavy operators: The AdS contribution,” JHEP **1112** (2011) 095 [hep-th/1109.6262](#).
- [18] Y. Kazama and S. Komatsu, “On holographic three point functions for GKP strings from integrability,” JHEP **1201** (2012) 110 [hep-th/1110.3949](#).
- [19] Y. Kazama and S. Komatsu, “Wave functions and correlation functions for GKP strings from integrability,” JHEP **1209** (2012) 022 [hep-th/1205.6060](#).
- [20] Y. Kazama and S. Komatsu, “Three-point functions in the SU(2) sector at strong coupling,” JHEP **1403** (2014) 052 [hep-th/1312.3727](#).
- [21] Y. Kazama, S. Komatsu and T. Nishimura, “Novel construction and the monodromy relation for three-point functions at weak coupling,” JHEP **1501** (2015) 095 [hep-th/1410.8533](#).
- [22] Y. Kazama, S. Komatsu and T. Nishimura, “On the singlet projector and the monodromy relation for $\mathfrak{psu}(2, 2|4)$ spin chains and reduction to subsectors,” JHEP **1509** (2015) 183 [hep-th/1506.03203](#).
- [23] Y. Kazama, S. Komatsu and T. Nishimura, “Classical Integrability for Three-point Functions: Cognate Structure at Weak and Strong Couplings,” JHEP **1610** (2016) 042 [hep-th/1603.03164](#).
- [24] D. E. Berenstein, J. M. Maldacena and H. S. Nastase, “Strings in flat space and pp waves from $\mathcal{N} = 4$ superYang-Mills,” JHEP 0204 (2002) 013 [hep-th/0202021](#)
- [25] M. Spradlin and A. Volovich, “Superstring interactions in a pp wave background,” Phys. Rev. D 66 (2002) 086004 [hep-th/0204146](#).
- [26] A. Pankiewicz and B. Stefanski, Jr., “PP wave light cone superstring field theory,” Nucl. Phys. B 657 (2003) 79 [hep-th/0210246](#).
- [27] C. S. Chu and V. V. Khoze, “Correspondence between the three point BMN correlators and the three string vertex on the pp wave,” JHEP 0304 (2003) 014 [hep-th/0301036](#).

- [28] P. Di Vecchia, J. L. Petersen, M. Petrini, R. Russo and A. Tanzini, “The Three string vertex and the AdS / CFT duality in the PP wave limit,” *Class. Quant. Grav.* 21 (2004) 2221 [hep-th/0304025](#).
- [29] S. Dobashi and T. Yoneya, “Resolving the holography in the plane-wave limit of AdS/CFT correspondence,” *Nucl. Phys. B* 711 (2005) 3 [hep-th/0406225](#).
- [30] H. Shimada, “Holography at string field theory level: Conformal three point functions of BMN operators,” *Phys. Lett. B* 647 (2007) 211 [hep-th/0410049](#).
- [31] Z. Bajnok and R. A. Janik, “String field theory vertex from integrability,” *JHEP* 1504 (2015) 042 [hep-th/1501.04533](#).
- [32] Z. Bajnok and R. A. Janik, “The kinematical $\text{AdS}_5 \times \text{S}^5$ Neumann coefficient,” *JHEP* 1602 (2016) 138 [hep-th/1512.01471](#).
- [33] Z. Bajnok and R. A. Janik, “From the octagon to the SFT vertex gluing and multiple wrapping,” *JHEP* 1706 (2017) 058 [hep-th/1704.03633](#).
- [34] B. Basso, S. Komatsu and P. Vieira, “Structure Constants and Integrable Bootstrap in Planar $\mathcal{N} = 4$ SYM Theory,” [hep-th/1505.06745](#).
- [35] M. Kim and N. Kiryu, “Structure constants of operators on the Wilson loop from integrability,” *JHEP* **1711**, 116 (2017) [hep-th/1706.02989](#).
- [36] N. Kiryu and S. Komatsu “Correlation Functions on the Half-BPS Wilson Loop: Perturbation and Hexagonalization,” *JHEP* **1902** 090 (2019) [hep-th/1812.04593](#).
- [37] M. Kim, N. Kiryu, S. Komatsu and T. Nishimura, “Structure Constants of Defect Changing Operators on the 1/2 BPS Wilson Loop,” *JHEP* **1712**, 055 (2017) [hep-th/1710.07325](#).
- [38] G. 'tHooft, “A Planar Diagram theory for Strong Interactions,” *Nucl. Phys. B* 360, 461 (1974).
- [39] N. Drukker, J. Plefka, “The Structure of n-point functions of chiral primary operators in $\mathcal{N} = 4$ super Yang-Mills at one-loop,” *JHEP* 0904 (2009) 001 [hep-th/0812.3341](#).
- [40] F. A. Dolan, L. Gallot and E. Sokatchev, “On four-point functions of 1/2-BPS operators in general dimensions,” *JHEP* 0409, 056 (2004) [hep-th/0405180](#).
- [41] M. Nirschl and H. Osborn, “Superconformal Ward identities and their solution,” *Nucl. Phys. B* 711 (2005) 409 [hep-th/0407060](#).
- [42] K. Okuyama, L. Tseng, “Three-point functions in $\mathcal{N} = 4$ SYM theory at one-loop”, *JHEP* 0408 (2004) 055 [hep-th/0404190](#).
- [43] R. Roiban, A. Volovich, “Yang-Mills correlation functions from integrable spin chains”, *JHEP* 0409 (2004) 032 [hep-th/0407140](#).

- [44] L. F. Alday, J. R. David, E Gava, K. S. Narain, “Structure constants of planar $\mathcal{N} = 4$ Yang Mills at one loop”, JHEP 0509 (2005) 070 [hep-th/0502186](#).
- [45] J. Escobedo, N. Gromov, A. Sever, P. Vieira, “Tailoring Three-point functions and Integrability”, JHEP 1109 (2011) 028 [hep-th/1012.2475](#).
- [46] Z. Bajnok and R. A. Janik, “String field theory vertex from integrability,” [hep-th/1501.04533](#).
- [47] B. Pozsgay, “Finite volume form factors and correlation functions at finite temperature,” [hep-th/0907.4306](#).
- [48] T. Fleury and S. Komatsu, “Hexagonalization of Correlation Functions,” JHEP **1701**, 130 (2017) [hep-th/1611.05577](#).
- [49] T. Fleury and S. Komatsu, “Hexagonalization of Correlation Functions II: Two-Particle Contributions,” JHEP **1802**, 177 (2018) [hep-th/1711.05327](#).
- [50] S. Komatsu, “Lectures on Three-point Functions in $\mathcal{N} = 4$ Supersymmetric Yang-Mills Theory,” [hep-th/1710.03853](#).
- [51] K. M. Watson, “Some general relations between the photoproduction and scattering of pi mesons,” Phys. Rev. 95 (1954) 228.
- [52] F. A. Smirnov, “Form-factors in completely integrable models of quantum field theory,” Adv. Ser. Math. Phys. 14 (1992) 1.
- [53] N. Beisert, B. Eden and M. Staudacher, “Transcendentality and Crossing,” J. Stat. Mech. 0701 (2007) P01021 [hep-th/0610251](#).
- [54] M. Lüscher, “Volume Dependence of the energy Spectrum in Massive Quantum Field Theories. 1. Stable Particle States,” Commun. Math. Phys. 104, 177 (1986).
- [55] R. A. Janik and T. Lukowski, “From nesting to dressing,” Phys. Rev. D78, 066018 (2008) [hep-th/0804.4295](#).
- [56] M. P. Heller, R. A. Janik and T. Lukowski, “A new derivation of Luscher F-term and fluctuations around the giant magnon,” JHEP 0806, 036 (2008) [hep-th/0801.4463](#).
- [57] R. A. Janik, “Review of AdS/CFT Integrability, Chapter III.5: Luscher corrections,” [hep-th/1012.3994](#).
- [58] B. Basso, A. Sever and P. Vieira, “Spacetime and Flux Tube S-Matrices at Finite Coupling for $\mathcal{N} = 4$ Supersymmetric Yang-Mills theory,” Phys. Rev. Lett. 111 (2013) 9, [hep-th/1303.1396](#).
- [59] B. Basso, A. Sever and P. Vieira, “Collinear Limit of Scattering Amplitudes at Strong Coupling,” Phys. Rev. Lett. 113 (2014) 26, 261604 [hep-th/1405.6350](#).
- [60] B. Basso, “Exciting the GKP string at any coupling”, Nucl.Phys. B857 (2012) 254-334 [hep-th/1010.5237](#).

- [61] B. Basso, A. V. Belitsky, “Luescher formula for GKP string”, Nucl.Phys. B860 (2012) 1-86 [hep-th/1108.0999](#).
- [62] B. Basso, V. Goncalves, S. Komatsu, P. Vieira, “Gluing Hexagons at Three Loops,” Nucl.Phys. B907 (2016) 695-716 [hep-th/1510.01683](#).
- [63] Y. Jiang, S. Komatsu, I. Kostov, D. Serban, “Clustering and the Three-Point Function,” J.Phys. A49 (2016) no.45, 454003 [hep-th/1604.03575](#).
- [64] B. Basso, V. Goncalves, S. Komatsu, P. Vieira, “Structure constants at wrapping order,” JHEP 1705 (2017) 124 [hep-th/1702.02154](#).
- [65] B. Basso, F. Coronado, S. Komatsu, H. T. Lam, P. Vieira, D. Zhong, “Asymptotic Four Point Functions,” [hep-th/1701.04462](#).
- [66] T. Fleury, S. Komatsu, “Hexagonalization of Correlation Functions II : Two-Particle Contributions,” JHEP 1802 (2018) 177, [hep-th/1711.05327](#).
- [67] F. Coronado, “Perturbative Four-Point Functions in Planar $\mathcal{N} = 4$ SYM from Hexagonalization,” [hep-th/1811.00467](#).
- [68] F. Coronado, “Bootstrapping the simplest correlator in planar $\mathcal{N} = 4$ SYM at all loops”, [hep-th/1811.03282](#).
- [69] T. Bargheer, J. Caetano, T. Fleury, S. Komatsu, P. Vieira, “Handling Handles I: Nonplanar Integrability,” [hep-th/1711.05326](#).
- [70] T. Bargheer, J. Caetano, T. Fleury, S. Komatsu, P. Vieira, “Handling Handles II: Stratification and Data Analysis,” JHEP 1811 (2018) 095 [hep-th/1809.09145](#).
- [71] K.G. Wilson, “Confinement of Quarks,” Phys. Rev. D10, 2445 (1974).
- [72] N. Drukker, D. J. Gross and H. Ooguri, “Wilson loops and minimal surfaces,” Phys. Rev. D 60 (1999) 125006. [hep-th/9904191](#).
- [73] J. Maldacena, “Wilson loops in large N field theories,” Phys. Rev. Lett. 80, 4859 (1998) [hep-th/9803002](#).
- [74] S. J. Rey and J. Yee, “Macroscopic strings as heavy quarks in large N gauge theory and anti-de Sitter supergravity,” Eur. Phys. J. C 22 (2001) 379 [hep-th/9803001](#).
- [75] K. Zarembo, “Supersymmetric Wilson loops,” Nucl.Phys. B643 (2002) 157-171 [hep-th/0205160](#).
- [76] G.W. Semenoff, K. Zarembo, “Wilson loops in SYM theory: from weak to strong coupling,” Nucl.Phys.Proc.Suppl. 108 (2002) 106-112 [hep-th/0202156](#).
- [77] J.K. Erickson, G.W. Semenoff, K. Zarembo, “Wilson loops in $\mathcal{N} = 4$ supersymmetric Yang-Mills theory,” Nucl.Phys. B582 (2000) 155-175 [hep-th/0003055](#).

- [78] N. Drukker, D. J. Gross, “An Exact prediction of $\mathcal{N} = 4$ SUSYM theory for string theory,” J.Math.Phys. 42 (2001) 2896-2914 [hep-th/0010274](#).
- [79] D. Berenstein, R. Corrado, W. Fischler and J. Maldacena, “The Operator Product Expansion for Wilson Loops and Surfaces in the Large N Limit,” Phys. Rev. D59, 105023 (1999) [hep-th/9809188](#).
- [80] N. Drukker and V. Forini, “Generalized quark-antiquark potential at weak and strong coupling,” [hep-th/1105.5144](#).
- [81] D. Correa, J. Henn, J. Maldacena, and A. Sever, “The cusp anomalous dimension at three loops and beyond,” [hep-th/1203.1019](#).
- [82] D. Correa, J. Henn, J. Maldacena, and A. Sever, “An exact formula for the radiation of a moving quark in $\mathcal{N} = 4$ super Yang Mills,” [hep-th/1202.4455](#).
- [83] N. Drukker, “Integrable Wilson loops”, JHEP10(2013)135 [hep-th/1203.1617](#).
- [84] M. A. Shifman, “Wilson Loop In Vacuum Fields,” Nucl. Phys. B 173 (1980) 13.
- [85] N. Drukker and S. Kawamoto, “Small deformations of supersymmetric Wilson loops and open spin-chains,” JHEP 0607 (2006) 024 [hep-th/0604124](#).
- [86] K. Okamura, Y. Takayama and K. Yoshida, “Open spinning strings and AdS/dCFT duality,” JHEP 0601 (2006) 112 [hep-th/0511139](#).
- [87] D. Berenstein and S. E. Vazquez, “Integrable open spin chains from giant gravitons,” JHEP 0506 (2005) 059 [hep-th/0501078](#).
- [88] O. DeWolfe and N. Mann, “Integrable open spin chains in defect conformal field theory,” JHEP 0404 (2004) 035 [hep-th/0401041](#).
- [89] D. Correa, J. Maldacena and A. Sever, “The quark anti-quark potential and the cusp anomalous dimension from a TBA equation,” JHEP 1208 (2012) 134 [hep-th/1203.1913](#).
- [90] S. Giombi and S. Komatsu, “Exact Correlators on the Wilson Loop in $\mathcal{N} = 4$ SYM: Localization, Defect CFT, and Integrability,” JHEP 1805 (2018) 109, [hep-th/1802.05201](#).
- [91] J. Maldacena and A. Zhiboedov, “Constraining Conformal Field Theories with A Higher Spin Symmetry,” J. Phys. A 46 (2013) 214011 [hep-th/1112.1016](#).
- [92] J. Maldacena and A. Zhiboedov, “Constraining conformal field theories with a slightly broken higher spin symmetry,” Class. Quant. Grav. 30 (2013) 104003 [hep-th/1204.3882](#).
- [93] I. R. Klebanov and A. M. Polyakov, “AdS dual of the critical $O(N)$ vector model,” Phys. Lett. B 550 (2002) 213 [hep-th/0210114](#).

- [94] S. Giombi and X. Yin, “Higher Spin Gauge Theory and Holography: The Three-Point Functions,” JHEP 1009 (2010) 115 [hep-th/0912.3462](#).
- [95] S. Giombi and X. Yin, “Higher Spins in AdS and Twistorial Holography,” JHEP 1104 (2011) 086 [hep-th/1004.3736](#).
- [96] S. Giombi and X. Yin, “The Higher Spin/Vector Model Duality,” J. Phys. A 46 (2013) 214003 [hep-th/1208.4036](#).
- [97] N. Beisert, C. Kristjansen, J. Plefka, G. W. Semenoff and M. Staudacher, “BMN correlators and operator mixing in $\mathcal{N} = 4$ superYang-Mills theory,” Nucl. Phys. B 650 (2003) 125 [hep-th/0208178](#).
- [98] N. I. Usyukina and A. I. Davydychev, “An Approach to the evaluation of three and four point ladder diagrams,” Phys. Lett. B 298 (1993) 363-370
- [99] J. K. Erickson, G. W. Semenoff, R. J. Szabo and K. Zarembo, “Static potential in $\mathcal{N} = 4$ supersymmetric Yang-Mills theory,” Phys. Rev. D 61 (2000) 105006 [hep-th/9911088](#).
- [100] C. Chamon, R. Jackiw, S. Y. Pi and L. Santos, “Conformal quantum mechanics as the CFT1 dual to AdS2,” Phys. Lett. B 701, 503 (2011) [hep-th/1106.0726](#).
- [101] S. H. Dong and R. Lemus. “A new dynamical group approach to the modified Poschl- Teller potential.” [quant-ph/0110157](#).
- [102] H. Kawai, D. C. Lewellen and S. H. H. Tye, “A Relation Between Tree Amplitudes of Closed and Open Strings,” Nucl. Phys. B 269, 1 (1986).
- [103] A. Kitaev, “A simple model of quantum holography,” KITP strings seminar and Entanglement 2015 program (Feb. 12, April 7, and May 27, 2015) . <http://online.kitp.ucsb.edu/online/entangled15/>.
- [104] S. Sachdev and J. Ye, “Gapless spin-fluid ground state in a random quantum heisenberg magnet,” Phys. Rev. Lett. 70 (May, 1993) 3339-3342. <http://link.aps.org/doi/10.1103/PhysRevLett.70.3339>.
- [105] D. J. Gross and V. Rosenhaus, “The Bulk Dual of SYK: Cubic Couplings,” JHEP 1705 (2017) 092 [hep-th/1702.08016](#).
- [106] J. Maldacena and D. Stanford, “Comments on the Sachdev-Ye-Kitaev model,” [hep-th/1604.07818](#).
- [107] D. J. Gross and V. Rosenhaus, “A line of CFTs: from generalized free fields to SYK,” JHEP 1707, 086 (2017) [hep-th/1706.07015](#).
- [108] J. Maldacena, D. Stanford, Z. Yang, “Conformal symmetry and its breaking in two dimensional Nearly Anti-de-Sitter space,” PTEP 2016 (2016) no.12, 12C104 , [hep-th/1606.01857](#).

- [109] A. B. Zamolodchikov, Fishnet Diagrams as a Completely Integrable System, Phys. Lett. 97B (1980) 63-66.
- [110] O. Gurdogan and V. Kazakov, New Integrable 4D Quantum Field Theories from Strongly Deformed Planar $\mathcal{N} = 4$ Supersymmetric Yang-Mills Theory, Phys. Rev. Lett. 117 (2016) 201602, [hep-th/1512.06704](#).
- [111] J. Caetano, O. Gurdogan and V. Kazakov, Chiral limit of $\mathcal{N} = 4$ SYM and ABJM and integrable Feynman graphs, JHEP 03 (2018) 077, [hep-th/1612.05895](#).
- [112] S. Giombi, R. Roiban and A. A. Tseytlin, “Half-BPS Wilson loop and AdS₂/CFT₁,” Nucl. Phys. B 922, 499 (2017) [hep-th/1706.00756](#).